2013

INVESTIGATING KEY POST-PKS ENZYMES FROM GILVOCARCIN BIOSYNTHETIC PATHWAY

Nidhi Tibrewal
University of Kentucky, nidhitibrewal@gmail.com

STUDENT AGREEMENT:

I represent that my thesis or dissertation and abstract are my original work. Proper attribution has been given to all outside sources. I understand that I am solely responsible for obtaining any needed copyright permissions. I have obtained and attached hereto needed written permission statements(s) from the owner(s) of each third-party copyrighted matter to be included in my work, allowing electronic distribution (if such use is not permitted by the fair use doctrine).

I hereby grant to The University of Kentucky and its agents the non-exclusive license to archive and make accessible my work in whole or in part in all forms of media, now or hereafter known. I agree that the document mentioned above may be made available immediately for worldwide access unless a preapproved embargo applies.

I retain all other ownership rights to the copyright of my work. I also retain the right to use in future works (such as articles or books) all or part of my work. I understand that I am free to register the copyright to my work.

REVIEW, APPROVAL AND ACCEPTANCE

The document mentioned above has been reviewed and accepted by the student's advisor, on behalf of the advisory committee, and by the Director of Graduate Studies (DGS), on behalf of the program; we verify that this is the final, approved version of the student's dissertation including all changes required by the advisory committee. The undersigned agree to abide by the statements above.

Nidhi Tibrewal, Student

Dr. Jürgen Rohr, Major Professor

Dr. Jim Pauly, Director of Graduate Studies

INVESTIGATING KEY POST-PKS ENZYMES FROM GILVOCARCIN BIOSYNTHETIC PATHWAY

DISSERTATION

A dissertation submitted in partial fulfillment of the requirement

for the degree of Doctor of Philosophy in the College of Pharmacy

at the University of Kentucky

By

Nidhi Tibrewal

Lexington, KY

Director: Dr. Jürgen Rohr

Professor of Pharmaceutical Sciences

Lexington, Kentucky

2013

ABSTRACT OF DISSERTATION

INVESTIGATING KEY POST-PKS ENZYMES FROM GILVOCARCIN BIOSYNTHETIC PATHWAY

Gilvocarcin V (GV) belongs to the angucycline class of antibiotics that possesses remarkable anticancer and antibacterial activities with low toxicity. Gilvocarcin exhibits its light induced anticancer activity by mediating crosslinking between DNA and histone H3. When photo-activated by near-UV light, the C8 vinyl group forms a [2+2] cycloadduct with thymine residues of double stranded DNA. D-fucofuranose is considered essential for histone H3 interactions. However, the poor water solubility has rendered it difficult to develop gilvocarcin as a drug. We aim to design novel gilvocarcin analogues with improved pharmaceutical properties through chemo-enzymatic synthesis and mutasynthesis. Previous studies have characterized many biosynthetic genes encoding the gilvocarcin biosynthetic skeleton. Despite these previous findings the exact functions of many other key genes are yet to be fully understood. Prior gene inactivation and cross-feeding experiments have revealed that the first isolable tetracyclic aromatic product undergoes a series of steps involving C–C bond cleavage followed by two *O*-methylations, a penultimate *C*-glycosylation and final lactone formation in order to fully develop the gilvocarcin structure.

To provide a deeper understanding of these complex biochemical transformations, three specific aims were devised: 1) synthesis of the proposed intermediate and *in vitro* enzyme reactions revealed GilMT and GilM's roles in gilvocaric biosynthesis; 2) utilizing *in vitro* studies the enzyme responsible for the C–C bond cleavage and its substrate were determined; 3) a small series of structural analogues of the intermediate from the gilvocarcin pathway was generated via chemical synthesis and fed to the

mixture of the enzymes, GilMT and GilM. These reaction mixtures were then analyzed to establish the diversity of substrates tolerated by the enzymes.

Keywords: Gilvocarcin, S-adenosylmethionine, *O*-methyltransferase, Baeyer-Villiger monooxygenases.

Nidhi Tibrewal

2013

INVESTIGATING KEY POST-PKS ENZYMES FROM GILVOCARCIN BIOSYNTHETIC PATHWAY

By

Nidhi Tibrewal

Dr. Jürgen Rohr
(Director of Dissertation)

Dr. Jim Pauly
(Director of Graduate Studies)

2013

Dedicated to my Mother

ACKNOWLEDGEMENTS

I would like to extend my sincere thanks to all individuals whose support and guidance made my roller-coaster journey towards completion of my dissertation a success.

It gives me immense pleasure in thanking my mentor Dr. Jürgen Rohr for providing me the chance to work again after dissolution of my previous lab. I am grateful to him for his expert guidance and insightful discussions throughout my graduate studies. I would also like to thank my committee members Dr. Steven Van Lanen, Dr. Kyung-Bo Kim and Dr. Ann Frances Miller for their invaluable advice and timely assistance over the years. I sincerely thank Dr. Sean Parkin for agreeing to serve as an outside examiner for my dissertation defense.

Special thanks to all the past and present members of Dr. Rohr's lab for their support and ideas; Dr. Guojun Wang, Theresa Downey, Jhong-Min Chen, Stevie Weidenbach, Dr. Madan Kharel, Dr. Pallab Pahari, Dr. Khaled Shaaban, and Dr. Micah Shepherd.

I would like to express my heartiest gratitude to all my friends for their unconditional love and support. Things would have been challenging without them.

Above all, I need to thank my parents, particularly my mother. Times were tough after she passed away but the belief and courage her face reflected always kept me going strong during these difficult times. I love her so much and I wish she was here with me. I

am really grateful to my sisters, Manisha and Swati and my little brother, Saahil, for their love and encouragement. Finally, I would like to express my deepest gratitude to the love of my life, my husband, Arpit Gattani, whose support and love have made the journey worthwhile so far.

TABLE OF CONTENTS

LIST OF TABLES

LIST OF FIGURES

LIST OF SCHEMES

LIST OF ABBREVIATIONS

ACP	acyl carrier protein
APCI	atmospheric pressure chemical ionization
AT	acyl transferase
BLAST	basic local alignment search tool
BVMOs	Baeyer-Villiger monooxygenases
bp	base pairs
CoA	coenzyme A
COSY	correlation spectroscopy
CYC	Cyclase
CYP450	cytochrome P-450 monooxygenases
DEBS	6-deoxyerythronolide B synthase
DH	dehydratase
DNA	deoxyribonucleic acid
DMSO	dimethylsulfoxide
E. coli	*Escherichia coli*
EI-HRMS	Electron impact high resolution mass spectrometry
ER	Enoyl reductase

ESI	electrospray ionization
FAD	flavin adenine dinucleotide
G-1-P	glucose-1-phosphate
GT	glycosyltransferse
GM	Gilvocarcin M
GV	gilvocarcin V
HMBC	heteronuclear multiple bond coherence
HPLC	high performance liquid chromatography
HSQC	heteronuclear single quantum coherence
IPTG	isopropyl-β-D-thiogalactoside
KS	ketoacyl synthase
KR	keto reductase
LB	lysogeny broth
MCAT	malonyl CoA acyl carrier protein transacylase
MT	methyltransferase
MW	molecular weight
NAD^+	nicotinamide adenine dinucleotide, oxidized form
NADPH	nicotinamide adenine dinucleotide phosphate, reduced form
NMR	nuclear magnetic resonance
NOESY	nuclear overhauser effect spectroscopy

ORF	open reading frame
PCP	peptidyl carrier protein
PCR	polymerase chain reaction
PKS	polyketide synthase
R_f	TLC retention time
SAR	structure activity relationship
SAM	*S*-adenosyl methionine
TE	thioesterase
TLC	thin layer chromatograpy
UV	ultraviolet radiation

Chapter 1. Introduction

Survival, instinct, and competitiveness are the key that frames these diverse chemical entities known as natural products within the organisms. Natural products have been the source of the majority of FDA-approved agents and continue to inspire researchers in the field of drug discovery. The serendipitous discovery of pencillin by Alexender Fleming in 1928 and its development for use as a medicine in 1941 by Howard Walter Florey, together with Ernst Chain constitute a major breakthrough in medical history.

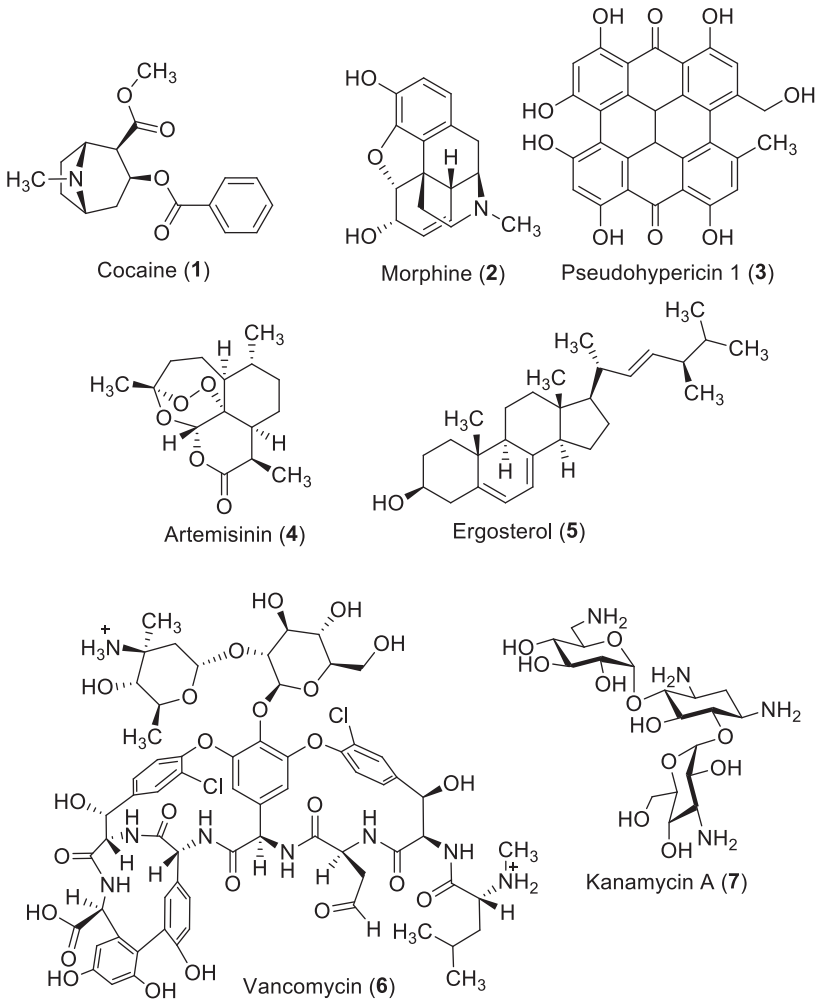

Figure 0.1 Natural Products

We broadly classify NPs into six categories based on their building blocks and biosynthetic routes: alkaloids (**1** and **2**), fatty acids and polyketides (**3**), terpenoids and steroids (**4** and **5**), nonribosomal peptides (**6**), and specialized carbohydrates (**7**) (Figure 1.1).(*1*)

1.1. Polyketides

Polyketides are complex small molecules that come from a variety of biological sources, mostly from microbes. Microorganisms, plants and insects make a wealth of these natural products to serve as pigments, virulence factors, or as defence weapons. Polyketides represent one of the major classes of natural products that exhibit a remarkable range of structural and functional diversity. Polyketides are known to possess a vast array of pharmaceutical functions such as antibiotic, immunosuppressant, antiparasitic, cholesterol-lowering, and antitumor properties. Others are infamous toxins or virulence factors.(*2*) Commercially important polyketides include antibiotics (oxytetracycline, erythromycin, monensin), anticancer agents (doxorubicin, mithramycin), immunosuppressants (FK506), antifungals (amphotericin B), and cholesterol-lowering (lovastatin) agents (Figure 1.2).(*1*)

Because of the high pharmaceutical significance of polyketides there have been constant efforts to synthesize their complex scaffolds. Synthetic chemistry has long been used to generate structural analogues of natural product drug candidates with improved pharmacological properties. Although total synthesis of natural products offers a promising opportunity to provide pharmacologically improved molecules frequently it becomes challenging to scale due to the structural complexity of these molecules. An alternative to this approach is mutasynthesis (or chemo-enzymatic synthesis), which utilizes synthetic chemistry to construct analogues of the intermediates in the pathway, leaving the remaining, more difficult, alterations to be accomplished by the enzymrs of the producing organism.(*3, 4*) To be able to construct the bioactive polyketides, a deeper knowledge of their biosynthesis is vital. Better understanding can allow us to become better polyketide engineers enabling us to create new and improved drug therapies.

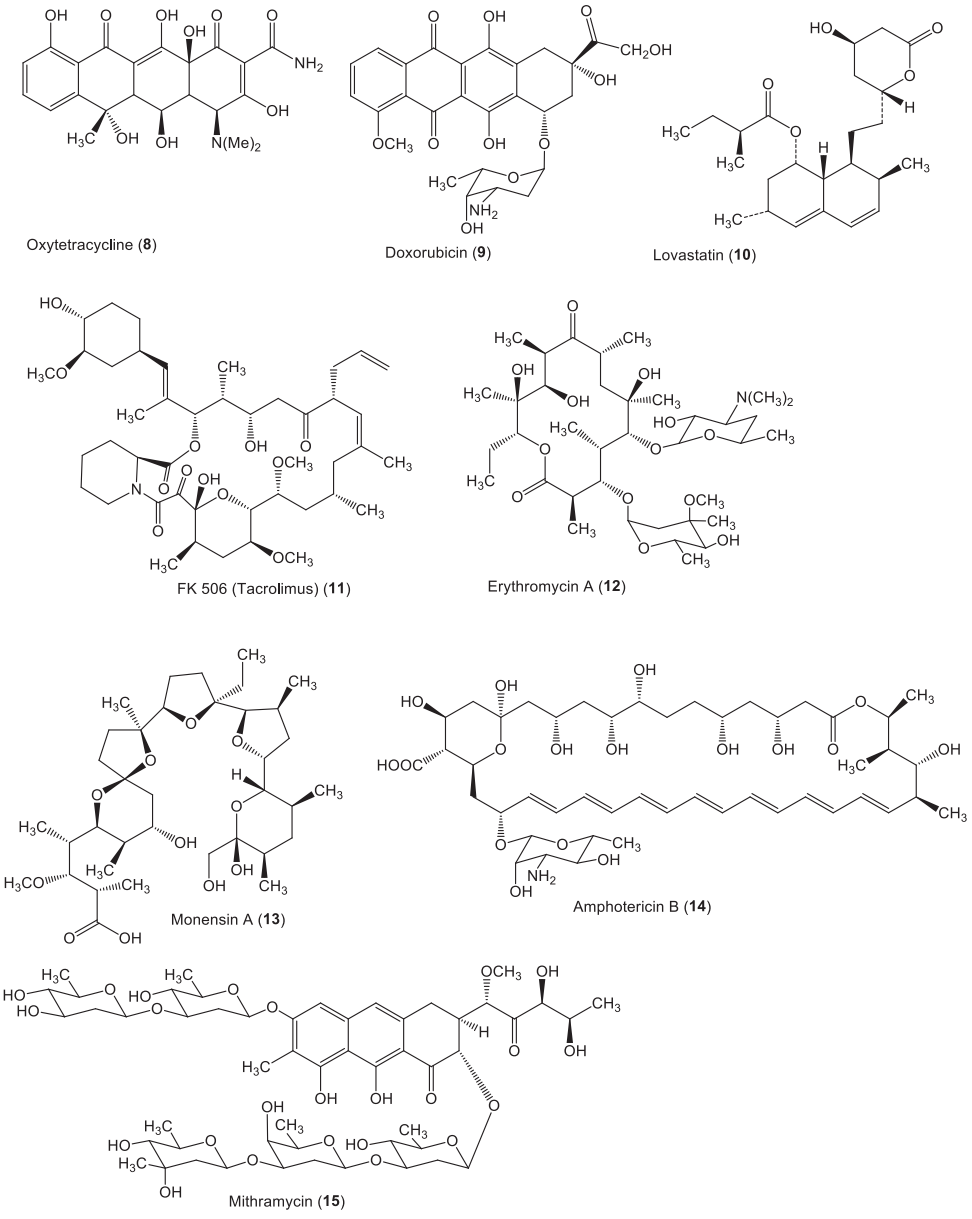

Figure 0.2 Polyketide drugs.

1.2. Polyketide biosynthesis

The most intriguing aspect of structurally complex polyketides is that they are derived from mostly simple building blocks in nature including, acetate and propionate.(5) Polyketide biosyntheses are catalyzed by complexes of mono or multi-functional enzymes called polyketide synthases (PKSs). The chemistry associated with PKSs is closely related to that of the well-studied fatty acid synthases (FASs). Polyketide

biosynthesis overlaps with fatty acid synthesis not only in terms of mechanistic details involved in chain elongation process but also in that both the utilize common precursors such as acetyl coenzyme A (CoA), malonyl CoA.(*6*) In general, fatty acids and polyketides are biosynthesized through the repititive decarboxylative condensations of activated acyl starter unit with malonyl-CoA derived extender units to generate poly *β*-ketoester intermediates (Scheme 1.1).

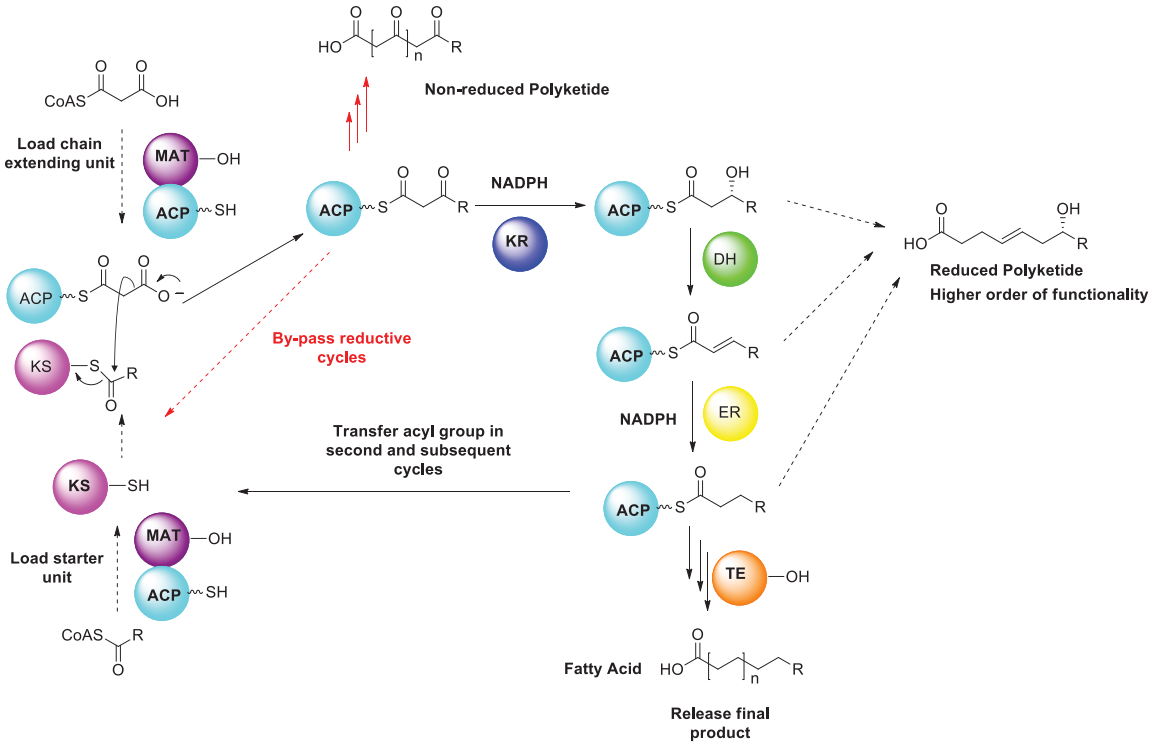

Scheme 0.1 The fatty acid and polyketide biosynthetic cycles. MAT: malonyl-acetyl transferase; ACP: acyl carrier protein; KS: ketosynthase; KR: ketoreductase; DH: dehydratase; ER: enoyl reductase.

FAS is a large multienzyme complex. The biosynthesis of fatty acids takes place two carbons at a time (Scheme 1.1), where the starter unit, derived from acetyl-CoA, is anchored to a ketosynthase (KS) and the extender unit, derived from manolyl-CoA, is tethered to an activated acyl carrier protein (holo-ACP). Release of carbon dioxide from malonic acid renders it nucleophilic enough to attack the KS bound acetyl-CoA resulting in the production of an ACP bound *β*-keto-acyl-thioester thus elongating the chain by two carbon atoms. The *β*-carbonyl generated during FA synthesis is reduced to an alcohol by a ketoreductase (KR), this resulting *β*-hydroxy is then dehydrated by a dehydrogenase

(DH) to give an alkene. Finally, the alkene will be hydrogenated by an enoylreductase (ER) to give a fully saturated fatty acyl ACP. This process of condensation, ketoreduction, dehydration and hydrogenation converts highly oxidized starter molecules to a fully saturated acyl backbone which can then return to the KS as two carbon extended chain and can go through this cycle again and again until a full length chain is obtained. The terminal step in the pathaway is the release of the full-length fatty acid by the enzyme ketoesterase (KE). In comparison to fatty acids, polyketides are more complex. Unlike FASs that only uses malonyl-CoA, PKSs can use a variety of building blocks, can terminate the chain elongation steps at any point in the reduction cycle, and can add modifications at any stage generating much higher level of functionality in a polyketide.

On the basis of their biosynthetic machinery, polyketides are usually categorized as type I-, type II- and type III-PKS derived.(*7*) Type I PKSs consist of large multifunctional enzyme complexes that can be further classified as either modular (for example, macrolides like erythromycin) or iterative (for example, the lovastatin nonaketide synthase).(*8*) Each of these type I modular proteins consists of multiple active domains organized into modules where each module consists of a minimal PKS (composed of KS, AT and ACP) along with optional *β*-keto processing domains (KR, DH, ER). Each catalytic and carrier domain is used only once as the growing chain is passed along the assembly line and is responsible for a single carbon–carbon bond formation followed by programmed reduction/ dehydration cycles. Thus, the number of modules determines the number of cycles catalyzed by a particular type I PKS and corresponds to the number of newly formed C–C bonds. The presence of KR, DH and ER domains depicts the degree of reduction that the *β*-keto group undergoes in each module. Overall, the number and organization of catalytic domains in each module largely reflects upon the chemical structure of the polyketide. The PKS involved in 6-deoxyerythronolide B (**16**) biosynthesis represents the textbook-example of a modular polyketide synthase (Scheme 1.2).

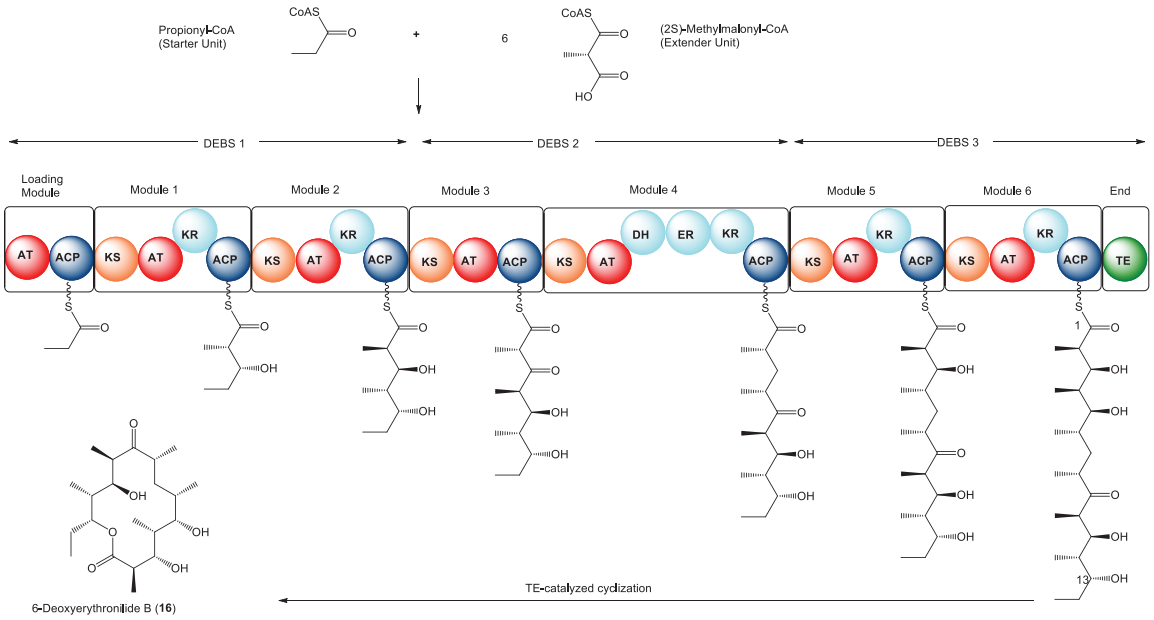

Scheme 0.2 6-deoxyerythronolide B (**16**) biosynthesis.

The cluster is composed of three very large proteins namely DEBS1, DEBS2 and DEBS3 producing a total of six modules in addition to a loading module and a termination enzyme.(*9-11*) The biosynthesis commences with the loading of a starter unit of propionyl-CoA to the holo-ACP domain; this is then passed onto the first module that also picks up a methylmalonyl-CoA. Decarboxylative claisen-condensation between the starter unit and the extender unit results in the formation of ACP-tethered diketide. The KR domain then reduces the *β*-carbonyl and results in the formation of a hydroxyl group at the C3 position. The AT domain catalyzes the transfer of the growing chain to the next module, module 2, that adds two more carbons and passes the chain to module 3. The third module lacks any reductive domain leaving the *β*-carbonyl intact after the addition of two carbons and passes the growing chain to the next module, module 4. The process continues through the remainder of the modules where the chain elongates until the designated chain length is achieved. In the final step the fully-grown chain reaches the terminal domain that has thioesterase (TE) activity. The TE catalyzes an intramolecular lactone formation while simultaneously releasing the fully-grown PKS product. The nucleophilic hydroxyl group at C13 position attacks the carbonyl carbon of the thioester facilitating the formation of 6-erythronolide B (**16**).

Apart from typical bacterial modular type I PKSs, there are other type I PKSs found in fungi characterized by an iteratively acting multidomain enzyme. These iterative type PKSs are mysterious in that it still remains unclear how a single multifunctional enzyme makes choices about the degree of reduction at each chain extending condensation. The iterative type I PKSs are typically found in the biosynthesis of fungal polyketides such as 6-methylsalicylic acid, lovastatin and aflatoxin. Lovastatin biosynthesis involves two type I PKSs, one being a noniterative PKS responsible for the formation of 2-methylbutyrate side chain and the other an iterative type I PKS (LovB) that specifies the formation of the main nonaketide-derived skeleton.(*12*) The KR, DH, and ER domains are optionally used in every round of chain elongation (Scheme 1.3).

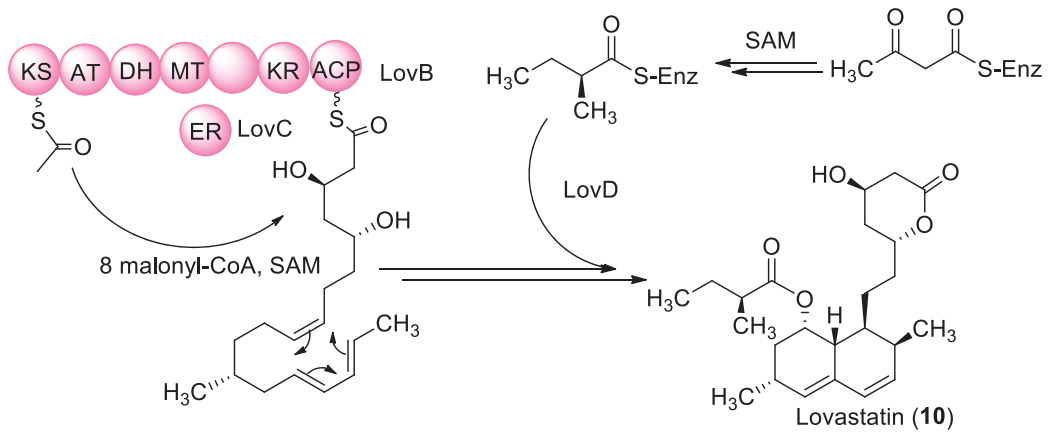

Scheme 0.3 Lovastatin biosynthesis.

Aromatic polyketides such as actinorhodin (**18**), landomycin A (**17**), kinamycin F (**20**), gilvocarcin V (**19**), and jadomycin A (**21**); are assembled by iteratively operating type II PKSs (Figure 1.3). Unlike type I PKSs, these multienzyme complexes iteratively use a ketosynthase heterodimer (KS_α and KS_β) that catalyzes condensation of a growing poly-*β*-keto ester chain with malonyl-CoA units. Ketoacyl synthases [KS_α and KS_β, also called chain length factor, CLF] and the ACP together constitute the minimal PKS (Scheme 1.4).(*13*) The major hallmark difference between type I and type II PKSs is that the latter does not include *β*-keto reduction cycles. Thus, at the end of chain enlongation the type I minimal PKS produces a highly reactive poly *β*-keto ester intermediate. Apart from the minimal PKS enzyme complex other tailoring enzymes such as ketoreductases

(KRs), cyclases (CYCs), and aromatases (AROs) are required to determine the folding, cyclization, and aromatization pattern of the polyketide chain. Type II PKSs are found in prokaryotes (*5*) and, with the exception of a few other Gram-negative bacteria, are found exclusively in the soil borne bacteria actinomycetes. (*14, 15*) The complete gene cluster for the biosynthesis of actinorhodin (**18**) was first cloned in 1984 followed by complete *Streptomyces coelicolor* genome sequencing in 1992.(*16, 17*) The starter unit incorporated in the biosynthesis is either acetyl-CoA or propionyl-CoA, and seven molecules of malonyl-CoA are used as the extender units. (Scheme 1.4).(*16*).

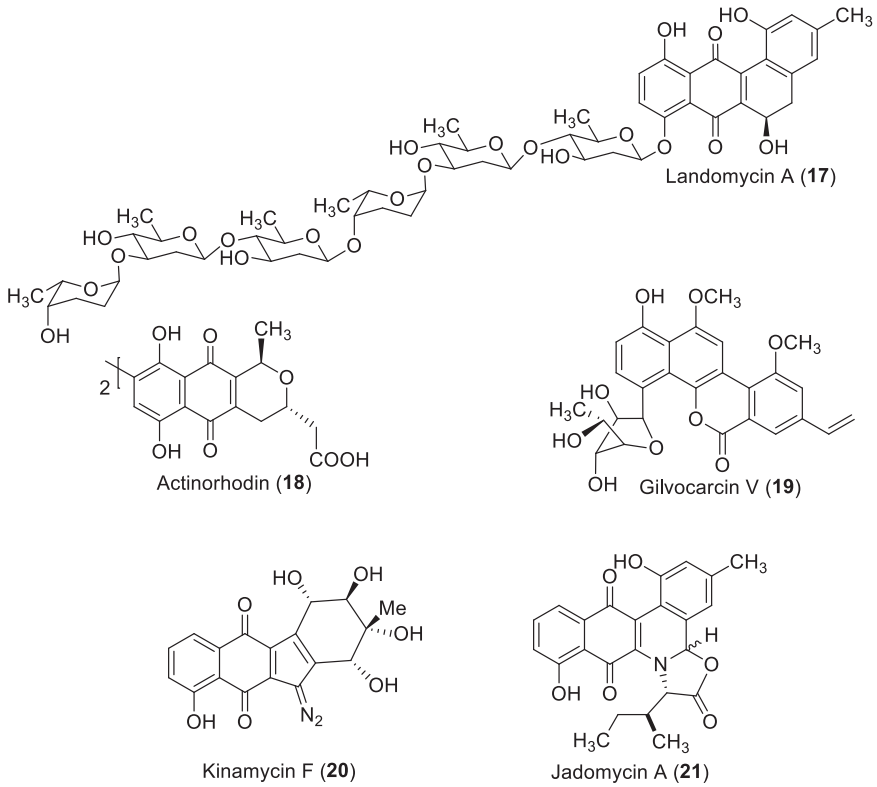

Figure 0.3 Some examples of type II PKS derived antibiotics.

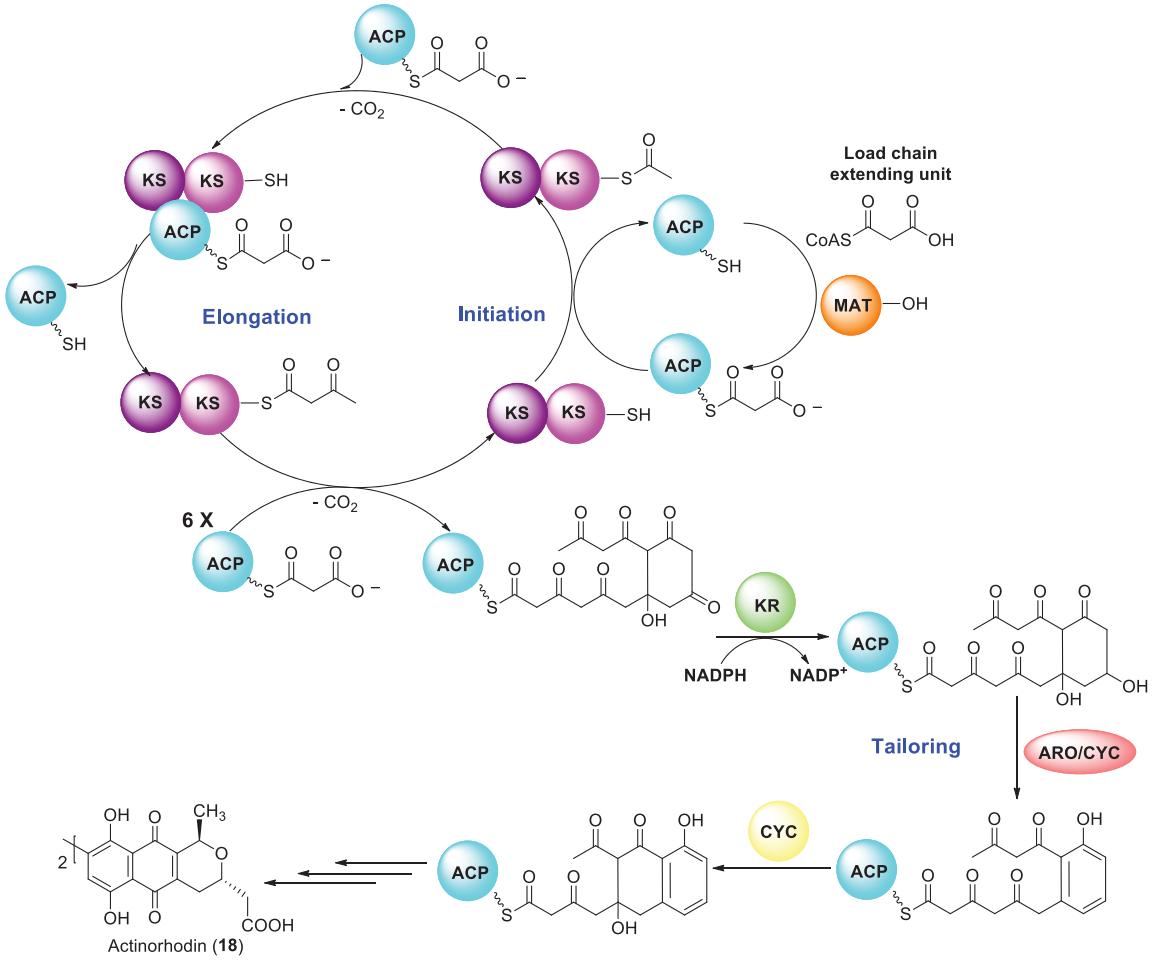

Scheme 0.4 Polyketide chain formation/elongation by type II PKSs.

The type III iterative PKSs are relatively small dimeric proteins that do not require an ACP with its phosphopantetheinyl arm on which the growing polyketide chains are tethered, and instead utilize acyl-CoA substrates directly.(*5*) Type III PKSs are most commonly found in plants. These enzymes are responsible for the synthesis of compounds such as stilbenes and chalcones and are more commonly known as stilbene/chalcone synthases (SHS or CHS). The first bacterial type III PKS, RppA, was reportedly from *Streptomyces griseus*, and catalyzes the synthesis of 1,3,6,8-tetrahydroxynaphthalene (THN). RppA utilizes five molecules of malonyl-CoA, which undergo spontaneous oxidation to form flaviolin (**22**) (Scheme 1.5).(*18*)

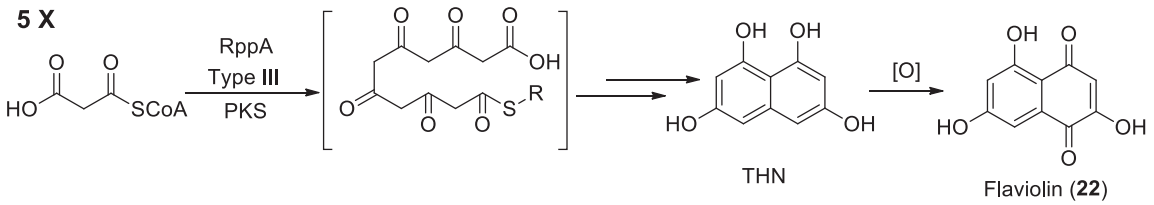

Scheme 0.5 Type III PKS-mediated biosynthesis of Flaviolin (**22**)**.**

In addition to the three broadly classified types of polyketide sythases there are other mixed type polyketide synthases, such as type I-type II, type I-type III, FAS-PKS hybrid and PKS-NRPS-hybrides (NRPS stands for non-ribosomal peptide synthase) as exemplified by lankacidin C, kendomycin, DIF-1, jamaicamide A, respectively.(*5, 19*)

1.3. Post-PKS tailoring enzymes

The fully condensed products of PKS catalyzed reactions usually undergo a series of tailoring events (also known as post-PKS events) such as glycosylation, methylation, oxidation, reduction, prenylation, and halogenation to generate biologically active structurally diverse compounds (Figure 1.4). Such tailorings can tremendously alter the pharmacological properties of the parent polyketides, impacting facors such as solubility or receptor binding ability of the modified parent compound. These post-PKS events usually result in the conversion of a biologically non-active polyketide into an active product. The conversion of inactive 6-deoxyerythronolide B (**16**), to potent antibacterial agent, Erythromycin A (**12**) well illustrates the effect of such tailoring events.(*20*) These post-PKS tailoring reactions provide a unique handle to decorate the initial natural product frame by means of combinatorial biosynthesis or precursor-directed biosynthesis. Tailoring enzymes such as oxidoreductases, group transferases, halogenases, cyclases, and deoxysugar biosynthetic enzymes have been extensively used to generate modified polyketides, occassionally with improved pharmacological properties.(*21*) Some commonly occuring post-PKS tailoring reactions are briefly discussed in the following section.

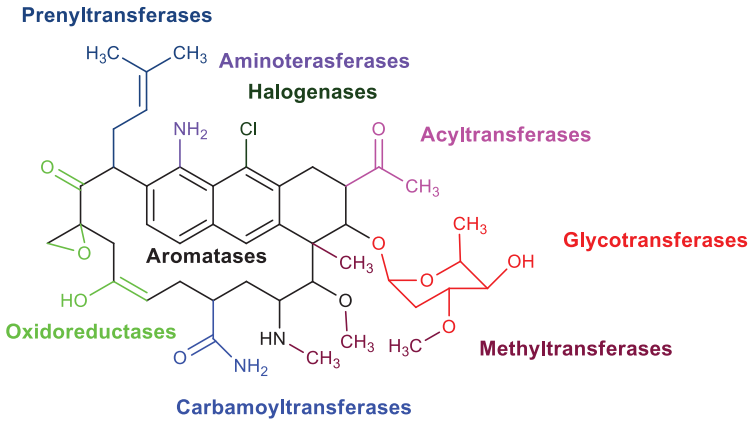

Figure 0.4 Post-PKS tailoring steps.Adapted from Olano et al.(*21*)

Oxygenases

The products of PKSs often go through multiple oxidative steps that introduce structural diversity to these molecules. The oxygenases modify the framework through the introduction of oxygen-containing functionalities, such as hydroxy, epoxide, aldehyde and keto groups, and through oxidative C–C bond cleavages, oxidative ring closing. Such oxidative events provide handles for other post-PKS modifications such as *O*-methylation and *O*-glycosylation. Common oxygenases known to play a role in natural product biosyntheses are cytochrome P-450 monooxygenases (CYP450s), flavin-dependent monooxygenases, dioxygenases, and co-factor free anthrone oxygenases. (*22, 23*) Oxygenases directly catalyze the addition of oxygen from molecular oxygen to the substrate. Depending on the number of oxygen atoms introduced into the substrate, they can be further classified as monooxygenases (uses one O-atom from an O_2-molecule) (Scheme 1.6) and dioxygenases (adds both O-atoms of an O_2-molecule). Most of the monooxygenases utilize NADH, NADPH or ascorbic acid as reducing equivalents to reduce the second oxygen molecule to water. The most studied examples of these monooxygenases are cyctochrome P-450 monooxygenases (CYP450s).(*23*)

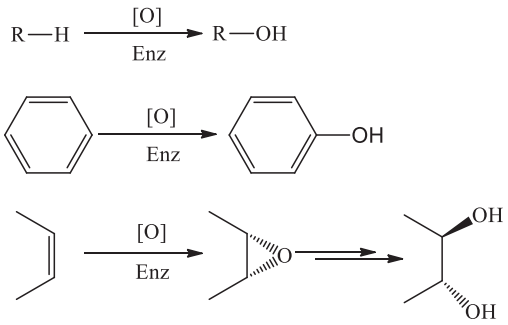

Scheme 0.6 Monooxygenases.

CPY450s belong to a very large and diverse family of proteins containing heme as a cofactor and, hence, are hemeproteins. CYP450s play a critical role in the primary and secondary metabolic pathways as well as in drug detoxification pathways. Most CYPs pair up with a multi-component electron transfer system that constitutes of a protein partner to supply one or more electrons for iron reduction. However, some CYPs can be one-component, i.e., they do not require any external reducing partner. In the presence of molecular oxygen, the cofactor NAD(P)H, and an electron transfer system the CYPs catalyze a diverse array of regio and sterospecific reactions including the epoxidation of C–C double bonds and aliphatic/ aromatic hydroxylations. CYP450 catalyzed reactions are commonly observed in post-PKS modifications. The understanding of CYP450 function is essential for the efficient engineering of *Streptomyces* strains capable of generating novel antibiotics. For example, the improved biosynthesis of pladienolide D from recombinant *Streptomyces platensis* will be discussed. *Streptomyces platensis* produces pladienolide B (**23**) and only minor amounts of its 16-hydroxylated derivative pladienolide D (**24**) that posseses strong anti-cancer activity. The pladienolide B 16-hydroxylase PsmA from *Streptomyces bungoensis* A-1544 was overexpressed in a recombinant *Streptomyces platensis* strain enhancing the production of pladienolide D (**24**) to a level comparable to that of pladienolide B (**23**).(*24*) Approaches that utilize substrate promiscuity of CYP450s have also been applied to generate novel analogues of erythromycin and pikromycin.(*25-27*)

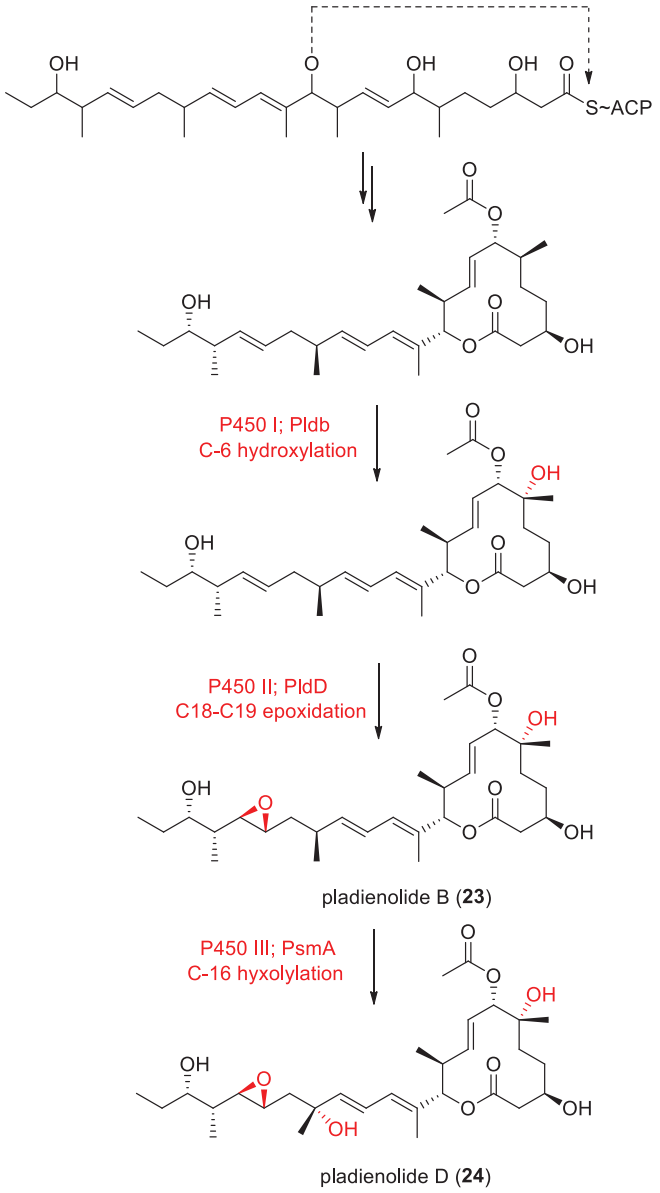

Scheme 0.7 Biosynthesis of the polyketide macrolide pladienolide D (**24**) in recombinant *Streptomyces platensis*: CYP450 mediated hydroxylations and epoxidation.

Another class of monooxygenases that have gained researchers' attention is that of the Baeyer-Villiger monooxygenase (BVMO). The flavin-dependent Baeyer-Villiger monooxygenases involved in secondary metabolite biosynthetic pathways catalyze C–C bond cleavage through the insertion of an oxygen atom in cyclic ketone to form a lactone. Examples of this activity are seen in the BVMOs MtmOIV in the mithramycin biosynthetic pathway and CmmOIV in the chromomycin biosynthetic pathway.(*28, 29*)

MTM biosynthesis proceeds through the polyketide derived tetracyclic premithramycinone, which undergoes glycosylation and methylation at the 9-position to give premithramycin B (**25**). A Baeyer-Villiger reaction catalyzed by MtmOIV then oxidatively cleaves the C-C bond in the the fourth ring generating the tricyclic aglycone core and highly functionalized pentyl side chain at the 3-position, mithramycin DK, the penultimate intermediate of the mithramycin biosynthetic pathway (Scheme 1.8).(*28, 30*) Mechanistically, two electrons and two protons are transferred from NADPH to FAD generating $FADH_2$ transiently. The reduced flavin immediately reacts with an atmospheric oxygen molecule to generate a reactive peroxyflavin. Nucleophilic attack of the peroxyflavin on the ketone carbon generates a tetrahedral intermediate also know as a Criegee intermediate. A subsequent concerted step involves the migration of one of the adjacent carbons to the oxygen thereby generating a lactone (Scheme 1.9).

Apart from cofactor-dependent monooxygenases, there are some monooxygenases that do not require any cofactor and/or a transition metal ion to activate molecular oxygen. Quinone forming monooxygenases compose a unique group of cofactor-free monooxygenases that catalyzes the oxidation of naphthacenone- and anthrone- type precursors of type II polyketides to form the corresponding quinone derivatives. For example, tetracenomycin F1 monooxygenase (TcmH) from the biosynthetic pathway of the antitumor antibiotic tetracenomycin C. (**33**) TcmH catalyzes the oxidation of the naphthacenone tetracenomycin F1 at position C-5 to the 5,12-naphthacenequinone tetracenomycin D3 (**29**) (Scheme 1.10). TcmH does not require any cofactor for catalysis and uses its substrate as the reducing equivalent for the reduction of one oxygen atom of molecular oxygen to water.(*31*) Other cofactor free anthrone oxygenases include ActVA-orf6 from *Streptomyces coelicolor* A3 (*32*) and ElmH from *Streptomyces olivaceus*.(*33*)

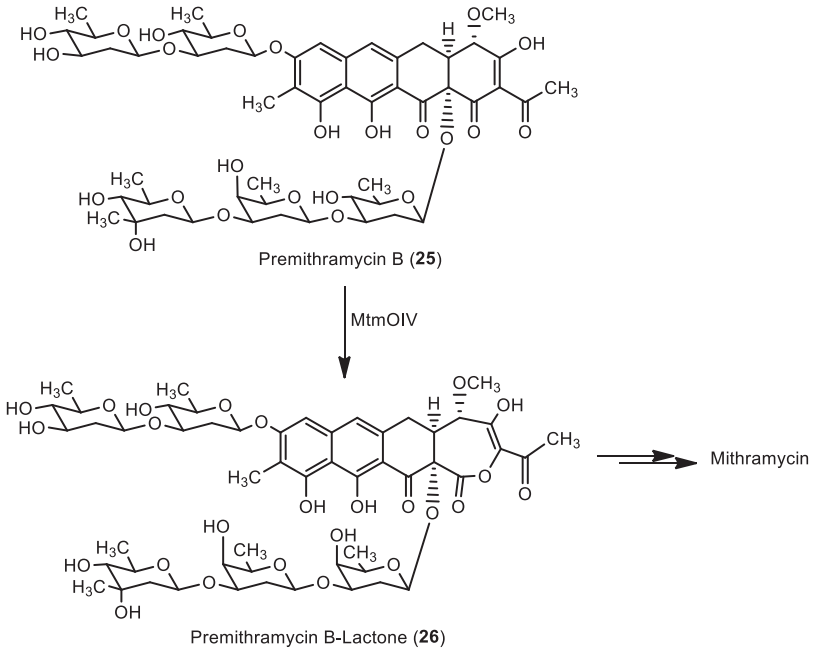

Scheme 0.8 MtmOIV-catalyzed Baeyer-Villiger oxidation of premithramycin B.

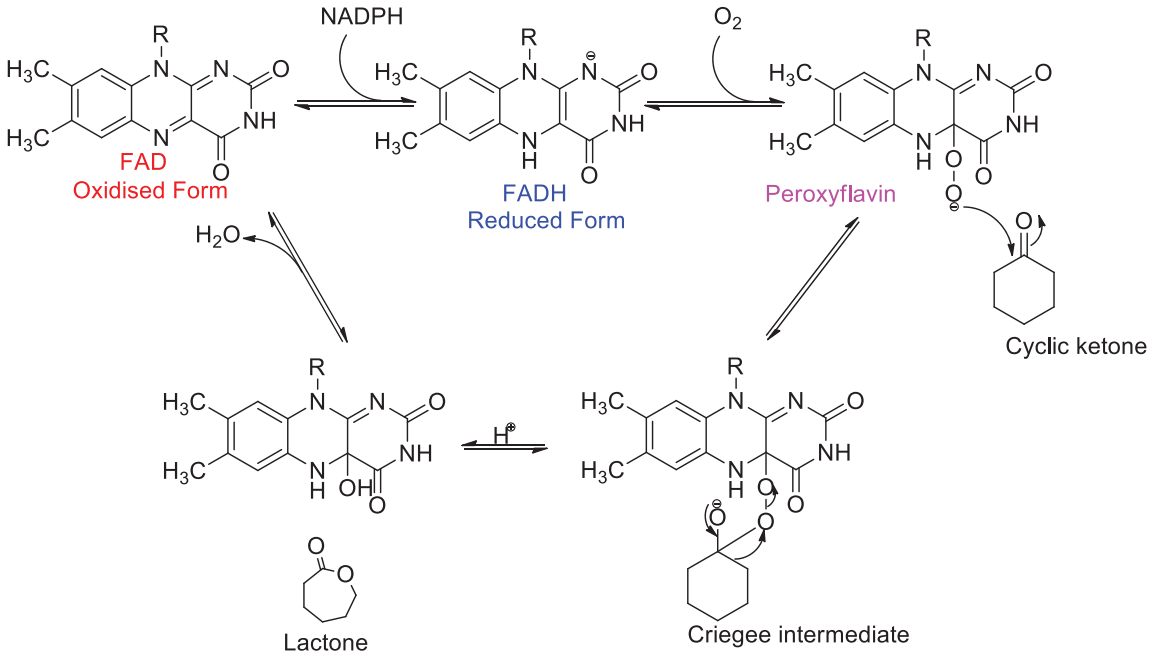

Scheme 0.9 Mechanism of BVMO catalysis.

Dioxygenases

As the name suggests, a dioxygenase incorporates both oxygen atoms of dioxygen into a substrate resulting in a dioxetane or a peroxide. These often a highly reactive species can rearrange or react further, e.g. into a 1,2-diol. Tetracenomycin A2's oxygenase TcmG from tetracenomycin C's (**33**) biosynthetic pathway catalyzes a triple hydroxylation in the final step to yield tetracenomycin C via a monooxygenase-dioxygenase mechanism (Scheme 1.10).(*34*)

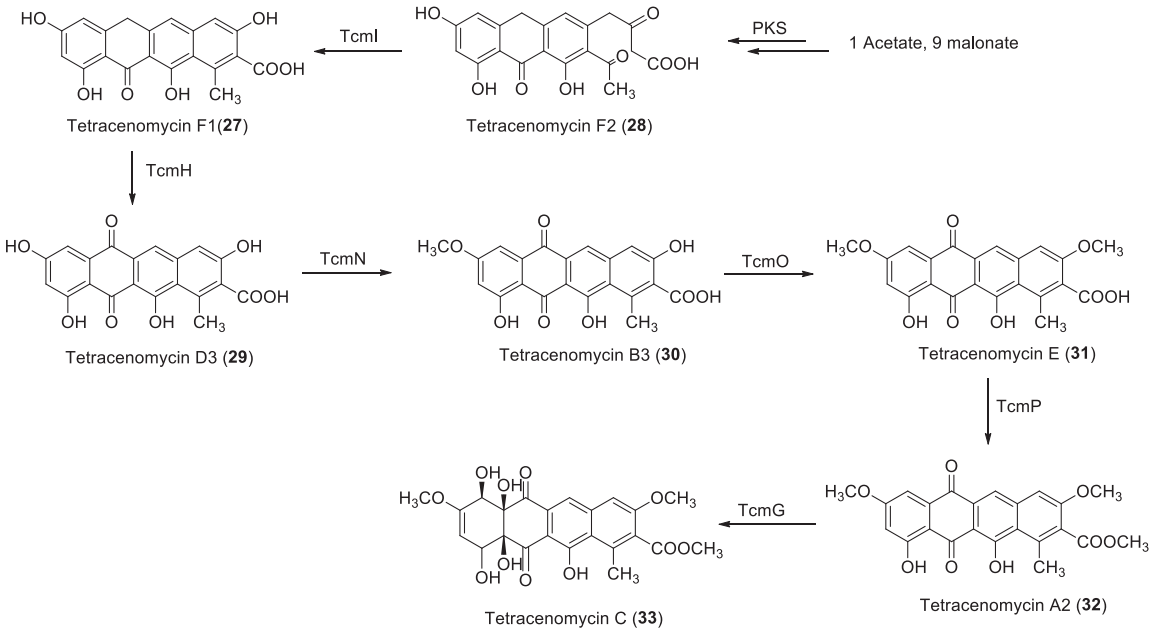

Scheme 0.10 Post-PKS tailoring steps in the biosynthetic pathway of the antibiotic tetracenomycin C (**33**).

Glycosylation

Glycosylation in natural product biosynthesis not only imparts structural diversity but also is important for the biological activity of these compounds. These sugars usually play a critical part in the molecular recognition of a molecules cellular target.(*35*) The classic textbook example includes activation of the inactive aglycon 6-DEB after glycosylation, which introduces two sugar moieties converting it into erythromycin, a potent antibiotic.(*11*) These sugars can be linked to the acceptor substrate as monosaccharides, disaccharides or oligosaccharides through *O*-, *C*-, *S*- or *N*-glycosidic

bonds. *O*-glycosides are by far the most widespread of the group in comparison to their realtively rare *N*-, *S*- and *C*-glycoside counter parts. Glycosylation typically occurs in the later stages of biosynthesis where the sugars are transferred to the corresponding acceptor substrate by an enzyme known as glycosyltransferases (GTs).

Based on the stereochemical outcome, the GTs can be classified as either inverting or retaining (Scheme 1.11).(*36*) Inverting glycosyltransferases mediate nucleophilic attack of the acceptor substrate at the anomeric carbon of the activated sugar, with the simultaneous release of the leaving group in an SN_2 fashion. This results in the inversion of the configuration of the anomeric carbon in the product with respect to the donor substrate. Koshland et al. first proposed the mechanism for the retaining GT in 1953. The retaining glycosyltransferases mediate the formation of a glycosidic bond via a double displacement mechanism that involves a covalently bound glycosyl-enzyme intermediate species (Scheme 1.11, A). An alternative SN_1 mechanism was also proposed where the activating group leaves first resulting in an enzyme-stabilized oxocarbenium ion intermediate species. This species is shielded on one face by the enzyme, thereby preventing back side attack of the incoming nucleophile and leading to complete retention of the anomeric configuration in the product (Scheme 1.11, B).(*36*)

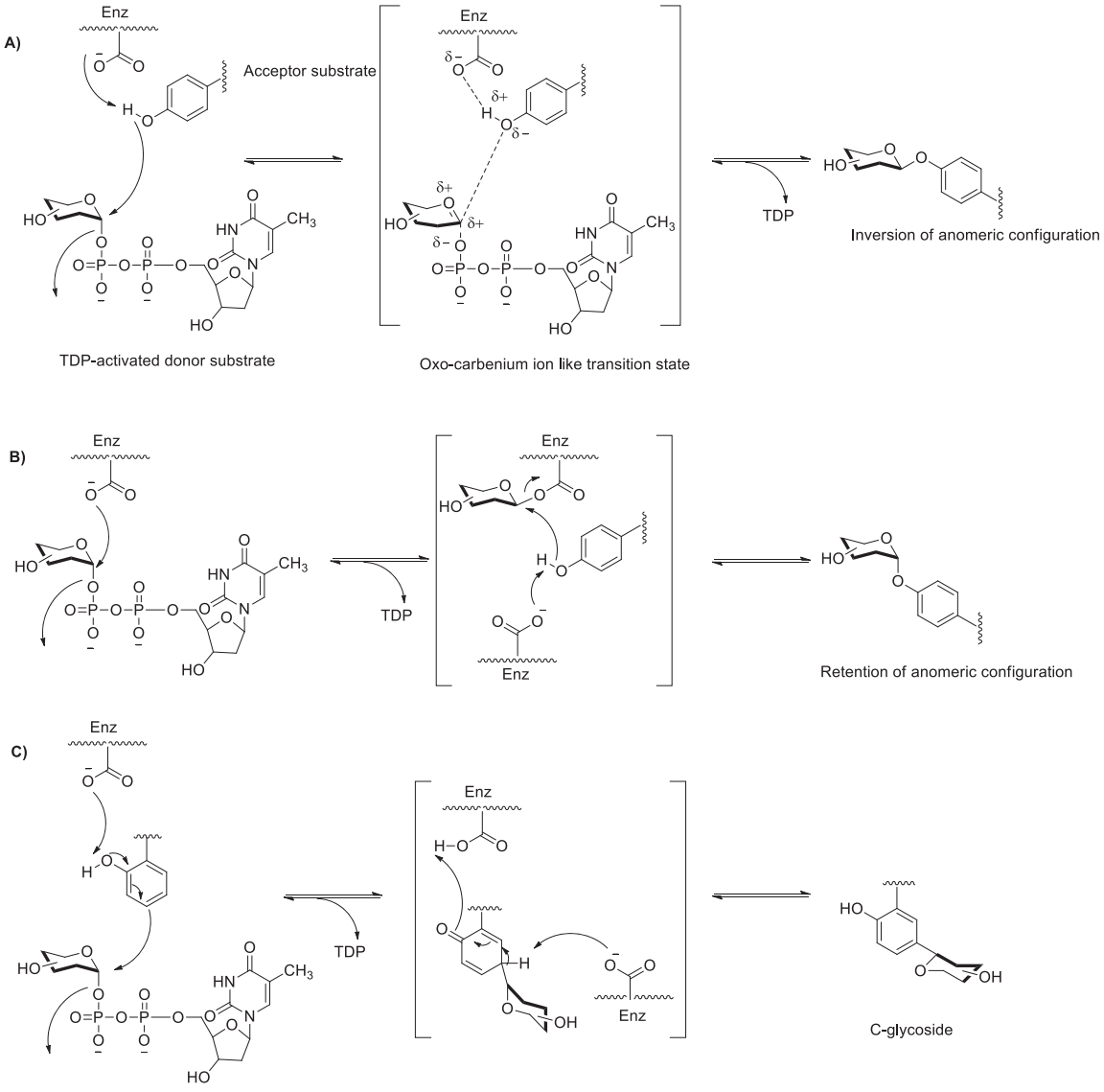

Scheme 0.11 Proposed mechanism for inverting (A) and retaining (B) type *O*-glycosyltransferases as well as *C*-glycoside formation (C).

The *C*-glycosides from microbial secondary metabolites are also interesting as *C*-glycosidic bonds unlike *O*-glycosidic bonds are quite stable. The sugar moiety is attached either at an ortho- or para-position with respect to an electron donating functional groups (e.g. hydroxyl) of the acceptor substrate's aromatic moiety. Such electron rich groups increase the electron density at these positions, and hence make it possible to attack the anomeric center of the activated sugar as in the case of urdamycin A and gilvocarcin

V.(*37, 38*) The exact mechanisms for *C*- or *N*-glycosylations are still obscure, however a hypothetical mechanism has been proposed (Scheme 1.11, C).

Methylation

Another common PKS modification occurring in the biosynthesis of a variety of natural products is methylation, catalyzed by enzymes referred to as methyltransferases. Most of the methyltransferases use the reactive methyl group bound to sulfur in S-adenosyl methionine (SAM) as the methyl donor. In a typical methylation reaction this methyl group is transferred to the acceptor substrate. The biosynthesis of the antitumor drug mithramycin by *Streptomyces argillaceus* presents an interesting example of both *O*- and *C*- methylations catalyzed by MtmMI and MtmMII respectively.(*39*)

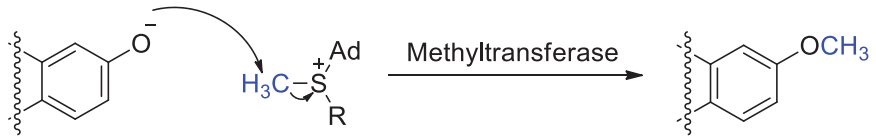

Scheme 0.12 Methyltransferase catalyzed reaction.

Once again, the biosynthesis of tetracenomycin C (**33**) provides an excellent example, since it requires three methylation steps, which are catalyzed by three different SAM-dependent methyltransferases TcmN, TcmO and TcmP (Scheme 1.10).(*40, 41*) TcmN is an interesting bifunctional enzyme whose *N*-ternimal functions as a cyclase and its *C*-terminal contains 3-*O*-MT activity that converts tetracenomycin D3 (**29**) into tetracenomycin B3 (**30**). In the next step, the 8-*O*-methyltransferase, TcmO converts Tetracenomycin B3 into tetracenomycin E (**31**), which in turn is converted into tetracenomycin A2 (**32**) by the C-9 carboxymethyltransferase, TcmP.

Another example is the biosynthesis of macrolide antibiotic, tylosin. While TylM and TylC3 catalyze an *N*-methylation and a *C*-methylation, respectively, during the biosynthesis on the NDP-sugars,(*42, 43*) TylE and TylF catalyze a double *O*-methylation in the final two steps of the tylosin biosynthesis.(*44*) Other well studied examples of *O*-methylations are seen in the biosynthesis of daunorubicin,(*45, 46*) and erythromycin.(*11*)

Mutasynthesis

The above described biosynthetic enzymes incorporate small and simple precursors into the complex natural products by catalyzing the reactions in chemoselective and stereoselective manner. Many efforts to mimic this highly evolved biosynthetic machinery have been made to synthesize clinically relevant complex natural products and their analogues in abiotic chemical environment. Chemical synthesis of large and highly functionalized molecules is a difficult task. Another approach that has been successfully employed to generate such complex natural products is mutasynthesis.(*3, 47*) Mutasynthesis is a technique that couples the power of chemical synthesis with metabolic engineering. In mutasynthesis, synthetic chemistry is used to construct analogues of biosynthetic intermediates. The intermediates are then fed to the mutant strains (that lack enzymes for an early key step/multiple biosynthetic steps) of producing organism, thereby forcing the cellular uptake of surrogate substrates and their incorporation into the natural product derivatives.

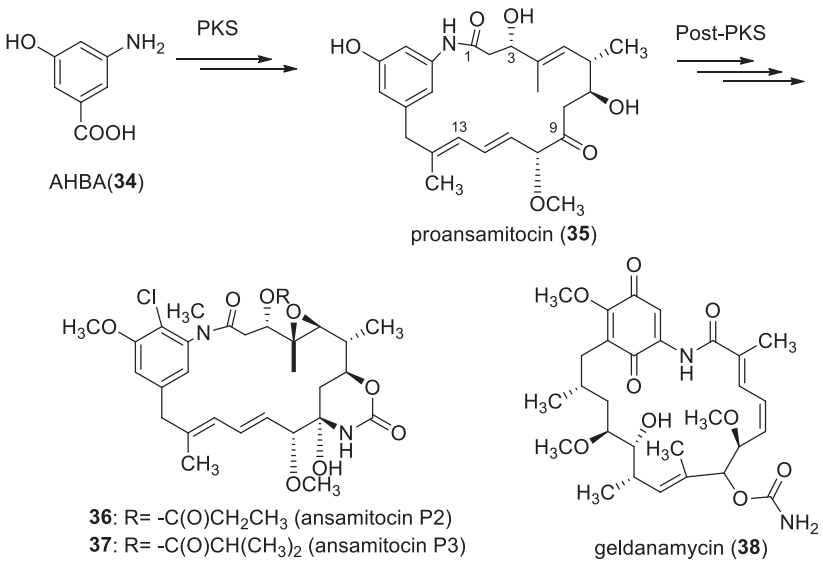

Scheme 0.13 Biosyntheses of ansamitocins.

One of the recent examples of mutasynthesis is the production of ansamitocin derivatives for structure-activity relationship study. The ansamitocins show high potency against the growth of different leukaemia cell lines as well as human solid tumors. Structurally similar ansamitocin and geldanamycin have related polyketide biosyntheses

with a common starter unit, aminohydroxybenzoic acid (AHBA, **34**). Andreas Kirschning and his group selected two early stage mutant strains that are blocked in the formation of AHBA (*Actinosynnema pretiosum* HGF073 for ansamitocins and *Streptomyces hygroscopicus var. geldanus* K390-61-1 for geldanamycin). A third late stage *A. pretiosum* mutant was also used. This mutant blocked in the post-PKS modifications (chlorination and carbamoylation) mostly accumulated proansamitocin (**35**) along with small amounts of 10-epi-proansamitocin. Proansamitocin was then derivatized to generate the analogues. Feeding of the proansamitocin derivatives along with proansamitocin and epi-proansamitocin to the (–)-AHBA blocked mutant of *S. hygroscopicus* successfully produced new carbamoylated metabolites. With semisynthetic approach, a few carbanalogues were also produced. All the derivatives were tested for their antiproliferative activity in mouse fibroblast cells and human tumor cell lines. The structure-activity relationship study revealed that the stereochemistry at C-9 is important for the activity, whereas the carbamate nitrogen is not crucial for the cytotoxicity (Figure 1.5).

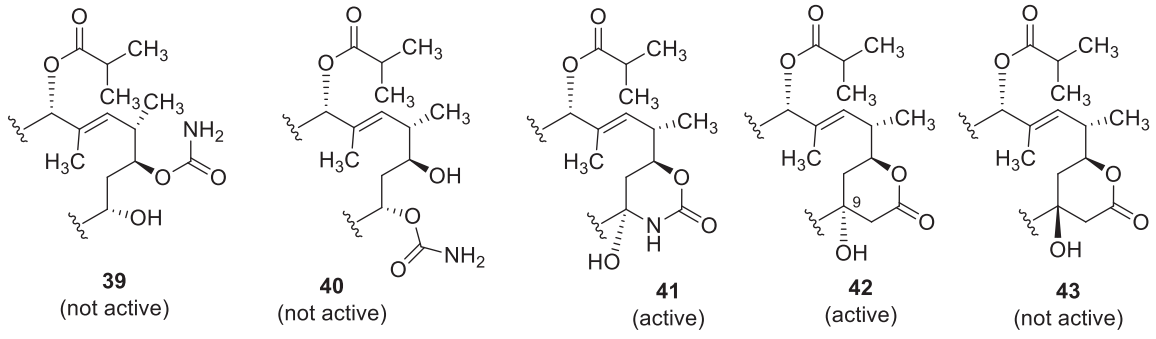

Figure 0.5 Antiproliferative activity of the selected ansamitocin derivatives synthesized via mutasynthesis-semisynthesis route.

Another example of mutasynthesis is diverization of the uridyl peptide antibiotic pacidamycin. The introduction of *prnA*, a gene encoding for halogenase activity from pyrrolnitrin biosynthesis, into *Streptomyces coeruleorubidus* resulted in the chlorinated pacidamycin. The installed chlorine provided a handle for funtionalization of the natural product via cross-coupling Suzuki reaction (Scheme 1.14).

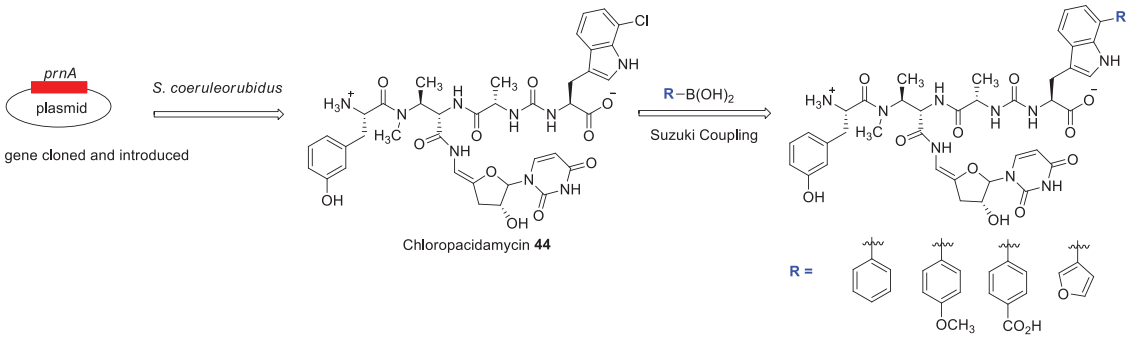

Scheme 0.14 Gene expression enabling synthetic diversification of placidamycin.

Antibiotic Gilvocarcin V

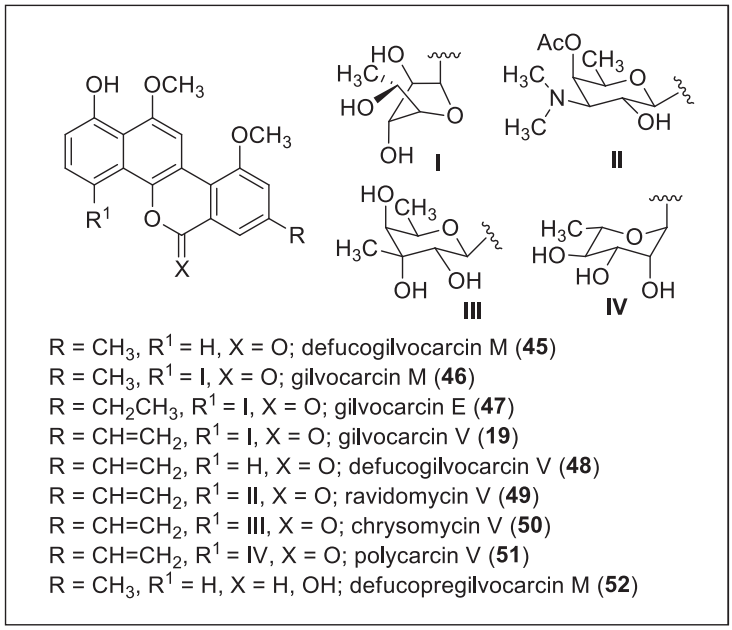

Figure 0.6 Representative members of the gilvocarcin group of natural products.

Gilvocarcin V (GV, **19**) also known as toromycin, is decorated with a *C*-glycosidically linked sugar moiety. It is the most important representative of the benzo[*d*]naptho[1,2-*b*]pyran-6-one antibiotics possessing significant antitumor activity. (*48, 49*) Chrysomycin V (**50**), ravidomycin V (**49**) and polycarcin V (**51**) (Figure 1.6) represent other members of the family that contain the same aromatic core attached to various sugar moieties. Nakano et al. first isolated GV in 1981 from *Streptomyces*

gilvotanareus.(*50-52*). GV exhibits high potency against tumor cell lines while maintaining a low *in vivo* toxicity. Addition, GV serves as an antiviral and antibacterial agent.(*49, 53, 54*) Elespuru and Gonda identified light exposure of the gilvocarcins in the presence of DNA as a significant requirement for potency in cell culture.(*55*) In 1987, McGee and coworkers reported that gilvocarcin V intercalates into DNA in the dark and undergoes covalent adduct formation with DNA only in the presence of the light.(*56*) A detailed mechanistic study later revealed that when photo-activated GV mediates a [2+2] cycloaddition reaction of the C-8-vinyl side chain with DNA thymine residues and additionally causes cross-linking to histone H3.(*57-60*) For the latter, the *C*-glycosidically-linked sugar moiety of the gilvocarcins appears to be crucial. GV photo activation at ~ 400 nm offers selective treatment of cancer, particularly lung cancer and colon cancer. Additionally, GV has the potential to treat brain cancer or cancer anywhere else that solid tumors can be reached through light capillaries.(*61-63*)

In spite of being rich in various biological activities, predominantly anticancer and antibacterial, gilvocarcin V has not been developed into a clinically applied drug mainly due to low water solubility. Additionally, structural complexity of GV makes total synthetic approaches to the development of analogues very challenging and expensive. A deeper understanding of how the organism generates such scaffolds is necessary to develop GV analogues with improved activity through mutasynthesis and combinatorial biosynthesis.

The GV producer, *Streptomyces griseoflavus* also produces two other minor congeners, gilvocarcin M (GM, **46**) and gilvocarcin E (GE, **47**). All three compounds (gilvocarcin V, M and E) have an identical tetracyclic aromatic moiety linked to D-fucofuranose through C-4 glycosidic linkage, but GM and GE have a methyl group and ethyl group respectively at the C-8 position instead of the vinyl group of GV. Gilvocarcins M and E are far less photoactive compared to GV confirming the importance of the vinyl side chain for antitumor activity.(*57*)

1.4. Biosynthetic Highlights of Gilvocarcin V

Initial feeding experiments with various ^{13}C labeled acetate and propionate precursors showed that the unique gilvocarcin backbone originates from acetate and propionate via the polyketide route and the pathway involves a series of oxidative events along with a C-C bond cleavage and O-methylations. (*64-66*) Gilvocarcins E and V incorporate propionate as starter unit resulting in a C-8 ethyl or vinyl side chain while gilvocarcin M incorporates acetate (Scheme 1.15).

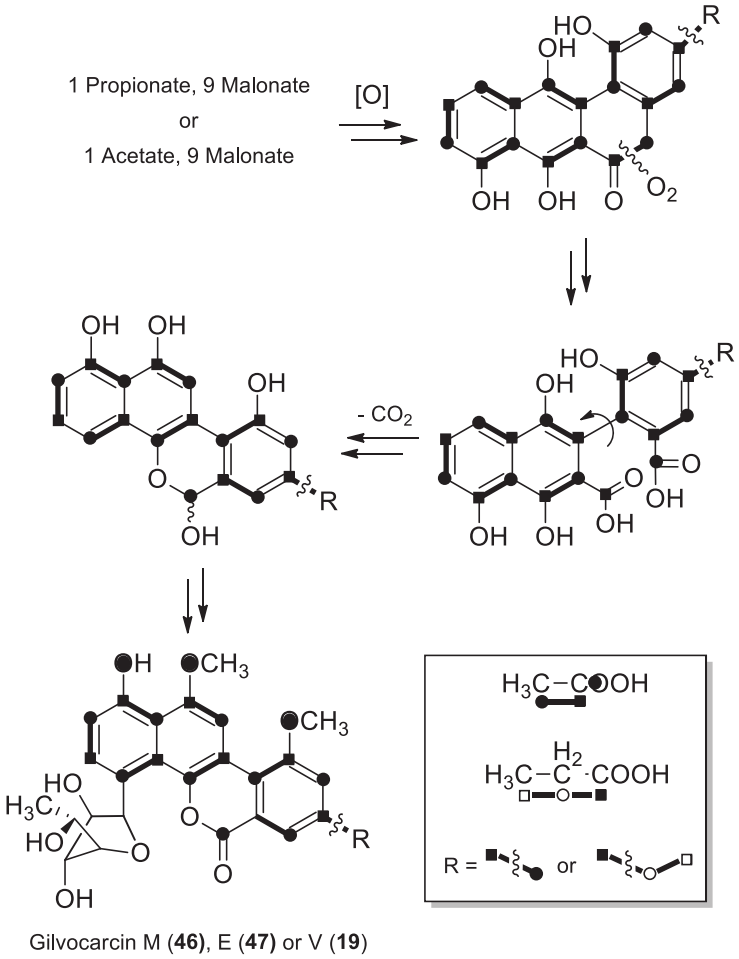

Scheme 0.15 Labeling pattern and hypothetical oxidative rearrangements.

In 2003, Rohr et al. isolated the gilvocarcin gene cluster on a single cosmid, cosG9B3, from *S. griseoflavus* Gö3592.(*67*) The heterologous reconstitution of the GV pathway, accomplished by expressing cosG9B3 in *S. lividans* TK24, confirmed the presence of the complete gilvocarcin biosynthetic locus (*gil*). Sequencing and

bioinformatics analysis revealed the presence of the expected type II PKS genes (*gilABCFKPQ*) in black (Figure 1.7), four putative oxygenases (encoded by *gilOI*, *OII*, *OIII*, *OIV*) in red, a *C*-glycosyltransferase (encoded by *gilGT*) in green, a methyltransferase gene (*gilMT*) in blue, an oxidoraductase gene (*gilR*) in pink, deoxysugar biosynthetic genes (*gilE, D* and *U*) in green, and several other genes with unknown function such as *gilNLVM* along with putative repressor and resistance genes (Figure 1.7).

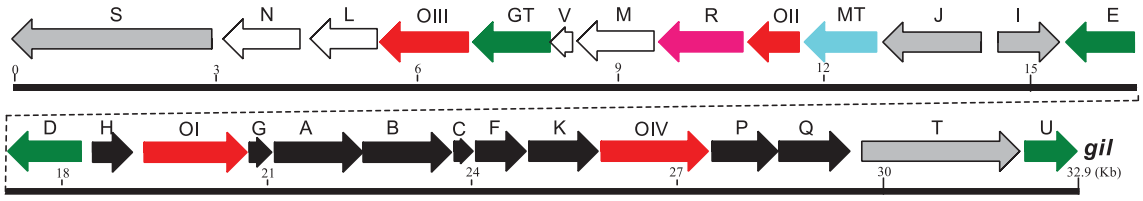

Figure 0.7 GV biosynthetic gene cluster.

After the isolation of the complete gene cluster initial studies involving the inactivation of the pathway oxygenases in cosG9B3 were conducted to determine the mode and sequence of the oxidative events involved in the generation of the gilvocarcin chromophore. The oxygenases were inactivated and the resulting mutant cosmids were heterologously expressed in *S. lividans* TK24. An observed accumulation of mostly gilvocarcin E (**47**) from Δ*gilOIII* mutant clearly disregarded gilOIII as being involved in C–C bond cleavage. However, absence of GV indirectly established the role of *gilOIII* in the formation of the vinyl side chain.(*38*) The culture broths of Δ*gilOI* or Δ*gilOI*Δ*gilOII*Δ*gilOIV* mutants accumulated homo-prejadomycin (**55-56**) while homo-rabelomycin (**72**) was identified as major metabolite from ΔGilOIV or GilOIVΔGilOII mutants(Scheme 1.13).(*68, 69*) Similarly dehydro-homo-rabelomycin (**74**) was isolated from a ΔGilOII mutant. None of the metabolites produced by single or sequential inactivations of *gilOI*, *gilOII* and/or *gilOIV* were the products of an oxidative rearrangement leading to the hypothesis that all three oxygenases were required for the C5–C6 bond cleavage. High sequence homologies between oxygenases from the similar gilvocarcin and jadomycin pathways indicated that both jadomycin A (**21**) and GV (**19**) biosynthetic pathways share a common oxidative route. The hypothesis was further

supported by the accumulation of similar metabolites when oxygenases (encoded by *jadF, jadG and jadH*) from the jadomycin pathway were inactivated (Scheme 1.17).(*70, 71*) More interestingly, cross complementation of the ΔGilOI and ΔGilOIV mutant strains with JadH and JadF, respectively, restored the production of gilvocarcin. However, Δ*gilOII*/*jadG* complementation did not restore GV production.(*69*) Despite the extensive studies, the enzymatic events and actual substrate for C–C bond cleavage remained obscure.

Rohr et al. inactivated several other genes as a means of delineating the gilvocarcin biosythtic pathway. The ΔGilR mutant accumulated pregilvocarcin V (**66**), a hemiacetal,(*72*) indirectly proving that gilvocarcin biosynthesis proceeds via an aldehyde-acid intermediate (**59**) as opposed to alternatives in the literature (example, the one shown is scheme 1.15) that suggested diacid intermediates for the GV and related pathways.(*73-75*) Inactivation of GilGT completely abolished the production of GV but accumulated defuco-GV (**48**) clearly indicating that GilGT was involved in the *C*-glycosylation.(*76*) Additionally, inactivation of *gilM* did not accumulate any product suggesting *gilM* to be critical for the pathway, although its exact role is not known. Deletion of a putative methyltransferase, encoded by *gilMT* also did not accumulate any product.

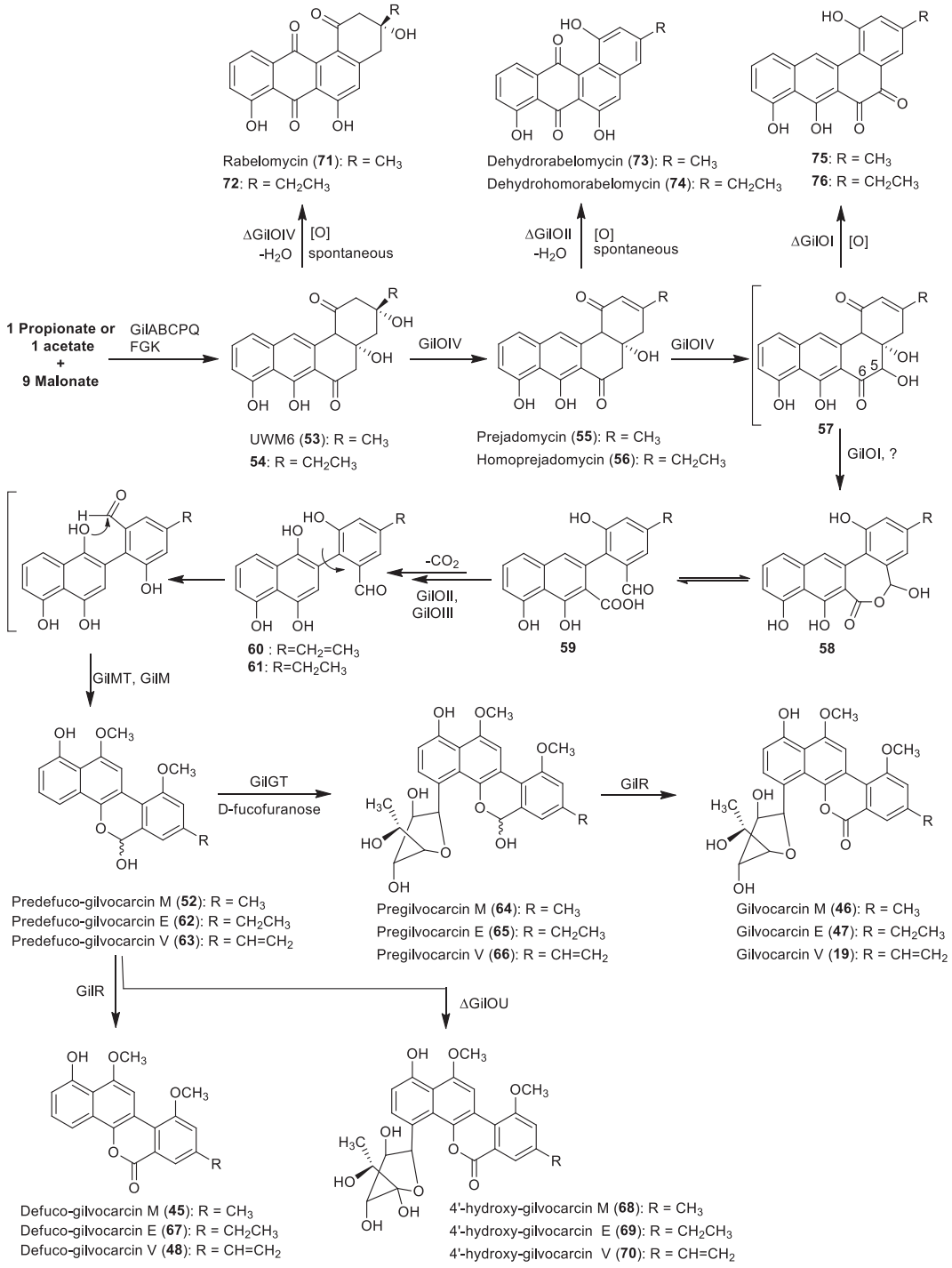

Scheme 0.16 Previously proposed pathway for GV biosynthesis.

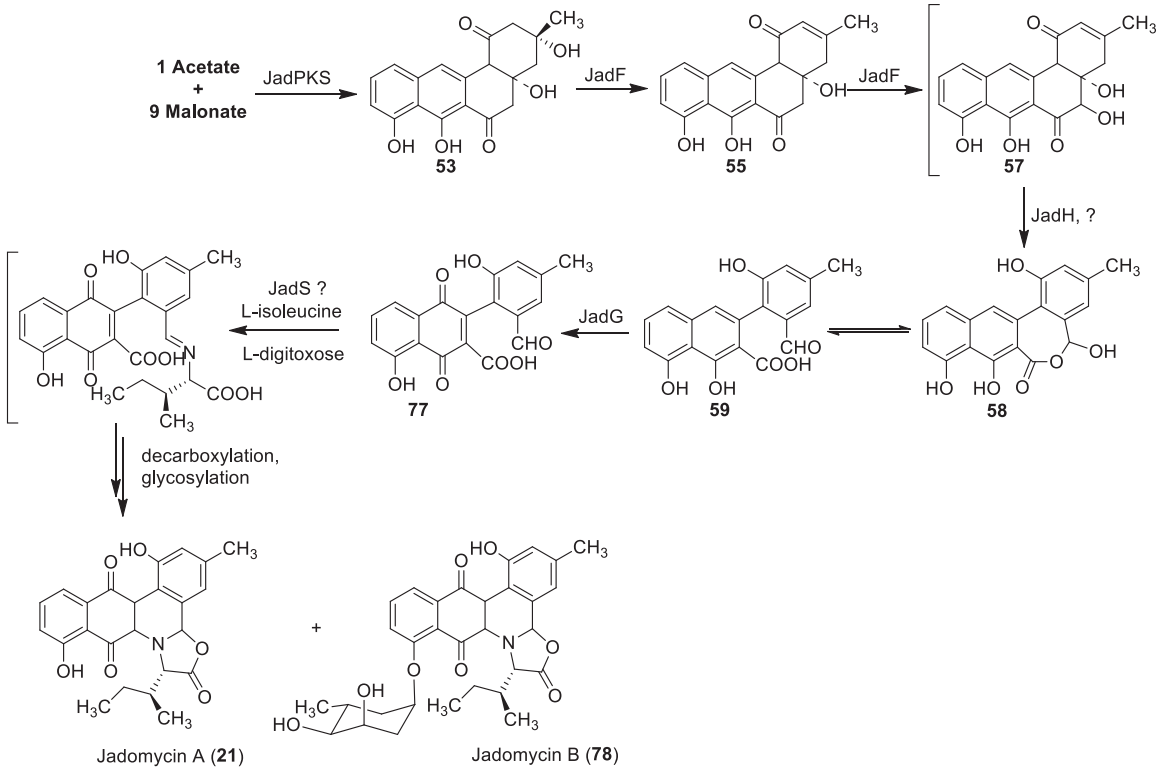

Scheme 0.17 Biosynthetic pathway of jadomycins A and B.

D-fucofuranose is a unique deoxysugar and is rarely found in glycosylated natural products. Inactivation of the putative deoxysugar 4-ketoreductase gene *gilU* resulted in the accumulation of a new GV derivative, 4′-hydroxy-GV (**70**), with an improved biological activity.(*77*) GilU reduces the 4-keto group of **79** (Scheme 1.18) in a stereospecific manner to generate TDP-D-fucose, which further undergoes a yet unknown ring-contraction and glycosylation steps to yield the D-fucofuranose moiety of GV (**81**).

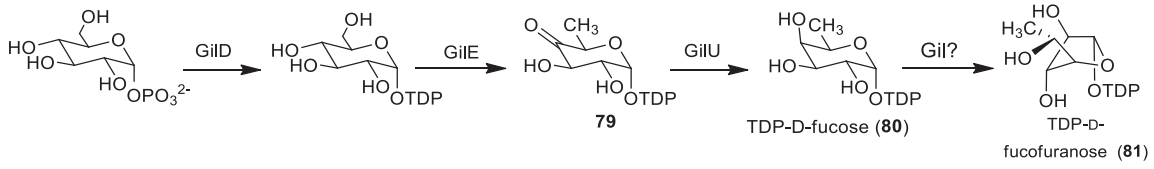

Scheme 0.18 TDP-D-fucofuranose biosynthesis.

Very recently, Rohr and co-workers demonstrated a combinatorial biosynthetic enzymology approach leading to the enzymatic total synthesis of defuco-gilvocarcin M

(**45**), a model compound with the complete gilvocarcin chromophore.(*78*) The total enzymatic synthesis of **45** from acetyl-CoA and malonyl-CoA, with systematic variations of the enzyme mixtures, revealed a simplified hypothetical pathway (Scheme 1.19) confirming that prejadomycin (**55**) and dehydrorabelomycin are intermediates in the GV biosynthesis pathway. Several attempts of crossfeeding studies and *in vitro* enzyme reactions failed to convert UWM6 (**53**) to **45**, confirming that **53**, which was previously considered the first post PKS tetracyclic intermediate, is a shunt product. However, when JadF, the homologue of GilOIV was added to the PKS enzyme mix, **55** was isolated, leading to a new hypothesis that GilOIV may actually act on angucyclic substrates (**82**) that are still bound to the ACP to directly give **55**. A spontaneous hydrolysis and decarboxylation of **82** would then result in **53**. Finally, the study revealed that GilOIV/JadF do not function as oxygenases but catalyze a 2,3-dehydration reaction along with PKS-release and therefore are crucial enzymes that bridge PKS and post-PKS reactions. The *in vitro* enzymatic analysis also showed that GilOI is an anthrone oxygenase responsible for the 12-hydroxylation of **55**.

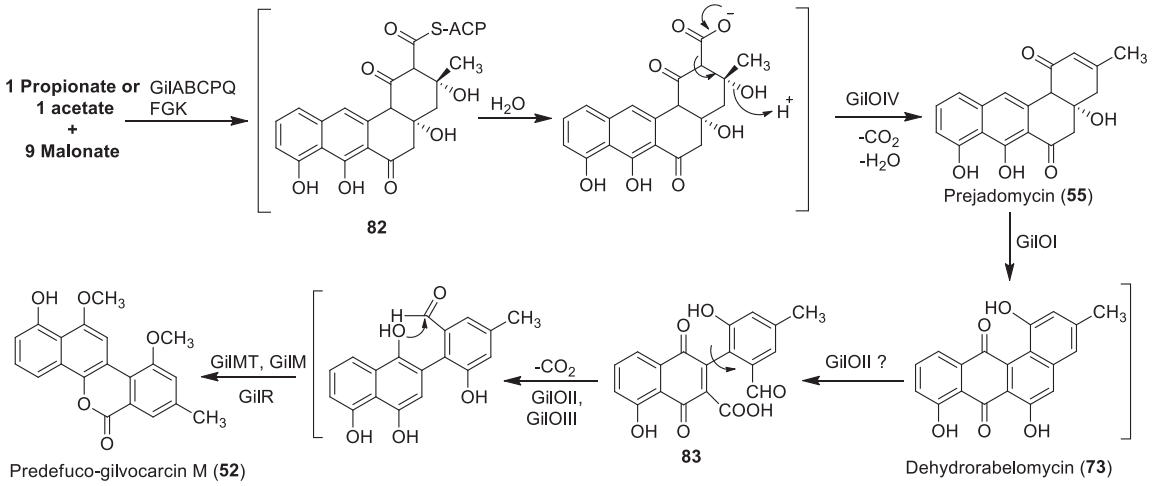

Scheme 0.19 A revised gilvocarcin biosynthetic pathway.

1.5. Summary

Nature creates a multitude of natural products also known as secondary metabolites with a diverse range of activities. Polyketides are complex small molecules that come from a variety of biological sources, mostly from microbes. Polyketides are

known to possess a vast array of pharmaceutical activities. Because of the high pharmaceutical significance, there have been constant efforts to synthesize these complex scaffolds. Total synthesis of natural products remains the most vital tool to provide pharmacologically improved molecules, but it sometimes becomes challenging because of structural complexities within the molecules. An alternative to this approach is mutasynthesis or chemo-enzymatic synthesis, which utilizes synthetic chemistry to construct analogues of the intermediates in the pathway, leaving the remaining, more difficult, alterations to be accomplished by the producing organism or enzymes. To be able to construct the bioactive polyketides, a deeper knowledge of their biosynthesis is vital. Our lab has been investigating gilvocarcin V (**19**) biosynthesis for quite a few years with focus on developing novel analogues either through mutasynthesis or a combinatorial biosynthetic approach for structure activity relationship (SAR) studies. Isolation of complete gene clusters followed by labeling studies, gene inactivation, and cross feeding analyses has helped to identify the functions of the PKS gene products along with some post-PKS enzymes. However, the exact biosynthetic intermediates and sequence of reactions remained elusive. A recent enzymatic total synthesis of defucogilvocarcin M (**45**) provided deeper insights into its biosynthesis and paved the way for further characterization of critical post PKS enzymes.(*78*)

1.6. Specific aims

The objectives of this study were to identify the intermediates in the biosynthetic pathway of GV and to elucidate the functional role of involved post-PKS tailoring enzymes along with their substrate specificities; the prerequisite for a successful chemo-enzymatic approach towards novel GV analogues. To accomplish this goal, the following specific aims were addressed:

Specific aim 1 was to investigate the roles of a putative methyltransferase, GilMT and an unknown enzyme GilM.

Synthesis of the proposed intermediate and *in vitro* enzyme reactions revealed GilMT as an S-adenosylmethionine (Ado-met) dependent *O*-methyltransferase and GilM

as an Ado-met bound reductive methyltransferase that acts on the monomethylated quinone and converts it into defuco-pregilvocarcin. GilM is unique in its functionality as it mediates its reducing capabilities by coupling with GilR, an FAD-dependent oxidoreductase. GilM utilizes reduced flavin produced in the GilR reaction and then regenerates FAD for the next catalytic cycle.

Specific aim 2 was to delineate C–C bond cleavage in gilvocarcin biosynthesis.

Through in vitro studies, the enzyme responsible for the C–C bond cleavage and the exact substrate were revealed. The crucial C–C bond cleavage was attributed to GilOII. The $FADH_2$ dependent GilOII catalyzes sequential three step reactions: the initial 5-hydroxylation and the following Baeyer-Villiger oxidation. Finally, GilOII aided the ring opening completing the oxidative cascade. In the process JadG, a GilOII homologue from jadomycin pathway was also studied. JadG was also shown to catalyze C–C bond cleavage via the same 3-step oxidation.

Specific aim 3 was to explore subsrate specificities for GilM and GilMT.

A small series of structural analogues of the intermediate of the gilvocarcin pathway were generated via chemical synthesis and were fed to the mixture of the post-PKS enzymes. The reaction mixtures were analyzed to establish the diversity of substrates tolerated by the enzymes. Through chemoenzymatic synthesis we proved that the two critical downstream enzymes, GilM and GilMT, are flexible enough to accommodate analogues with small variations.

Chapter 2. Investigating roles of a putative methyltransferase GilMT and an unknown enzyme GilM.

The role of many of the post PKS gene products have been assigned based on gene inactivation, cross-feeding, and labeling studies.(*39, 49, 69, 72, 78-80*) Most of the genes of the three known biosynthetic clusters(*81*) of this group have been assigned to certain enzymatic activities allowing us to predict the biosynthetic steps en route to gilvocarcins (Scheme 1.17). Despite rigorous efforts, most of the post PKS gene functions remained unclear. The major hurdle in completely elucidating the pathway is the lack of isolable substrates.

Among other downstream genes, *gilM* (encoding an enzyme of unknown function) and *gilMT* (encoding a methyltransferase) appear to be crucial for the biosynthesis of gilvocarcin and were proposed to be involved in *O*-methylation reactions. However, the exact functions of their genes products, GilM and GilMT, remained obscure. The mutant strains created by deletion of their corresponding genes did not accumulate any isolable metabolites, and thus provided no clue regarding their potential substrates and thus providing no insight into the structure of key biosynthetic intermediates.

2.1. Design and synthesis of the model substrate

A recent combinatorial biosynthetic approach based on enzymology led to the enzymatic total synthesis of defuco-gilvocarcin M (**45**) from acetyl-CoA and malonyl-CoA, a model compound with the complete gilvocarcin chromophore. Moreover, systematic variations of the enzyme mixtures revealed a greatly simplified hypothetical pathway (Scheme 1.19) suggesting that 2-aryl-5-hydroxy-1,4-naphthoquinone-3-carboxylic acid (**83**) is likely the product of the critical oxidative C–C bond cleavage and thereby a key intermediate of the gilvocarcins. The results also suggested that only three more enzymes, namely GilM, GilMT and GilR, were necessary to finish the biosynthesis of **45**. To confirm this hypothesis and fully enlighten the “biosynthetic black box”, a

potential model substrate, 2-aryl-5-hydroxy-1,4-naphthoquinone (**84**) was synthesized and subsequently used to interrogate the function of GilM and GilMT.

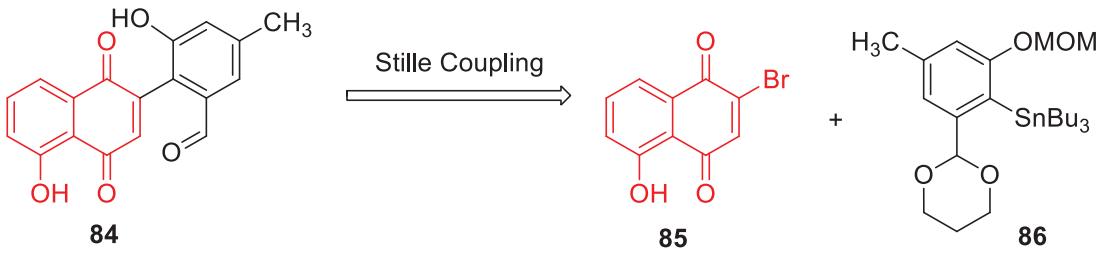

Scheme 2.1 Retrosynthetic analysis of model compound **84**.

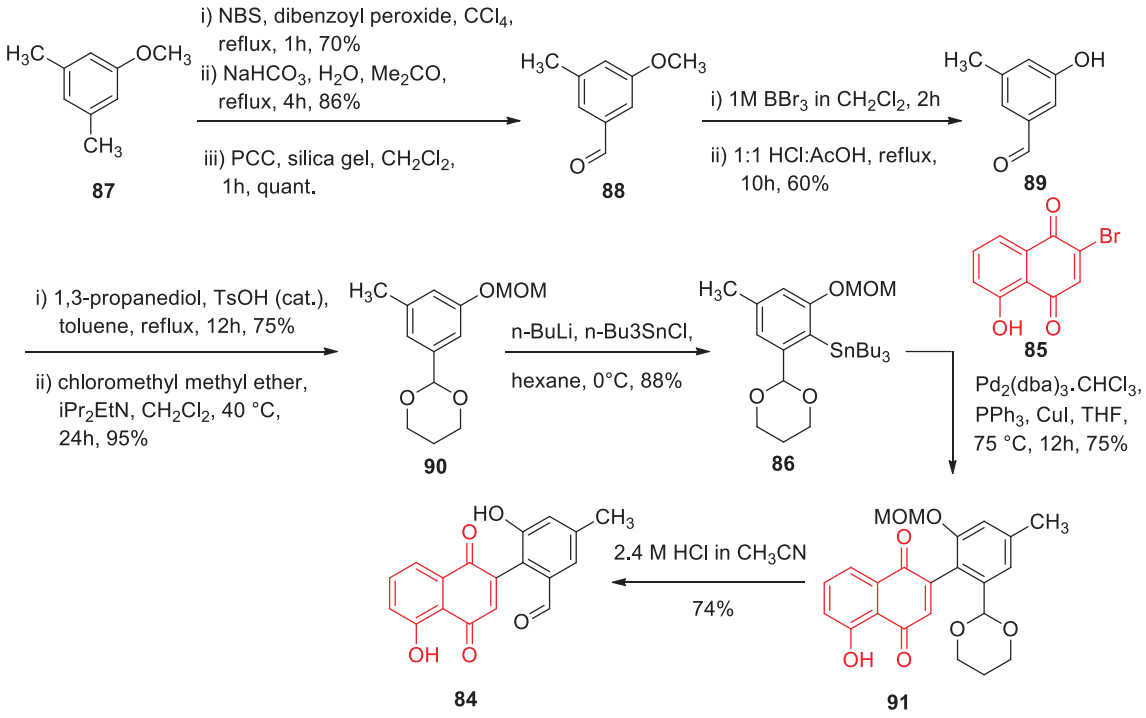

Scheme 0.1 Synthesis of 84**.**

2.2. Results and discussions

The model compound **84** could be prepared by sewing together **85** and **86** via Stille coupling (Scheme 2.1). Synthesis of compound **86** began with commercially

available dimethyl anisole (**87**).(*82*) Bromination with NBS and benzoyl peroxide provided mono bromo benzyl derivative. A sequential hydroxylation followed by oxidation with PCC afforded **88** in 60% yield from **87**.(*82*) Removal of the methoxy group was achieved in 60% yield by treatment with BBr_3 at r.t., followed by acidic hydrolysis. Protection of the aldehyde as a cyclic acetal and the phenolic OH as methoxylmethyl ether provided **90**. An ortho-metalation with tributyltinchloride yielded the required stannane **84** in 88% yield.(*83*) 2-bromonaphthoquinone (**85**) was prepared from juglone using the reported protocol.(*84*) A facile Stille coupling between **85** and **86** provided **91**. **91** was then exposed to harsh acidic conditions (2.4 M HCl in CH_3CN) for 4 min to provide fully unprotected 2-aryl-1,4-naphthaquinone **84** in 74% yield.(*83*)

With a potential substrate in hand, both *gilM* and *gilMT* genes were cloned into pET28a and expressed in *E. coli* to yield soluble proteins that were purified to near homogeneity. Synthetic **84** when incubated with purified GilM produced a complex mixture (Fig. 2.1, trace C). In contrast, HPLC-MS analysis of **84** with GilMT and S-adenosylmethionine (SAM) revealed a decrease in the amount of substrate and formation of a new product (Fig. 2.1, trace E). In the absence of SAM, no product was formed (Fig. 2.1, trace D). The GilMT product was isolated and characterized using NMR and HRMS. The analysis revealed the product as mono-methylated derivative **92**. Nuclear Overhauser enhancement (nOe) studies further confirmed that the hydroxyl group of the phenyl ring of substrate **84** was methylated.

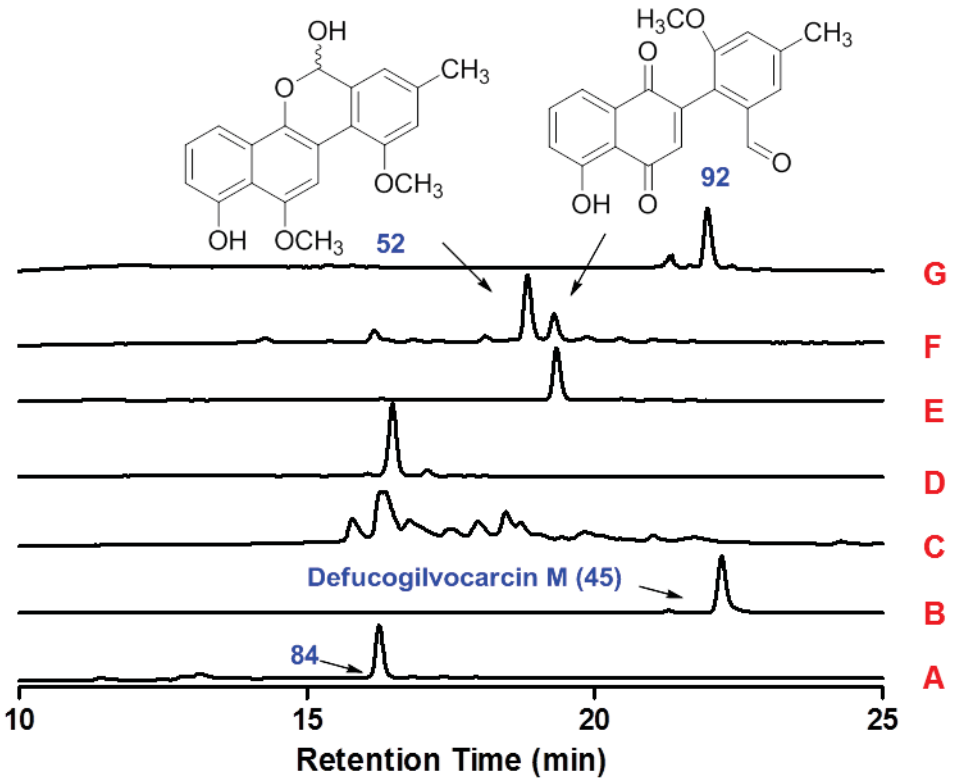

Figure 0.1 HPLC traces of the enzymatic reactions with 2-aryl-1,4-naphthaquinone (**84**): (A) standard 2-aryl-1,4-naphthaquinone (**84**); (B) standard defuco-gilvocarcin M (**7**); (C) **84** + GilM; (D) **84** + GilMT; (E) **84** + GilMT+ SAM; (F) **84** + GilMT + GilM + SAM; (G) **84** + GilMT + GilM + GilR + SAM.

When compound **84** was incubated with both GilM and GilMT along with SAM, a new product along with **92** accumulated (Figure 2.1, trace F). The new compound was identified as defuco-pregilvocarcin M (**52**) by NMR experiments (^{1}H NMR, HSQC). Adding GilR led to the accumulation of defuco-gilvocarcin M (**45**) (Figure 2.1, trace G), further confirming the structure of the GilM/MT product as **52**. In total the results suggested that GilMT is a typical SAM-dependent *O*-methyltransferase, while GilM was responsible for the reduction of the quinone moiety necessary for the observed second *O*-methylation. BLAST analysis (*85, 86*) revealed GilM to have low similarity (34-37% sequence identity) to nucleotidyl-*S*-transferases such as thiopurine-*S*-methyltransferases from *Rhodococcus equi* or *Mycobacterium avium* as well as to benzoquinone methyltransferases from *Mycobacterium tuberculosis* (33% sequence identity). The

translated amino acid sequence of GilM contains VLDLGCGLG as residues 49-57, which appear to be a SAM binding motif (generally hh(D/E)hGXGXG, where h represents a hydrophobic residue). Thus, it remained unclear at this point whether GilMT or GilM catalyzes the second *O*-methylation. To solve this ambiguity, product **92** from the GilMT reaction was used as a substrate for GilM in the presence of SAM. The reaction accumulated **52**, suggesting that GilM not only mediates reduction of the quinone but also catalyzes the second *O*-methylation. Surprisingly, the GilM reaction seemed to convert **92** to **52** even in absence of SAM, which prompted us to further investigate GilM for any bound SAM cofactor.

GilM catalyzes reductive methylation without any external cofactor. However, the BLAST analysis showed a very vague similarity to thiopurine-S-methyltransferases. To analyze any bound cofactor, the enzyme was boiled for 5 minutes and centrifuged (12000 ×g, 5 min). The supernatant was then subjected to LC-MS analysis. A linear gradient of acetonitrile and 0.1% formic acid-water (solvent A = 0.1% formic acid-H_2O; solvent B = acetonitrile; 0-15 min 25% B to 100% B; 16-24 min 100% B; 25-26 min 100% to 25% B; 27-29 min 25% B) with flow rate of 0.5 mL/min was used to separate the compounds in a Waters Symmetry C_{18} (4.6 × 250 mm, 5μm) column. The supernatant showed UV-absorption at 260, typical of an adenosine spectrum, indicated co-purified SAM. To further verify presence of loosely bound S-adenosylmethionine, standard solution of S-adenosylmethionine was prepared in 50 mM phosphate buffer and was used in parallel for comparison. GilM was found to be co-purifying with S-adenosylmethionine (Figure 2.2).

.

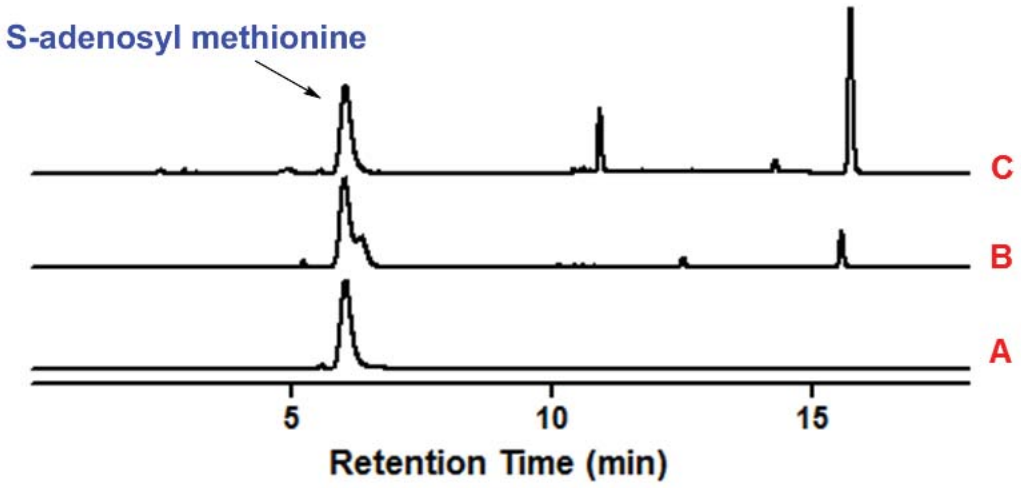

Figure 0.2 HPLC traces of the released cofactor: (A) standard S-adenosylmethionine; (B) Cofactor released from GilM; (C) S-adenosylmethionine boiled for 5 min.

To further analyze the reaction sequence catalyzed by GilM, compound **92** was incubated with GilM and the reaction was studied at different time points (Figure 2.3). With stoichiometric enzyme quantities, the substrate was 80% converted into the product after 15 minutes (Figure 2.3, trace D). When the reaction was analyzed by reversed phase HPLC-MS in 3-5 min intervals, a new peak (**93**) appeared with shorter retention time than the overall product **52** (Figure 2.3). Although NMR analysis of **93** was impossible due to its instability, LC-MS analysis suggested it to be demethyl-defuco-pregilvocarcin M (*m*/*z* 323 $[M-H]^-$). To prove that **93** was an intermediate en route to **52** and not a shunt product, **93** was incubated with GilM, and, as anticipated, was rapidly converted to **52** (Figure 2.3, trace F). Overall, the results showed that GilM catalyzes a sequence of three reactions: (i) quinone reduction, (ii) hemiacetal formation and (iii) *O*-methylation, to construct the tetracyclic core of the gilvocarcins.

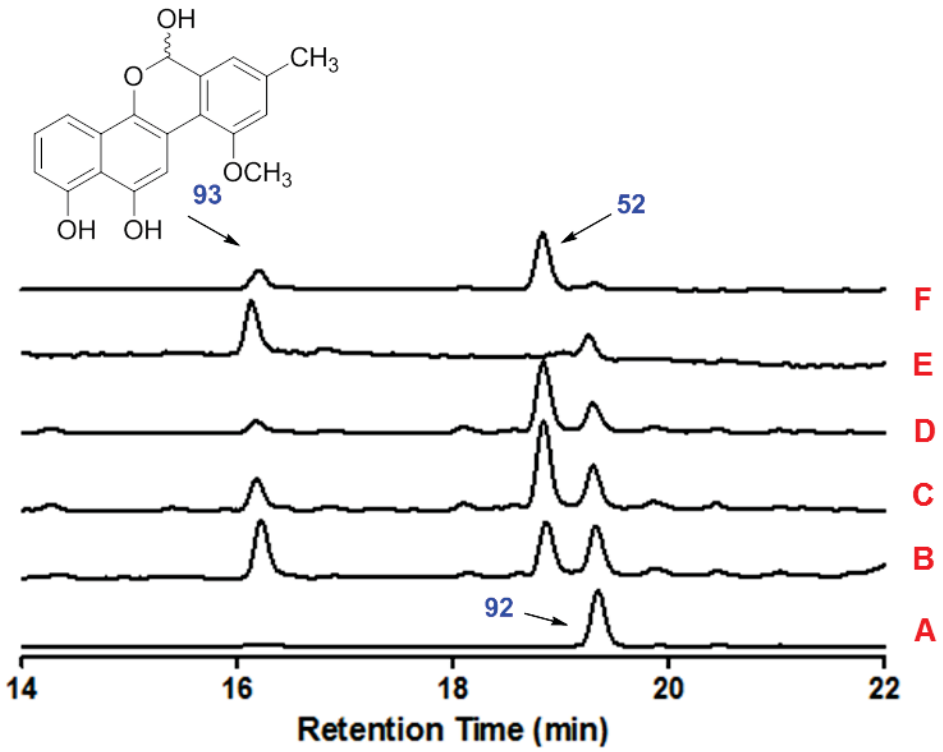

Figure 0.3 HPLC traces of the enzymatic reactions with **92**: (A) standard **92**; (B) **92** + GilM + SAM + 5 min; (C) **92** + GilM + SAM + 10 min; (D) **92** + GilM + SAM + 15 min; (E) intermediate (**93**) isolated from HPLC (mixture of closed and open form); (F) **93** + GilM.

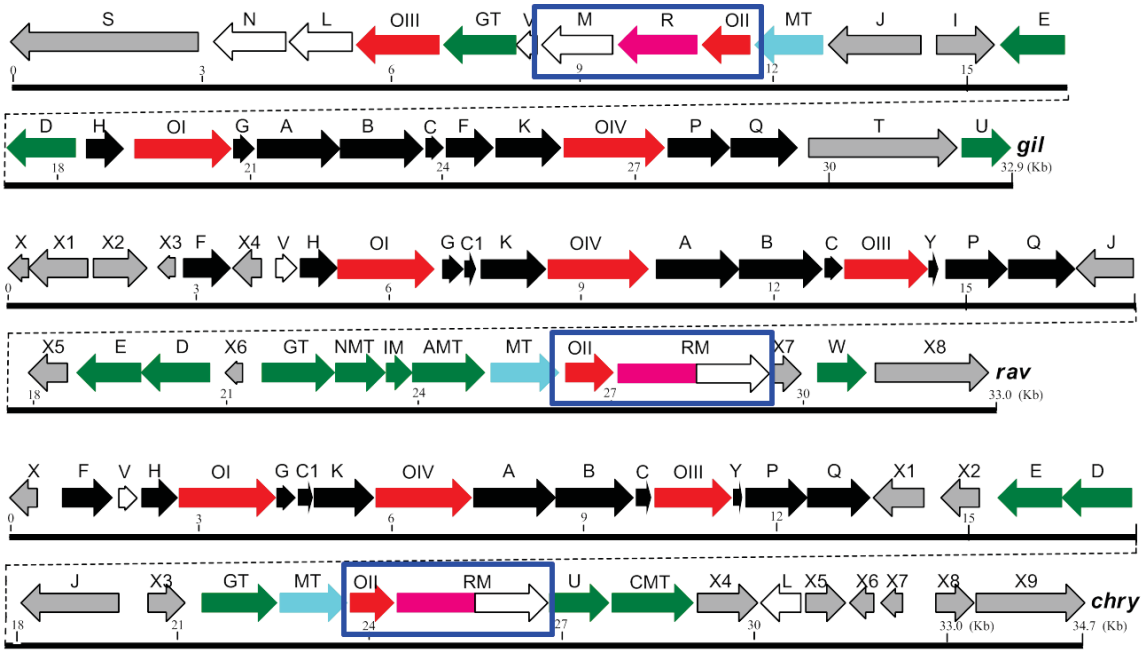

Figure 0.4 R and M genes in gilvocarcin, ravidomycin and chrysomcin gene clusters.

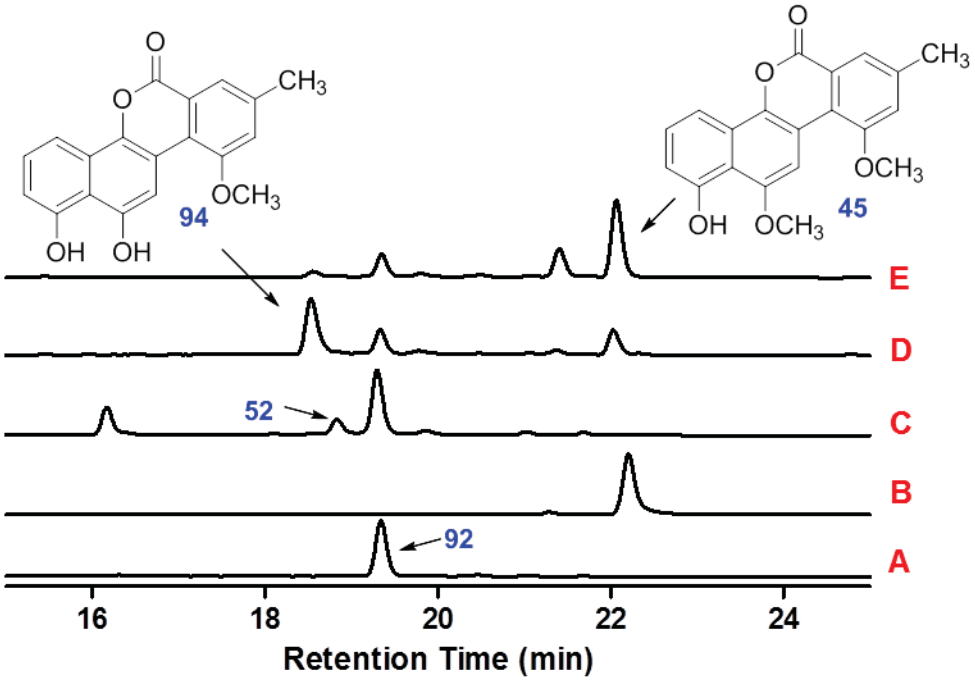

Figure 0.5 HPLC traces of the enzymatic reactions with **92**: (A) standard **92**; (B) standard defuco-gilvocarcin M (**45**); (C) **92** + GilM; (D) **92** + GilM + GilR; (E) **92** + GilM + GilR + SAM.

The only remaining question was the regeneration of GilM after reduction of the quinone. Interestingly, the respective GilM-activity in the biosynthetic pathways of other structurally related compounds, chrysomycin A and ravidomycin V, is encoded on the same gene as the oxidoreductase GilR-activity,(*81*) while in the gilvocarcin pathway, *gilM* and *gilR* are two separate genes (Figure 2.4).(*49*) This prompted us to propose that GilM could be working in conjunction with GilR, an FAD dependent oxidoreductase that catalyzes the very last step in gilvocarcin biosynthesis by converting pregilvocarcin to gilvocarcin, but also was shown to convert sugar free defuco-pregilvocarcins.(*38, 87*) We hypothesized that GilM utilizes the reduced flavin generated in the GilR reaction to reduce the quinone thereby regenerating oxidized flavin for the next catalytic cycle. To validate this hypothesis, compound **92** was incubated with GilM and GilR (Figure 2.5). The assistance of GilR for the reducing capabilities of GilM was established by measuring the amounts of the products formed in the reactions. Catalytic amounts of GilM alone accumulated mostly starting material along with minor production of **52** (Figure 2.5, trace C). In the absence of SAM, GilM and GilR accumulated a new peak (Figure 2.5, trace D) that corresponds to demethyl-defuco-gilvocarcin M(*88*) (**94**, *m*/*z* 321 $[M-H]^-$). Adding SAM to the GilM-GilR reaction mixture led to the accumulation of **7** (Figure 2.5, trace E). A 10-fold increase in the formation of **45** in the GilM-GilR reaction versus using GilM alone confirmed that GilM works synergistically with GilR.

Overall, these results described here allowed us to fully prove the post-PKS reaction sequence of the gilvocarcin biosynthetic pathway as shown in Scheme 2.3. The fact that the easy to synthesize compound **84** is an intermediate of the gilvocarcin pathway opens up future possibilities of generating gilvocarcin analogues through chemo-enzymatic synthesis or mutasynthesis,(*89, 90*) thus coupling the power of chemical synthesis with metabolic engineering.

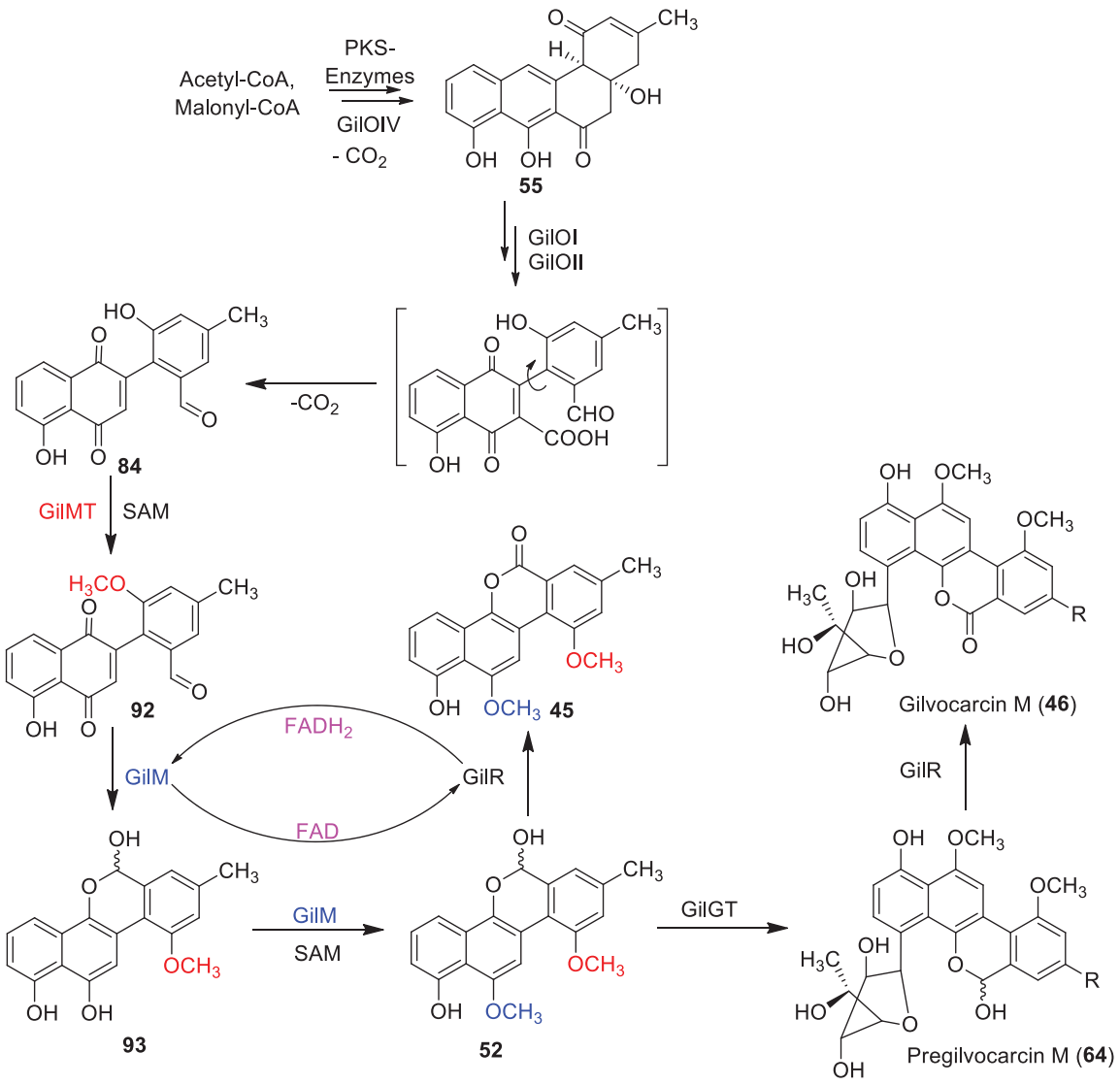

Scheme 0.2 Key follow-up sequence of events involving GilMT and GilM reactions en route to defucogilvocarcin M (**45**) and gilvocarcin M (**46**).

2.3. Experimental

Section A: General Information

General Remarks: ^{1}H and ^{13}C spectra were recorded using Agilent instruments (^{1}H frequencies 300, 400 and 500 MHz, corresponding ^{13}C frequencies are 75, 100, 125 MHz, respectively). Chemical shifts are quoted in parts per million (ppm) relative to TMS. *J* values are recorded in Hz. A photodiode array detector (Waters 2996) along with a Micromass ZQ 2000 mass spectrometer (Waters Corporation) equipped with an

electrospray ionization (ESI) probe was used to detect the molecular ions and analyze the compounds. 60-200 mesh silica gel was used for flash column chromatography. Thin layer chromatography was carried out using aluminum backed plates coated with silica gel. The plates were visualized under UV light at 254 nm and /or vanillin stain. R_f values were obtained by elution in the stated solvent ratios (v/v). All small-scale dry reactions were carried out under Nitrogen using standard syringe-septum technique.

Section B: Synthetic protocols

3-Methoxy-5-methylbenzaldehyde (88): This was prepared in 3 steps.

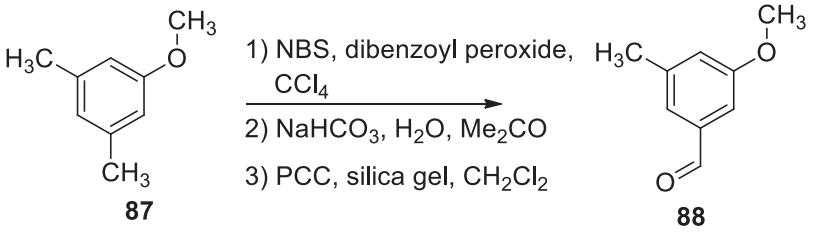

To a magnetically stirred solution of the dimethyl anisole (500 mg, 3.68 mmol) in CCl_4 (40 mL) was added NBS (622 mg, 3.5 mmol) and benzoyl peroxide (10 mg). After refluxing for 1h, the reaction mixture was filtered and the filtrate was successively washed with aqueous HCl (3 N), saturated aqueous $NaHCO_3$, H_2O and brine. The organic layer was dried over Na_2SO_4 and the solvent was evaporated to give a residue that was purified on a silica gel column (30% CH_2Cl_2–hexane, R_f = 0.56) to furnish the bromide (70%).

To a stirred solution of the above bromide (2.15 g, 9.95 mmol) in acetone (60 mL) and H_2O (100 mL) was added $NaHCO_3$ (1.05 g, 12.5 mmol). The reaction mixture was refluxed for 4h then cooled to r.t. and extracted with EtOAc (3×50 mL). The combined organic layer was washed with brine and dried (Na_2SO_4). Evaporation of the solvent and purification of the residue on a silica gel column (20% EtOAc–hexane, R_f = 0.2) furnished the alcohol (86%).(*89*)

To a stirred suspension of pyridinium chlorochromate (2.0 g, 14.4 mmol) and silica gel (2.0 g) in anhydrous CH_2Cl_2 (10 mL) was added a solution of the above alcohol

(1.3 g, 9.6 mmol) in CH_2Cl_2 (5 mL). After stirring the reaction mixture for 1h at r.t., it was filtered through a small silica gel column. The column was eluted with excess CH_2Cl_2 and the solvent was evaporated under reduced pressure to furnish the benzaldehyde as oil (quant.) (40% CH_2Cl_2–hexane, R_f = 0.45). ^{1}H NMR ($CDCl_3$, 300 MHz) δ 9.90 (s, 1H), 7.25 (bs, 1H), 7.18 (bs, 1H), 6.97 (bs, 1H), 3.82 (s, 3H), 2.38 (s, 3H); ^{13}C NMR ($CDCl_3$, 75 MHz) δ 192.3, 160.1, 140.4, 137.7, 124.4, 122.2, 109.5, 55.6, 21.5.

3-Hydroxy-5-methylbenzaldehyde (89)

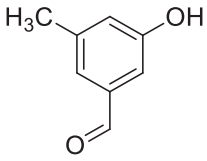

1M BBr_3 in CH_2Cl_2 (6.6 mL, 6.6 mmol) was added dropwise to a stirred solution of **88** (500 mg, 3.3 mmol) in anhydrous CH_2Cl_2 (10 mL) under nitrogen at r.t. After stirring for 2h, 3 mL of each HCl and AcOH were added and reaction mixture was refluxed for 10h. The reaction was cooled, diluted with H_2O and extracted with CH_2Cl_2. The combined organic layer was dried over Na_2SO_4 and the solvent was evaporated to give a residue that was purified on silica gel (20% EtOAc-hexane, R_f = 0.25) to give deprotected derivative as yellowish solid in 60% yield.(*91*) ^{1}H NMR (CD_3OD, 300 MHz) δ 9.76 (s, 1H), 7.09 (bs, 1H), 7.04 (bs, 1H), 6.87 (bs, 1H), 2.27 (s, 3H); ^{13}C NMR (CD_3OD, 75 MHz) δ 194.2, 158.8, 141.4, 138.9, 123.5, 113.1, 54.7, 21.3.

2-(3-Methoxymethoxy-5-methylphenyl)-1,3-dioxane (90): This protected benzaldehyde was prepared in 2 steps.

(a) 2-(3-Hydroxy-5-methylphenyl)-1,3-dioxane

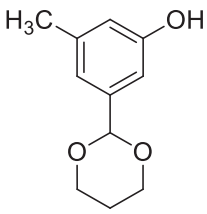

A mixture of **89** (200 mg, 1.5 mmol), 1,3-propanediol (0.16 mL, 2.2 mmol) and TsOH.H_2O (6 mg, 0.03 mmol) in toluene was refluxed with the azeotropic removal of H_2O. After starting material was consumed completely, the reaction mixture was cooled and the solvent was removed under pressure to give a residue. The crude residue was purified on silica (EtOAc-hexane, R_f = 0.32) to give the protected aldehyde(*88*) as a white solid in 75% yield. ^{1}H NMR ($CDCl_3$, 300 MHz) δ 6.84 (bs, 1H), 6.70 (bs, 1H), 6.49 (bs, 1H), 6.45 (bs, 1H), 5.39 (s, 1H), 4.27–4.21 (m, 2H), 3.99–3.92 (m, 2H), 2.22 (s, 3H), 2.20–2.14 (m, 1H), 1.44–1.38 (m, 1H); ^{13}C NMR ($CDCl_3$, 75 MHz) δ 155.7, 139.6, 139.4, 118.7, 116.8, 110.4, 101.7, 67.4, 25.8, 21.5; HRMS (+EI): Calc'd for $C_{11}H_{14}O_3$: 194.0943, observed: 194.0944.

(b) 2-(3-Methoxymethoxy-5-methylphenyl)-1,3-dioxane (90)

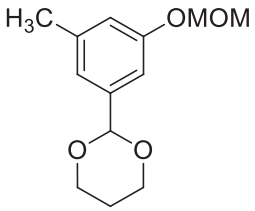

To a stirred solution of the above phenyl acetal (165 mg, 0.85 mmol) and diisopropylethylamine (0.23 mL, 1.35 mmol) in anhydrous CH_2Cl_2 was dropwise added chloromethyl methyl ether (0.14 mL, 1.69 mmol) and the mixture was heated at 40 °C. After 24h, reaction mixture was washed with H_2O and brine. The combined organic layer was dried over Na_2SO_4 and the solvent was removed under vacuum to give MOM ether(*17*) as colorless oil in 95% yield. ^{1}H NMR ($CDCl_3$, 300 MHz) δ 6.97 (bs, 1H), 6.82 (bs, 1H), 5.42 (s, 1H), 5.15 (s, 2H), 4.26–4.20 (m, 2H), 3.98–3.89 (m, 2H), 3.44 (s, 3H), 2.32 (s, 3H), 2.28–2.12 (m, 1H), 1.42–1.36 (m, 1H); ^{13}C NMR ($CDCl_3$, 75 MHz) δ 157.0, 139.8, 139.3, 120.1, 117.2, 110.8, 101.4, 94.2, 67.3, 55.9, 25.8, 21.5; HRMS (+EI): Calc'd for $C_{13}H_{18}O_4$: 238.1205, observed: 238.1204.

(2-(1,3-dioxan-2-yl)-6-(methoxymethoxy)-4-methylphenyl)tributylstannane (86)

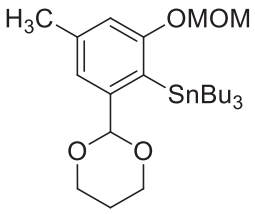

The above MOM ether (300 mg, 1.26 mmol) was co-evaporated twice with anhydrous toluene and was dissolved in freshly dried hexane (10 mL). At 0 °C, *n*-BuLi (0.6 mL, 2.5M in hexane, 1.5 mmol) was added and the mixture was stirred for 30 min. A white precipitate indicates the formation of lithiated species. After 30 min, *n*-Bu_3SnCl (0.5 mL, 1.89 mmol) was added and the mixture was further stirred for 30 min. It was then diluted with hexane-Et_2O (1:1, v/v), followed by the addition of saturated aqueous $NaHCO_3$. The mixture was stirred at 0 °C for 30 min. After separation, the aqueous layer was extracted twice with hexane-Et_2O (1:1, v/v). The combined organic layers were washed with brine and dried over Na_2SO_4. The solvent was removed under vacuum and the residue was subjected to purification on silica to give the required stannane(*83*) (3% EtOAc-hexane, R_f = 0.5) as colorless oil (88%). ^{1}H NMR ($CDCl_3$, 300 MHz) 7.24 (bs, 1H), 6.90 (bs, 1H), 5.38 (s, 1H), 5.11 (s, 2H), 4.26-4.21 (bs, 2H), 3.99 (bs, 2H), 3.45 (s, 3H), 2.34 (s, 3H), 2.30-2.12 (m, 1H), 1.56-0.87 (m, 28H); δ ^{13}C NMR ($CDCl_3$, 75 MHz) δ 161.9, 146.6, 140.3, 125.8, 120.6, 113.7, 102.5, 94.5, 67.4, 56.0, 29.4, 27.7, 26.0, 21.8, 14.0, 12.4; HRMS (ESI): Calc'd for $[C_{25}H_{44}O_4Sn+H]^+$: 529.2339, observed: 529.2342.

2-(2-(1,3-dioxan-2-yl)-6-(methoxymethoxy)-4-methylphenyl)-5-hydroxy-1,4-napthaquinone (91)

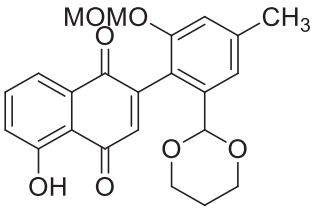

To a solution of 2-Bromo-8-hydroxy-1,4-naphthaquinone **85** (96 mg, 0.38 mmol), stannane **86** (200 mg, 0.38 mmol), and CuI (7.6 mg, 0.04 mmol) in THF (5 mL) was added a solution of $Pd_2(dba)_3$•$CHCl_3$ (9.8 mg, 0.009 mmol) and PPh_3 (10.5 mg, 0.04

mmol) in THF (1 mL). The mixture was heated at 75 °C for 12h. The mixture was cooled to 0 °C and diluted with EtOAc (25 mL). Saturated aqueous $NaHCO_3$ (25 mL) was added and the mixture was stirred for 30 min. The layers were separated and the aqueous layer was extracted twice with EtOAc (50 mL). The combined organic layers were washed with brine and dried over Na_2SO_4. The solvent was removed under vacuum and the resulting residue was subjected to flash silica gel column chromatography to provide the coupled product(*83*) (35% EtOAc-hexane, R_f = 0.6) as orange solid (75%). ^{1}H NMR ($CDCl_3$, 400 MHz) δ 12.33 (s, 1H), 7.80 (dd, J = 8.5, 7.5 Hz, 1H), 7.61 (dd, J = 7.5, 1 Hz, 1H), 7.39 (bs, 1H), 7.36 (dd, J = 8.5, 1 Hz, 1H), 7.18 (bs, 1H), 6.99 (s, 1H), 2.43 (s, 3H); ^{13}C NMR ($CDCl_3$, 100 MHz) δ 190, 5, 184.5, 162.5, 156.1, 147.5, 142.1, 138.7, 137.7, 137.3, 133.5, 126.4, 124.8, 124.7, 123.3, 119.2, 116.4, 21.1.

3-hydroxy-2-(5-hydroxy-1,4-dioxo-1,4-dihydronaphthalen-2-yl)-5-methylbenzaldehyde (84)

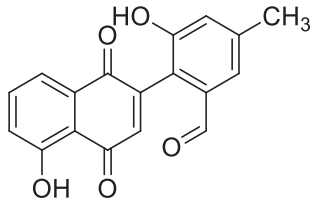

To **91** (60 mg, 0.14 mmol) in a 250 mL flask at r.t. was added a solution of concentrated HCl (2 mL) in 10 mL CH_3CN. The mixture was stirred for 4 min and then was quenched with $NaHCO_3$ (60 mL) followed by addition of EtOAc (50 mL). After separation of the layers, the aqueous layer was extracted with EtOAc twice. The combined organic layers was washed with brine, dried over Na_2SO_4 and the solvent was removed under vacuum. The resulting residue was subjected to purification by flash silica gel column chromatography to provide the desired product(*83*) (35% EtOAc-hexane, R_f = 0.25) as orange solid (74%). ^{1}H NMR (acetone-d_6, 500 MHz) δ 12.06 (bs, 1H), 9.90 (s, 1H), 7.80 (dd, J = 8.5, 7.5 Hz, 1H), 7.61 (dd, J = 7.5, 1 Hz, 1H), 7.39 (bs, 1H), 7.36 (dd, J = 8.5, 1 Hz, 1H), 7.18 (bs, 1H), 6.99 (s, 1H), 2.43 (s, 3H); ^{13}C NMR (acetone-d_6, 100 MHz) δ 193.0, 190.5, 184.5, 162.5, 156.1, 147.5, 142.1, 138.7, 137.7, 137.3, 133.5,

126.4, 124.8, 124.7, 123.3, 119.2, 116.4, 21.1; HRMS (+EI): Calc'd for $C_{18}H_{12}O_5$: 308.0685, observed: 308.0686.

Section C: Expression and Purification of Enzymes

gilM, *gilMT*, and *gilR* genes were expressed using pET28a(+) expression constructs in *E. coli* BL21 (DE3) with an *N*-terminal polyhistidine tag. A single colony was transferred to 10 mL LB supplemented with 50 µg/mL kanamycin and grown at 37 °C and 250 rpm for 5h. Subsequently, 500 mL LB supplemented with 50 µg/mL kanamycin was inoculated with 5 mL of the culture and was grown at 37 °C until OD600 reached to 0.5. Gene expression was induced with isopropyl-*β*-D-1-thiogalactopyranoside (IPTG, 0.2 mM final concentration) and the culture was allowed to grow at 18 °C for 16h. The cell pellets were collected by centrifugation (4000 × g, 15 min) and were washed twice with 20 mL of lysis buffer (50 mM KH_2PO_4, 300 mM KCl, 10 mM imidazole, pH 8.0). The cells were lysed using a French Press and the crude soluble enzyme fractions were collected through centrifugation (16000 × g, 1h). The crude enzymes were loaded onto a Talon metal affinity resin (BD Biosciences) column and were washed three times with lysis buffer. The enzymes were then eluted with elution buffer (50 mM KH_2PO4, 300 mM KCl, 250 mM imidazole, pH 8.0). The purified proteins were concentrated using an Amicon Ultra centrifugal filter (Millipore Corp.) and stored as 25% glycerol stocks at -20 °C. The concentration of protein was determined by the Bradford method using a calibration curve of the known concentrations of BSA. The concentrations for GilM, GilMT and GilR were found to be 6.7, 12.5 and 2.4 mg mL^{-1} respectively.

Section D: Cofactor Analysis of GilM

GilM catalyzes reductive methylation without any external cofactor. However, the BLAST analysis showed a very vague similarity to thiopurine-S-methyltransferases. To analyze any co-purified cofactor, the enzyme was boiled for 5 minutes and centrifuged (12000 ×g, 5 min). The supernatant was then subjected to LC-MS analysis. A linear gradient of acetonitrile and 0.1% formic acid-water (solvent A = 0.1% formic acid-H_2O; solvent B = acetonitrile; 0-15 min 25% B to 100% B; 16-24 min 100% B; 25-26 min

100% to 25% B; 27-29 min 25% B) with flow rate of 0.5 mL/min was used to separate the compounds in a Waters Symmetry C_{18} (4.6 × 250 mm, 5µm) column. The supernatant showed UV-absorption at 260, typical of adenosine spectrum. To further verify presence of loosely bound S-adenosylmethionine a standard solution of S-adenosylmethionine was prepared in 50 mM phosphate buffer and was used in parallel for comparison. GilM was found to be co-purifying with S-adenosylmethionine.

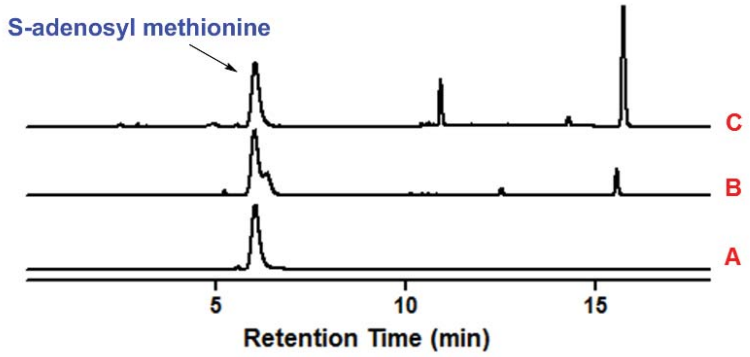

Figure 0.6 HPLC traces of the released cofactor: (A) standard S-adenosylmethionine; (B) Cofactor released from GilM; (C) S-adenosylmethionine boiled for 5 min.

Section E: Kinetic Profile

GilM

A typical reaction mixture (50 µM) composed of substrate (**92**), 50 mM phosphate buffer, 20 µM enzyme (final concentration) was incubated at 25 °C. After 5 min reaction was extracted twice with EtOAc (300 µl) and combined organic layers were dried under vacuum. The residue was then dissolved in 50 µl acetonitrile and 20 µl was injected onto HPLC following the protocol described in Section D. The amount of product formed was estimated by plotting the peak area in the standard calibration curve. The data resulting from incubating 7 different substrate concentrations with enzyme were fit to the Michael-Menten equation with nonlinear regression. k_{cat} and K_M values were calculated using

GraphPad Prism 5.0. The analysis was done in triplicate and the average was taken. The analysis yielded a k_{cat} of 0.02930 and a K_M of 35.38μM.

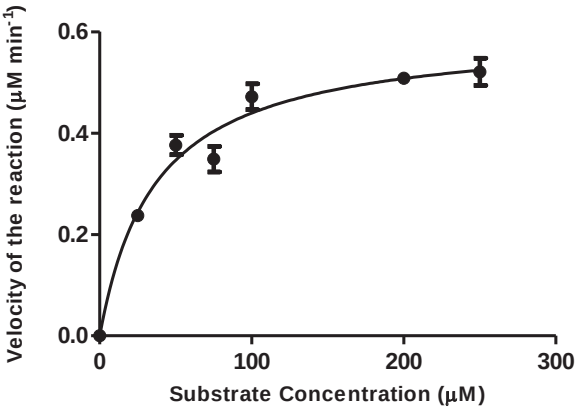

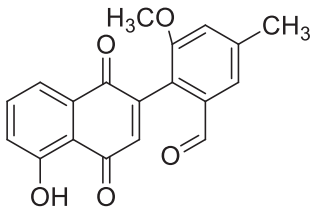

92

GilMT

A typical reaction mixture (100 μM) composed of substrate (**84**), 50 mM phosphate buffer, S-adenosylmethionine (excess), 13.7 μM GilMT (final concentration) was incubated at 25 °C for 5–15 min to optimize the analysis condition. The kinetic profile for GilMT could not be generated due to solubility issues. The substrate concentration above 1 mM resulted in substrate precipitation while less enzyme concentration failed to produce substantial amount of product to be monitored by HPLC.

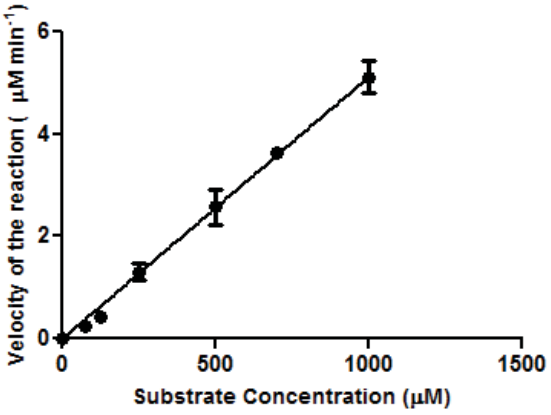

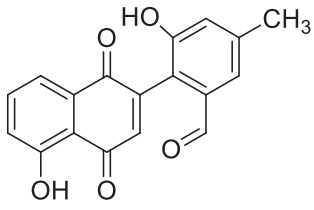

84

Section F: In vitro enzymatic reactions

Enzymatic synthesis of 2-(5-hydroxy-1,4-dioxo-1,4-dihydronaphthalen-2-yl)-3-methoxy-5-methylbenzaldehyde (92)

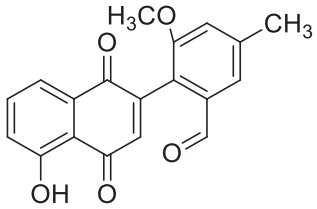

An assay mixture (5 mL) composed of phosphate buffer (pH 6.5, 50 mM), substrate **84** (100 μM), S-adenosylmethionine (excess), and GilMT (10 μM) was incubated at 30 °C for 12h. The reaction was extracted with EtOAc (2 × 10 mL). The organic solvent was dried at low pressure and the crude product was dissolved in CH_3CN. The product showed UV-absorbance at 420 and was purified through HPLC using the conditions as described in Section D. The reaction produced the desired methylated product in 40% yield. ^{1}H NMR ($CDCl_3$, 400 MHz) δ 12.03 (s, 1H), 9.85 (s, 1H), 7.64-7.60 (m, 2H), 7.33 (bs, 1H), 7.28 (dd, J = 7.5, 2 Hz, 1H), 7.05 (bs, 1H), 6.82 (s, 1H), 3.77 (s, 3H), 2.48 (s, 3H); ^{13}C NMR ($CDCl_3$, 100 MHz) δ 191.7, 190.2, 183.3, 161.5, 157.3, 147.5, 141.6, 137.1, 136.4, 135.8, 132.7, 125.7, 124.2, 119.8, 117.7, 115.6, 56.3, 21.8; HRMS (+EI): Calc'd for $C_{19}H_{14}O_5$: 322.0841, observed: 322.0850.

Enzymatic synthesis of defuco-pregilvocarcin M (52)

An assay mixture (1 mL) composed of phosphate buffer (pH 6.5, 50 mM), substrate **92** (100 μM), S-adenosylmethionine (excess), and GilM (8 μM) was incubated at 30 °C for 4h. The reaction was extracted with EtOAc (2 × 2 mL). The organic solvent was removed at low pressure and the crude product was dissolved in CH_3CN. The cyclized product showed a sharp absorbance at 375 nm and was purified through HPLC (conditions as described in Section D). The reaction produced the desired product in 60% yield. HRMS (+EI): Calc'd for $C_{20}H_{18}O_5$: 338.1154, observed: 338.1160.

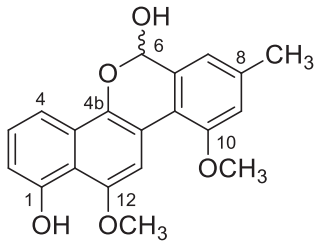

Table 2.1 ^{1}H and HSQC data for defuco-pregilvocarcinM (**52**) in $CDCl_3$ (500 MHz, relative to internal TMS, J in Hz).

Position	**^{1}H NMR**	**Multiplicity(Hz)**	**HSQC**
1-OH	9.43	S	
2	6.88	d (1)	113.6
3	7.38	dd (8.5, 7.5)	125.4
4	7.83	dd (8.5, 1)	
6	6.40	d (6.5)	93.1
6-OH	3.02	d (6.5)	
7	6.89	d (2)	119.4
8-CH_3	2.41	S	21.8
9	6.86	Bs	111.2
10-OCH_3	3.97	S	56.0
11	8.04	S	103.6
12-OCH_3	4.08	S	56.2

Enzymatic synthesis of demethyl-defuco-pregilvocarcin M (93)

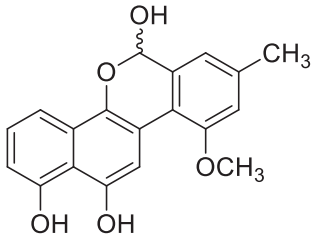

An assay mixture (50 μl) composed of phosphate buffer (pH 6.5, 50 mM), substrate **92** (0.8 μM), and GilM (0.04 μM) was incubated at 30 °C for 5 min. The reaction was extracted with EtOAc (2 × 2 mL). The organic solvent was dried at low pressure and the crude product was dissolved in CH_3CN. The solution was injected onto HPLC (conditions described in Section D). The reaction produced the desired intermediate in 10 % yield. HRMS (ESI): Calc'd for $[C_{19}H_{16}O_5\text{-}H]^-$ 323.0919, observed: 323.0919.

Enzymatic synthesis of demethyl-defuco-gilvocarcin M (94)

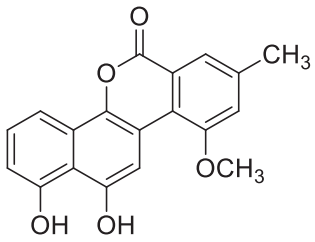

An assay mixture (100 μl) composed of phosphate buffer (pH 6.5, 50 mM), substrate **92** (2 μM), GilM (0.1 μM) and GilR (0.2 μM) was incubated at 30 °C for 1h. The reaction was extracted with EtOAc (2 × 2 mL). The organic solvent was dried at low pressure and the crude product was dissolved in CH_3CN. The solution was injected onto HPLC (conditions described in Section D). The reaction produced the desired product in 31 % yield. HRMS (+EI): Calc'd for $C_{19}H_{14}O_5$ 322.0841, observed: 322.0846.

This Chapter has been reproduced with permission from the following publication: copyright ACS publications

Tibrewal, N., Downey, T. E., Van Lanen, S. G., Ul Sharif, E., O'Doherty, G. A., Rohr, J. "Roles of the Synergistic Reductive O-Methyltransferase GilM and of O-Methyltransferase GilMT in the Gilvocarcin Biosynthetic Pathway." *J. Am. Chem. Soc.*, **2012**, *134*, 12402–12407.

Chapter 3. Investigating C–C bond cleavage in the gilvocarcin biosynthetic pathway

C–C bond cleavages initiate one of the most significant structural rearrangements in the biosynthesis of many natural products, through which numerous unique scaffolds are generated. Most of these cleavage reactions are also crucial for the biological activity of the natural products also (e.g., mithramycin, aflatoxin). Thus, great attention has been devoted to identifying the relevant enzymes and cleavage mechanisms. One of the important examples is found during the biosynthesis of gilvocarcins.

It has been proven that the early biosynthetic steps generate an angucyclinone intermediate (e.g., prejadomycin/homo-prejadomycin **55**/**56**, dehydrorabelomycin **73**; Schemes 3.1) that subsequently undergoes a complex structural rearrangement via an oxidative C5–C6 bond cleavage to form the benzonaphthopyranone skeleton of the gilvocarcins.(*49, 78, 79, 92*) Another intriguing group of natural products, the jadomycins (e.g., **21** and **78**), are believed to share their initial biosynthetic pathway including the oxidative rearrangement reaction.(*69*) To date, however, it has not been unambiguously proven at which exact step and by which mechanism these oxidative rearrangements take place. In this chapter, we unambiguously confirmed that GilOII (JadG for the jadomycin pathway) is the sole enzyme responsible for this oxidative C–C bond cleavage, and on the basis of the structure of an isolated pivotal intermediate, we were also able to propose a mechanism for this reaction.

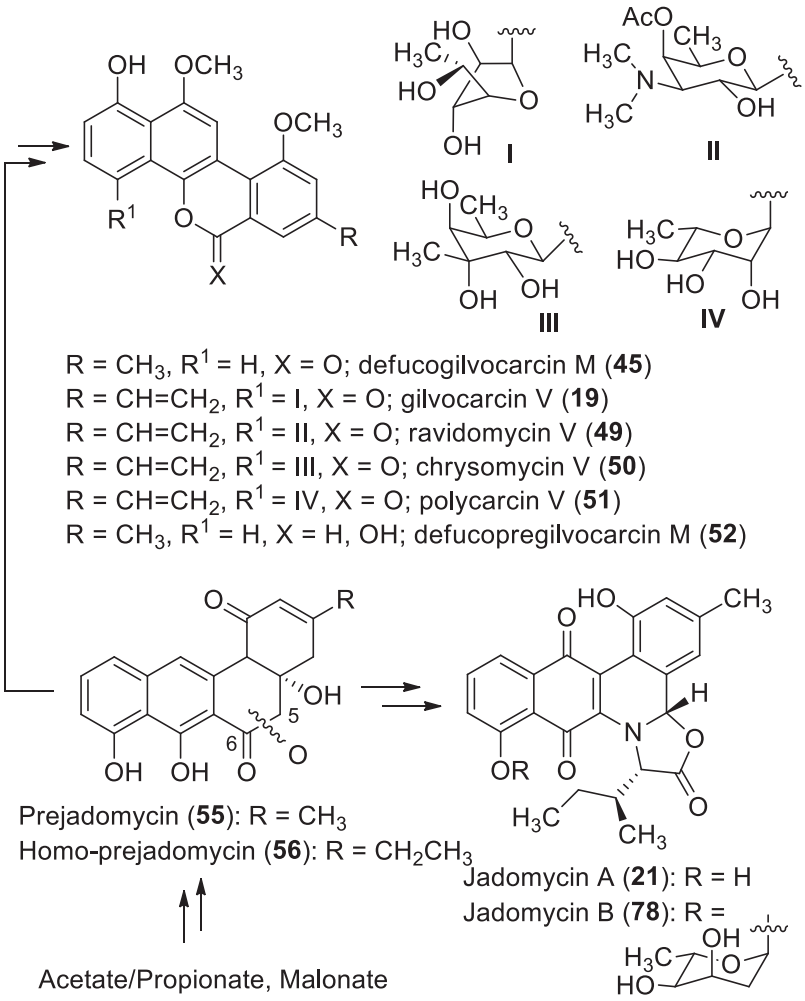

Scheme 0.1 Representative members of the gilvocarcin and jadomycin groups of natural products sharing common biosynthetic intermediate, prejadomycin (**55**).

3.1. Results

A recent report on the enzymatic total synthesis of defucogilvocarcin M (**45**) confirmed that only four enzymes, namely oxygenase GilOII, methyltransferase GilMT, methyltransferase/reductase GilM, and oxidoreductase GilR are needed to convert the angucyclinone intermediate dehydrorabelomycin (**73**) to **45**.(*78*)

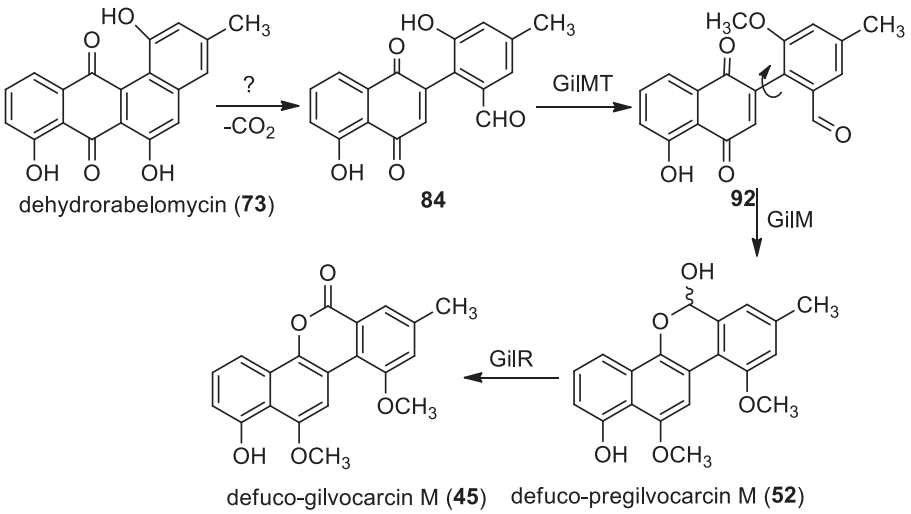

Scheme 0.2 Sequence of events en route to defucogilvocarcin M.

GilR is an FAD dependent oxidoreductase that catalyzes the very last step in gilvocarcin biosynthesis by converting pregilvocarcin to gilvocarcin, but also was shown to convert sugar free defuco-pregilvocarcins.(*30, 69*) GilMT, an S-adenosylmethionine dependent *O*-methyltransferase, works on the intermediate **84**, plausibly derived from the oxidative cleavage of dehydrorabelomycin (**73**). A subsequent sequence of reactions catalyzed by the S-adenosylmethionine dependent reductive *O*-methyltansferase, GilM, then generates the tetracyclic hemiacetal core, defucopregilvocarcin M (**52**), prompting us to impute the C-C bond cleavage reaction to GilOII. However, it remained unclear whether GilOII can catalyze the crucial C-C bond cleavage reaction alone or whether some support by one or more of the downstream enzymes were needed. Thus, we interrogated reactions of dehydrorabelomycin (**73**) with individual enzymes and a cocktail of downstream enzymes. GilOII, GilMT, GilM and GilR were expressed in *E. coli* and purified as His_6-tagged proteins following a procedure described earlier.(*78*) Substrate **73** was prepared enzymatically from prejadomycin (**55**), a proven intermediate of both the gilvocarcin M and the jadomycin biosynthetic pathways as well as of many other anguclycines, which was isolated from a Δ*gilOI* mutant strain *S. lividans* TK24 (cosG9B3–OI¯) following the reported procedure (see experimental section).(*69*)

As anticipated, the bi-functional enzyme GilM alone did not react with **73**. GilMT alone reacted with **73** unexpectedly, yielding three different compounds (**95**–**97**), the major product was dimethyldehydrorabelomycin (**95**), and the other two minor products were identified as monomethylated dehydrorabelomycins **96** and **97** (Figure 3.1 trace D, Scheme 3.3). The low yields confirmed our prior findings that GilMT normally acts after the C–C bond cleavage on aldehyde intermediate **84**.(*92*) Neither **95**, **96** nor **97** were converted to defucogilvocarcin M (**45**) when treated with a mixture of GilOII, GilM, GilMT and GilR, proving that the C–C bond cleavage reaction requires a nonmethylated substrate, while **73** with a cocktail of GilOII, GilMT and GilM did accumulate defuco-pregilvocarcin M (Figure 3.1, trace C).

Investigating GilOII

The reaction of **73** with GilOII alone resulted in consumption of all the starting material, but unexpectedly, no product was seen. After careful screening of different cofactors (FMN, FAD, NADH, NADPH) and cofactor regeneration enzymes, we found the correct conditions by incubating **73** with GiOII, FAD, and NADPH and adding E. coli flavin reductase (Fre), which is known to regenerate $FADH_2$ from FAD using NADPH, and an NADPH-regeneration system containing glucose-6-phosphate and glucose-6-phosphate dehydrogenase that maintained a constant supply of NADPH in the reaction.

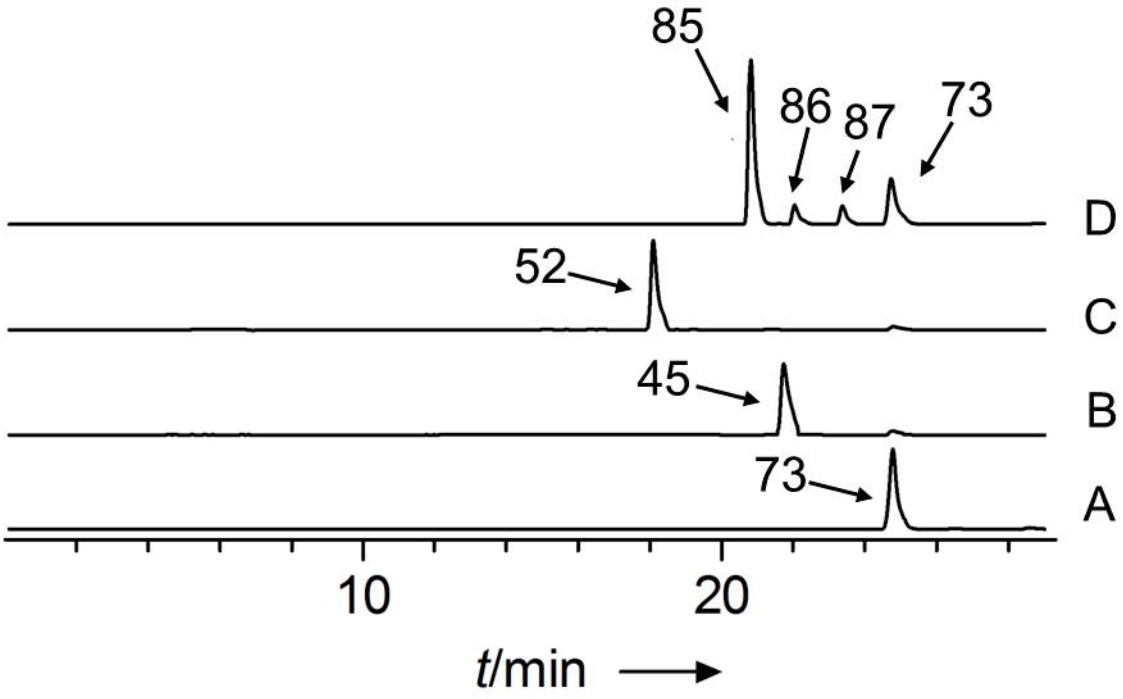

Figure 0.1 HPLC traces of the enzymatic reactions: A) standard dehydrorabelomycin (**73**), B) **73** + GilOII + GilMT + GilM + GilR producing defucogilvocarcin M (**45**), C) **73** + GilOII + GilM + GilMT producing defucopregilvocarcin M (**52**), D) **73** + GilMT.

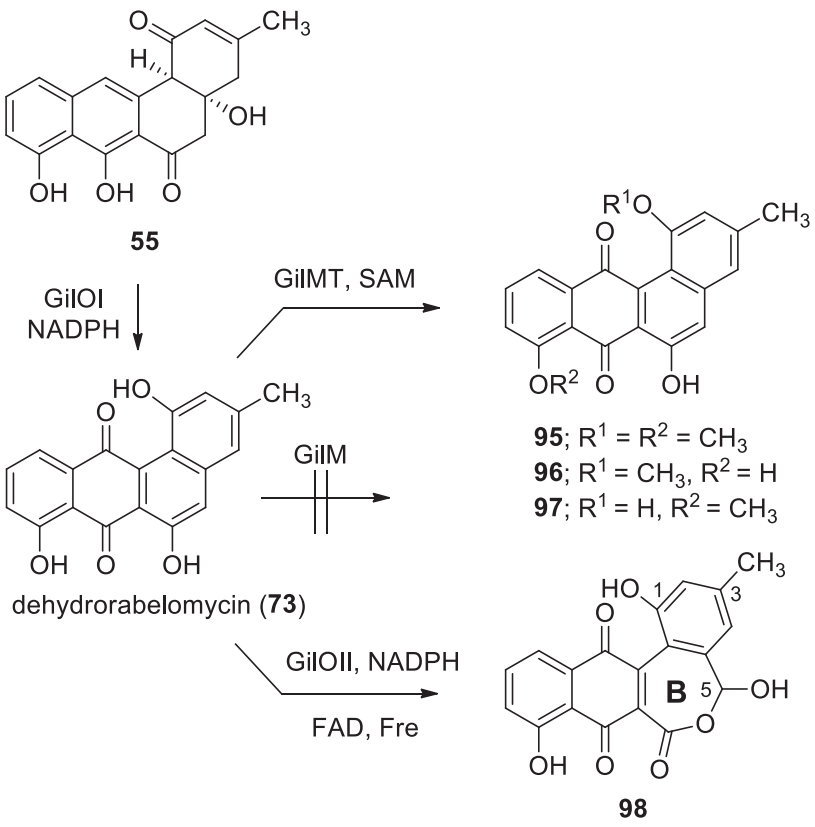

Scheme 0.3 Enzymatic reaction of dehydrorabelomycin (**73**) with GilMT and GilOII; Fre: *E. coli* flavin reductase.

Under these conditions, a new peak (**98**) was observable at a wavelength of 420 nm (Figure 3.2, trace A). After the reaction was run several times, ca. 90 µg of **98** were isolated for NMR characterization. The ^{1}H NMR spectrum of the new compound showed a considerable upfield shift of H5, which also showed a coupling with a new proton signal at δ 3.56. The latter was exchangeable with D_2O. The complete spectral characterization along with high-resolution mass spectrometry revealed **98** to possess a tetracyclic core with a unique hydroxy-oxepinone ring B (**98**, Scheme 3.3). The production of **98** clearly proved that GilOII is solely responsible for the key C–C bond cleavage. In the absence of FAD, NADPH or flavin reductase Fre, the assay failed to consume any starting material or to yield any product (Figure 3.2, trace B).

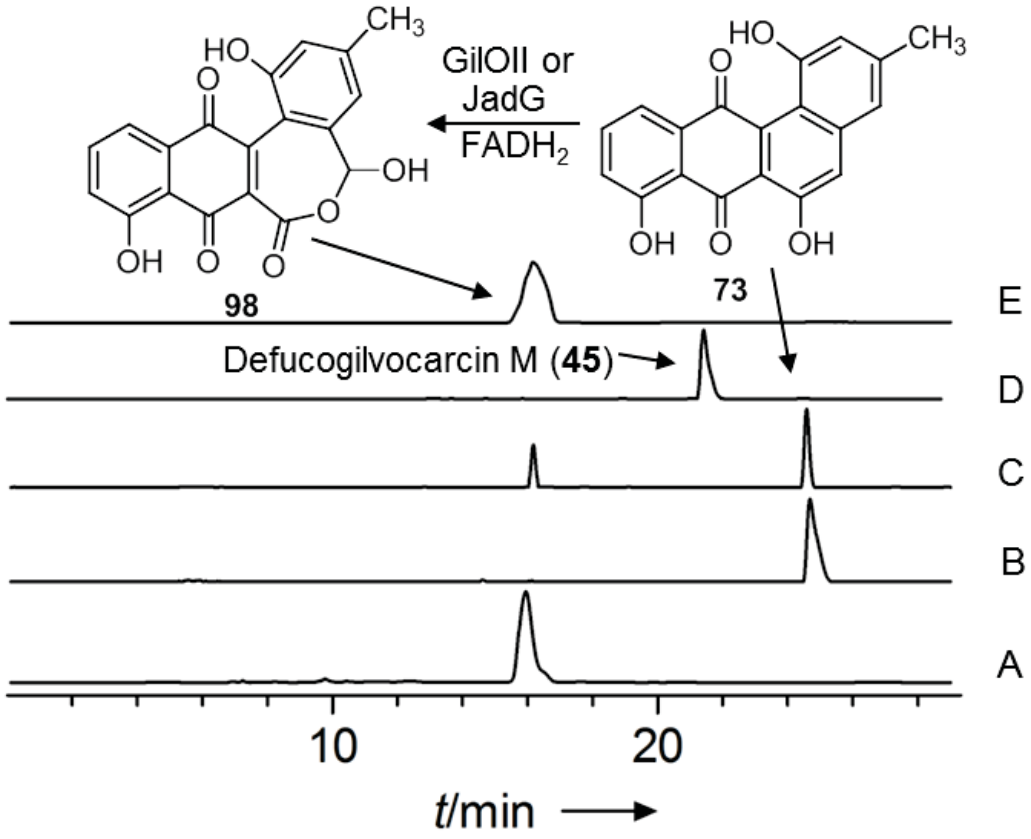

Figure 0.2 HPLC traces of the enzymatic reactions: A) dehydrorabelomycin (**73**) + GilOII + NADPH + FAD + Fre, B) **73** + GilOII C) **73** + GilOII + NADPH + Fre (traces of **98** were formed due to traces of FAD co-purified with Fre), D) **73** + JadG + GilMT + GilM + GilR producing defucogilvocarcin M (**45**), E) **73** + JadG + NADPH + FAD + Fre.

This proved that co-factor $FADH_2$ (here produced in situ from FAD and NADPH by Fre) is absolutely necessary, although the BLAST analysis showed that GilOII has no recognizable FAD-binding site. In fact, the enzyme resembles mostly co-factor free anthrone oxygenases, and we had considered that GilOII might act by a mechanism similar to that recently proposed for the cofactor-independent dioxygenase DpgC(*93*) involved in the biosynthesis of the dihydroxyphenylglyoxylate building block of glycoprotein antibiotics, as a possible alternative to the earlier proposed Baeyer-Villiger oxidation mechanism [Scheme 3.4, path B (in blue) vs path A (in green)]. The above described GilOII reaction and the isolated compound **98** were also critical for solving this mechanistic ambiguity. The stepwise mechanism, 5-hydroxylation followed by Baeyer-

Villiger oxidation (Scheme 3.4, path A, green) was corroborated, while the dioxygenase mechanism involving a dioxetane intermediate (Scheme 3.4, path B, blue) could be refuted. The observation that the experiment without FAD also produced a small amount of the product **98** (Figure 3.2, trace C) was tracked to small quantities of FAD that were co-purified with Fre. The insufficient supply of FAD in the experiment monitored by trace C (Figure 3.2) also explained well the incomplete conversion of starting material **73** to **98**.

Next we wanted to verify that compound **98** is a true intermediate of the pathway, and not a shunt product. We monitored conversion of **98** to defucogilvocarcin M (**45**) when it was incubated with a mixture of GilM, GilMT, and GilR. However, any combination of these three enzymes and suitable cofactors failed to convert **98** to **45**. Only upon addition of GilOII was **98** converted to **45** (Figure 3.3). This clearly proves oxepinone **98** is a pathway intermediate of the gilvocarcin biosynthesis. When **98** was incubated with GilOII alone, it was completely consumed, but no product was accumulated. This could be attributed to the unstable nature of the expected aldehyde (**84** or its carboxylated analogue). Overall, GilOII not only mediates C-5 hydroxylation and the following Baeyer-Villiger oxidation, but is also critical for the ring opening.

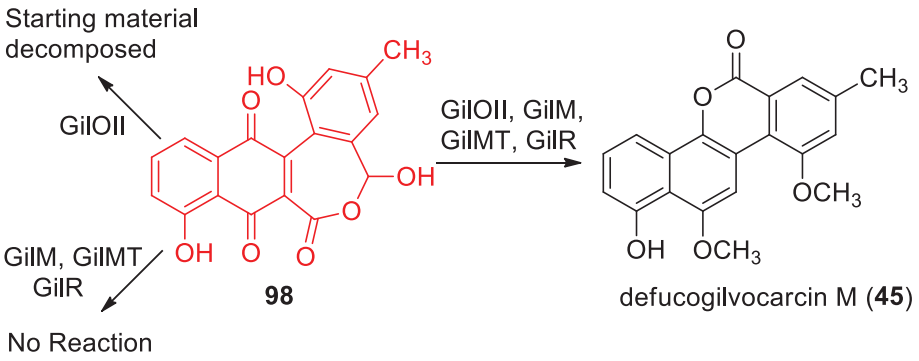

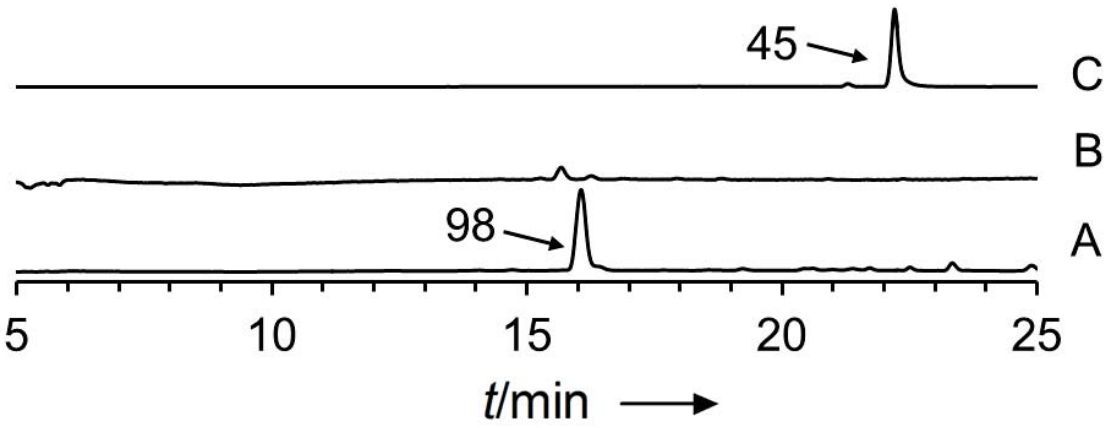

Figure 0.3 (Top) In vitro reactions of **98** with different combinations of downstream enzymes; GilOII, GilM, GilMT and GilR. (Bottom) HPLC traces of the enzymatic reactions: A) **98** + GilMT + GilM + GilR + Fre + FAD + NADPH; B) **98** + GilOII; C) **98** + GilOII + GilMT + GilM + GilR + Fre + FAD + NADPH.

Investigating JadG

Finally we wanted to investigate whether the closely related jadomycin biosynthesis also follows the same pathway regarding the C–C bond cleavage. It had recently been reported that dehydrorabelomycin (**73**) is also a biosynthetic intermediate of the jadomycin A pathway.(*94*, *95*) Among the three oxygenases reported in the biosynthetic pathway of jadomycin, JadG (also a seemingly co-factor free anthrone oxygenase) showed the highest similarity with GilOII (51.5%). Thus, JadG was expressed in *E. coli*, purified to near-homogeneity, and incubated with a mixture of GilM, GilMT, GilR, and the substrate **73**. All the substrate was converted into **45** (Figure 3.2, trace D), confirming our hypothesis. The results here demonstrate the functional equivalence of GilOII and JadG, although earlier cross-complementation experiments showed that swapping of *gilOII* with *jadG* in the *gilOII*-deleted mutant failed to restore gilvocarcin production.(*69*) Adding JadG to a mixture of NADPH, FAD, Fre, and dehydrorabelomycin (**73**) successfully produced hydroxyoxepinone **98** (Figure 3.2, trace E). Thus, the jadomycin biosynthesis shares the same C–C bond key cleavage reaction in its biosynthetic pathway as found for the gilvocarcin pathway.

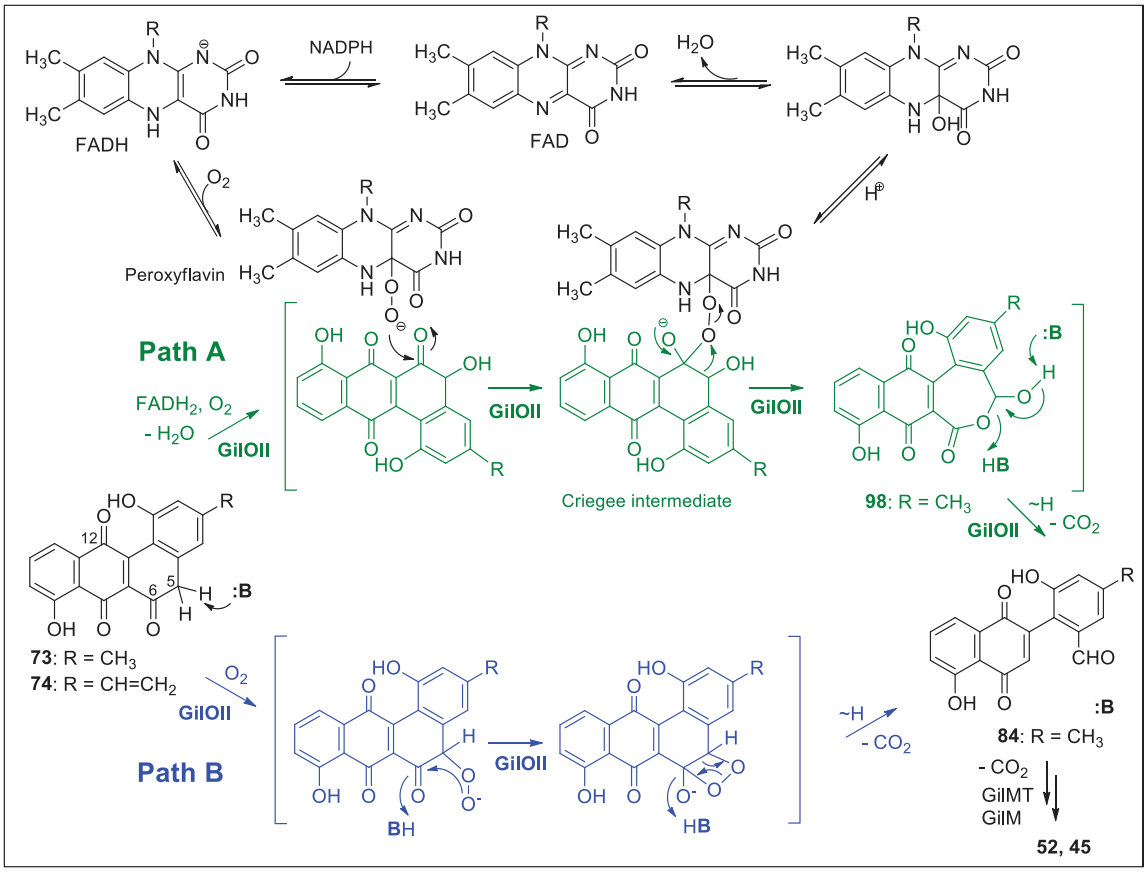

Scheme 0.4 Mechanistic alternatives for the key C–C bond cleavage reaction.

3.2. Discussion

In conclusion, we have shown that two previously believed cofactor free oxygenases, GilOII and JadG, are indeed $FADH_2$-depedent and are responsible for the critical C5–C6 bond cleavage of the benz[*a*]-anthracene skeleton of angucyclinone intermediate **73** and the subsequent rearrangements during the biosyntheses of gilvocarcin and jadomycin, respectively. These enzymes are not cofactor-independent, despite misleading BLAST search results indicating that these enzymes mostly resemble cofactor-free anthrone oxygenases, such as TcmH (43% aa-identity with GilOII)(*31*) or AknX (34% aa-identity with GilOII).(*96*) Anthrone oxygenases require a second oxidation (dehydrogenation) of the immediate hydroquinone to the corresponding quinone to produce the necessary two H atoms for the formation of the second product, a molecule of H_2O. Although GilOII and JadG catalyze a similar first reaction, namely

formation of an 'ortho-hydroquinone', this is not further oxidized to an ortho-quinone, and requires $FADH_2$ instead for the H_2O-formation. Since the product FAD has to leave the active site to be re-reduced to $FADH_2$ (in our experiment by Fre and in the *gil*-pathway presumably by GilH), the cofactor has to move freely and cannot have a tight binding site. The reaction is sequential and requires 2 equiv of $FADH_2$ since the enzymes catalyze both an initial 5-hydroxylation and the following Baeyer-Villiger oxidation, which initiates the scaffold rearrangements in these pathways. The work described here closes the gaps of the gilvocarcin and jadomycin biosyntheses, since oxepinone **98** opens under decarboxylation into aldehyde **84**, which had been synthesized and proven to be an intermediate of both the gilvocarcin(*92*) and jadomycin(*18*) pathways. Baeyer-Villiger monooxygenases(*97*) were also suggested or proven to play key roles in the biosynthesis of other natural products, e.g., the pentalenolactones,(*98*) the aureolic acids,(*30*) BE7585A,(*99*) the aflatoxins,(*100*) and in addition play major roles in degradation processes such as the recently deciphered toxoflavin degradation.(*101*)

3.3. Experimental

Section A. Bacterial strains culture conditions and isolation of compounds

Standard prejadomycin for the large scale preparation of dehydrorabelomycin (**73**) and defucogilvocarcin M (**45**) were isolated from the *S. lividans* TK24 (cosG9B3-OI$^-$) and *S. lividans* TK24 (cosG9B3-GT$^-$) mutant respectively, following previously reported procedure.(*69*) The spores of cultured *Streptomyces* strains on apramycin sulfate (50 μg mL^{-1}) supplemented M2 agar were inoculated into SG liquid medium (100 mL). The seed culture thus prepared was then taken for inoculation of production scale SG medium (5 L; 100 mL × 50 flasks) and grown for 7 days. The culture broth was separated from the mycelia through centrifugation (4000×g, 30 min) and the culture broth was extracted twice with equal volumes of ethyl acetate. The mycelia portion was extracted with acetone by sonication. Both the acetone and the ethyl acetate extract were dried together and the product was purified using preparative scale HPLC (monitored at 254 nm). A linear gradient of acetonitrile and water (solvent A = H_2O; solvent B = acetonitrile; 0–15 min 25% B to 100% B; 16–24 min 100% B; 25–26 min 100% to 25%

B; 27–29 min 25% B) with flow rate of 2.5 mL/min was used to separate the compounds in a Waters Symmetry Prep C_{18} 7μm (19 × 150 mm) column. A photodiode array detector (Waters 2996) along with a Micromass ZQ 2000 mass spectrometer (Waters Corporation) equipped with an atmospheric pressure chemical ionization (APCI) probe was used for the identification of the compounds.

Section B. List of primers used in this study

Table 0.1 List of primers used in this study

Name of the primers	Oligonucleotide sequence (5′→3′)
GilOII_for	GGCCATATGCCGATCATCGAGCCCGAGAAC
GilOII_rev	CGGGAATTCTCACGACGCGTACCCCTCGACCGA
JadG_for	ATCATATGCCTCTGATCAACCCCGAAG
JadG_rev	ATGAATTCCTACTCCGCCGAGCGCGAGTG
GilM_for	CGCCATATGCCAACGGGCAGCACGGAGAAGATC
GilM_rev	CGGGAATTCTCATGCCGGGCTCTCCGATCGGGT
GilMT_for	GACCATATGACCATTACTGCATCGGGATCG
GilMT_rev	CGGGAATTCTCACCGGCTGCGGGGAGAGCCCGG

Section C. Expression and purification of enzymes

All of the genes were expressed with *N*-terminal polyhistidine tag using pET-28a-expression constructs in *E. coli* BL21 (DE3). For the purpose of seed culture a single colony was selected and grown in LB liquid (20 mL) supplemented with kanamycin sulfate (50 μg mL^{-1}) for 4 h. The seed was used to inoculate (10 mL/L) a large scale LB culture and grown at 37 °C until OD600 reached 0.5. The protein production was induced by the addition of isopropyl-*β*-D-1-thio-galactopyranoside (IPTG, 0.2 mM final concentration) and the culture was allowed to grow at 18 °C for 12 h. The cell pellets were collected by centrifugation and washed with lysis buffer (50 mM KH_2PO_4, 300 mM KCl, 10 mM imidazole, pH 8.0). A French Press (Thermo Electron Corporation) was used to disrupt the cells and the crude soluble *N*-terminal $(His)_6$-tagged enzyme fractions were purified through metal talon affinity resin (BD Biosciences) using elution buffer (50 mM KH_2PO_4, 300 mM KCl, 250 mM imidazole, pH 8.0). The size exclusion filters were used for final desalting. The protein concentrations were determined by the Bradford

method using a calibration curve of the known concentrations of BSA and the purities were estimated by sodium dodecylsulfate-polyacrylamide gel electrophoresis (SDS-PAGE) analyses.(*102*) The measured sizes of the proteins were in good agreement with the calculated one. For storage purpose of the purified enzymes 50 mM phosphate buffer (pH 7.5) supplemented with glycerol (25% final volume) were used.

Section D. Combinatorial biosynthetic enzymology experiments

Enzymatic reactions carried out using dehydrorabelomycin (**73**) as substrate along with different combinations of enzymes are described below. All the reactions for the combinatorial studies contained phosphate buffer (pH 6.5, 50 mM), dehydrorabelomycin (50 μM), NADPH (50 μM), FAD (50 μM), SAM (100 μM), *E. coli* Fre (2 μM), and an NADPH regeneration system consisting of glucose-6-phosphate (10 mM) and glucose-6-phosphate dehydrogenase (10 μM). 1 mL assay mixture was incubated with different combinations of enzymes (10–15 μM of each) for 6–8 h and the reactions were monitored using the HPLC conditions described in section A at 375 nm.

Table 0.2 *In vitro* enzymatic reactions of **73**.

Expt. No.	GilOII/JadG	GilM	GilMT	GilR	Product(s)
1	+	+	+	+	defucogilvocarcin M (**45**)
2	+	+	+	-	defucopregilvocarcin M (**52**)
3	+	+	-	-	Starting material decomposed

Section E. In vitro enzymatic reactions

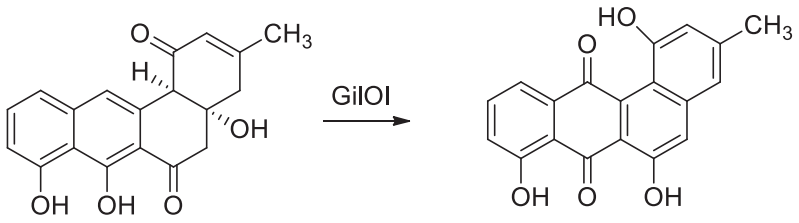

Prejadomycin (**55**) Dehydrorabelomycin (**73**)

Synthesis of dehydrorabelomycin (73) from prejadomycin

An assay mixture (10 mL) containing phosphate buffer (pH 6.5, 50 mM), prejadomycin (80 μM), GilOI (15 μM), NADPH (20 μM), glucose-6-phosphate (2 mM), and glucose-6-phosphate dehydrogenase (10 μM) was incubated at 28 °C for 6 h. The reaction was extracted with ethyl acetate (3 × 20 mL), concentrated under reduced pressure and purified using preparative scale HPLC following the conditions mentioned in section A (monitored at 460 nm). The product dehydrorabelomycin (**73**) was obtained almost in quantitative amounts.(*78*)

Reaction of dehydrorabelomycin (73) with GilMT

An assay mixture (5 mL) containing phosphate buffer (pH 6.5, 50 mM), dehydrorabelomycin (**73**) (60 μM), GilMT (120 μM), and S-adenosylmethionine chloride (SAM) (200 μM) was incubated at 28 °C for 4 hours. The reaction was stopped by flash-cooling to -78 ºC (dry ice/acetone bath) and the product was extracted with ethyl acetate (3 × 10 mL). The organic layer was dried under reduced pressure and purified using HPLC following the conditions mentioned in section A (monitored at 460 nm). The yield of the product **95** was ~ 90% while both of the **96** and **97** was produced < 1%.

Table 0.3 High resolution mass spectroscopy data of compounds **95–97.**

Compound	HRMS (+EI)	
	Calc'd	Observed
95; $C_{21}H_{16}O_5$	348.0998	348.0999
96; $C_{20}H_{14}O_5$	334.0841	334.0850
97; $C_{20}H_{14}O_5$	334.0841	334.0847

Reaction of dehydrorabelomycin (73) with GilOII to produce compound 98

A typical assay mixture (1 mL) containing phosphate buffer (pH 6.5, 50 mM), dehydrorabelomycin (**73**) (50 μM), GilOII (12 μM), glucose-6-phosphate (1 mM), glucose-6-phosphate dehydrogenase (10 μM), FAD (50 μM), NADPH (20 μM), and *E. coli* Fre (2 μM) was incubated at 28 °C for 8 hours. The reaction was stopped by flash-cooling to -78 ºC (dry ice/acetone bath) and the product was extracted with ethyl acetate (3 × 2 mL). The organic layer was dried under reduced pressure and purified using HPLC following the conditions mentioned in section A (monitored at 420 nm). This reaction was repeated ~ 200 times to yield a combined product **98** of ~ 90 μg. HRMS (ESI): $[M - H_2O]^+$ Calc'd for $C_{19}H_{12}O_7$: 335.0555, observed: 335.0555.

Section F. Spectral data

The NMR spectra were acquired on a Varian MR 400 spectrometer (B_0 9.4 T*)* and a Bruker Avance 600 (B_0 14.09 T) spectrometer equipped with a 1.7 mm cryoprobe and a Bruker Avance 500 (B_0 11.74 T) spectrometer equipped with a 5 mm cryoprobe. Deuterated chloroform was used as NMR solvent for all spectra recorded.

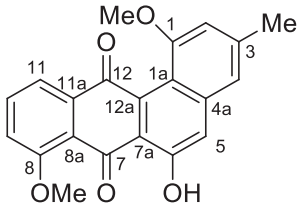

1,8-Dimethoxy dehydrorabelomycin (**95**)

Table 0.4 ^{1}H, ^{13}C , NOESY and gHMBC data for 1,8-Dimethoxy dehydrorabelomycin (**95**) in $CDCl_3$ (500 MHz, relative to internal TMS, J in Hz).

Position	^{1}H NMR	^{13}C NMR	1D NOESY	gHMBC
1	-	157.1	-	-
1-OMe	3.92 (s, 3H)	56.1	-	1
1a	-	115.8	-	
2	6.64 (s, 1H)	108.6	1-OMe, 3-Me	4, 3-Me
3	-	141.6	-	-
3-Me	2.47 (s, 3H)	22.5	-	2, 3, 4
4	7.06 (s, 1H)	118.6	3-Me, 5-H	1a, 2, 5
4a	-	137.0	-	-
5	7.34 (s, 1H)	117.1	4-H	1a, 4, 6, 12a
6	-	157.1	-	-
6-OH	12.25 (s, 1H)	-	-	5, 6, 12a
7	-	188.9	-	-
7a	-	140.4	-	-
8	-	160.1	-	-
8a	-	120.2	-	-
8-OMe	4.06 (s, 3H)	56.8	-	8
9	7.27 (d, 1H, J = 8.0 Hz)	116.8	8-OMe, 10-H	8a, 11
10	7.72 (dd, 1H, J = 8.0, 7.5 Hz)	136.2	-	8, 11a
11	7.66 (d, 1H, J = 7.5 Hz)	118.8	-	8a, 9, 12
11a	-	139.4	-	-
12	-	186.7	-	-
12a	-	119.7	-	-

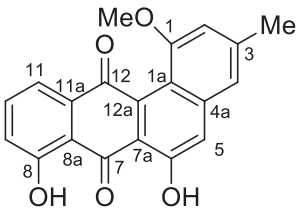

1-Methoxy dehydrorabelomycin (**96**)

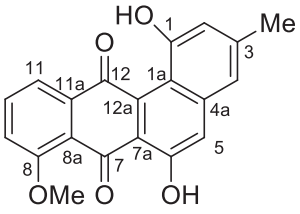

8-Methoxy dehydrorabelomycin (**97**)

Table 0.5 ^{1}H data for **96** and **97** in $CDCl_3$ (500 MHz, relative to internal TMS, J in Hz).

Position	^{1}H NMR of **96**	^{1}H NMR of **97**
1	-	-
1-OMe/1-OH	3.92 (s, 3H)	10.12 (s, 1H)
1a	-	-
2	6.65 (s, 1H)	6.94 (s, 1H)
3	-	-
3-Me	2.48 (s, 3H)	2.44 (s, 3H)
4	7.07 (s, 1H)	7.09 (s, 1H)
4a	-	-
5	7.36 (s, 1H)	7.65 (s, 1H)
6	-	-
6-OH	11.67 (s, 1H)	12.72 (s, 1H)
7	-	-
7a	-	-
8	-	-
8a	-	-
8-OH/8-OMe	11.58 (s, 1H)	4.09 (s, 3H)
9	7.38 (d, 1H, J = 9.0 Hz)	7.27 (d, 1H, J = 8.5 Hz)
10	7.72 (dd, 1H, J = 8.0, 7.5 Hz)	7.78 (dd, 1H, J = 8.0, 8.5 Hz)
11	7.58 (dd, 1H, J = 7.5, 1.5 Hz)	7.91 (dd, 1H, J = 7.5, 1.0 Hz)

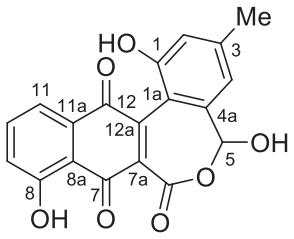

Oxepinone derivative **98**

Table 0.6 ^{1}H, ^{13}C , gHSQC and gHMBC data for **98** in $CDCl_3$

Position	^{1}H NMR	^{13}C NMR	HSQC	HMBC
1	-	155.1	-	
1-OH	10.89 (s)	-		1a, 1, 2
1a	-	108.2*		
2	6.96 (s)	122.0	122.0	1a, 4
3	-	not observed		
3-Me	2.38 (s)	21.4	21.4	2, 4, 4a
4	6.74 (s)	119.1	119.1	1a, 2, 3-CH_3, 5
4a	-	143.7*		
5	6.52 (d, J = 5.5 Hz)	94.5	94.5	
5-OH	3.56 (d, J = 5.5 Hz) D_2O exchangeable	-		
6	-	not observed		
7	-	183.7		
7a	-	144.2		
8	-	161.8		
8-OH	11.72 (s)	-		8a, 8, 9
8a	-	113.5*		
9	7.31 (d, J = 8.5 Hz)	125.4	125.4	8a
10	7.67 (dd, J = 8.5, 7.5 Hz)	137.3	137.3	
11	7.83 (d, J = 7.5 Hz)	121.5	121.5	8a, 9,12
11a	-	132.4		
12	-	186.7*		
12a	-	140.9		

* From HMBC

Tibrewal, N., Pahari, P., Wang, G., Kharel, M. K., Morris, C., Downey, T., Hou, Y., Bugni, T. S., Rohr, J. Baeyer-villiger C–C bond cleavage reaction in gilvocarcin and jadomycin biosynthesis *J. Am. Chem. Soc.* **2012**, *134*, 18181–18186.

Chapter 4. Exploring promiscuous GilM and GilMT: Chemoenzymatic synthesis of pre-defucogilvocarcin M analogues

Constructing gilvocarcin's core is a difficult synthetic venture. In the past two decades several synthetic groups tried and demonstrated a long streak of steps required to generate the core.(*103-106*) Recently, Snieckus and James reported a 20 step long total synthesis of defucogilvocarcin M (**45**).(*104*) Despite several attempts, none of the synthetic groups succeeded in providing protocols that are short and practical. Synthetic chemistry has long been used to generate natural products and their structural analogues. Additionally, chemical synthesis offers great opportunities to provide pharmacologically improved molecules. Unfortunatly, these syntheses occasionally become challenging to scale up because of structural complexities within these molecules. In such cases, it becomes imperative to develop new strategies that can overcome synthetic hurdles.

The catalytic power of the enzymes from biosynthetic pathways could be harnessed and used to aid traditional synthetic protocols in the efficient and economical generation of natural product analogues.(*107-111*) A deep understanding of the gene products involved in the biosynthetic manufacturing of gilvocarcin has enabled us to exploit various downstream enzymes in the achievement of difficult synthetic steps (Scheme 4.1). In this section, we report our initial attempts to explore the proposed chemoenzymatic synthesis, where two critical downstream enzymes, GilM and GilMT, were investigated with respect to their substrate flexibility. A small series of analogues of compound **84** generated via chemical route were fed to various mixtures of the enzymes and the reactions were analyzed to establish the diversity of substrates tolerated.

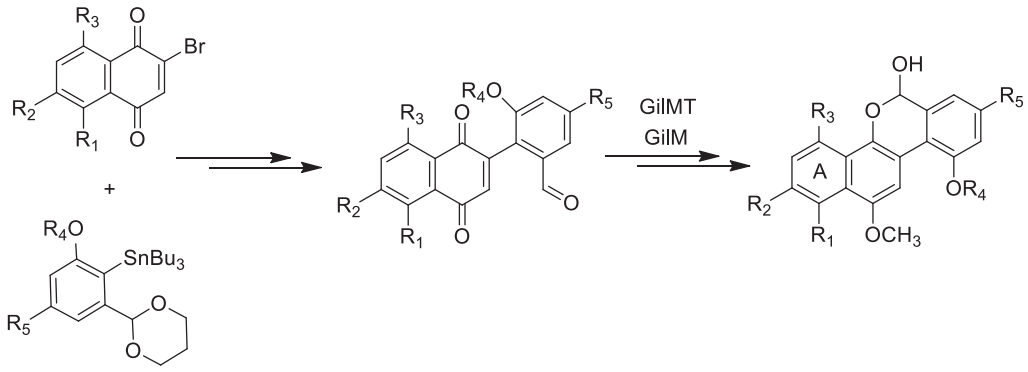

Scheme 0.1 Chemoenzymatic strategy for the synthesis of pre-defucoGM analogues.

4.1. Results and Discussions

Our strategy capitalized on the easy and practical synthesis of compound **84** as discussed in chapter 2. We used the synthetic route to compound **84,** utilizing Stille coupling, as a framework for generating analogues. Our initial attempts focused on varying the position of hydroxyl group on ring A. With this idea in mind, we attempted controled introduction of bromine into the 3-position of the commercially available juglone (Scheme 4.2).(*112, 113*) The treatment with bromine was followed by debromination of the crude dibrominated adduct selectively gave 3-bromojuglone (**99**) as an orange solid. The differences in melting point and the polarities of the 2- and 3-regioisomers assisted in an easy separation of the two. A palladium catalyzed Stille coupling reaction between **86** and **99** yielded the coupled product in 75% yield. A careful acidic treatment with concentrated HCl in acetonitrile provided the desired product, containing a hydroxyl group at position-8, as an orange solid.

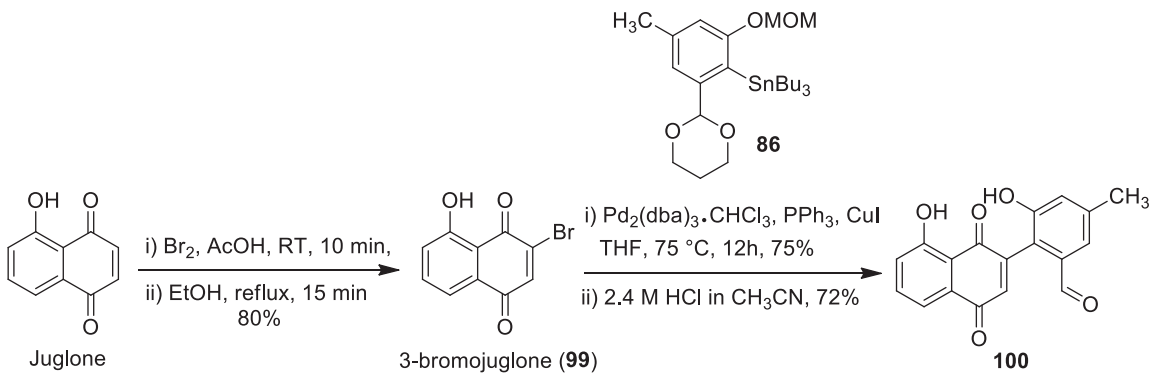

Scheme 0.2 Synthesis of **100**.

We also considered analogues with additional hydroxyl groups as suitable substrates for GilM and GilMT. We envisaged that an additional hydroxyl or amino group should add more polar properties into the molecule, rendering it more water-soluble. The compound **101** with an additional hydroxyl group in 10-position was proposed to be assembled by a Stille coupling between dihydroxy-bromojuglone (**102**) and **86** (Scheme 4.3). **102** was prepared by a Diels–Alder addition of 1-methoxy-1,3-bis(trimethylsilyloxy)-1,3-butadiene (**105**) to 2,5-dibromo-1,4-benzoquinone (**107**) in dry benzene (Scheme 4.3).(*114*) The latter was synthesized via ceric ammonium nitrate (CAN)-mediated oxidative demethylation of 2,5-dibromo-1,4-dimethoxybenzene.(*115*) The diene **105** was prepared from silyl enol ether **104** (Scheme 4.4) that in turn was accessible from methyl acetoacetate following a procedure reported in literature.(*116*) A solution of freshly distilled methyl acetoacetate and triethylamine in hexane was treated with trimethylsilyl chloride and stirred for 18 h. The resulting mixture was passed through celite and the filtrate was concentrated and distilled (100 °C/20 mmHg) to give methyl-3-(trimethylsiloxy)-2-butenoate (**104**). Methyl-3-(trimethylsiloxy)-2-butenoate was deprotonated with freshly prepared LDA in THF at -78 °C followed by silylation with trimethylsilylchloride to give the desired diene in 95% yield. A palladium catalyzed coupling between **102** and **86** yielded the protected coupled product (**108**) in 4% yield. The routine treatment of the protected compound **108** with 2.4 M HCl in acetonitrile resulted in decomposition of the material. We tried acidifying the reaction mixture at low

temperatures but that was also unsuccesful. Unfortunately, several attempts to deprotect the MOM group failed to yield the desired product (**101**).

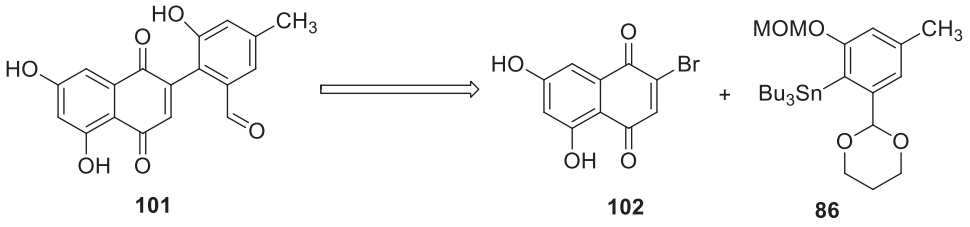

Scheme 0.3 Retrosynthetic analysis of **101**.

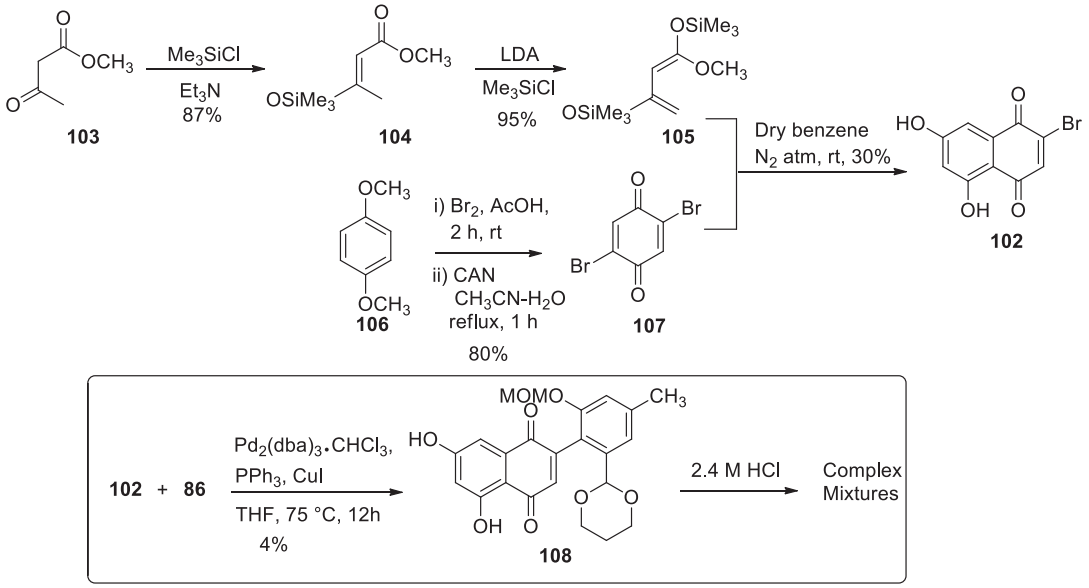

Scheme 0.4 Attempted synthesis of **101**.

We then moved our focus to the substituted hydroxyl derivative (**112**). The formation of 2-chloro-6-methoxy-8-hydroxy-1,4-naphthoquinone (**111**) was achieved through a Diels-Alder cycloaddition of the Bassard's diene (**109**)(*117*) onto the commercially available 2,6-dichloro-1,4-benzoquinone (**110**). This reaction was perfomed at -30 °C in THF followed by a vigorous aromatization for 24 h at room temperature in presence of excess deactivated silica (Scheme 4.5).(*118*) The resulting napthoquinone (**111**) was coupled with stannane **86** and subsequently subjected toacidic deprotection. A room temperature acid treatment resulted in decomposition of the starting material with no product formation. However, a very careful HCl treatment at 0°C

provided the desired analogue in very low yields (2%). Acidification at even lower temperatures did not affect the yield.

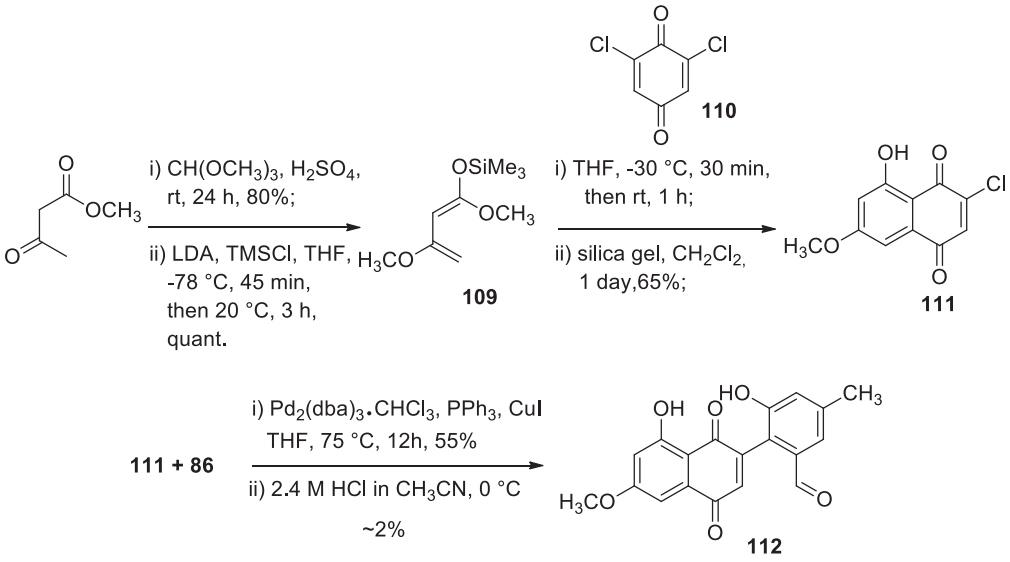

Scheme 0.5 Synthesis of **112**.

Another venture was to see whether the enzymes can handle more bulky substrate, i.e. to see how strict GilM was with respect to sterical requirements. Thus, a benzylated substrate was well suited for the study. Benzylation of bromojuglone (**85**) was carried out with freshly prepared silver oxide and benzyl chloride. Palladium catalyzed coupling with **86** followed by global acidic deprotection provided the benzylated substrate (**114**) (Scheme 4.6).

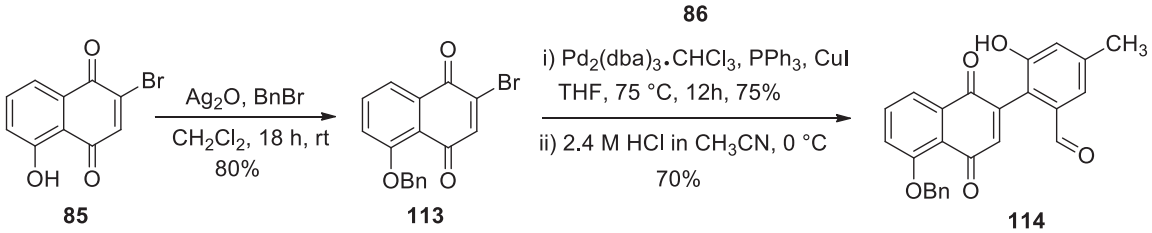

Scheme 0.6 Synthesis of benzylated derivative **114**.

We also sought to check if the hydroxyl group in 5'-position in the natural substrate (**84**) and methyl group in 5-position were critical for enzyme activity. Coupling

between commercially available 2-bromo-1,4-naphthoquinone (**115**) and the stannane **86** followed by acidic deprotected yielded the required fully deprotected analogue (**116**).

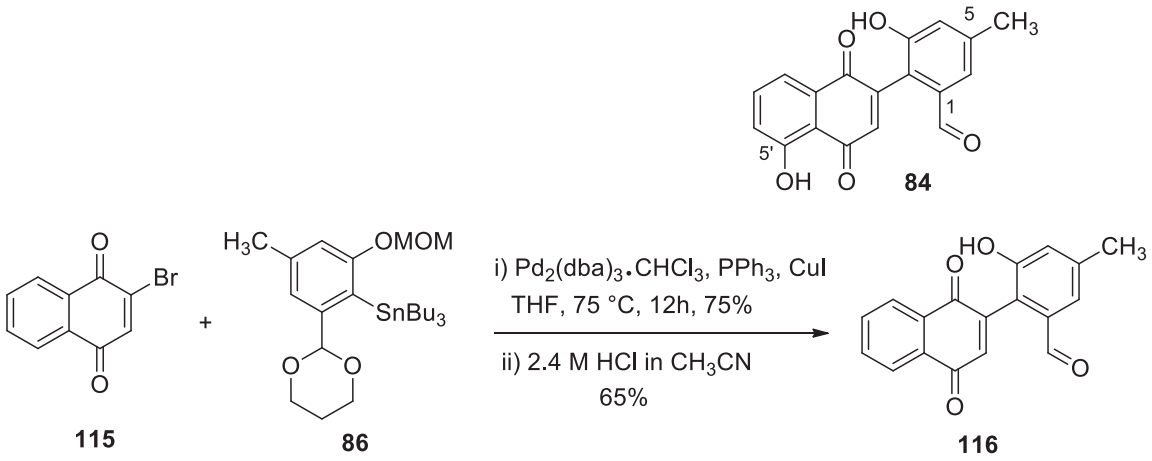

Scheme 0.7 Synthesis of **116**.

The demethylated analogue (**120**) was prepared by coupling bromo-juglone (**85**) and stannane (**119**) (Scheme 4.8). Synthesis of the latter began from commercially available m-hydroxybenzaldehyde (**117**). Protection of the hydroxyl group as a MOM ether and the aldehyde as a cyclic acetal group provided substrate (**118**) for ortho-lithiation. *n*-Butyl lithium-mediated selective ortho-deprotonation followed by quenching with tributyltinchloride gave the required stannane (**119**) in 88% yield. A low-temperature acidic treatment of the coupled product provided analogue **120** along with small quantities of the MOM-protected derivative **121**, which we thought was a great analogue to test if the enzymes could tolerate ethers other than methyl ether (**92**).

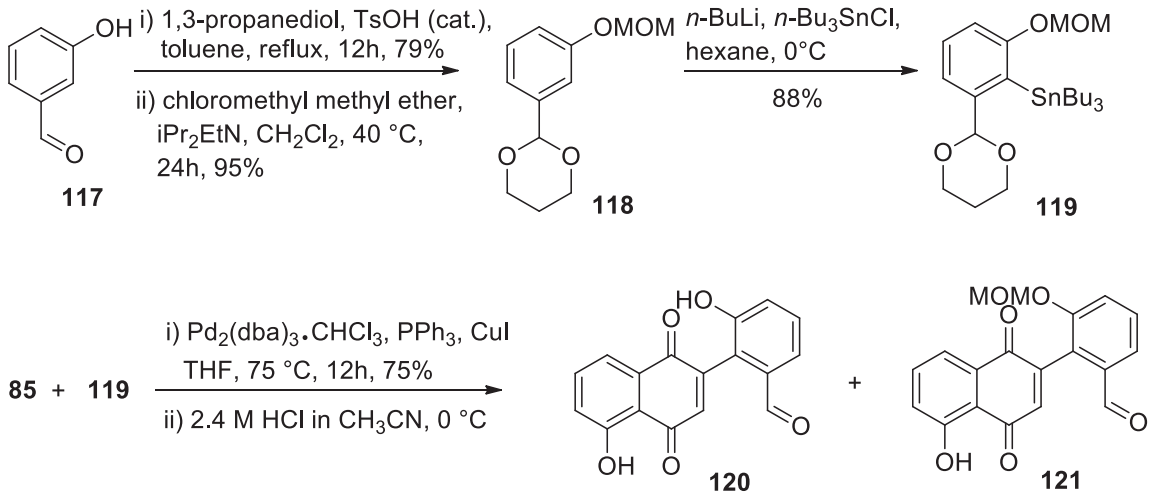

Scheme 0.8 Synthesis of derivatives **120** and **121**.

After developing a small series of analogues with different substituents decorating the core substrate, we fed them to a mixture of GilM and GilMT and analyzed the reactions at different time points. An assay mixture (0.5 mL) composed of phosphate buffer (pH 6.5, 50 mM), substrate analogue (10 μM), S-adenosylmethionine (excess), GilMT (1 μM), and GilM (1 μM) was incubated at 30 °C. 100 μl of assay mixture was withdrawn at progressive time intervals of time and was extracted with EtOAc (2 × 250 μL). The organic solvent was dried at low pressure and the crude product was dissolved in CH_3CN. The solution was then subjected to LC-MS analysis. A linear gradient of acetonitrile and 0.1% formic acid-water (solvent A = 0.1% formic acid-H_2O; solvent B = acetonitrile; 0-15 min 25% B to 100% B; 16-24 min 100% B; 25-26 min 100% to 25% B; 27-29 min 25% B) with flow rate of 0.5 mL/min was used to separate the compounds in a Waters Symmetry C_{18} (4.6 × 250 mm, 5μm) column.

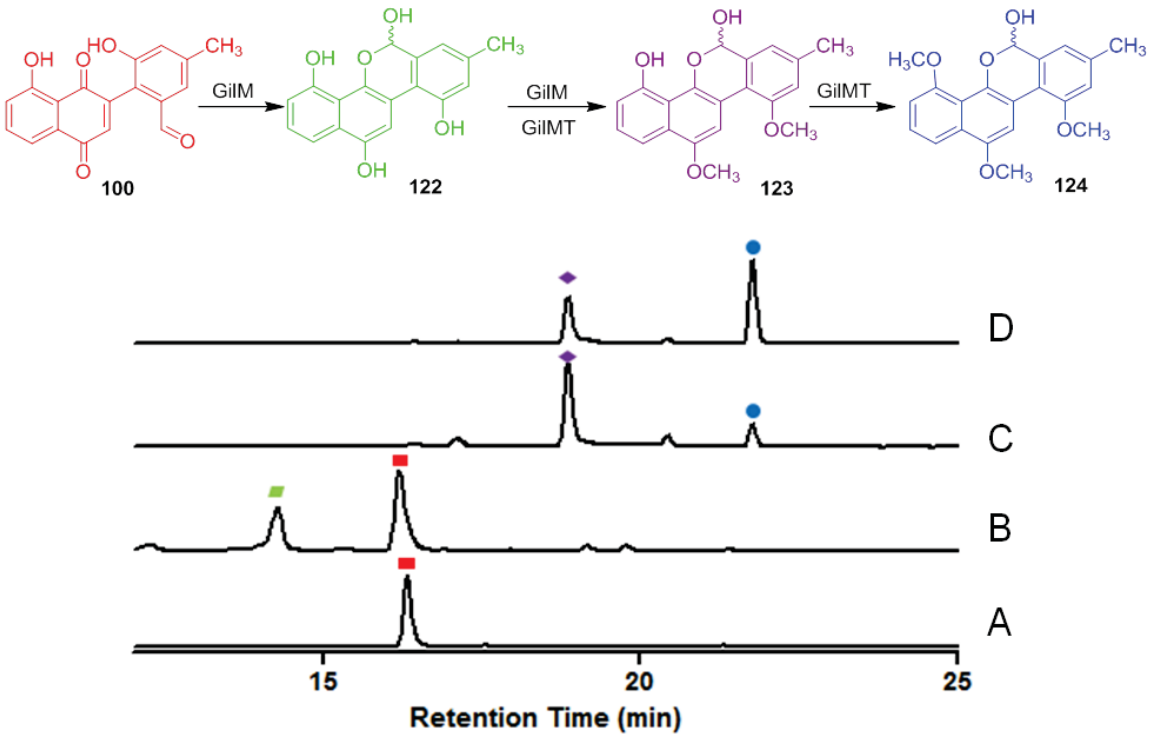

Figure 0.1 HPLC traces of the enzymatic reactions with **100**: (A) standard **100**; (B) **100** + GilM + GilMT + SAM + 15 min; (C) **100** + GilM + GilMT + SAM + 2 h; (D) **100** + GilM + GilMT + SAM + 18 h.

Figure 4.1 shows the HPLC traces of the enzymatic reactions of analogue **100** with GilM and GilMT in presence of SAM. Compound **100** underwent initial quinone reduction to generate the hydroquinone, followed by subsequent intramolecular cyclization to give hemiacetal **122** (Figure 4.1, trace B). GilM, as expected, catalyzed the first *O*-methylation followed by a GilMT-mediated second *O*-methylation to give the anticipated defuco-pregilvocarcin M analogue **123** (Figure 4.1, trace C). Further incubation of the enzyme mixture for 18 h resulted in over methylated product **124** (Figure 4.1, trace D). The ability of GilM and GilMT to catalyze the series of the reactions leading from **100** to **123**, shows that both GilM and GilMT are broad enough to accommodate other regioisomers with respect to the hydroxyl group in ring A.

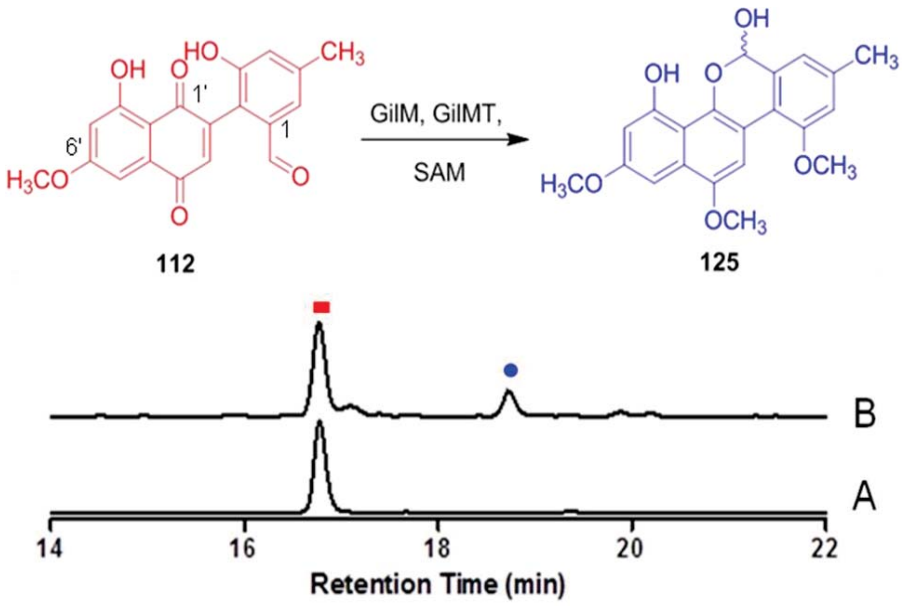

Figure 0.2 HPLC traces of the enzymatic reactions with **112**: (A) standard **112**; (B) **112** + GilM + GilMT + SAM + 18 h.

When compound **112,** with an additional methoxy group in 6'-position, was incubated with GilM and GilMT, no new product was produced after the first 4 h. However, after overnight incubation, a new peak was formed with a longer retention time in comparison to the starting material and a chromophore similar to that of defuco-pregilvocarcin M. Low-resolution mass analysis of the new peak is consistent with compound structure **125** (Figure 4.2; trace B). Based on the area under curve of the HPLC peak the conversion was 15%. The very slow turnover of **112** by GilM shows that GilM's binding pocket can hardly accommodate an additional methoxy group in 6'-position. To further test GilM's ability to handle bulky substrates, we incubated the benzylated derivative **114** with GilM and GilMT. This reaction did not accumulate any cyclized product clearly indicating that the GilM catalytic pocket has enough extra room to accommodate smaller substituents but is too tight for bulky substituents like benzyl groups.

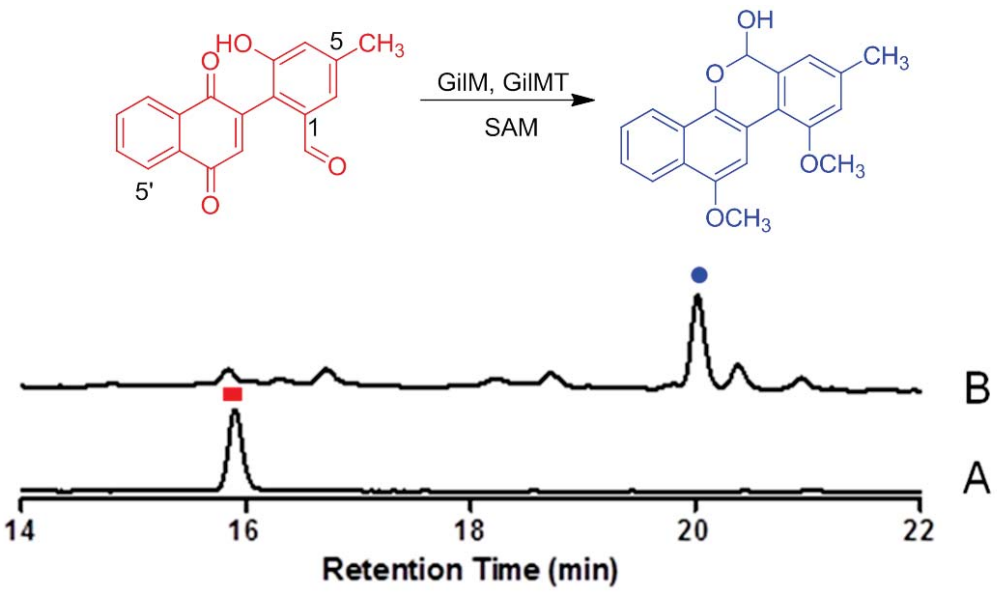

Figure 0.3 HPLC traces of the enzymatic reactions with **116**: (A) standard **116**; (B) **116** + GilM + GilMT + SAM + 2 h.

To further explore the sterical effects and interrogate whether the hydroxyl group in 5'-position and methyl group in 5-position of compound **84** are critical for enzyme activities, we incubated demethylated derivative **116** with GilM and GilMT. As anticipated, after 2 h **116** was fully converted to **126** (Figure 4.3; trace B). Compound **116** is of particular interest as it would be useful in solving the often-asked question of whether or not the 1-OH of predefuco-gilvocarcin M (**52**) directs the glycosylation reaction in 4-position. The demethylated derivative **120** was also tested and found to be successfully turned over by a mixture of GilM and GilMT (Figure 4.4).

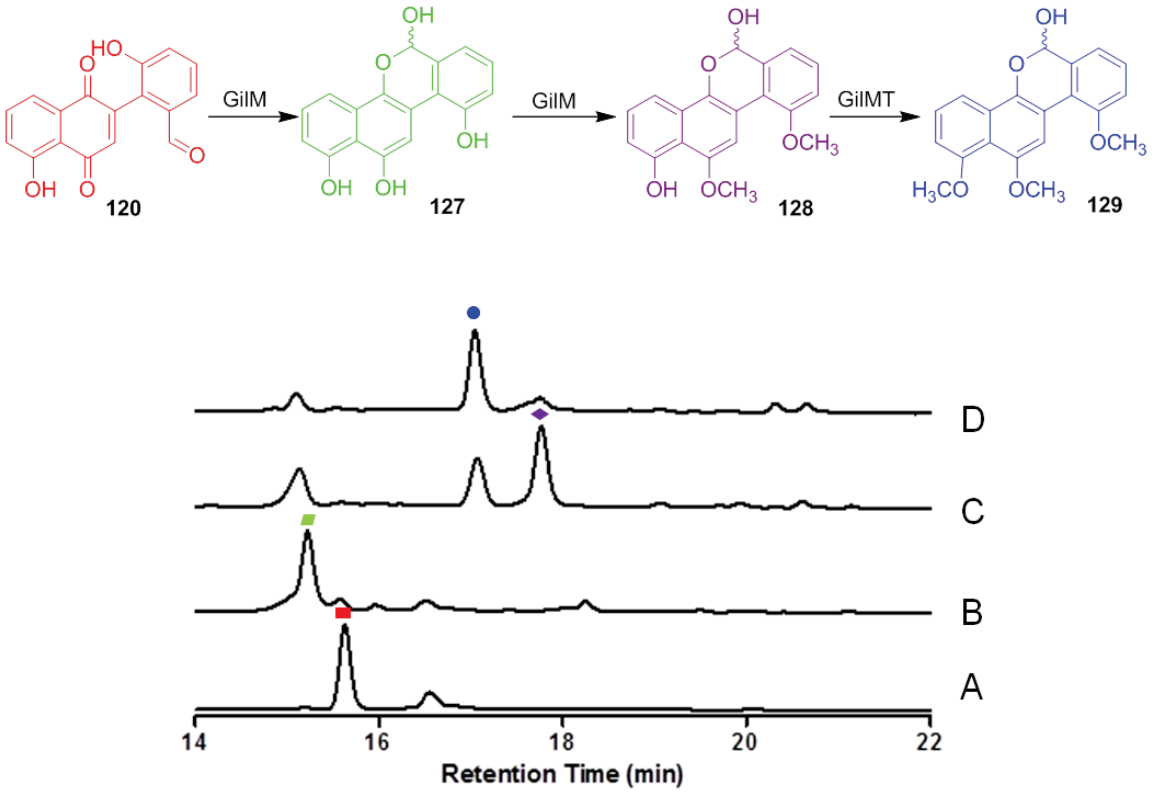

Figure 0.4 HPLC traces of the enzymatic reactions with **120**: (A) standard **120**; (B) **120** + GilM + GilMT + SAM + 15 min; (C) **120** + GilM + GilMT + SAM + 2 h; (D) **120** + GilM + GilMT + SAM + 18 h.

Furthermore, compound **121** with its 3-OH presubstituted with the bulkier methoxy methyl ether, was additionally found to be smoothly accepted as a substrate by both GilM and GilMT (Figure 4.5). After incubation with GilM for 15 min, **121** underwent quinone reduction and cyclization to form the hemiacetal, a demethyl-predefucogilvocarcin **130** type derivative (Figure 4.5; trace B). After an 18 h incubation period, compound **132** was isolated (Figure 4.5; trace D). Strikingly, GilM is promiscuous enough to accommodate a wide variety of substrates. The enzymatic conversion of **121** to **132** is a major stepping-stone towards total chemoenzymatic synthesis of gilvocarcin type compounds with diverse range of pharmacophores.

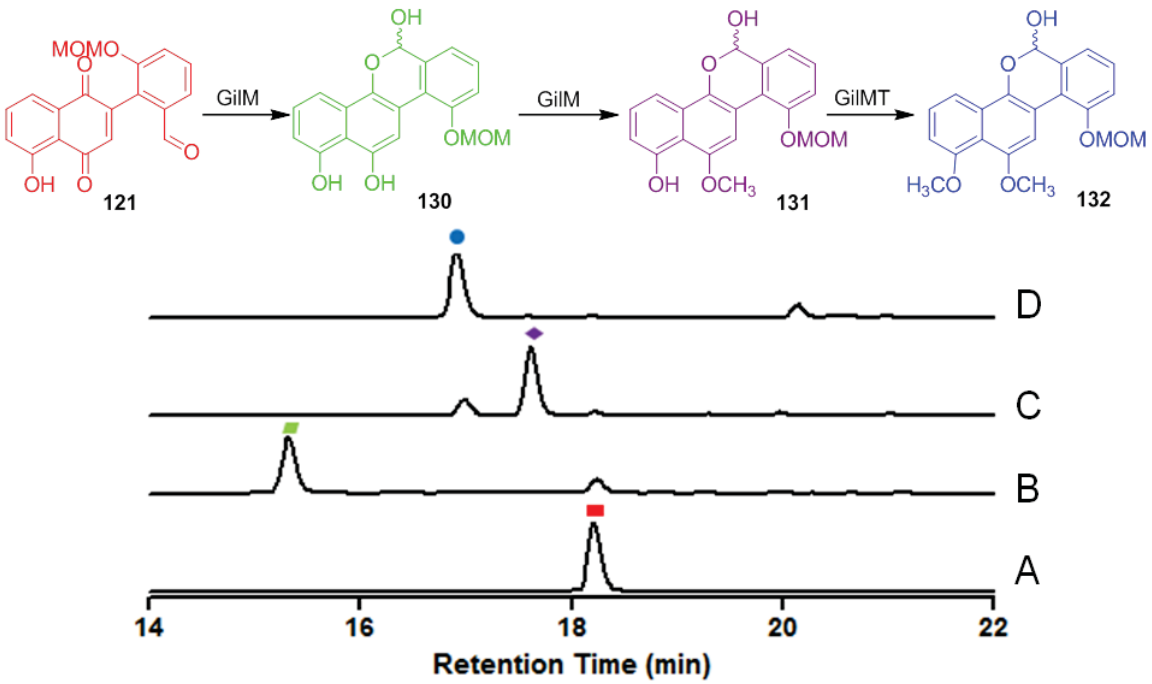

Figure 0.5 HPLC traces of the enzymatic reactions with **121**: (A) standard **121**; (B) **121** + GilM + GilMT + SAM + 15 min; (C) **121** + GilM + GilMT + SAM + 2 h; (D) **121** + GilM + GilMT + SAM + 18 h.

All analogues, except the bulky benzylated derivative **114**, showed a sequence of events similar to those displayed by the natural substrate **84**. GilM was shown to be relatively accommodating towards aromatic substitution patterns different from the natural substrate. Additonally, GilMT was shown to be more promiscuous than GilM. Interesting, it was also found that when the reaction mixtures were left for 18 h or more GilMT catalyzed a second *O*-methylation despite occupation of the first catalytic site. This initial testing of substrates for GilM and GilMT and chemoenzymatic synthesis of defuco-preGM type analogues forges the way for future exploration of more drastic substrates. From the drug development standpoint, our findings make the future prospectives of a gilovocarcin type anticancer antibiotic look even brighter then previously thought.

4.2. Experimental

3-bromojuglone (**99**)

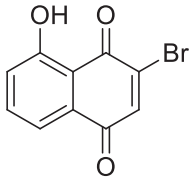

A suspension of commercially available juglone (1.2 g, 6.89 mmol) in acetic acid (18 mL) was treated with bromine (6.89 mmol, 0.36 mL) in the dark at 25 °C. After stirring for 15 min, the reaction mixture was poured onto ice and the resulting slurry stirred. After 10 min the dibrominated intermediate was filtered off under reduced pressure. The resulting solid was washed with 5 mL of ice-water followed by immediate washing with ethanol (10 mL) and stirring for 10 min under reflux. The mixture was cooled down to room temperature and the resulting red precipitate was filtered off under reduced pressure. After washing with cold ethanol, the residue was subjected to silica gel chromatography to give 3-bromojuglone **99**(*113*) as an orange solid (1.4 g, 80%). M.p. 170 °C; ^{1}H NMR (500 MHz, $CDCl_3$) δ 11.7 (s, 1H), 7.66–7.61 (m, 2H), 7.47 (s, 1H), 7.29 (dd, J = 8 Hz, 1.5 Hz, 1H).

Compound 100

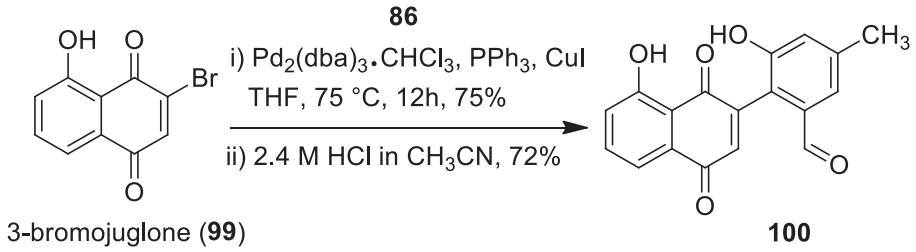

A suspension of 3-bromo-5-hydroxy-1,4-naphthaquinone **99** (48 mg, 0.19 mmol), stannane **86** (100 mg, 0.19 mmol), and CuI (3.8 mg, 0.02 mmol) in THF (4 mL) was added to a solution of $Pd_2(dba)_3$•$CHCl_3$ (4.9 mg, 0.0045 mmol) and PPh_3 (5.4 mg, 0.02 mmol) in THF (1 mL). The mixture was heated at 75 °C for 12 h. The mixture was cooled to 0°C and diluted with EtOAc (10 mL). Saturated aqueous $NaHCO_3$ (10 mL) was added and the mixture was stirred for 30 min. The layers were separated and the aqueous layer extracted twice with EtOAc (25 mL). The combined organic layers were washed with brine and dried over Na_2SO_4. The solvent was removed under vacuum and the

resulting residue subjected to flash silica gel column chromatography to provide the coupled product (20% EtOAc-hexane, R_f = 0.25) as an orange solid (75%). 1H NMR (acetone-d_6, 500 MHz) δ 12.0 (s, 1H), 7.80 (dd, J = 8.5, 7.5 Hz, 1H), 7.65 (dd, J = 7.5, 1.0 Hz, 1H), 7.35 (dd, J = 8.5, 1 Hz, 1H), 7.16 (d, J = 0.5 Hz, 1H), 7.07 (d, J = 0.5 Hz, 1H), 6.89 (s, 1H), 5.50 (s, 1H), 5.13 (s, 2H), 4.03–3.96 (m, 2H), 3.86–3.75 (m, 2H), 3.33 (s, 3H), 2.39 (s, 3H), 1.98–1.85 (m, 1H); ^{13}C NMR (acetone-d_6, 125 MHz) δ 190.5, 184.6, 162.4, 155.4, 148.2, 140.8, 139.2, 138.9, 137.5, 124.7, 121.3, 119.1, 115.8, 100.7, 95.3, 67.6, 56.3, 26.4, 23.3, 21.8, 14.4. (+EI): Calc'd for $C_{23}H_{22}O_7$ 410.1365, observed: 410.1362.

A solution of concentrated HCl (2 mL) in 10 mL CH_3CN was added to the above coupled product (55 mg, 0.13 mmol) in a 250 mL flask at r.t. The mixture was stirred for 4 min, quenched with $NaHCO_3$ (60 mL), and EtOAc (50 mL) was added. After separation of the layers, the aqueous layer was extracted with EtOAc twice. The combined organic layer was washed with brine, dried over Na_2SO_4. The solvent was then removed under vacuum. The resulting residue was subjected to purification by flash silica gel column chromatography (40% EtOAc-hexane, R_f = 0.25) to provide the desired product **100** as an orange solid (72%). ^{1}H NMR (acetone-d_6, 400 MHz) δ 11.93 (bs, 1H), 9.94 (s, 1H), 9.02 (bs, 1H), 7.83 (t, J = 10.5 Hz, 1H), 7.66–7.64 (m, 1H), 7.41–7.34 (m, 2H), 7.20–7.18 (m, 1H), 6.95 (s, 1H), 2.39 (s, 3H); ^{13}C NMR (acetone-d_6, 100 MHz) δ 193.0, 190.5, 184.5, 162.5, 156.1, 147.5, 142.1, 138.7, 137.7, 137.3, 133.6, 126.4, 124.8, 124.7, 123.3, 119.2, 116.4, 21.1; HRMS (+EI): Calc'd for $C_{18}H_{12}O_5$: 308.0685, observed: 308.0686.

1,3-Bis(trimethylsiloxy)-1-methoxybuta-1,3-diene (105)

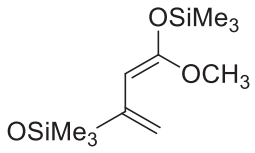

Trimethylsilyl chloride (1.3 mL, 9.2 mmol) in dropwise increments was added to a solution of freshly distilled methyl acetoacetate (1.0 mL, 9.2 mmol) and triethylamine (1.5 mL, 11.1 mmol) in hexane (10 mL). The resulting mixture was stirred at room

temperature for 18 h. The mixture was then passed through a short pad of celite and the filtrate concentrated in vacuo. The residue was distilled (100 °C/20 mmHg) to give methyl 3-(trimethylsiloxy)-2-butenoate (**104**) (80%). **104** (0.75g, 3.7 mmol) was added dropwise to a freshly prepared solution of LDA (4 mmol) in THF at –78 °C. After 30 min trimethylsilyl chloride (0.6 mL, 5 mmol) was slowly added and the reaction mixture warmed to 0 °C. After 1 h, all volatile materials were removed in vacuo at room temperature, and the residue washed with dry hexane. The residue was further distilled (50 °C/0.01 mmHg) to give **105** (97%).(*116*)

2,5-Dibromo-1,4-benzoquinone (107)

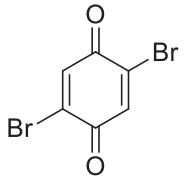

At room temperature, Br_2 (4 mL, 72.5 mmol) in acetic acid (5 mL) was added dropwise to a solution of 1,4-dimethoxybenzene (**106**, 5g, 36.25 mmol) in acetic acid (10 mL). After stirring for 2 h, the solution was cooled and the resulting white precipitate of 2,5-dibromo-1,4-dimethoxybenzene filtered. The filtrate was further diluted with water (15 mL) and extracted with $CHCl_3$ (2 X 10 mL). The organic layer was washed with 10% aqueous $NaHCO_3$, dried over Na_2SO_4 and dried under vacuum to yielding a total amount of 10 g of 2,5-dibromo-1,4-dimethoxybenzene. A portion of the white solid (5 g, 16.9 mmol) was dissolved in CH_3CN (50 mL) in an oil bath at 100 °C. A solution of cerium ammonium nitrate (25.0 g, 45.6 mmol) in water (150mL) was added to the boiling CH_3CN solution. After completion of the addition, the heat was turned off and the reacting mixture was left to cool to room temperature. The precipitate formed on cooling was filtered and washed with water (30 mL), yielding 3.8 g (80% overall) of **107**, as a yellow solid.(*115*) HRMS (+EI): Calc'd for $C_6H_2Br_2O_2$: 263.8422, observed: 263.8416.

2-Bromo-5,7-dihydroxy-1,4-naphthoquinone (102)

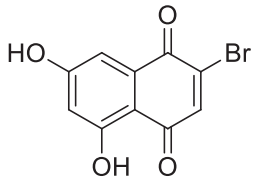

At room temperature and under nitrogen, a solution of diene **105** (1.0 g, 4 mmol) in dry benzene (10 mL) was added dropwise to a solution of **107** (0.94 g, 3.5 mmol) in dry benzene (10 mL). After stirring the reaction mixture overnight, the solvent was removed in vacuo to yield a crude residue. The residue was purified by flash chromatography (10% ethyl acetate–hexane; R_f = 0.25), followed by washing with methylene chloride to afford the adduct **102** (0.25 g, 25%) as a bright orange solid, mp 193.8 °C.(*114*) ^{1}H NMR (acetone-d_6, 500 MHz) δ 11.93 (bs, 1H), 10.5 (bs, 1H), 7.51 (s, 1H), 7.11 (d, J = 2.0 Hz, 1H), 6.62 (d, J = 2.5 Hz, 1H); ^{13}C NMR (acetone-d_6, 125 MHz) δ 186.7, 177.9, 165.8, 165.3, 141.7, 141.6, 139.7, 133.7, 110.8, 109.6, 108.8.

Compound 108

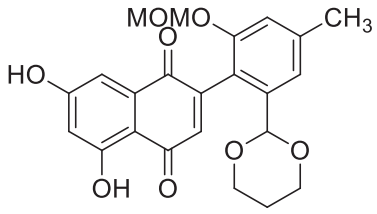

A solution of 2-Bromo-5,7-dihydroxy-1,4-naphthoquinone **102** (50 mg, 0.18 mmol), stannane **86** (115 mg, 0.18 mmol), and CuI (3.8 mg, 0.02 mmol) in THF (4 mL) was added to a solution of $Pd_2(dba)_3$•$CHCl_3$ (5.0 mg, 0.0045 mmol) and PPh_3 (5.4 mg, 0.02 mmol) in THF (1 mL). The mixture was heated at 75 °C for 12 h, cooled to 0 °C, and diluted with EtOAc (10 mL). Saturated aqueous $NaHCO_3$ (10 mL) was added and the mixture was stirred for 30 min. The layers were separated and the aqueous layer was extracted twice with EtOAc (25 mL). The combined organic layers were washed with brine and dried over Na_2SO_4. The solvent was removed under vacuum and the resulting residue was subjected to flash silica gel column chromatography to provide the coupled product (25% EtOAc-hexane, R_f = 0.2) as orange solid (4%). 1H NMR (acetone-d_6, 400 MHz) δ 12.25 (bs, 1H), 7.13 (bs, 1H), 7.08 (d, J = 3.0 Hz, 1H), 7.02 (bs, 1H), 6.80 (s,

1H), 6.65 (bs, J = 3.0 Hz, 1H), 5.44 (s, 1H), 5.08 (s, 2H), 4.03–3.97 (m, 2H), 3.87–3.75 (m, 2H), 3.31 (s, 3H), 2.37 (s, 3H), 1.99–1.90 (m, 2H); ^{13}C NMR (acetone-d_6, 100 MHz) δ 189.4, 183.2, 165.7, 165.1, 155.4, 148.9, 140.6, 139.1, 135.4, 132.8, 129.6, 121.2, 115.9, 110.1, 109.1, 108.1, 100.7, 95.3, 67.7, 67.5, 56.3, 26.4, 21.7.

Compound 111

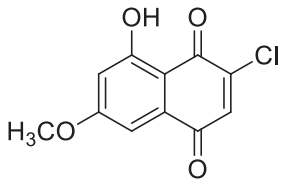

A solution of (1,3-dimethoxy-buta-1,3-dienyloxy)trimethylsilane(*117*) (3.4 g, 16.9 mmol) in dry THF (16 mL) was added dropwise at -30 °C to a solution of commercially available 2,6-dichloro-1,4- benzoquinone (1.0 g, 5.6 mmol) in dry THF (26 mL) followed by the addition of excess deactivated silica. The reaction was stirred for 24 h and warmed to room temperature. The mixture was passed through a short pad of celite and the filtrate was concentrated in vacuo. The resulting residue was subjected to flash silica gel column chromatography (10% ethyl acetate–hexane; R_f = 0.40) to provide the desired adduct in 50% yield as an orange solid.(*118*) 1H NMR ($CDCl_3$, 400 MHz) δ 11.89 (s, 1H), 7.16 (d, J = 3 Hz, 1H), 7.10 (s, 1H), 6.46 (d, J = 2 Hz, 1H), 3.89 (s, 3H); ^{13}C NMR ($CDCl_3$, 100 MHz) δ 182.0, 181.0, 166.9, 165.2, 146.8, 136.2, 133.5, 109.1, 109.0, 106.3, 56.4.

Compound 112

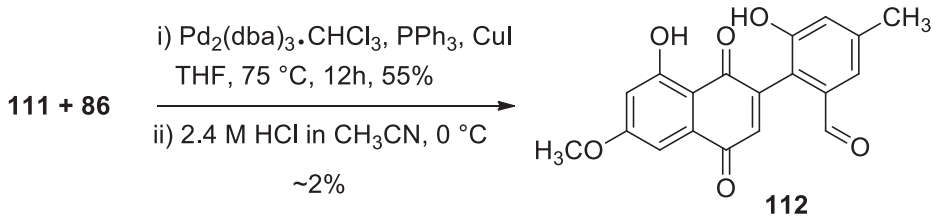

To a solution of **111** (60 mg, 0.25 mmol), stannane **86** (130 mg, 0.25 mmol), and CuI (5.0 mg, 0.026 mmol) in THF (4 mL) was added a solution of $Pd_2(dba)_3$•$CHCl_3$ (6.4 mg, 0.006 mmol) and PPh_3 (6.9 mg, 0.026 mmol) in THF (1 mL). The mixture was heated at

75 °C for 12 h. The mixture was cooled to 0 °C and diluted with EtOAc (10 mL). Saturated aqueous $NaHCO_3$ (10 mL) was added and the mixture was stirred for 30 min. The layers were separated and the aqueous layer was extracted twice with EtOAc (25 mL). The combined organic layers were washed with brine and dried over Na_2SO_4. The solvent was removed under vacuum and the resulting residue was subjected to flash silica gel column chromatography to provide the coupled product (20% EtOAc-hexane, R_f = 0.25) as orange solid (55%). 1H NMR ($CDCl_3$, 400 MHz) δ 12.33 (s, 1H), 7.22 (d, J = 2.4 Hz, 1H), 7.15 (bs, 1H), 6.99 (bs, 1H), 6.84 (s, 1H), 6.67 (d, J = 2 Hz, 1H), 5.31 (s, 1H), 5.08 (dd, J = 18 Hz, 7.2 Hz, 2H), 4.09 (dd, J = 11.6 Hz, 4 Hz, 2H), 3.90 (s, 3H), 3.78–3.68 (m, 2H), 3.34 (s, 3H), 2.37 (s, 3H), 2.07–1.97 (m, 2H); ^{13}C NMR ($CDCl_3$, 100 MHz) δ 187.5, 184.6, 166.1, 164.6, 154.6, 148.1, 141.0, 137.7, 137.6, 134.1, 120.7, 119.1, 115.6, 109.9, 107.2, 106.5, 100.4, 94.7, 67.4, 56.3, 25.6, 21.9. (+EI): Calc'd for $C_{24}H_{24}O_8$ 440.1471, observed: 440.1482.

A solution of concentrated HCl (2 mL) in 10 mL CH_3CN was added to the above coupled product (30 mg, 0.07 mmol) in a 250 mL flask at 0 °C. The mixture was stirred for 4 min and then was quenched with $NaHCO_3$ (60 mL) followed by addition of EtOAc (50 mL). After separation of the layers, the aqueous layer was extracted twice with EtOAc. The combined organic layers were washed with brine, dried over Na_2SO_4 and the solvent was removed under vacuum. The resulting residue was subjected to purification by flash silica gel column chromatography (25% EtOAc-hexane, R_f = 0.20) to provide the desired product **112** as an orange-red solid (~2%). ^1H NMR (acetone-d_6, 400 MHz) δ 12.21 (s, 1H), 9.93 (s, 1H), 8.97 (bs, 1H), 7.39 (d, *J* = 0.8 Hz, 1H), 7.18–7.15 (m, 2H), 6.89 (s, 1H), 6.80 (d, *J* = 2.4 Hz, 1H), 5.63 (s, 1H), 4.00 (s, 3H), 2.43 (s, 3H); ^{13}C NMR (acetone-d_6, 100 MHz) δ 191.9, 187.7, 183.4, 166.2, 155.1, 146.9, 141.0, 137.2, 136.4, 134.1, 125.1, 122.2, 106.7, 105.6, 55.8, 20.1; (+EI): Calc'd for $C_{19}H_{14}O_6$ 338.0790, observed: 338.0798.

Compound 113

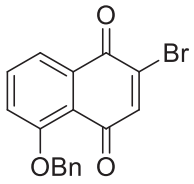

BnBr (0.75 mL, 6.25 mmol) at room temperature was added to a solution of **85** (0.8 g, 3.12 mmol) in CH_2Cl_2 (10 mL), followed by the addition of freshly prepared Ag_2O (1.4 g, 6.2 mmol). The suspension was stirred at r. t. for 18 h, then filtered and rinsed with EtOAc. The filterate was concentrated under reduced pressure to give a residue which was subjected to silica gel column chromatography (20% EtOAc-hexane, R_f = 0.45) to give the desired product **113**(*83*) as a yellow solid (1.0 g, 93%).^{1}H NMR (CDCl3, 500 MHz): δ 7.83 (dd, *J* = 8.0, 1.0 Hz, 1H); 7.65 (dd, *J* = 8.5, 8.0 Hz, 1H), 7.63 (dd, *J* = 7.0, 0.5 Hz, 2H), 7.43–7.40 (m, 3H), 7.37–7.33 (m, 3H), 5.30 (s, 2H).

Compound 114

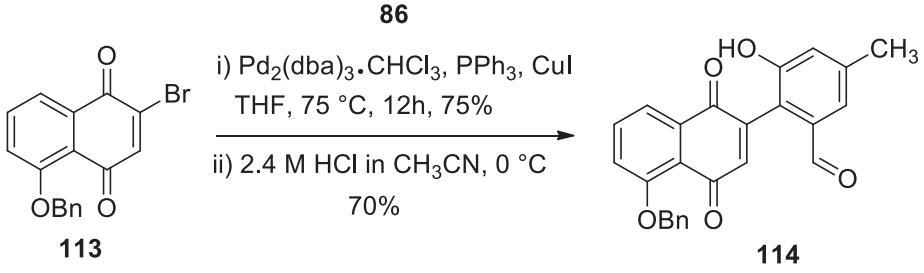

A solution of $Pd_2(dba)_3$•$CHCl_3$ (35 mg, 0.033 mmol) and PPh_3 (35 mg, 0.14 mmol) in THF (2 mL) was added to a solution of **113** (228 mg, 0.66 mmol), stannane **86** (350 mg, 0.66 mmol), and CuI (25 mg, 0.14 mmol) in THF (5 mL). The mixture was heated at 75°C for 12 h. The mixture was cooled to 0°C and diluted with EtOAc (10 mL). Saturated aqueous $NaHCO_3$ (10 mL) was added and the mixture was stirred for 30 min. The layers were separated and the aqueous layer extracted twice with EtOAc (25 mL). The combined organic layers were washed with brine and dried over Na_2SO_4. The solvent was removed under vacuum and the resulting residue was subjected to flash silica gel column chromatography to provide the coupled product (30% EtOAc-hexane, R_f = 0.40) as a yellow solid (75%).(*83*) ^{1}H NMR ($CDCl_3$, 400 MHz) δ 7.84–7.74 (m, 2H), 7.64–7.61 (m, 2H), 7.53–7.35 (m, 3H), 7.12 (bs, 1H), 7.00 (bs, 1H), 6.84 (s, 1H), 5.38 (s, 1H), 5.37–

5.31 (m, 2H), 5.12–5.03 (m, 2H), 4.12–4.04 (m, 2H), 3.8–3.71 (m, 2H), 3.31 (s, 3H), 2.38 (s, 3H), 2.05–1.95 (m, 1H), 1.34–1.29 (m,1H); ^{13}C NMR ($CDCl_3$, 100 MHz): δ 184.6, 183.8, 158.4, 154.5, 144.8, 140.6, 139.6, 137.5, 136.3, 135.0, 134.8, 128.8, 128.0, 126.8, 120.6, 120.5, 120.5, 120.0, 115.6, 100.2, 94.6, 71.0, 67.4, 67.3, 56.2, 25.6, 21.9.

A solution of concentrated HCl (4 mL) in 20 mL CH_3CN at 0 °C was added to the above coupled product (100 mg, 0.2 mmol) in a 250 mL flask. The mixture was stirred for 4 min, quenched with $NaHCO_3$ (75 mL), and EtOAc (50 mL) added. After separation of the layers, the aqueous layer was extracted with EtOAc twice. The combined organic layer was washed with brine, dried over Na_2SO_4. The solvent was then removed under vacuum and the resulting residue was subjected to purification by flash silica gel column chromatography (30% EtOAc-hexane, R_f = 0.25) to provide the desired product **114** as a yellow solid (70%).(*83*) ^{1}H NMR (DMSO, 500 MHz) δ 9.97 (s, 1H), 9.83 (s, 1H), 7.82 (dd, *J* = 8.4, 7.8 Hz, 1 H), 7.68 (d, *J* = 8.0 Hz, 1H), 7.63–7.61 (m, 3H), 7.45 (dd, *J* = 7.8, 7.8 Hz, 2H), 7.35-7.33 (m, 1H), 7.31 (s, 1H), 7.08 (s, 1H), 6.78 (s, 1H), 5.38 (s, 2H), 2.38 (s, 3H).

Compound 116

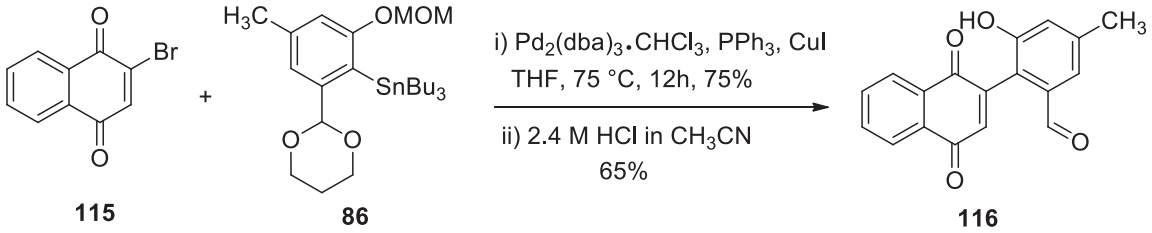

A solution of $Pd_2(dba)_3$•$CHCl_3$ (5.4 mg, 0.005 mmol) and PPh_3 (5.5 mg, 0.021 mmol) in THF (1 mL) was added to a solution of **115** (50 mg, 0.21 mmol), stannane **86** (114 mg, 0.21 mmol), and CuI (4.0 mg, 0.021 mmol) in THF (4 mL). The mixture was heated at 75 °C for 12 h. The mixture was then cooled to 0 °C and diluted with EtOAc (10 mL). Saturated aqueous $NaHCO_3$ (10 mL) was added and the mixture was stirred for 30 min. The layers were separated and the aqueous layer was extracted twice with EtOAc (25 mL). The combined organic layers were washed with brine and dried over Na_2SO_4. The solvent was removed under vacuum and the resulting residue was subjected to flash silica

gel column chromatography to provide the coupled product (20% EtOAc-hexane, R_f = 0.20) as a yellow solid (75%). ^{1}H NMR (acetone-d_6, 500 MHz) δ 8.12-8.09 (m, 2H), 7.89-7.87 (m, 2H), 7.16 (dd, J = 1.5, 1.0 Hz, 1H), 7.05 (dd, J = 1.5, 1.0 Hz, 1H), 6.91 (s, 1H), 5.47 (s, 1H), 5.09 (d, J = 1 Hz, 2H), 4.02–3.95 (m, 2H), 3.84–3.72 (m, 2H), 3.31 (s, 3H), 2.38 (s, 3H), 1.98–1.88 (m, 2H); ^{13}C NMR (acetone-d_6, 125 MHz) δ 185.3, 183.8, 155.3, 148.3, 140.5, 139.1, 137.8, 134.8, 134.6, 133.4, 133.1, 127.3, 126.6, 121.2, 115.8, 100.7, 95.2, 67.5, 56.2, 26.4, 21.8; HRMS (+EI): Calc'd for $C_{23}H_{22}O_6$: 394.1416, observed: 394.1424.

A solution of concentrated HCl (4 mL) in 20 mL CH_3CN at 0 °C was added to the above coupled product (100 mg, 0.2 mmol) in a 250 mL flask. The mixture was stirred for 4 min and then was quenched with $NaHCO_3$ (75 mL) followed by addition of EtOAc (50 mL). After separation of the layers, the aqueous layer was extracted with EtOAc twice. The combined organic layer was washed with brine, dried over Na_2SO_4 and the solvent was removed under vacuum. The resulting residue was subjected to purification by flash silica gel column chromatography (30% EtOAc-hexane, R_f = 0.20) to provide the desired product **116** as a yellow solid (65%). ^{1}H NMR (acetone-d_6, 500 MHz) δ 9.91 (s, 1H), 8.90 (bs, 1H), 8.13-8.07 (m, 2H), 7.93-7.88 (m, 2H), 7.71-7.53 (m, 2H), 7.38 (s, 1H), .18 (s, 1H), 6.97 (s, 1H), 2.45 (s, 3H); ^{13}C NMR (acetone-d_6, 100 MHz) δ 192.8, 185.2, 184.4, 155.3, 147.5, 141.8, 137.8, 137.2, 134.8, 133.7, 133.3, 132.8, 129.6, 127.3, 126.6, 126.0, 123.2, 21.6, HRMS (+EI): Calc'd for $C_{18}H_{12}O_4$: 292.0735, observed: 292.0745.

2-(3-(Methoxymethoxy)phenyl)-1,3-dioxane (118): This protected benzaldehyde was prepared in 2 steps.

(a) 3-(1,3-dioxan-2-yl)phenol

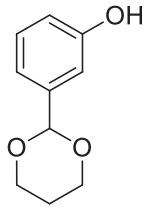

A mixture of commercially available 3-hydroxybenzaldehyde (1.0 g, 8.19 mmol), 1,3-propanediol (0.9 mL,1 2.29 mmol), and TsOH.H_2O (60 mg, 0.3 mmol) in toluene was refluxed with the azeotropic removal of H_2O. After the starting material was consumed completely, the reaction mixture was cooled and the solvent was removed under pressure to give a residue. The crude residue was purified on silica (35% EtOAc-hexane, R_f = 0.23) to give the protected aldehyde as a white solid in 79% yield. ^{1}H NMR ($CDCl_3$, 500 MHz) δ 7.18 (t, J = 7.5 Hz, 1H), 7.016 (dd, J = 7.5, 0.5 Hz, 1H), 6.92 (dd, J = 2.0, 1.5 Hz, 1H), 6.72 (ddd, J = 3.5, 2.5, 1.0 Hz, 1H), 6.22 (bs, OH), 5.45 (s, 1H), 4.27 (dd, J = 11.0, 4.5 Hz, 2H), 4.0–3.95 (m, 2H), 2.25–2.20 (m, 1H), 1.45–1.42 (m, 1H); ^{13}C ($CDCl_3$, 125 Hz) δ 155.9, 139.8, 129.7, 118.3, 116.3, 113.3, 101.6, 67.5, 25.7; HRMS (+EI): Calc'd for $C_{10}H_{12}O_3$: 180.0786, observed: 180.0784.

(b) 2-(3-(methoxymethoxy)phenyl)-1,3-dioxane (118)

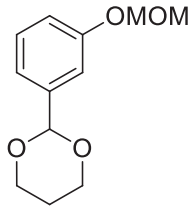

Chloromethyl methyl ether (0.17 mL, 2.2 mmol) was added dropwise to a stirred solution of the above phenyl acetal (200 mg, 1.10 mmol) and diisopropylethylamine (0.29 mL, 1.76 mmol) in anhydrous CH_2Cl_2 and the mixture was heated at 40 °C. After 24h, the reaction mixture was washed with H_2O and brine. The combined organic layers were dried over Na_2SO_4 and the solvent was removed under vacuum to give MOM ether as colorless oil in 95% yield. ^{1}H NMR ($CDCl_3$, 500 MHz) δ 7.28 (t, J = 8.0 Hz, 1H), 7.20-7.19 (m, 1H), 7.15-7.11 (m, 1H), 7.01 (ddd, J = 3.5, 2.5, 1.0 Hz, 1H), 5.44 (s, 1H), 5.15 (s, 2H), 4.22–4.19 (m, 2H), 3.94–3.88 (m, 2H), 3.44 (s, 3H), 2.21–2.11 (m, 1H), 1.38–1.33 (m, 1H); ^{13}C NMR ($CDCl_3$, 125 MHz) δ157.0, 140.2, 129.1, 119.4, 116.5, 113.6, 101.1, 94.1, 67.1, 55.7, 25.5; HRMS (+EI): Calc'd for $C_{12}H_{16}O_4$: 224.1048, observed: 224.1047.

Compound **119**

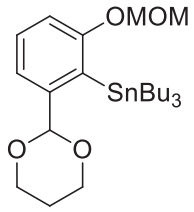

The above MOM ether (360 mg, 2.0 mmol) was co-evaporated twice with anhydrous toluene and was dissolved in freshly dried hexane (10 mL). At 0 °C, *n*-BuLi (0.96 mL, 2.5M in hexane, 1.2 mmol) was added and the mixture was stirred for 30 min. A white precipitate indicated the formation of lithiated species. After 30 min, *n*-Bu_3SnCl (0.9 mL, 2.0 mmol) was added and the mixture was further stirred for 30 min, diluted with hexane-Et_2O (1:1, v/v), and saturated aqueous $NaHCO_3$ added. The mixture was stirred at 0 °C for 30 min. After separation, the aqueous layer was extracted twice with hexane-Et_2O (1:1, v/v). The combined organic layers were washed with brine and dried over Na_2SO_4. The solvent was removed under vacuum and the residue subjected to purification on silica to give the required stannane (4% EtOAc-hexane, R_f = 0.5) as colorless oil (88%). ^{1}H NMR ($CDCl_3$, 500 MHz) δ 7.40 (d, J = 7.5 Hz, 1H), 7.31 (t, J = 8.0 Hz, 1H), 7.07 (d, J = 8.5 Hz, 1H), 5.40 (s, 1H), 5.12 (s, 2H), 4.24 (dd, J = 11.5, 4.5 Hz, 2H), 3.97 (t, J = 11.5 Hz, 2H), 3.44 (s, 3H), 2.26–2.18 (m, 1H), 1.55–0.88 (m, 28H); ^{13}C NMR ($CDCl_3$, 125 MHz) δ 161.8, 147.0, 130.1, 129.7, 119.9, 112.7, 102.3, 94.5, 67.2, 55.9, 29.2, 27.6, 25.8, 13.8, 12.2; LRMS (+EI) [M-Bu]: 457.

Compound 120 and 121

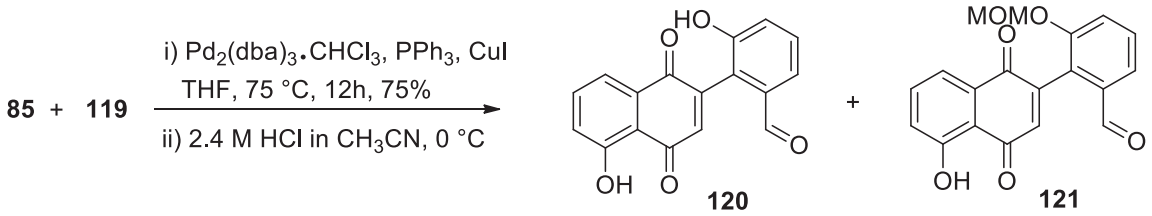

A solution of $Pd_2(dba)_3$•$CHCl_3$ (5.0 mg, 0.005 mmol) and PPh_3 (5.0 mg, 0.019 mmol) in THF (1 mL) was added to a solution of **85** (48 mg, 0.19 mmol), stannane **119** (100 mg, 0.19 mmol), and CuI (4.0 mg, 0.019 mmol) in THF (4 mL). The mixture was heated at 75 °C for 12 h. The mixture was cooled to 0 °C and diluted with EtOAc (10 mL). Saturated

aqueous $NaHCO_3$ (10 mL) was added and the mixture was stirred for 30 min. The layers were separated and the aqueous layer was extracted twice with EtOAc (25 mL). The combined organic layers were washed with brine and dried over Na_2SO_4. The solvent was removed under vacuum and the resulting residue was used in next step without further purification.

A solution of concentrated HCl (2 mL) in 10 mL CH_3CN at 0 °C was added to the above coupled product (30 mg, 0.07 mmol) in a 250 mL flask. The mixture was stirred for 4 min, quenched with $NaHCO_3$ (50 mL), and EtOAc (25 mL) added. After separation of the layers, the aqueous layer was extracted twice with EtOAc. The combined organic layers were washed with brine, dried over Na_2SO_4. The solvent was then removed under vacuum and the resulting residue subjected to purification by flash silica gel column chromatography to provide the desired product **120** along with partially protected MOM derivative **121**.

Compound 120: ^{1}H NMR (acetone-d_6, 400 MHz) δ 12.05 (bs, 1H), 9.96 (s, 1H), 9.08 (bs, 1H), 7.81–7.77 (m, 1H), 7.62–7.57 (m, 3H), 7.37–7.34 (m, 2H), 7.02 (s, 1H); ^{13}C NMR (acetone-d_6, 100 MHz) δ 191.8, 190.2, 182.6, 161.2, 155.1, 148.0, 136.5, 136.4, 131.7, 130.5, 128.6, 124.3, 123.6, 121.8, 120.4, 118.9, 115.3; HRMS (+EI): Calc'd for $C_{17}H_{10}O_5$: 294.0528, observed: 294.0518.

Compound 121: ^{1}H NMR (acetone-d_6, 500 MHz) δ 12.05 (bs, 1H), 10.03 (s, 1H), 7.83–7.81 (dd, J = 8.5, 7.5 Hz, 1H), 7.73 (dd, J = 8.0, 6.0 Hz, 2H), 7.68–7.60 (m, 2H), 7.39 (dd, J = 9.0, 1.0 Hz, 1H), 7.02 (s, 1H), 5.27–5.22 (m, 2H), 3.37 (s, 3H); ^{13}C NMR (acetone-d_6, 100 MHz) δ 192.6, 191.0, 183.5, 155.9, 148.8, 137.6, 137.6, 137.1, 133.5, 131.6, 126.0, 125.0, 124.7, 121.3, 120.0, 116.2, 95.6, 56.5; HRMS (+EI): Calc'd for: $C_{19}H_{14}O_6$: 338.0790, observed: 338.0791.

Summary

A complete understanding of the biosynthetic machinery of the gilvocarcin pathway provides the foundation for our ultimate goal, to create gilvocarcin V analogues with improved pharmaceutical properties. In this context, it is imperative to understand the key C–C bond cleavage, intramolecular cyclization, and *O*-methylations that produce the unique structural scaffold. The isolation of the gilvocarcin gene cluster from *S. griseoflavus* in 2003 established the genetic basis for further biochemical studies. Now after a decade, GilOII has been unambiguously identified as the key enzyme performing the crucial C–C bond cleavage reaction and is responsible for the unique rearrangement of a benz[*a*]anthracene skeleton to the benzo[*d*]naphthopyranone backbone typical of the gilvocarcin-type natural anticancer antibiotics. Further investigation of this enzyme led to the isolation of a hydroxyoxepinone intermediate and thus several important conclusions regarding the cleavage mechanism. The $FADH_2$-dependent oxygenase GilOII mediates C5–C6 bond cleavage via Baeyer-Villiger oxidation to give an acid-aldehyde intermediate which then undergoes decarboxylation to give the substrate for GilMT. The discovery has filled the puzzling decade old gap in the gilvocarcin biosynthetic pathway.

GilMT and GilM, with previously unclear functions, were also investigated by *in vitro* studies using purified recombinant enzymes and synthetically prepared intermediates. The studies revealed GilMT as a typical S-adenosylmethionine dependent *O*-methyltransferase and GilM was identified as a pivotal enzyme in the pathway that exhibits dual functionality catalyzing the reduction of the quinone intermediate to a hydroquinone along with stabilizing *O*-methylation and a hemiacetal formation. GilM mediates its reductive catalysis by using the reduced flavin generated in GilR reaction. GilR catalyzes the final step in the gilvocarcin biosynthesis by converting pregilvocarcin to gilvocarcin. A 10-fold increase in the formation of defucogilvocarcin in the GilR-GilM reaction versus GilM alone confirmed the synergistic effects of GilR. However, to fully understand the complex interactions between GilM and $FADH_2$, which is bicovalently tethered to GilR, we will need GilM structure. Other helpful information may be gained

from the structures of the corresponding enzymes ChryRM or RavRM, as both chrysomycin A and ravidomycin V contain the R- and the M-activity on the single gene.

We extended our knowledge of post-PKS enzymes through our initial attempts of chemoenzymatic synthesis of defuco-pregilvocarcin M. In this perspective, we designed and synthesized a series of structural analogues of pathway intermediates. The *in-vitro* enzyme reactions with these analogues revealed that GilM and GilMT are both promiscuous enzymes. The two critical enzymes were shown to tolerate most of the substrates in the study. Following up on these preliminary studies, a more robust series of analogues must be designed and synthesized for a braoder structure-activity-relationship study. Particularly, analogues with more polar substituents like amino, sulfonic acid residues could serve as a solution to the difficult problem of developing water-soluble GV analogues. Small variations around the aromatic core could be very useful in increasing GV potency. Future studies involving characterization of GilGT, the glycosyltransferase involved in the pathway, are essential for the total chemoenzymatic synthesis of gilvocarcin type analogues.

Spectral data

3-Methoxy-5-methylbenzaldehyde (88)

^{1}H NMR ($CDCl_3$, 300 MHz)

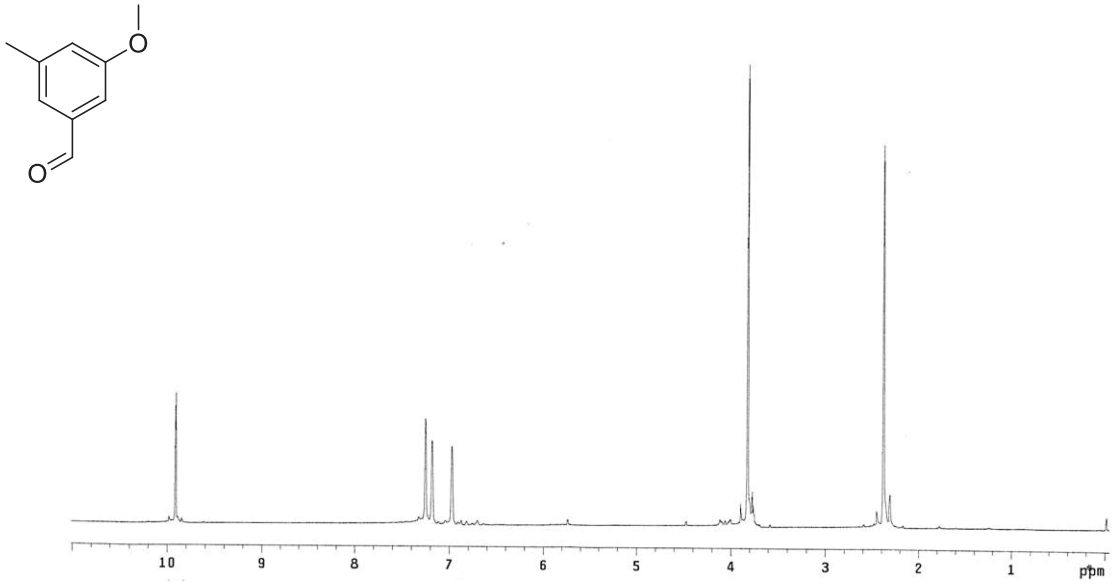

3-Methoxy-5-methylbenzaldehyde (88)

^{13}C NMR ($CDCl_3$, 75 MHz)

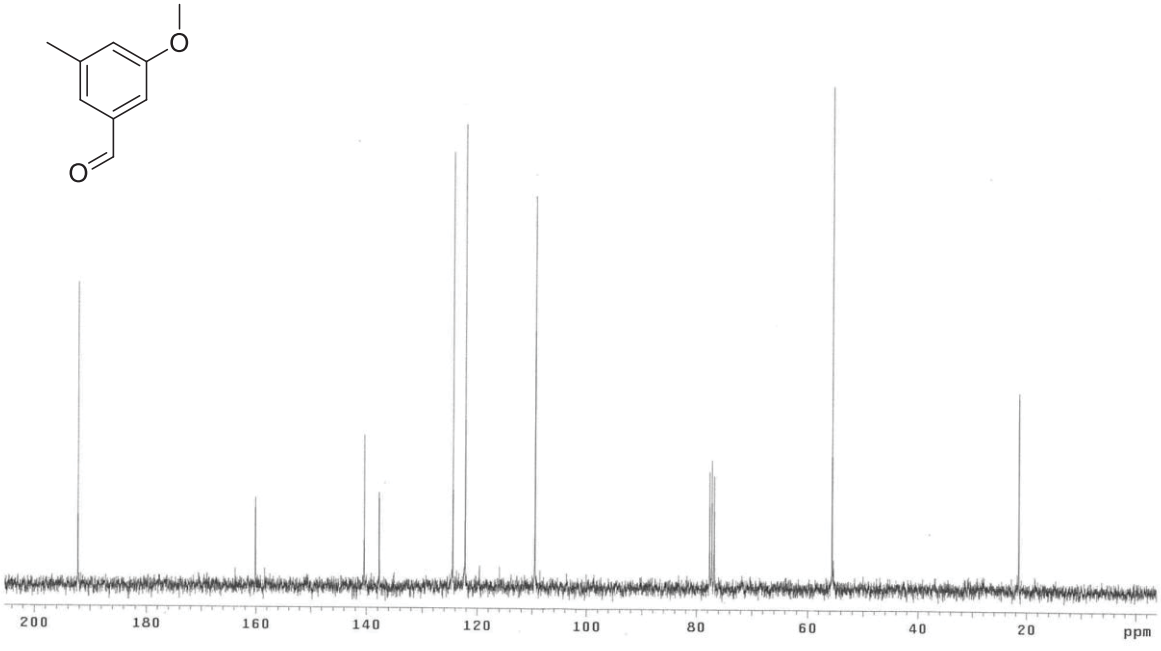

3-Hydroxy-5-methylbenzaldehyde (89)

^{13}C NMR (CD_3OD, 75 MHz)

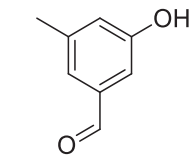

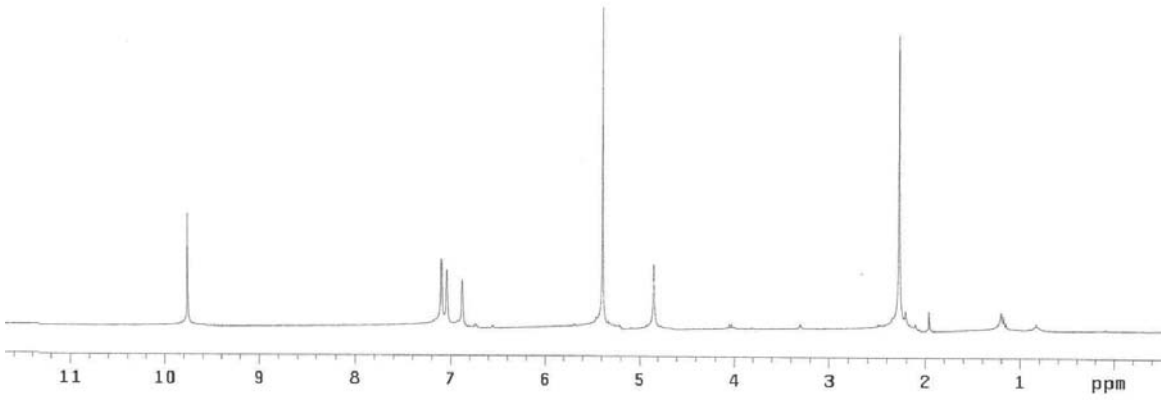

3-Hydroxy-5-methylbenzaldehyde (89)

^{1}H NMR (CD_3OD, 300 MHz)

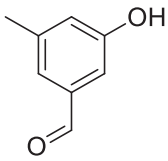

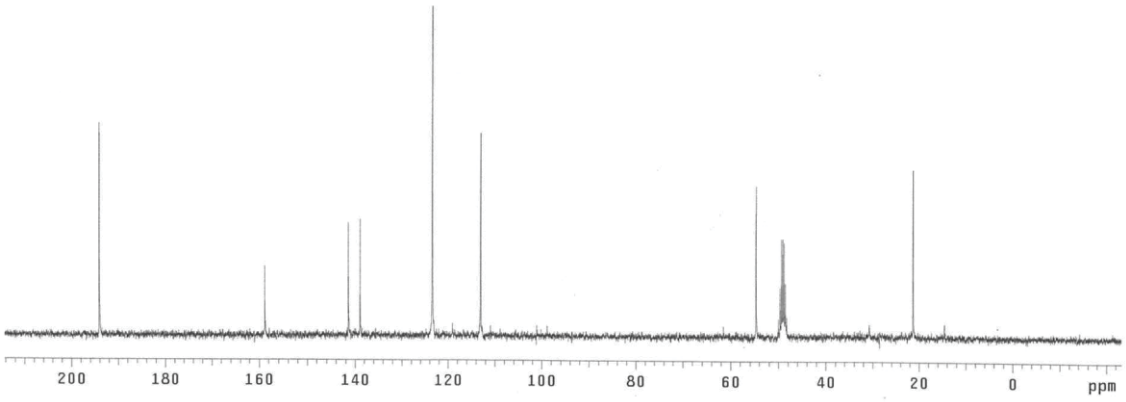

2-(3-Hydroxy-5-methylphenyl)-1,3-dioxane

^{1}H NMR ($CDCl_3$, 300 MHz)

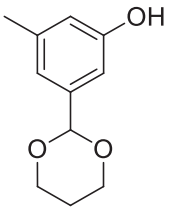

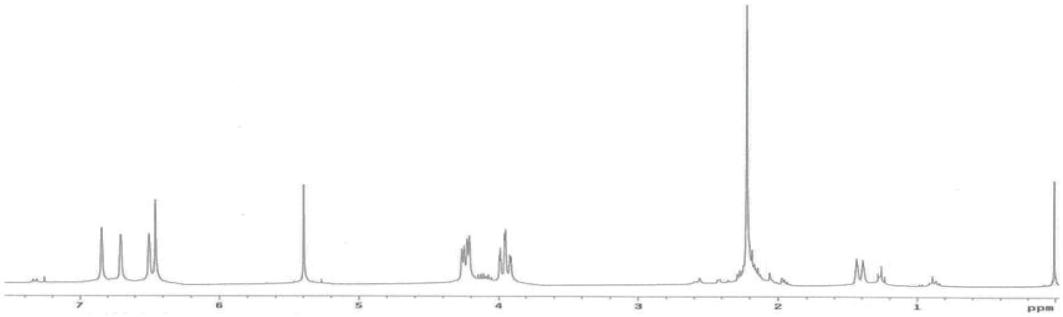

2-(3-Hydroxy-5-methylphenyl)-1,3-dioxane

^{13}C NMR ($CDCl_3$, 75 MHz)

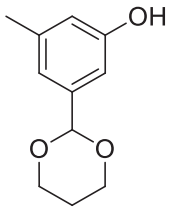

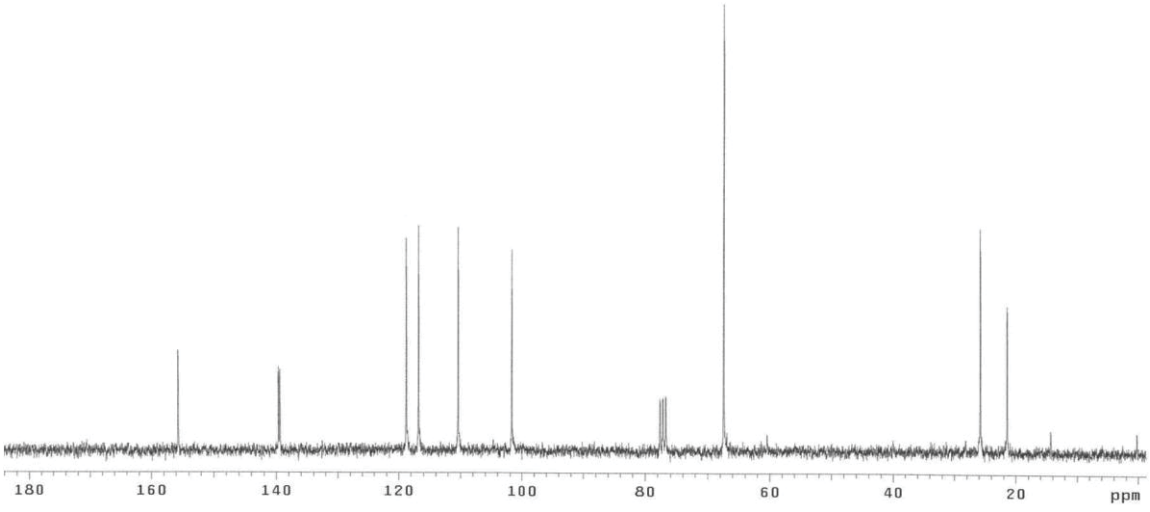

2-(3-Methoxymethoxy-5-methylphenyl)-1,3-dioxane (90)

^{1}H NMR ($CDCl_3$, 300 MHz)

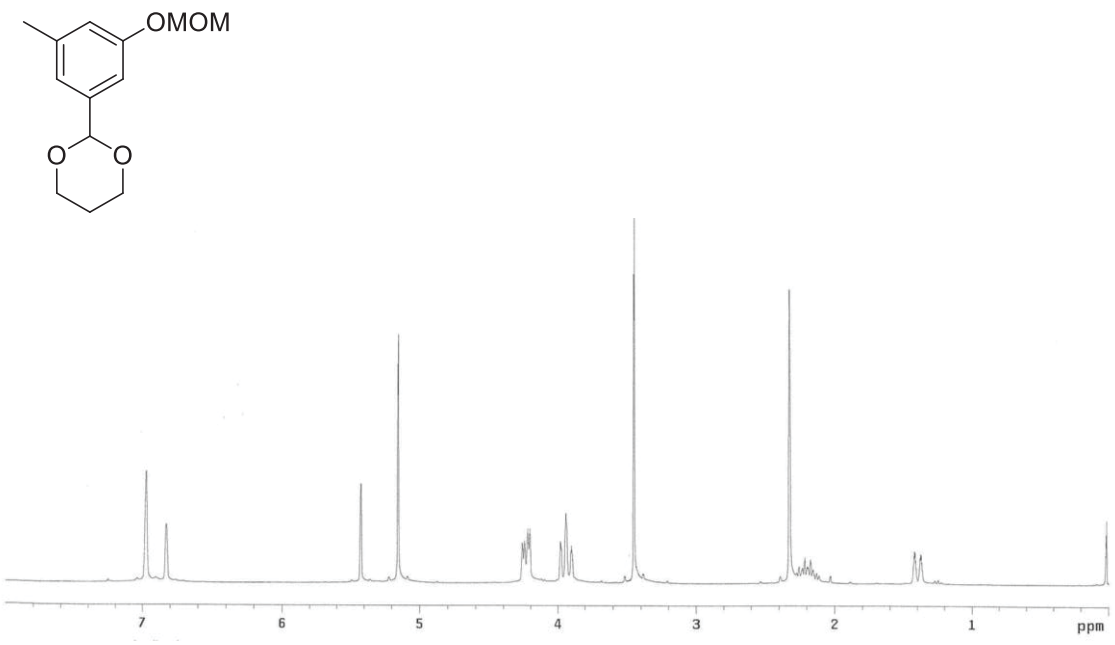

2-(3-Methoxymethoxy-5-methylphenyl)-1,3-dioxane (90)

^{13}C NMR ($CDCl_3$, 75 MHz)

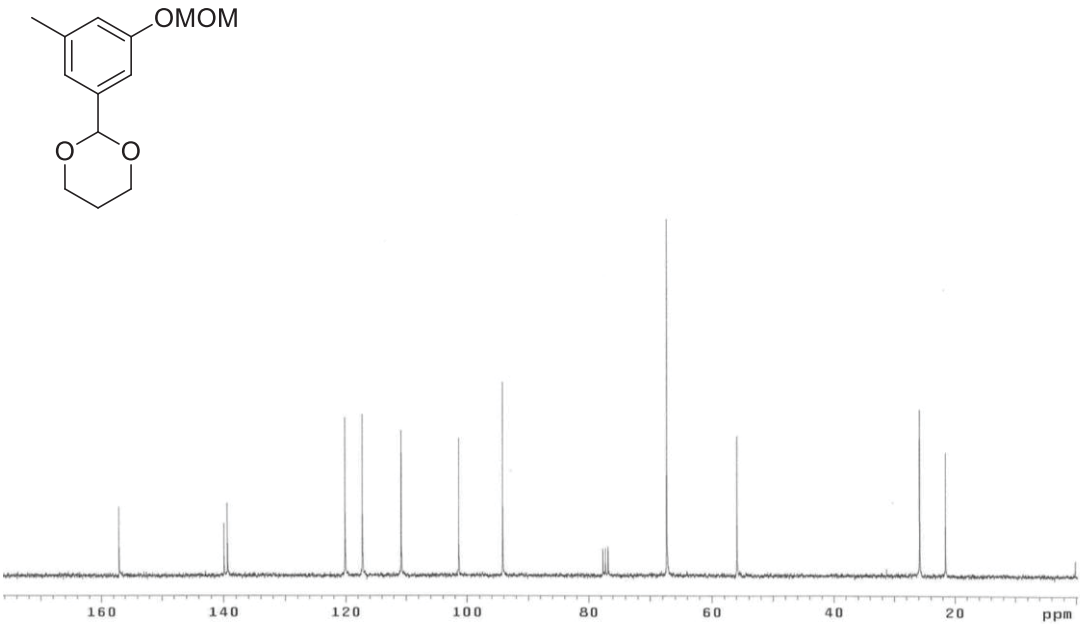

(2-(1,3-dioxan-2-yl)-6-(methoxymethoxy)-4-methylphenyl)tributylstannane (86)

^{1}H NMR ($CDCl_3$, 300 MHz)

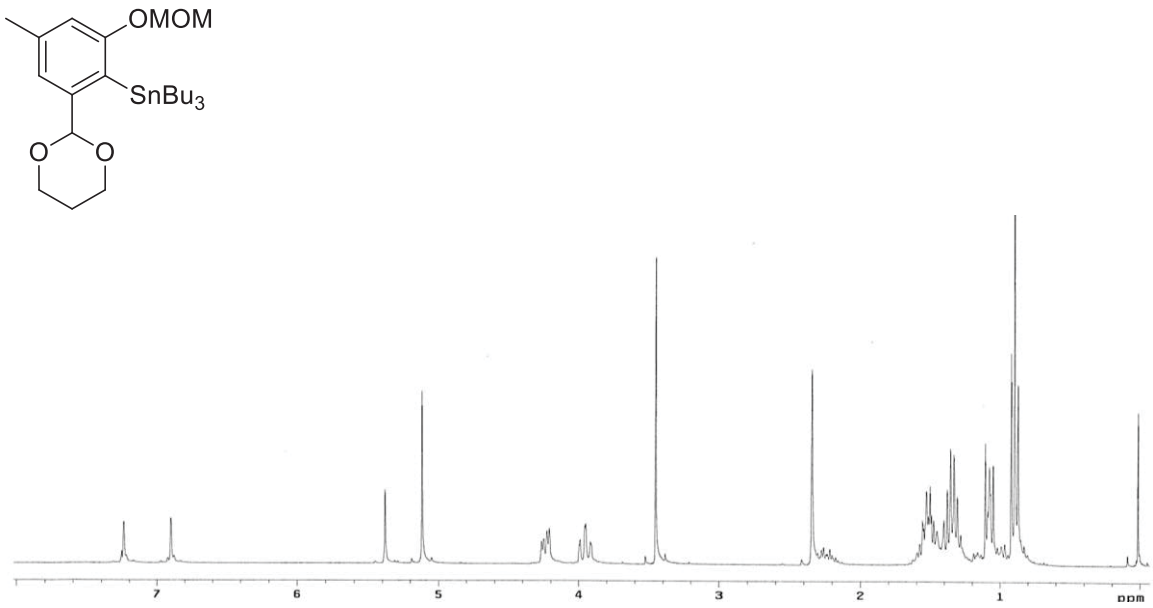

(2-(1,3-dioxan-2-yl)-6-(methoxymethoxy)-4-methylphenyl)tributylstannane (86)

^{13}C NMR ($CDCl_3$, 75 MHz)

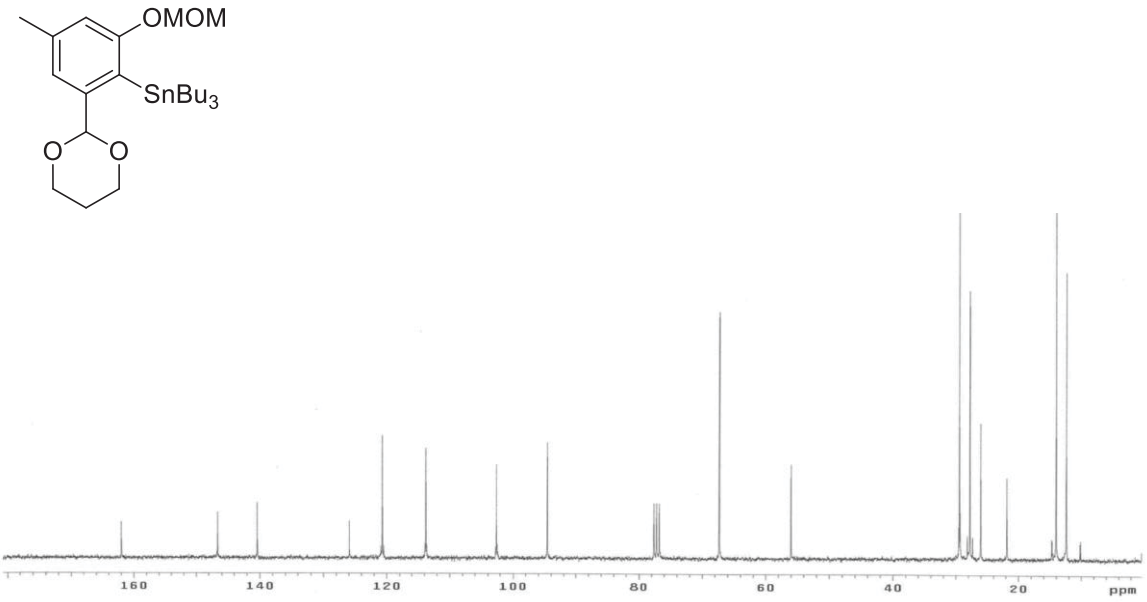

2-(2-(1,3-dioxan-2-yl)-6-(methoxymethoxy)-4-methylphenyl)-5-hydroxy-1,4-napthaquinone (91)

^{1}H NMR ($CDCl_3$, 400 MHz)

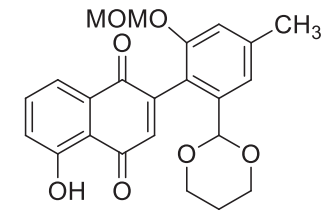

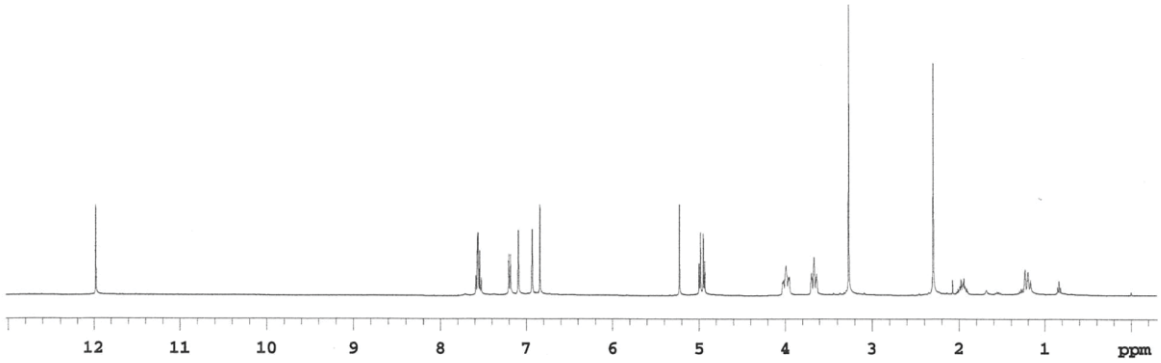

2-(2-(1,3-dioxan-2-yl)-6-(methoxymethoxy)-4-methylphenyl)-5-hydroxy-1,4-napthaquinone (91)

^{13}C NMR ($CDCl_3$, 100 MHz)

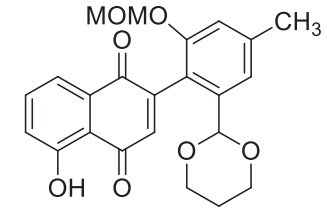

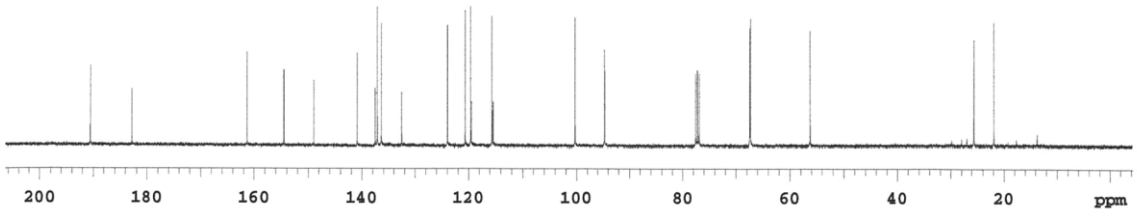

3-Hydroxy-2-(5-hydroxy-1,4-dioxo-1,4-dihydronaphthalen-2-yl)-5-methylbenzaldehyde (84)

^{13}C NMR (acetone-d_6, 100 MHz)

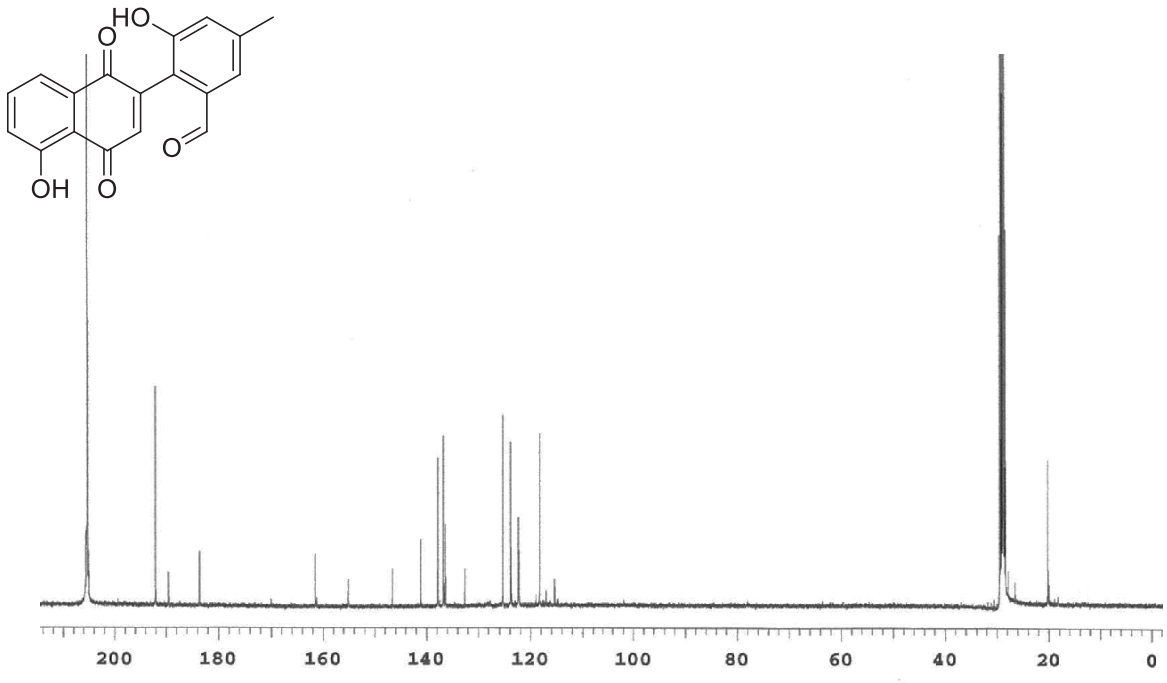

3-Hydroxy-2-(5-hydroxy-1,4-dioxo-1,4-dihydronaphthalen-2-yl)-5-methylbenzaldehyde (84)

^{1}H NMR (acetone-d_6, 500 MHz)

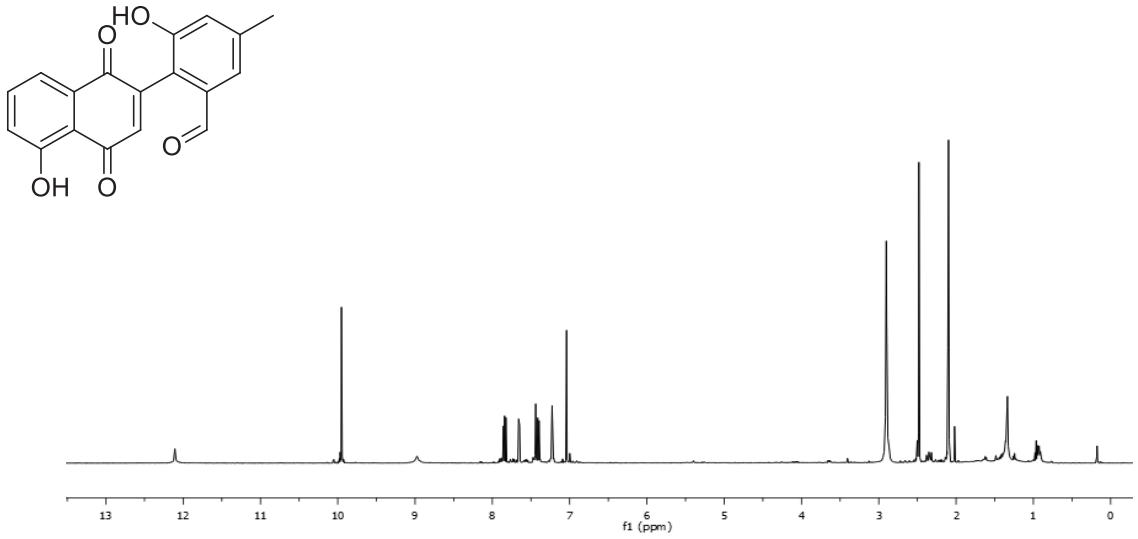

2-(5-hydroxy-1,4-dioxo-1,4-dihydronaphthalen-2-yl)-3-methoxy-5-methylbenzaldehyde (92)

^{1}H NMR ($CDCl_3$, 400 MHz)

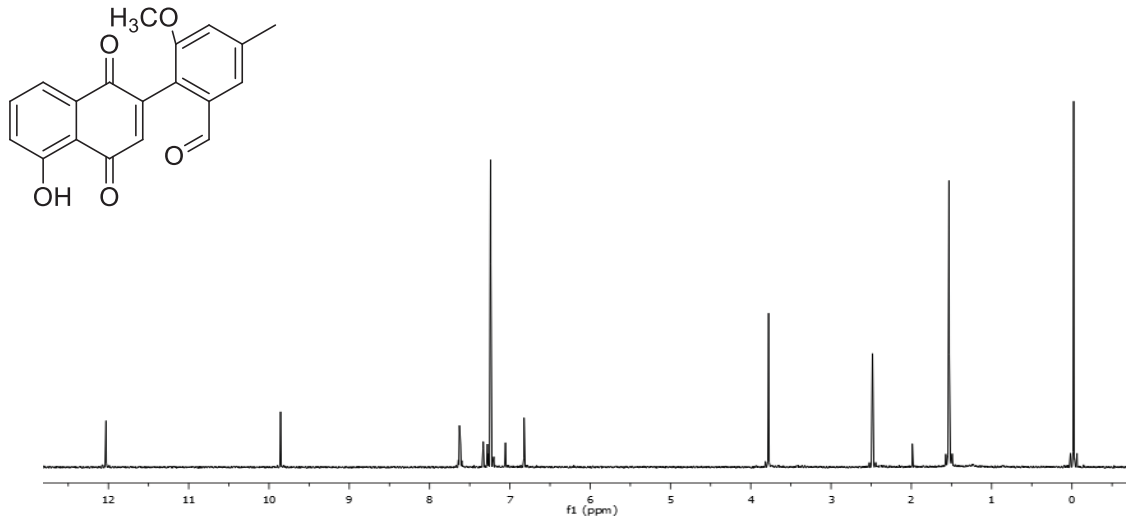

2-(5-hydroxy-1,4-dioxo-1,4-dihydronaphthalen-2-yl)-3-methoxy-5-methylbenzaldehyde (92)

^{13}C NMR ($CDCl_3$, 100 MHz)

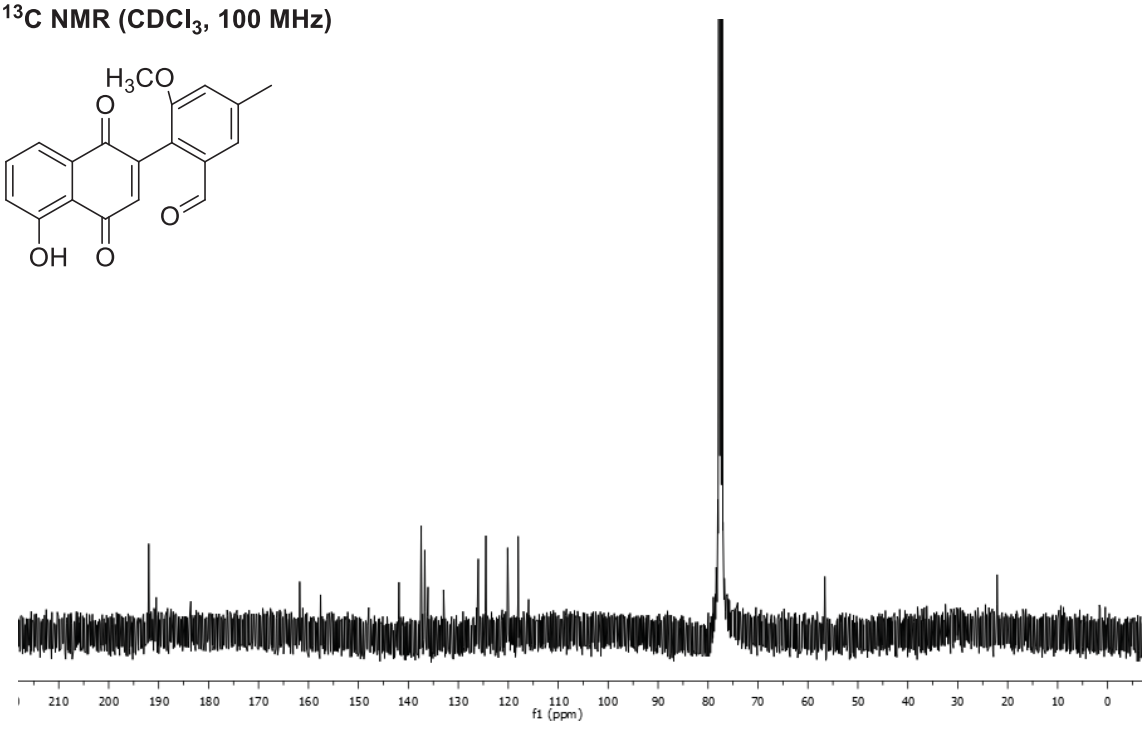

2-(5-hydroxy-1,4-dioxo-1,4-dihydronaphthalen-2-yl)-3-methoxy-5-methylbenzaldehyde (92)

NOE ($CDCl_3$, 400 MHz)

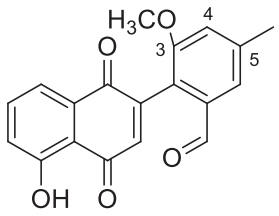

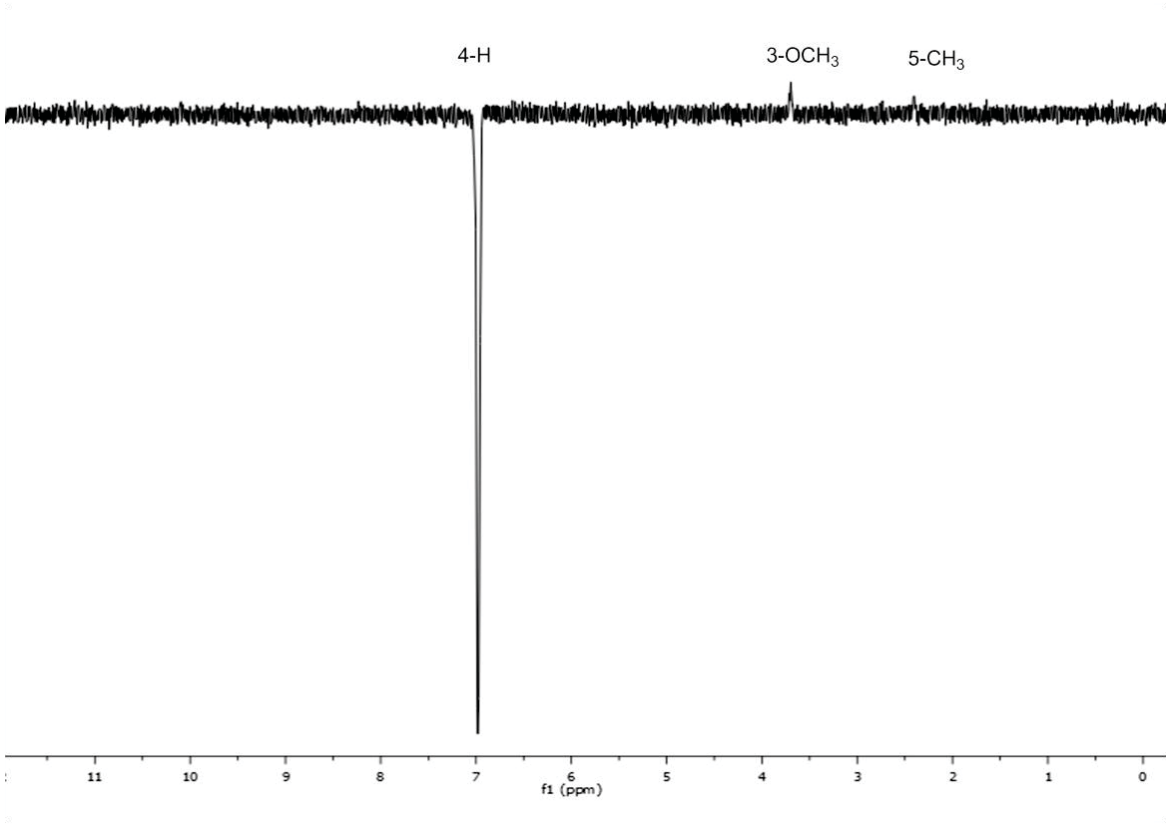

Defuco-pregilvocarcin M (52)

^{1}H NMR ($CDCl_3$, 500 MHz)

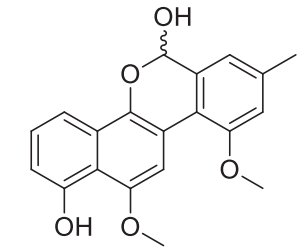

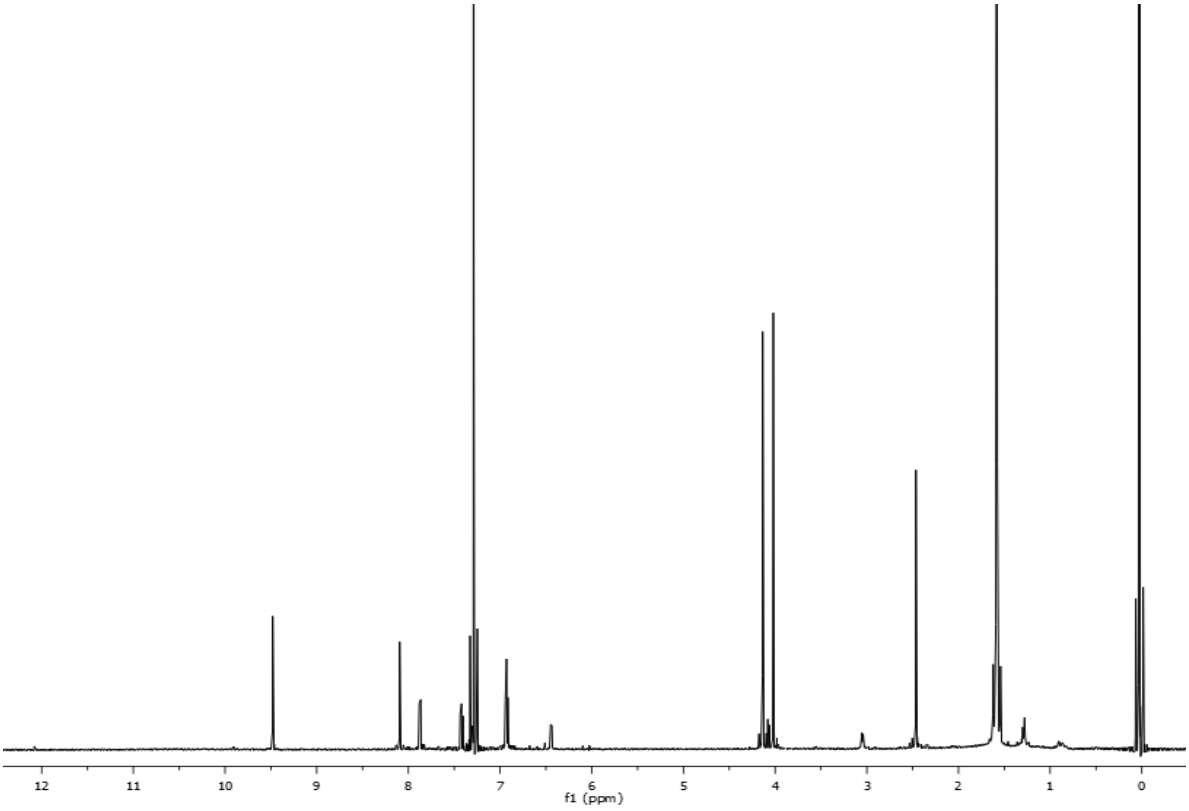

Defuco-pregilvocarcin M (52)

gHSQC ($CDCl_3$, 500 MHz)

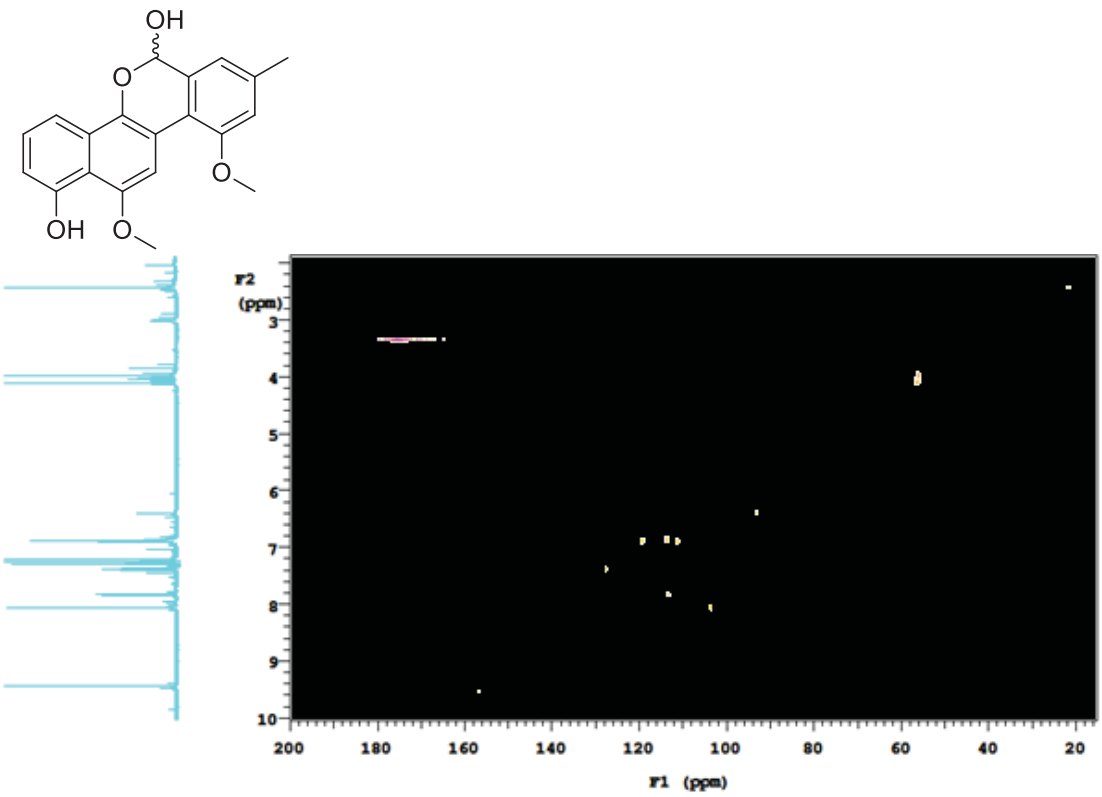

1,8-Dimethoxy dehydrorabelomycin (95)

^{1}H NMR ($CDCl_3$, 400 MHz)

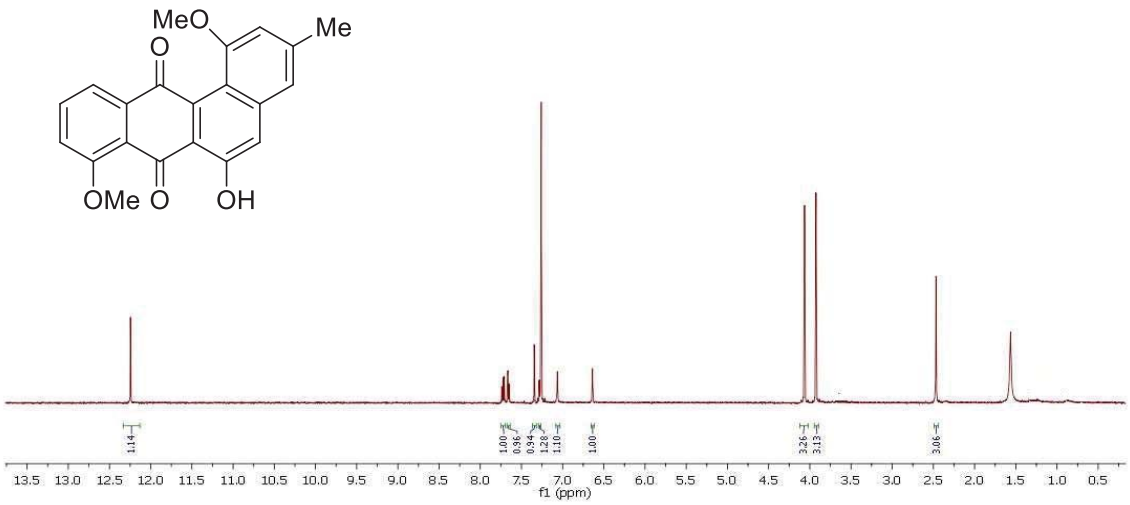

1,8-Dimethoxy dehydrorabelomycin (95)

^{13}C NMR ($CDCl_3$, 100 MHz)

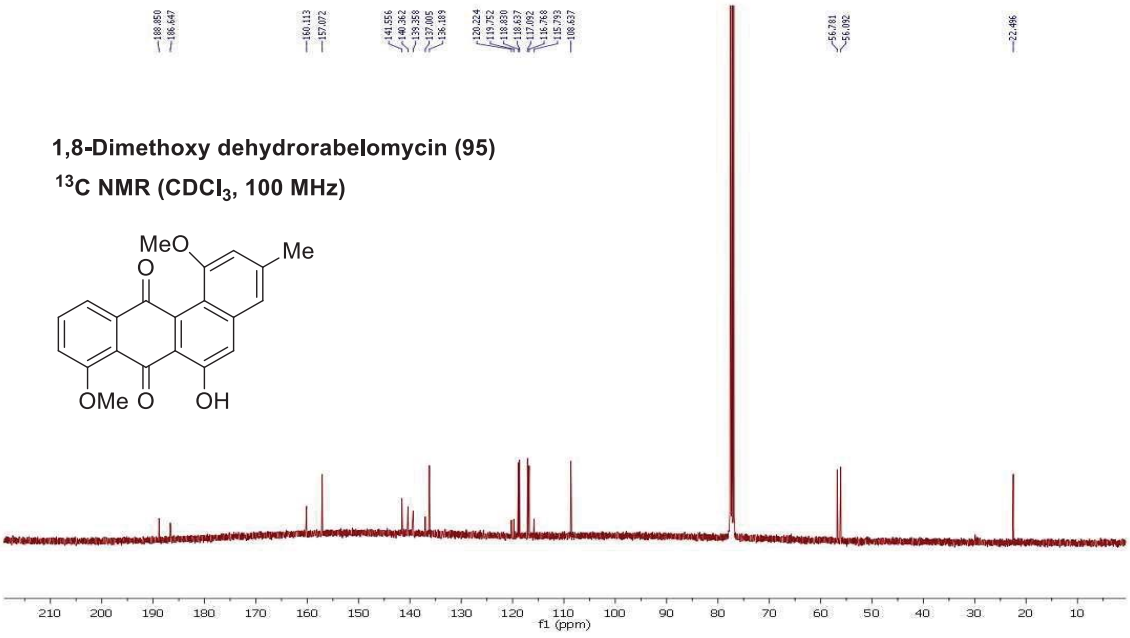

1,8-Dimethoxy dehydrorabelomycin (95)

gHMBC ($CDCl_3$, 400 MHz)

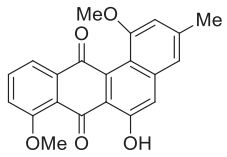

1,8-Dimethoxy dehydrorabelomycin (95)

gHSQC ($CDCl_3$, 400 MHz)

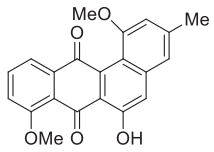

1,8-Dimethoxy dehydrorabelomycin (95)

NOESY1D ($CDCl_3$, 400 MHz)

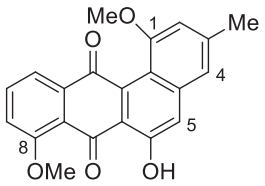

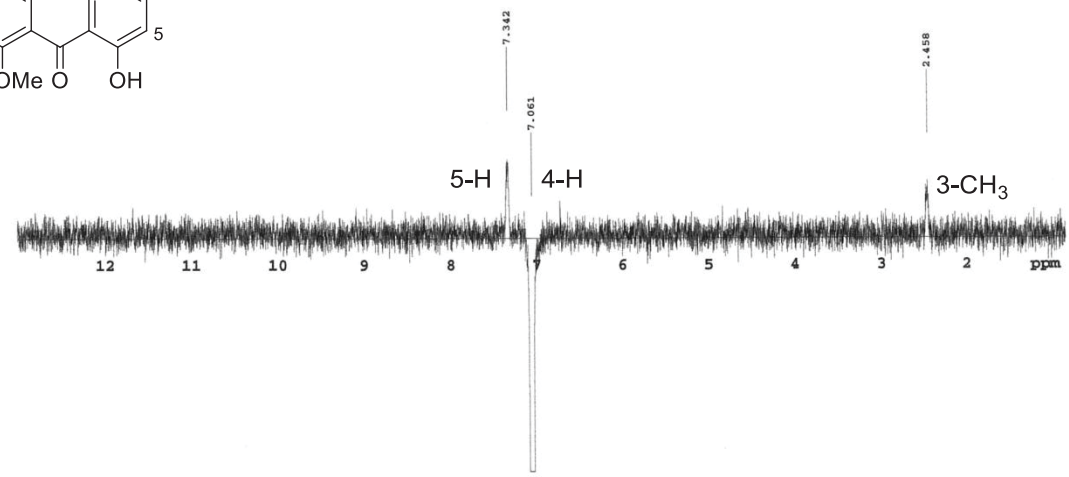

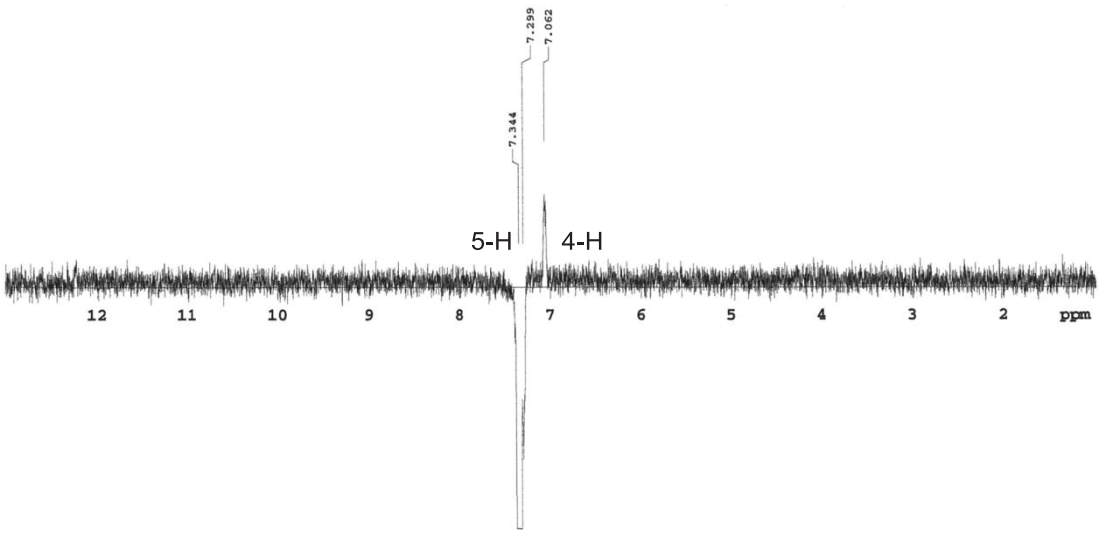

1,8-Dimethoxy dehydrorabelomycin (95)

NOESY1D ($CDCl_3$, 400 MHz)

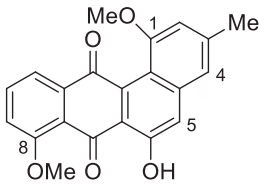

8-Methoxy dehydrorabelomycin (96)

^{1}H NMR ($CDCl_3$, 400 MHz)

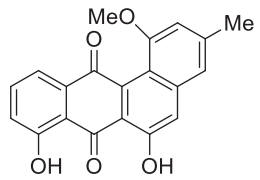

1-Methoxy dehydrorabelomycin (97)

^{1}H NMR ($CDCl_3$, 400 MHz)

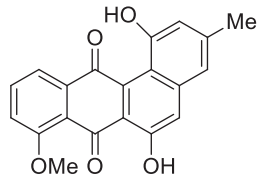

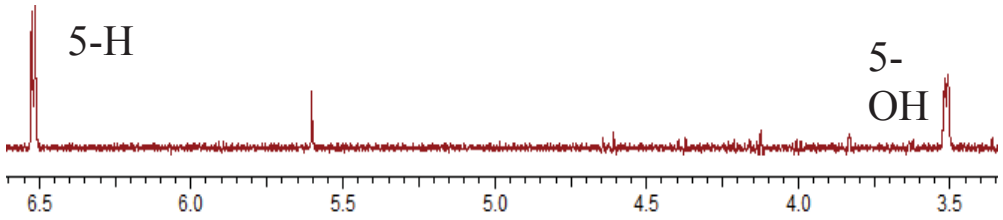

Oxepinone derivative (98)

^{1}H NMR ($CDCl_3$, 400 MHz)

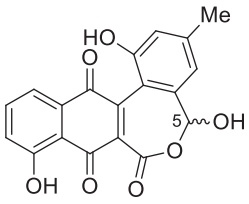

Oxepinone derivative (98)

^{13}C NMR ($CDCl_3$, 125 MHz)

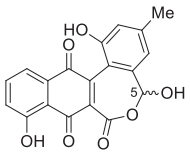

Oxepinone derivative (98)

HSQC ($CDCl_3$, 600 MHz)

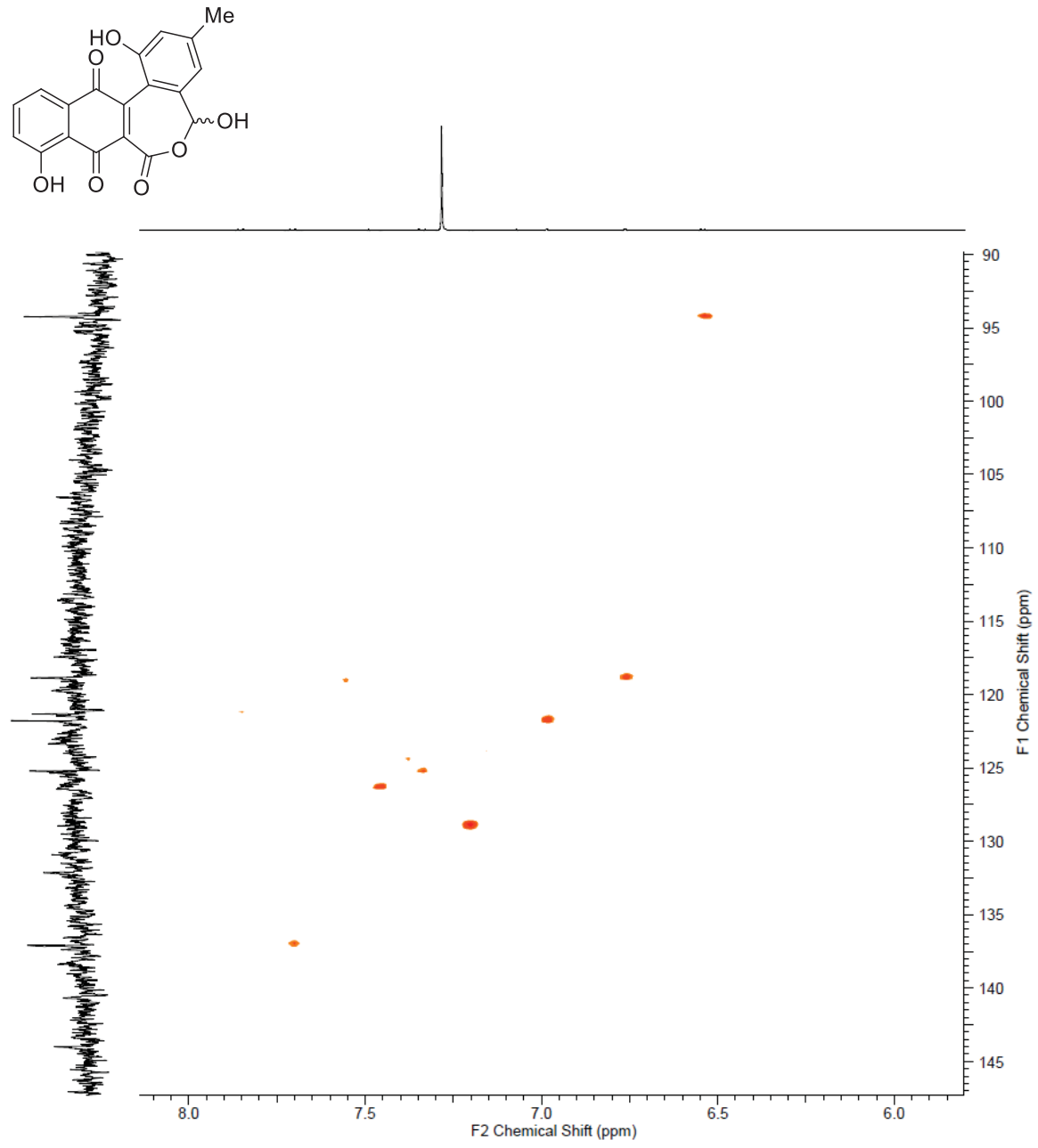

Oxepinone derivative (98)

HMBC ($CDCl_3$, 600 MHz)

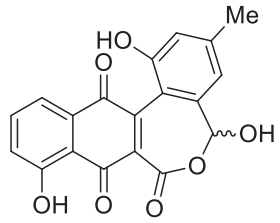

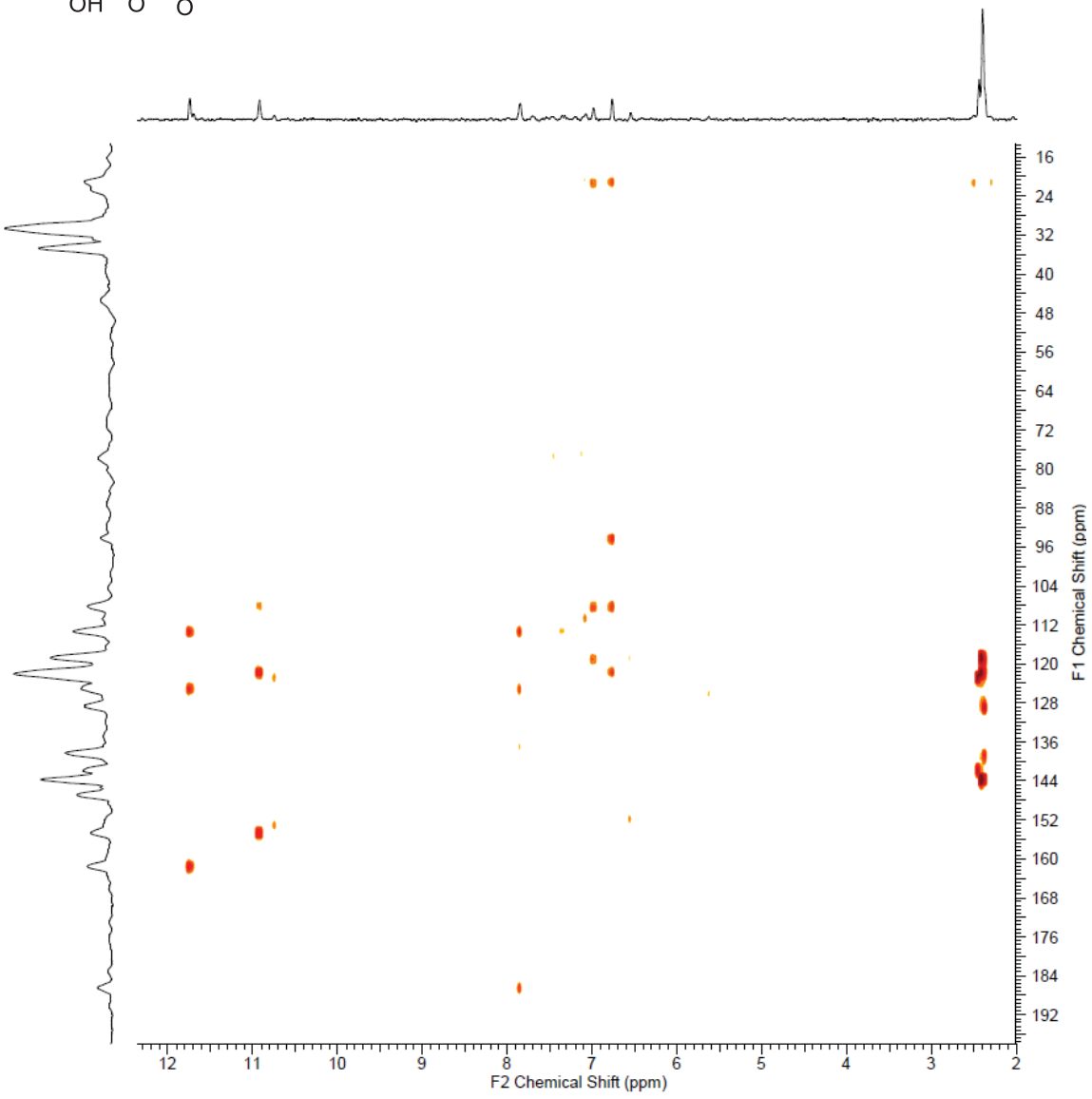

3-bromojuglone (99)

^{1}H NMR ($CDCl_3$, 500 MHz)

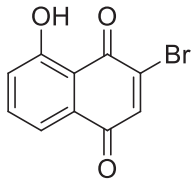

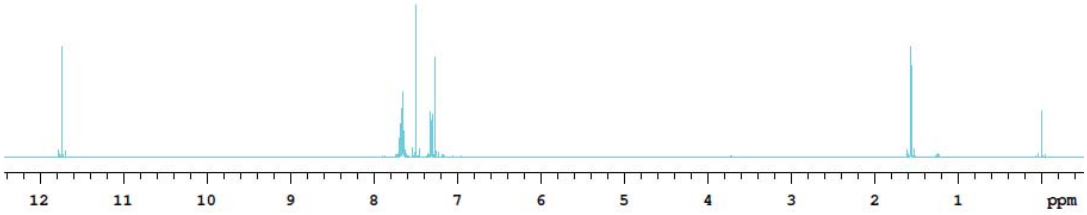

2-(2-(1,3-dioxan-2-yl)-6-(methoxymethoxy)-4-methylphenyl)-8-hydroxynaphthalene-1,4-dione

^{1}H NMR (acetone-d_6, 500 MHz)

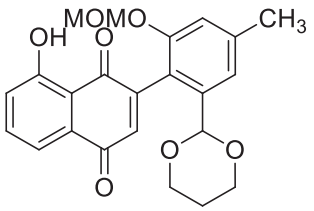

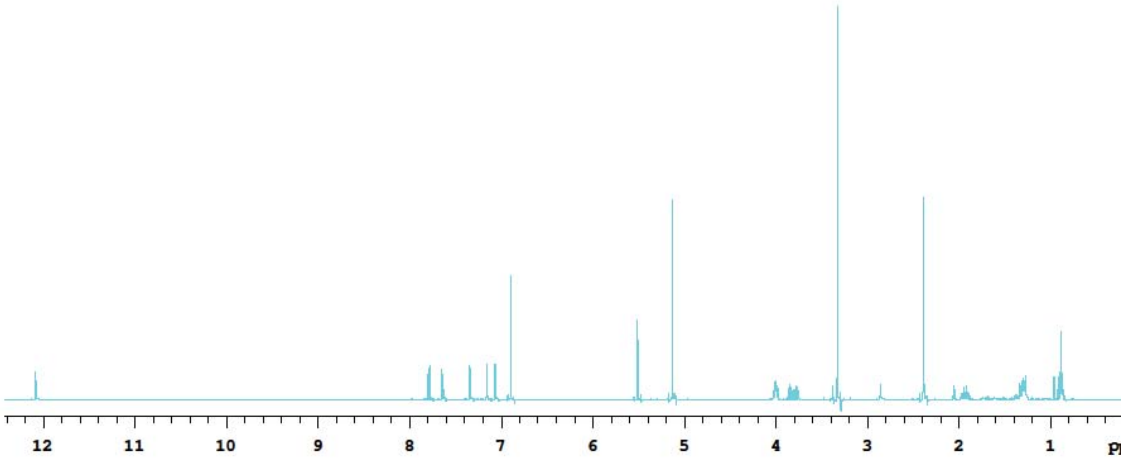

2-(2-(1,3-dioxan-2-yl)-6-(methoxymethoxy)-4-methylphenyl)-8-hydroxynaphthalene-1,4-dione

^{13}C NMR (acetone-d_6, 125 MHz)

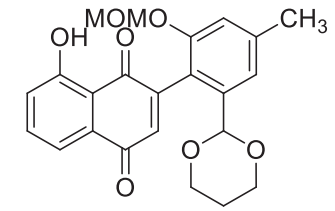

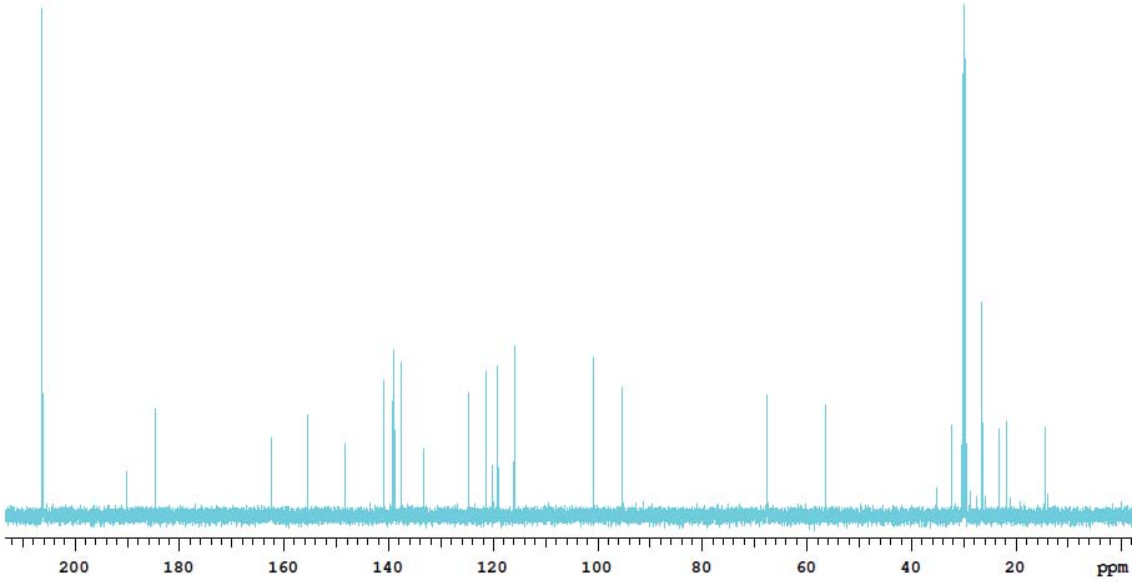

3-hydroxy-2-(8-hydroxy-1,4-dioxo-1,4-dihydronaphthalen-2-yl)-5-methylbenzaldehyde (100)

^{1}H NMR (acetone-d_6, 400 MHz)

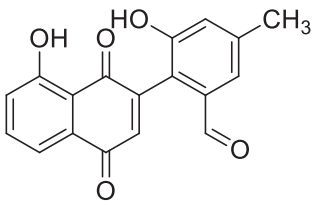

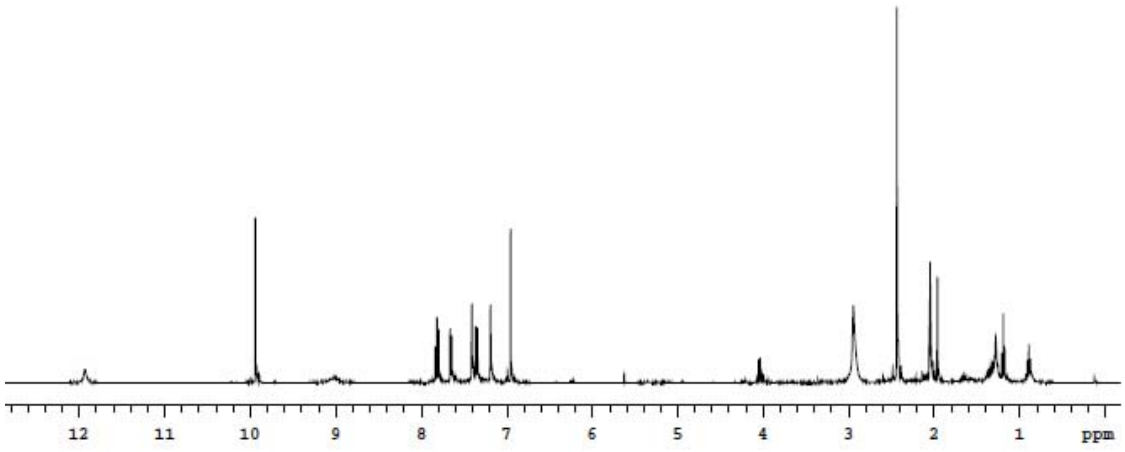

3-hydroxy-2-(8-hydroxy-1,4-dioxo-1,4-dihydronaphthalen-2-yl)-5-methylbenzaldehyde (100)

^{13}C NMR (acetone-d_6, 100 MHz)

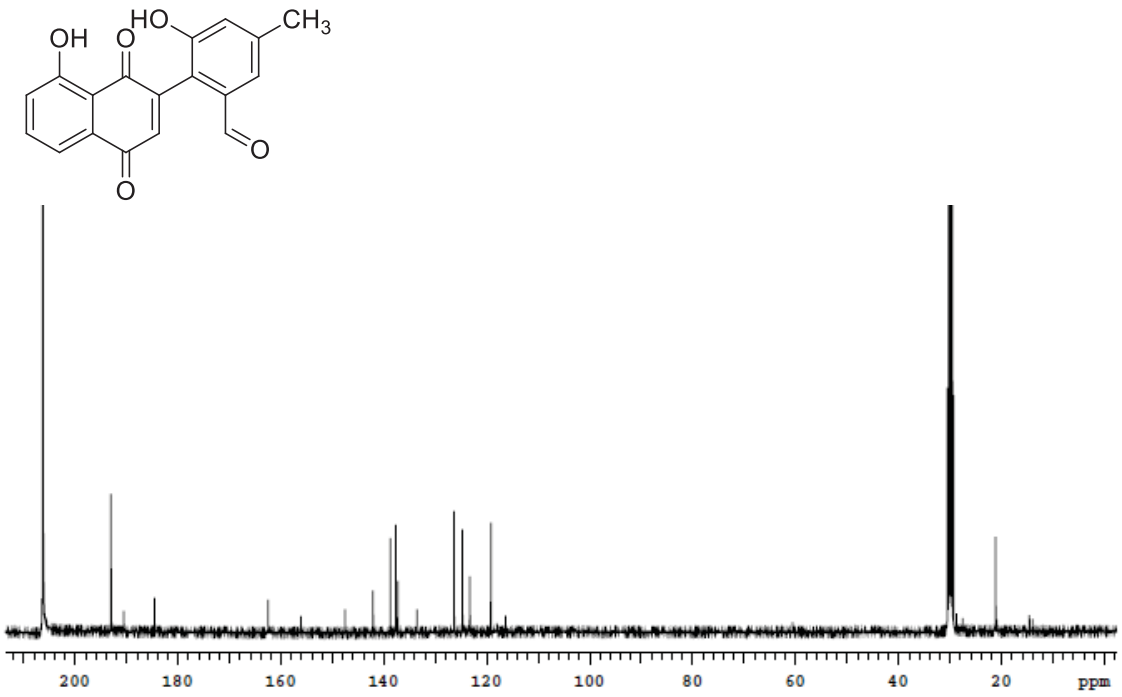

2-bromo-5,7-dihydroxynaphthalene-1,4-dione (101)

^{1}H NMR (acetone-d_6, 500 MHz)

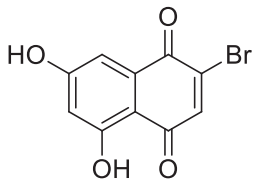

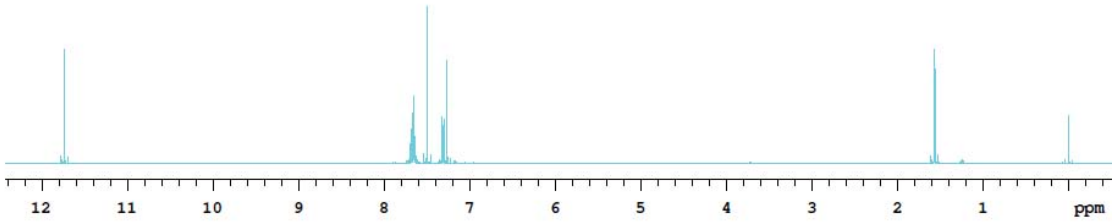

2-bromo-5,7-dihydroxynaphthalene-1,4-dione (101)

^{13}C NMR (acetone-d_6, 125 MHz)

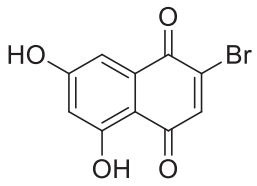

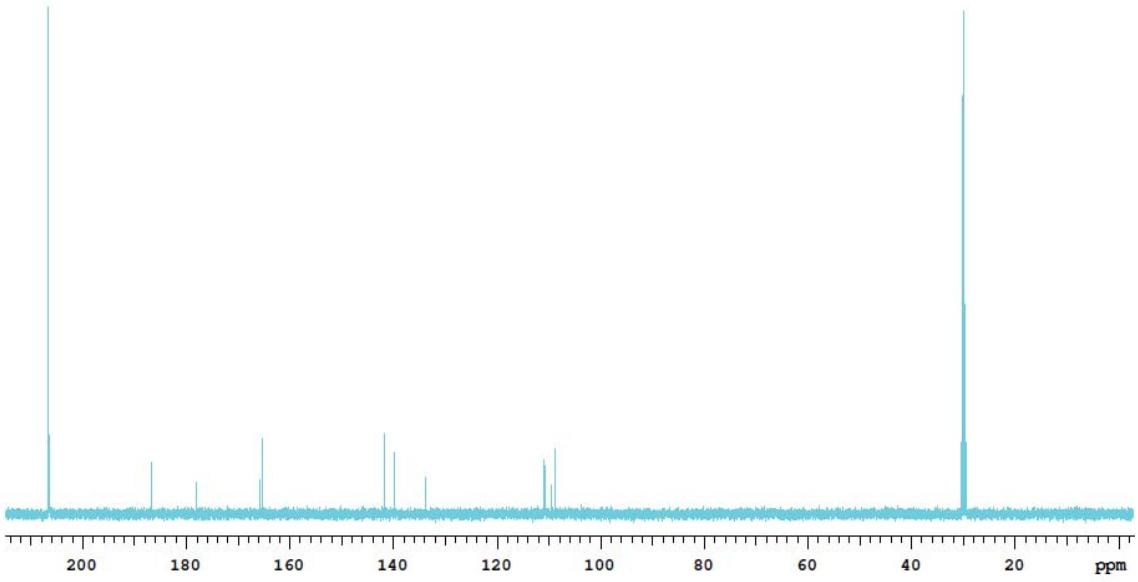

2-(2-(1,3-dioxan-2-yl)-6-(methoxymethoxy)-4-methylphenyl)-5,7-dihydroxynaphthalene-1,4-dione (108)

^{1}H NMR (acetone-d_6, 400 MHz)

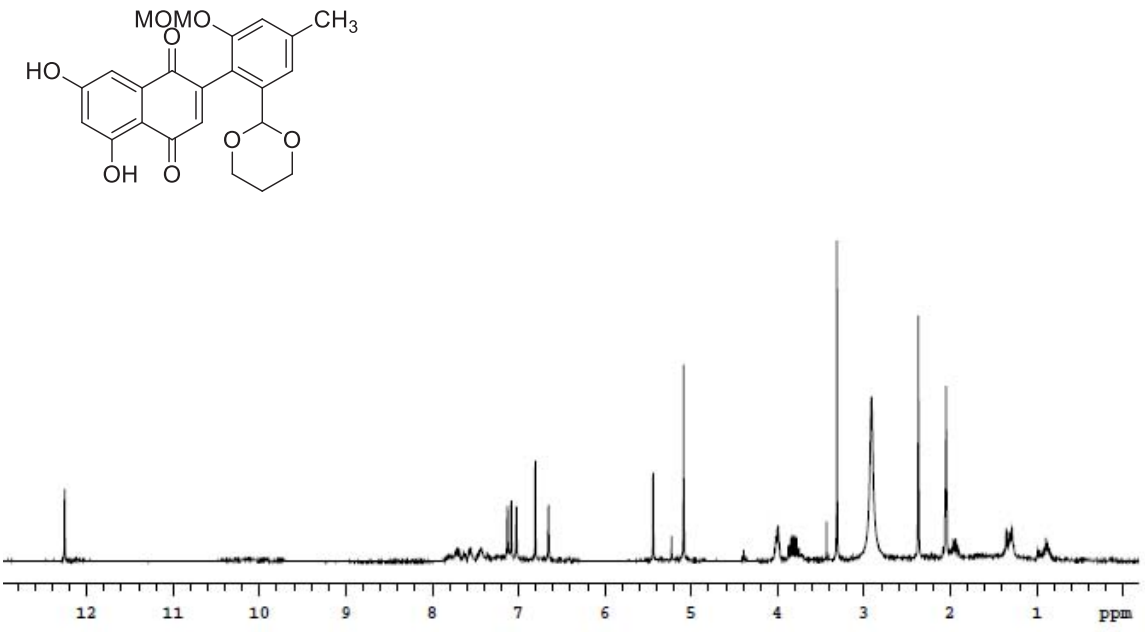

2-(2-(1,3-dioxan-2-yl)-6-(methoxymethoxy)-4-methylphenyl)-5,7-dihydroxynaphthalene-1,4-dione (108)

^{13}C NMR (acetone-d_6, 100 MHz)

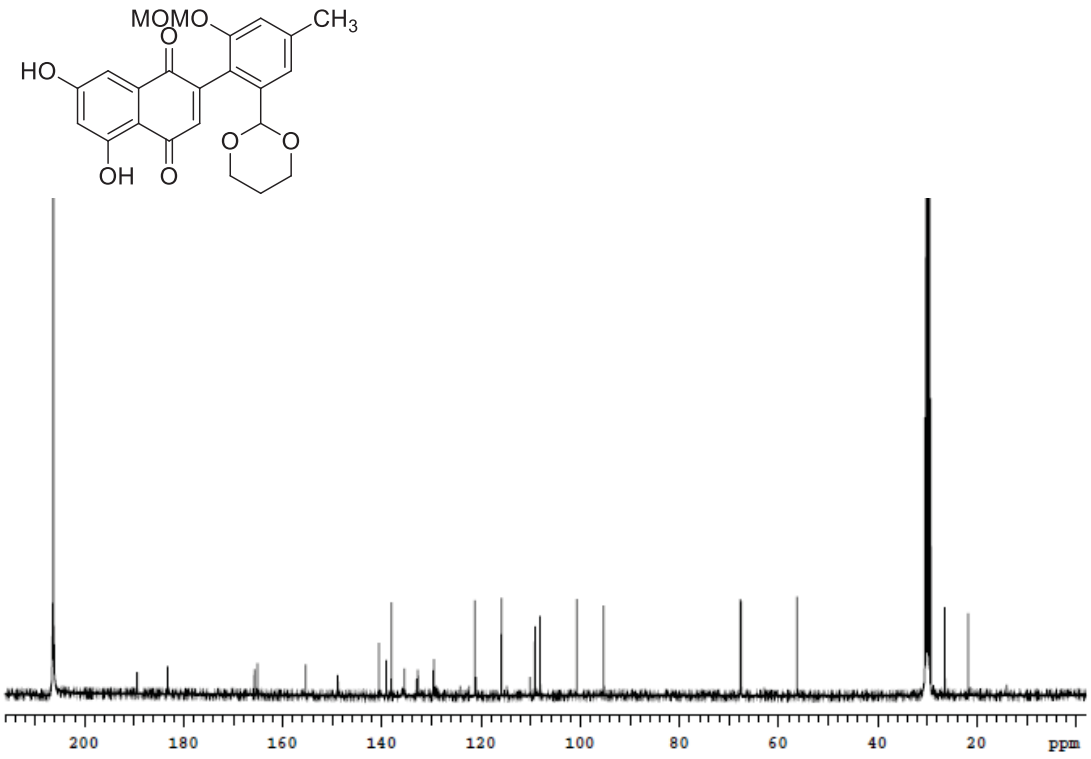

2-chloro-8-hydroxy-6-methoxynaphthalene-1,4-dione (111)

^{1}H NMR ($CDCl_3$,400 MHz)

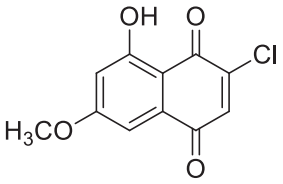

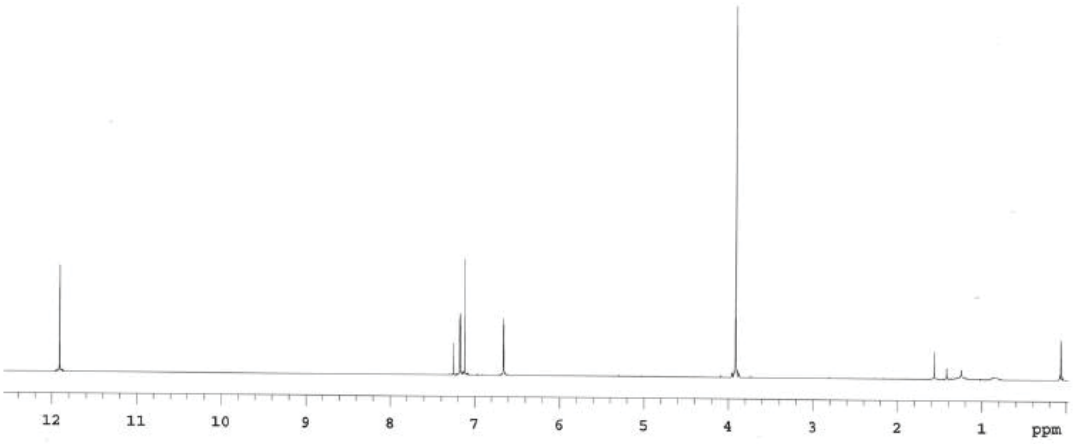

2-chloro-8-hydroxy-6-methoxynaphthalene-1,4-dione (111)

^{13}C NMR ($CDCl_3$,100 MHz)

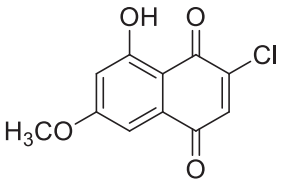

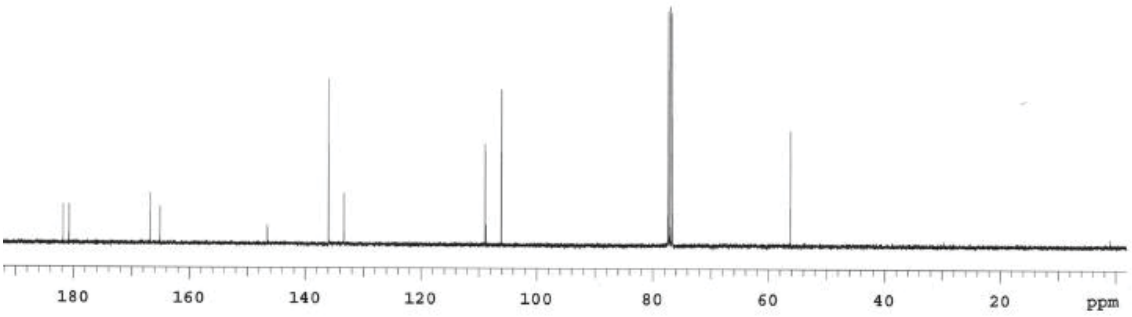

2-(2-(1,3-dioxan-2-yl)-6-(methoxymethoxy)-4-methylphenyl)-8-hydroxy-6-methoxynaphthalene-1,4-dione

^{1}H NMR ($CDCl_3$,400 MHz)

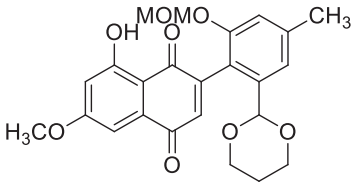

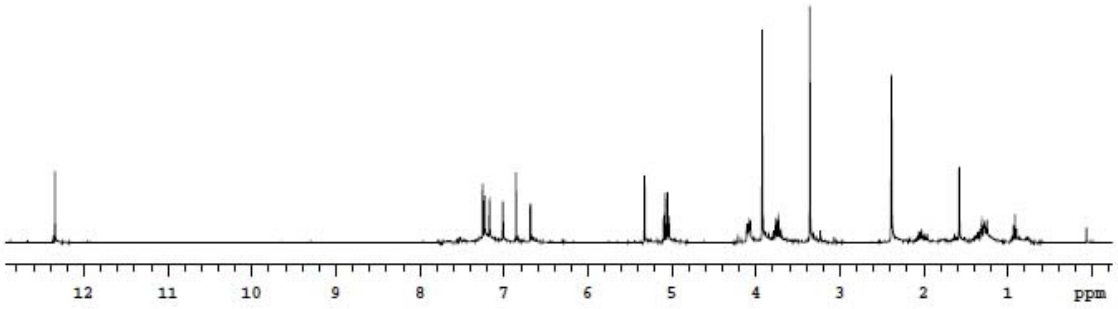

2-(2-(1,3-dioxan-2-yl)-6-(methoxymethoxy)-4-methylphenyl)-8-hydroxy-6-methoxynaphthalene-1,4-dione

^{13}C NMR ($CDCl_3$,100 MHz)

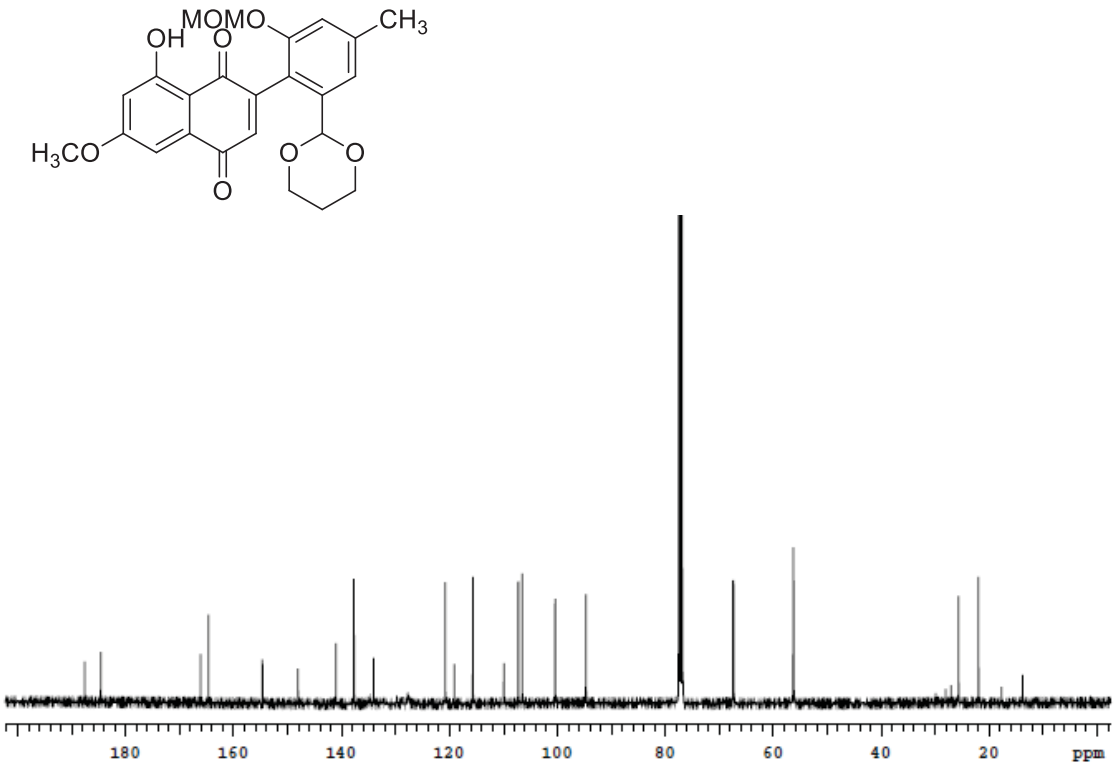

3-hydroxy-2-(8-hydroxy-6-methoxy-1,4-dioxo-1,4-dihydronaphthalen-2-yl)-5-methylbenzaldehyde (112)

^{1}H NMR (acetone-d_6, 400 MHz)

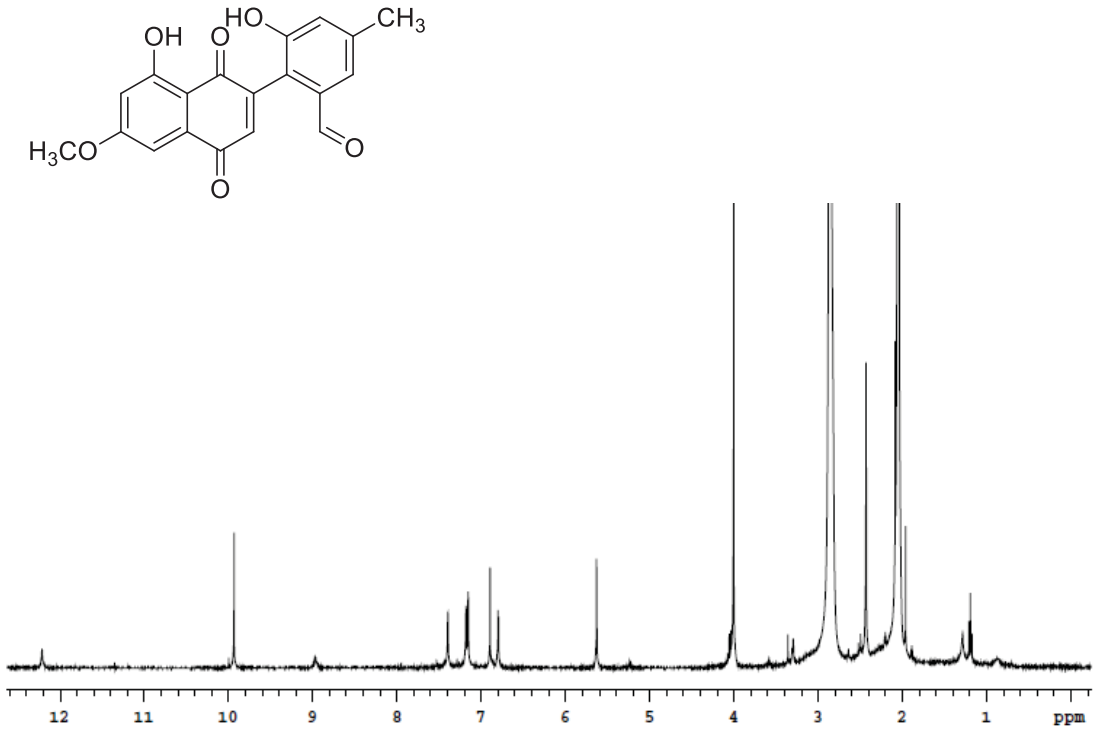

3-hydroxy-2-(8-hydroxy-6-methoxy-1,4-dioxo-1,4-dihydronaphthalen-2-yl)-5-methylbenzaldehyde (112)

^{13}C NMR (acetone-d_6, 100 MHz)

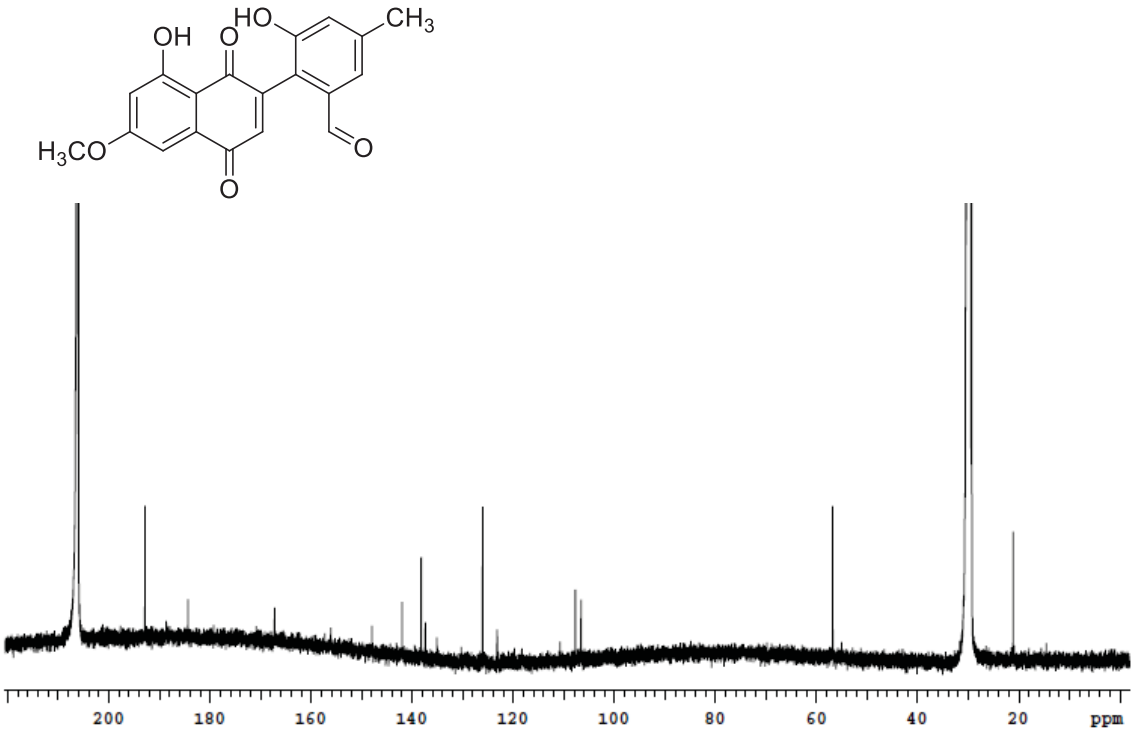

5-(benzyloxy)-2-bromonaphthalene-1,4-dione (113)

^{1}H NMR ($CDCl_3$, 500 MHz)

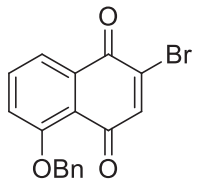

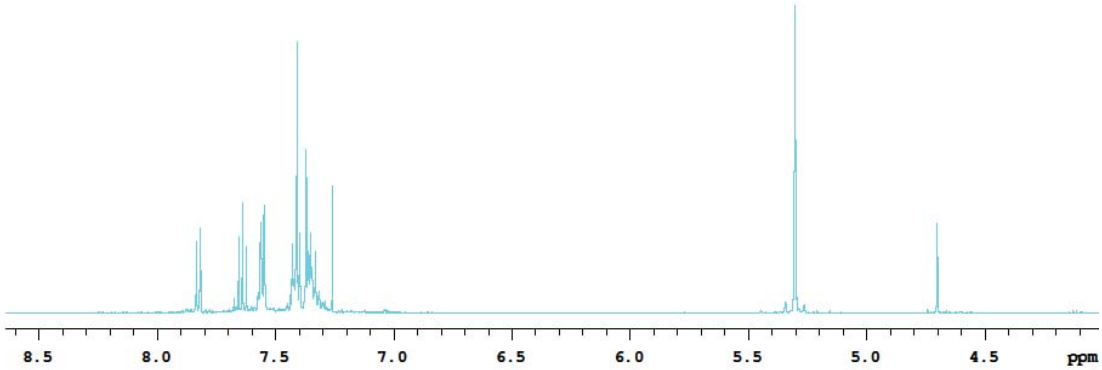

2-(2-(1,3-dioxan-2-yl)-6-(methoxymethoxy)-4-methylphenyl)-5-(benzyloxy)naphthalene-1,4-dione

^{1}H NMR ($CDCl_3$, 400 MHz)

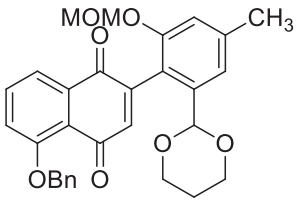

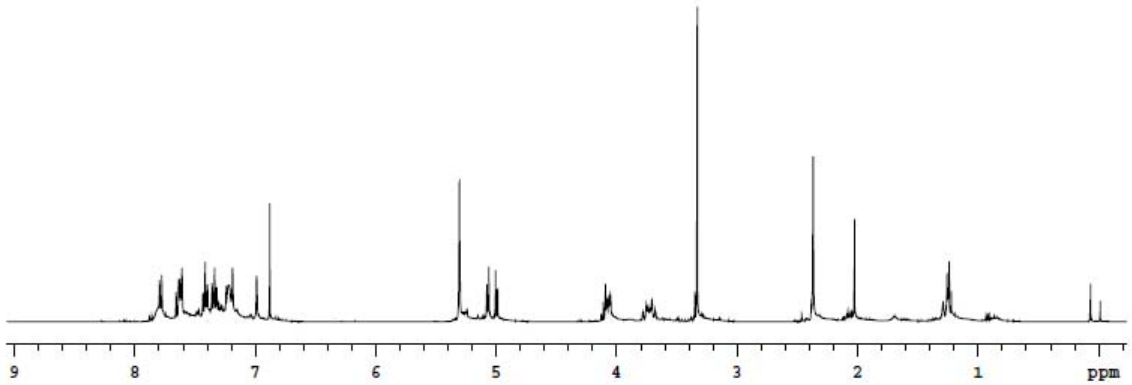

2-(2-(1,3-dioxan-2-yl)-6-(methoxymethoxy)-4-methylphenyl)-5-(benzyloxy)naphthalene-1,4-dione

^{13}C NMR ($CDCl_3$, 100 MHz)

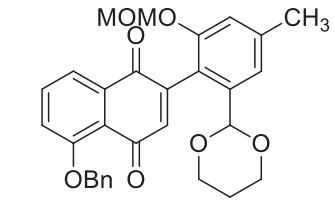

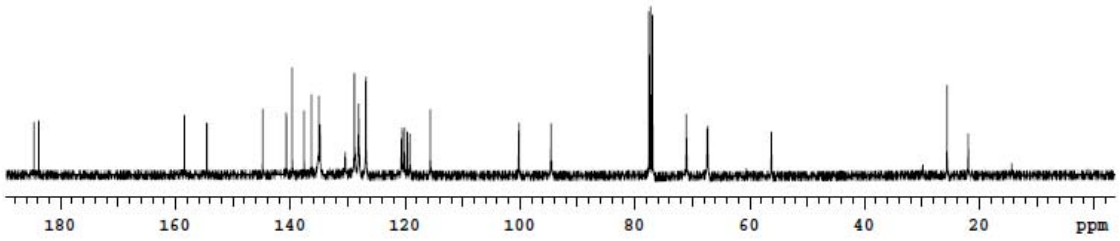

2-(5-(benzyloxy)-1,4-dioxo-1,4-dihydronaphthalen-2-yl)-3-hydroxy-5-methylbenzaldehyde (114)

^{1}H NMR (DMSO, 500 MHz)

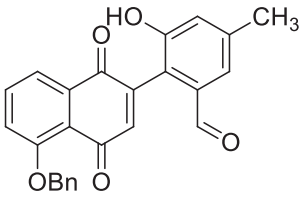

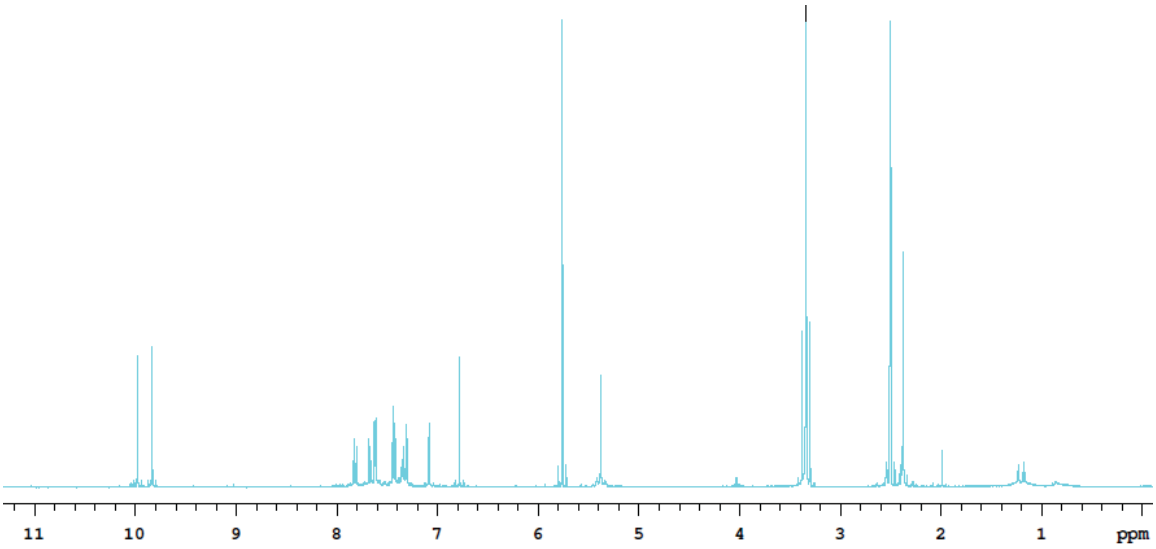

2-(2-(1,3-dioxan-2-yl)-6-(methoxymethoxy)-4-methylphenyl)naphthalene-1,4-dione

^{1}H NMR (acetone-d_6, 500 MHz)

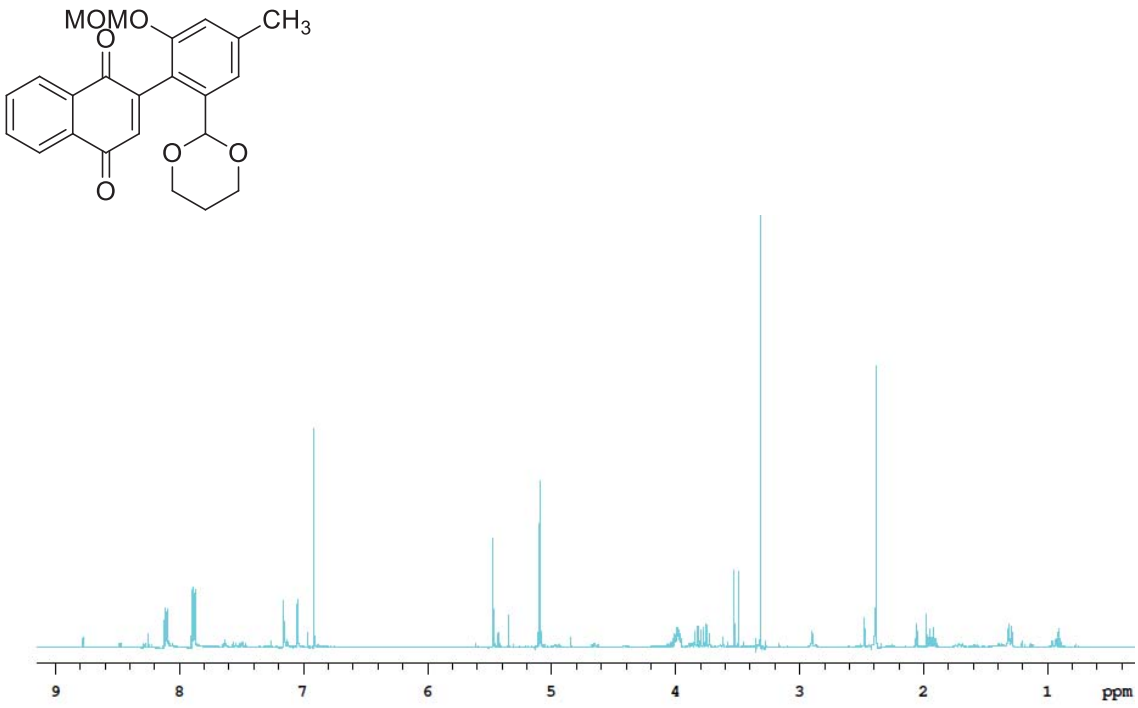

2-(2-(1,3-dioxan-2-yl)-6-(methoxymethoxy)-4-methylphenyl)naphthalene-1,4-dione

^{13}C NMR (acetone-d_6, 125 MHz)

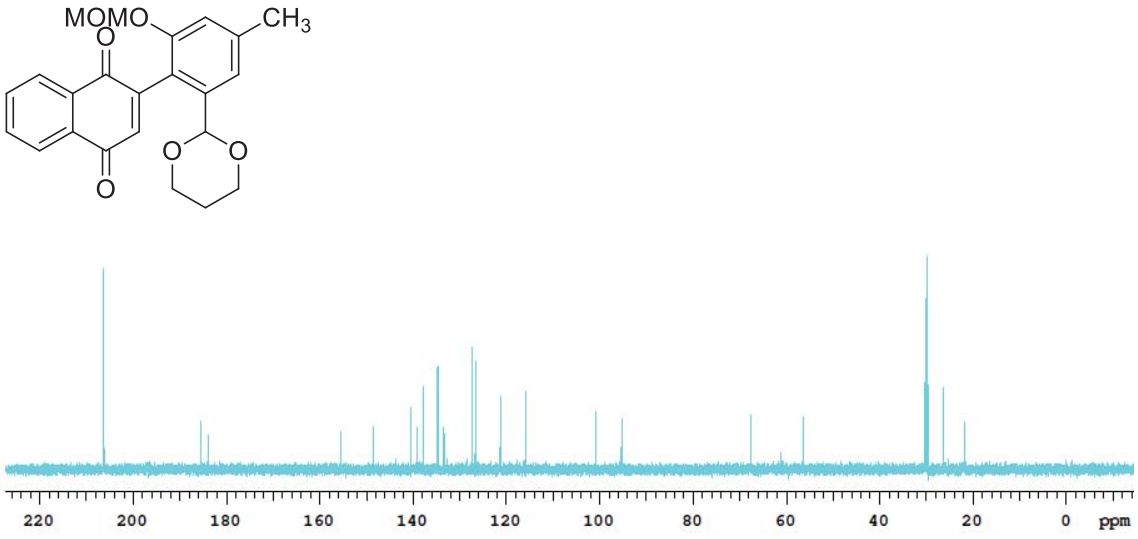

2-(1,4-dioxo-1,4-dihydronaphthalen-2-yl)-3-hydroxy-5-methylbenzaldehyde (116)

^{1}H NMR (acetone-d_6, 500 MHz)

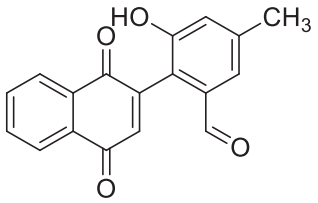

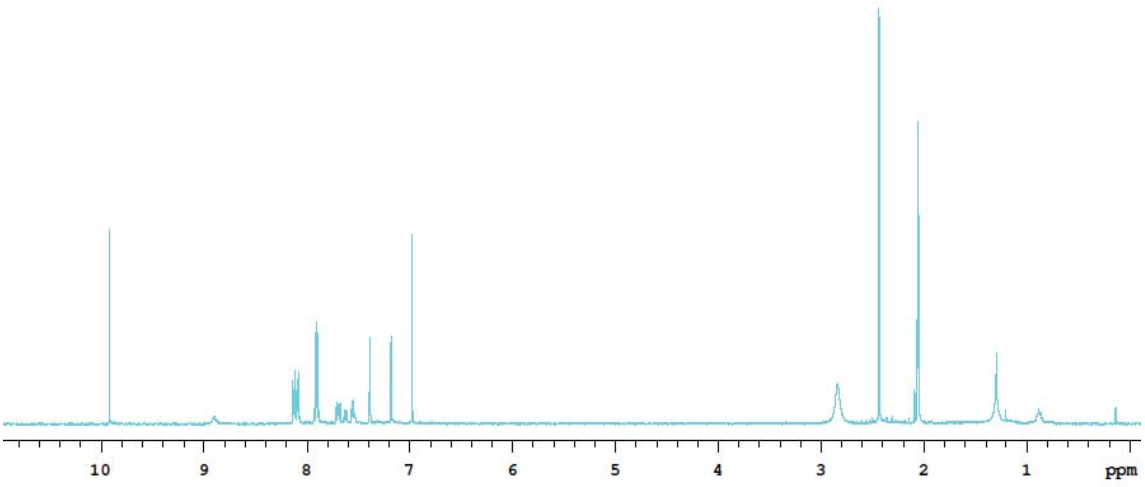

2-(1,4-dioxo-1,4-dihydronaphthalen-2-yl)-3-hydroxy-5-methylbenzaldehyde (116)

^{13}C NMR (acetone-d_6, 100 MHz)

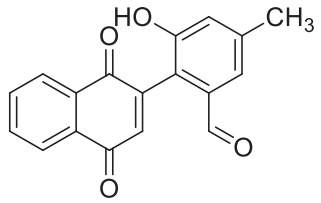

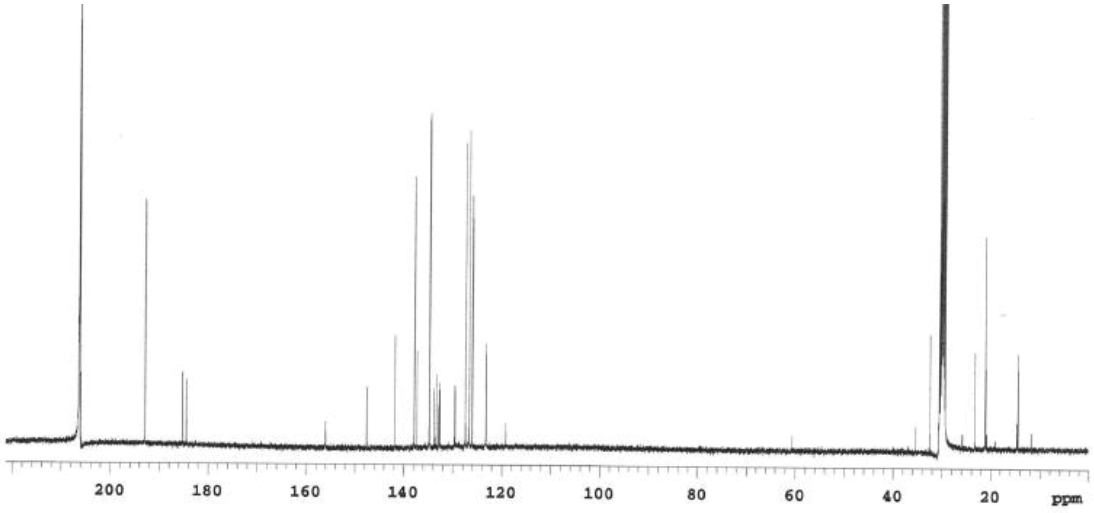

3-(1,3-dioxan-2-yl)phenol

^{1}H NMR ($CDCl_3$, 500 MHz)

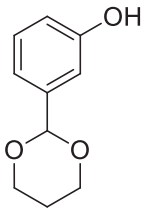

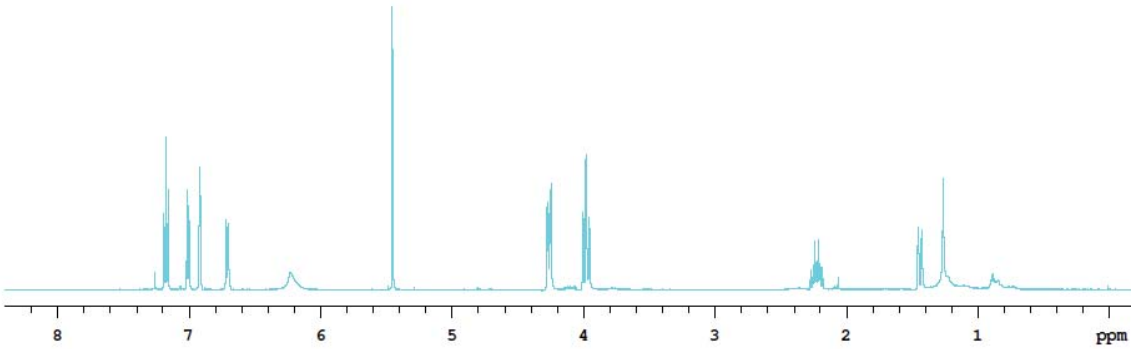

3-(1,3-dioxan-2-yl)phenol

^{13}C NMR ($CDCl_3$, 125 MHz)

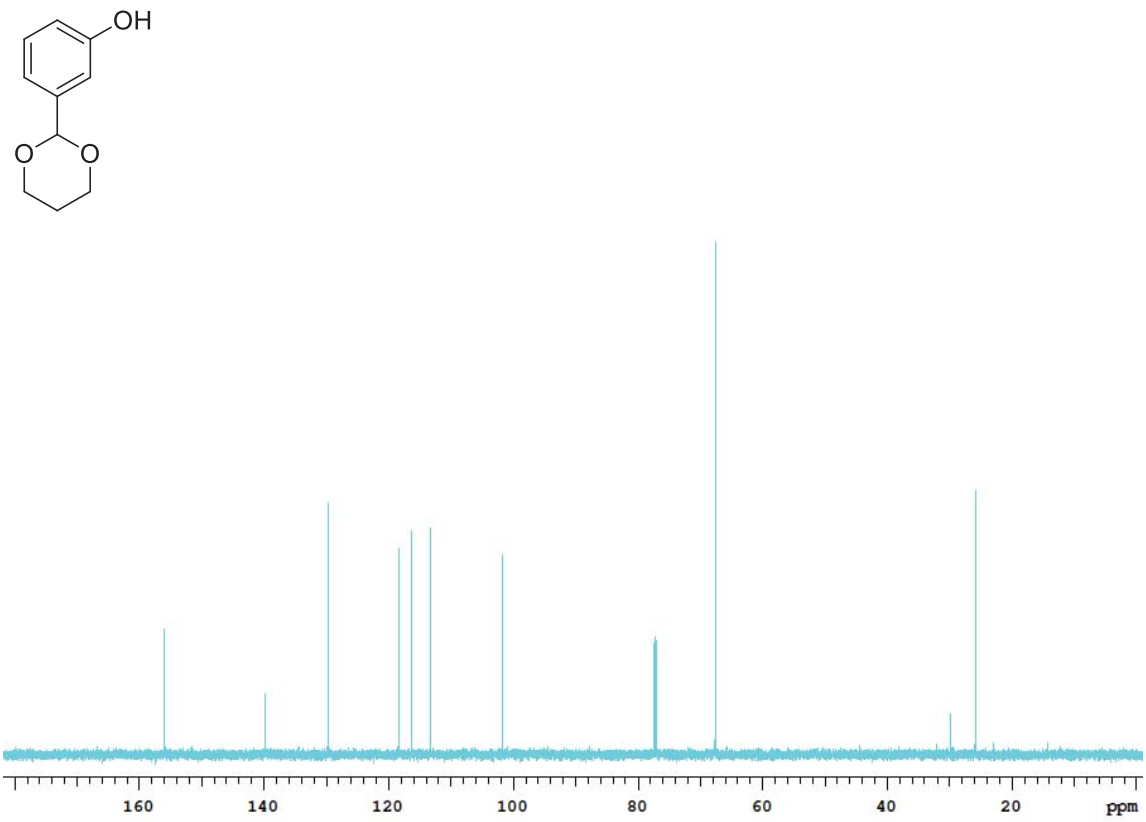

2-(3-(methoxymethoxy)phenyl)-1,3-dioxane (118)

^{1}H NMR ($CDCl_3$, 500 MHz)

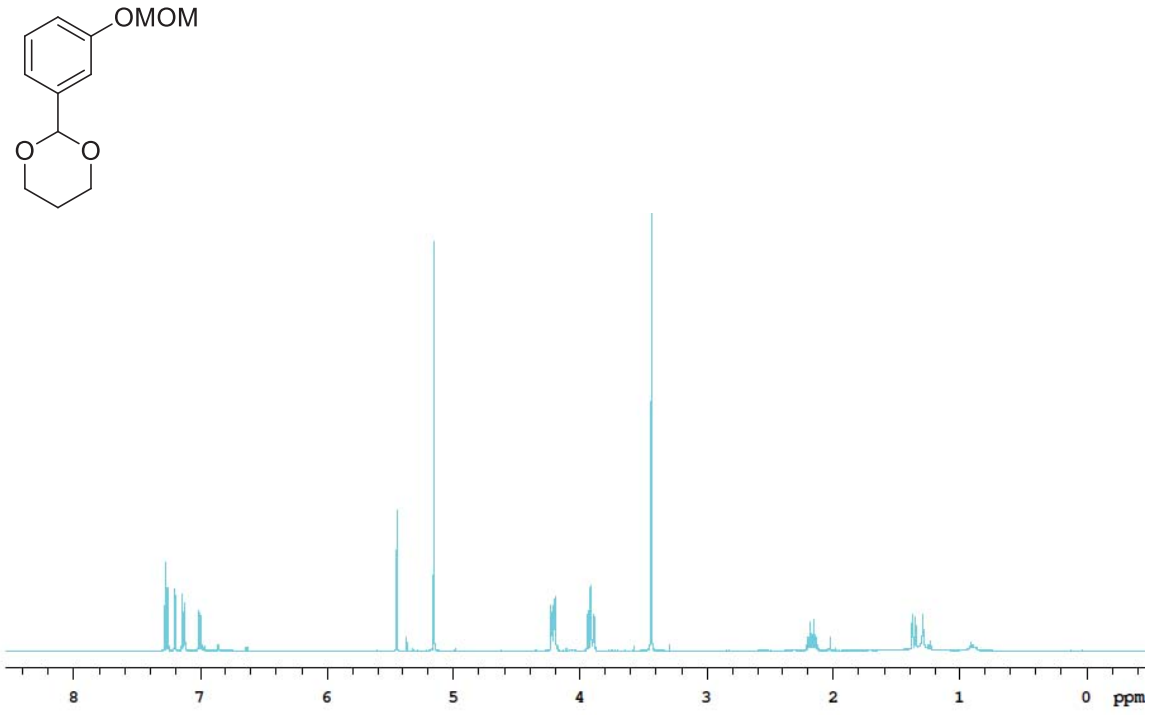

2-(3-(methoxymethoxy)phenyl)-1,3-dioxane (118)

^{13}C NMR ($CDCl_3$, 125 MHz)

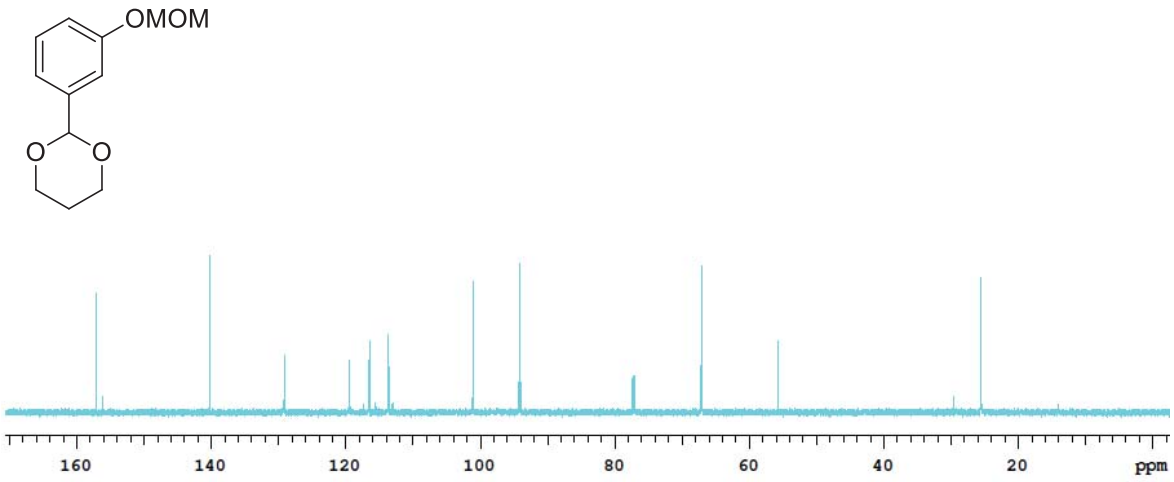

(2-(1,3-dioxan-2-yl)-6-(methoxymethoxy)phenyl)tributylstannane (119)

^{1}H NMR ($CDCl_3$, 500 MHz)

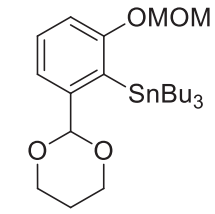

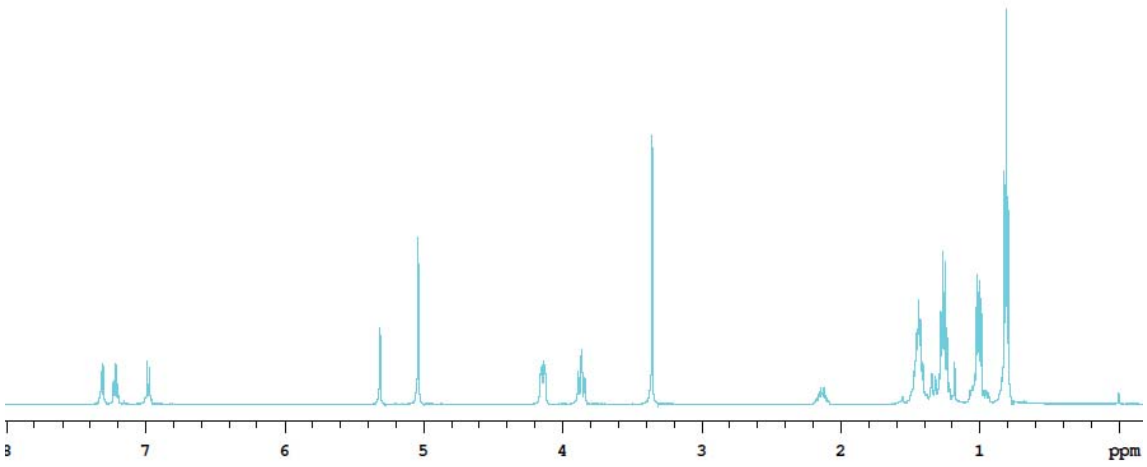

(2-(1,3-dioxan-2-yl)-6-(methoxymethoxy)phenyl)tributylstannane (119)

^{13}C NMR ($CDCl_3$, 125 MHz)

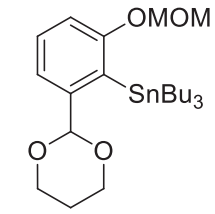

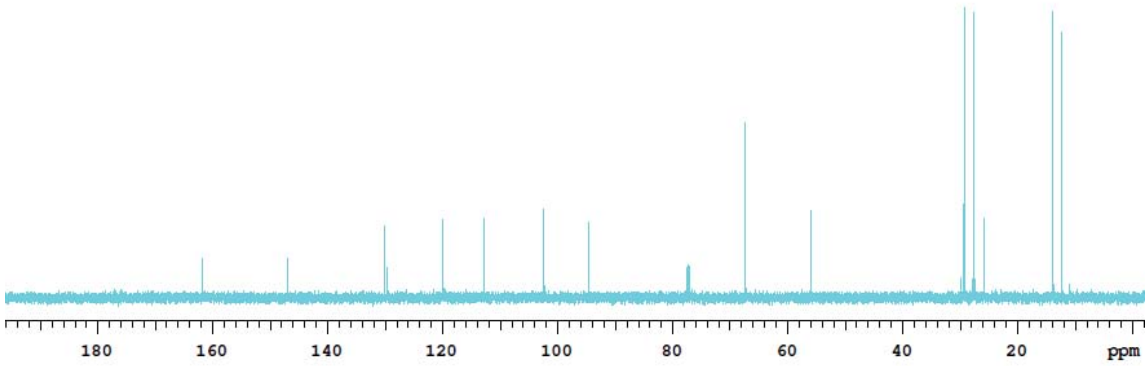

3-hydroxy-2-(5-hydroxy-1,4-dioxo-1,4-dihydronaphthalen-2-yl)benzaldehyde (120)

^{1}H NMR (acetone-d_6, 400 MHz)

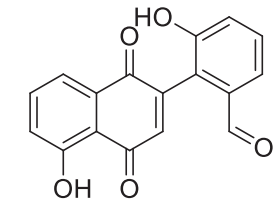

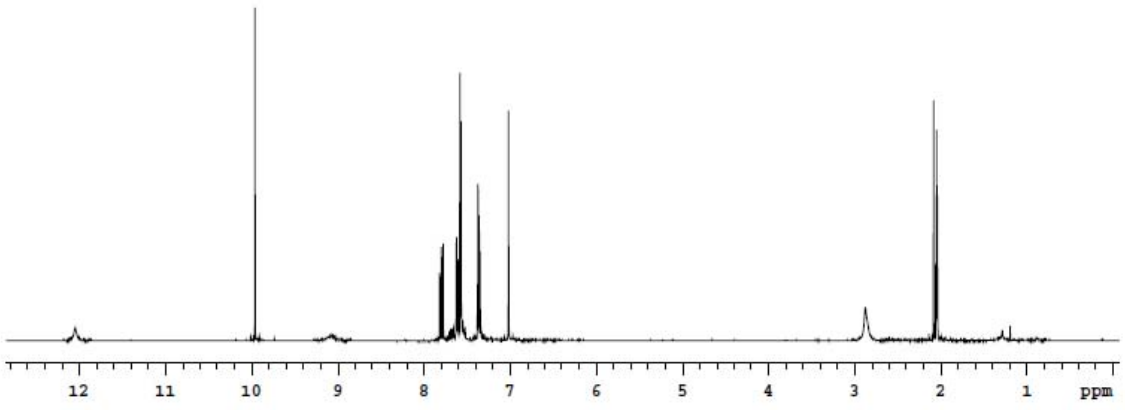

3-hydroxy-2-(5-hydroxy-1,4-dioxo-1,4-dihydronaphthalen-2-yl)benzaldehyde (120)

^{13}C NMR (acetone-d_6, 100 MHz)

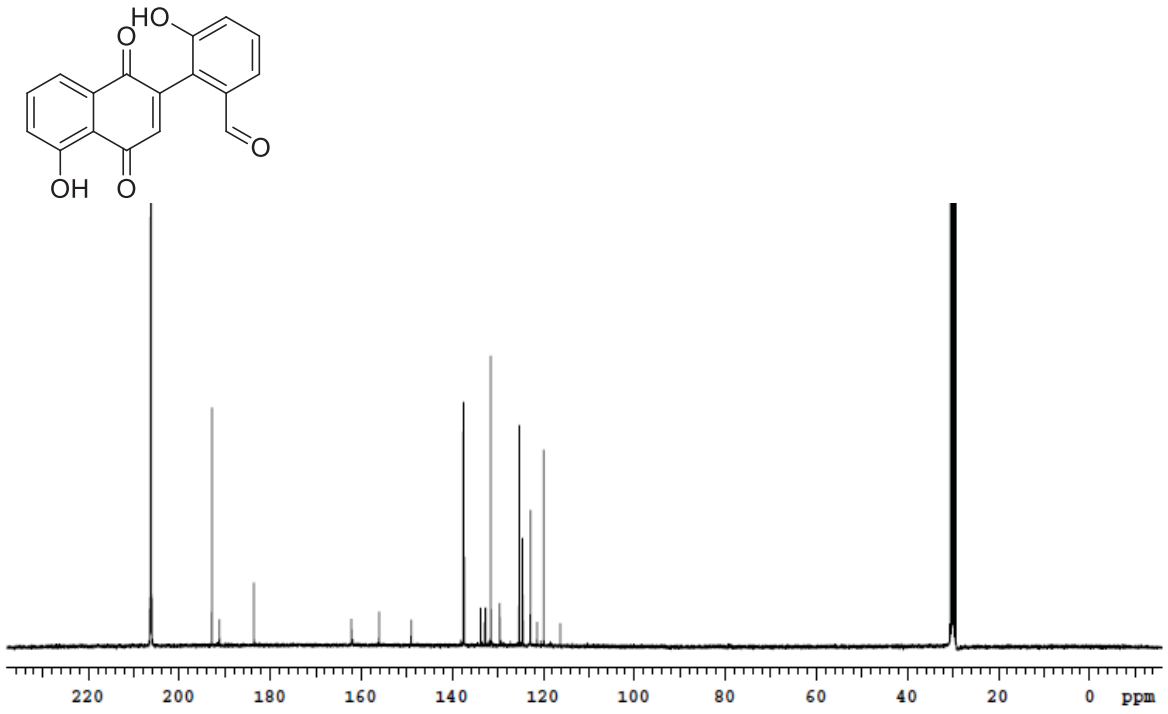

2-(5-hydroxy-1,4-dioxo-1,4-dihydronaphthalen-2-yl)-3-(methoxymethoxy)benzaldehyde (121)

^{1}H NMR (acetone-d_6, 500 MHz)

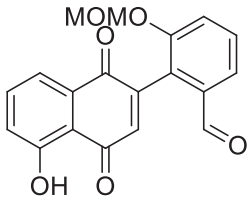

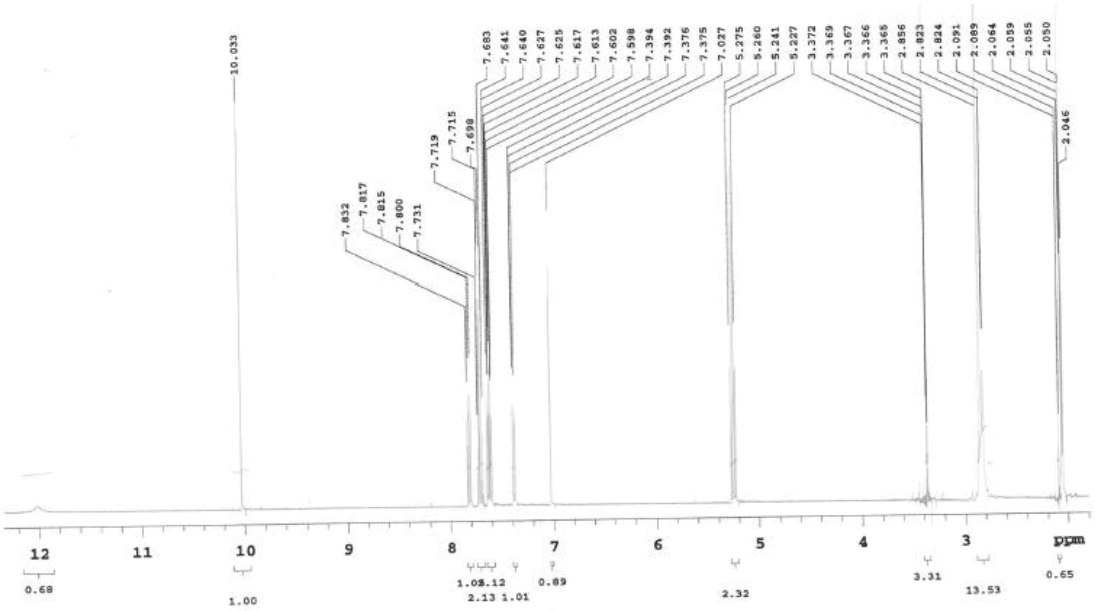

2-(5-hydroxy-1,4-dioxo-1,4-dihydronaphthalen-2-yl)-3-(methoxymethoxy)benzaldehyde (121)

^{13}C NMR (acetone-d_6, 100 MHz)

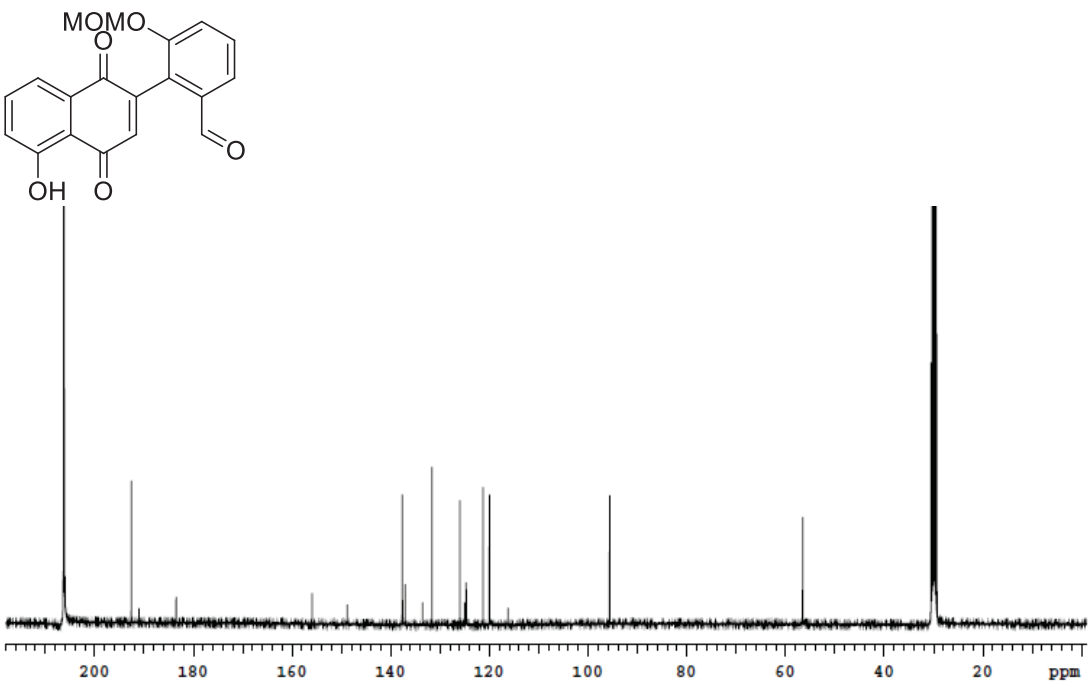

References

1. Dewick, P. (2007) *Medicinal Natural Products; Second Edition ed.; John Wiley & Sons, Ltd*.
2. O'Hagan, D. (1991) *The Polyketides Metabolites, Ellis Horwood, Chichester.*
3. Thiericke, R., and Rohr, J. (1993) Biological variation of microbial metabolites by precursor-directed biosynthesis., *Natural Product Reports 10* 265-289.
4. Weist, S., and Sussmuth, R. D. (2005) Mutational biosynthesis - a tool for the generation of structural diversity in the biosynthesis of antibiotics, *Appl Microbiol Biot 68*, 141-150.
5. Hertweck, C. (2009) The Biosynthetic Logic of Polyketide Diversity, *Angew Chem Int Edit 48*, 4688-4716.
6. Smith, S., and Tsai, S. C. (2007) The type I fatty acid and polyketide synthases: a tale of two megasynthases, *Natural Product Reports 24*, 1041-1072.
7. Hopwood, D. A. (1997) Genetic contributions to understanding polyketide synthases, *Chem. Rev. 97*, 2465-2497.
8. Fischbach, M. A., and Walsh, C. T. (2006) Assembly-line enzymology for polyketide and nonribosomal Peptide antibiotics: logic, machinery, and mechanisms, *Chem Rev 106*, 3468-3496.
9. Donadio, S., Staver, M. J., McAlpine, J. B., Swanson, S. J., and Katz, L. (1991) Modular organization of genes required for complex polyketide biosynthesis, *Science 252*, 675-679.
10. Walsh, C. T. (2003) Antibiotics, *Antibiotics, ASM press, washington DC, USA*, 175-191.
11. Rawlings, B. J. (2001) Type I polyketide biosynthesis in bacteria (Part A--erythromycin biosynthesis), *Natural Product Reports 18*, 190-227.
12. Ma, S. M., Li, J. W., Choi, J. W., Zhou, H., Lee, K. K., Moorthie, V. A., Xie, X., Kealey, J. T., Da Silva, N. A., Vederas, J. C., and Tang, Y. (2009) Complete reconstitution of a highly reducing iterative polyketide synthase, *Science 326*, 589-592.
13. McDaniel, R., Ebertkhosla, S., Hopwood, D. A., and Khosla, C. (1995) Rational design of aromatic polyketide natural products by recombinant assembly of enzymatic subunits, *Nature 375*, 549-554.
14. Sandmann, A., Dickschat, J., Jenke-Kodama, H., Kunze, B., Dittmann, E., and Muller, R. (2007) A Type II polyketide synthase from the gram-negative Bacterium Stigmatella aurantiaca is involved in Aurachin alkaloid biosynthesis, *Angew Chem Int Ed Engl 46*, 2712-2716.
15. Brachmann, A. O., Joyce, S. A., Jenke-Kodama, H., Schwar, G., Clarke, D. J., and Bode, H. B. (2007) A type II polyketide synthase is responsible for anthraquinone biosynthesis in Photorhabdus luminescens, *Chembiochem 8*, 1721-1728.
16. Malpartida, F., and Hopwood, D. A. (1984) Molecular cloning of the whole biosynthetic pathway of a Streptomyces antibiotic and its expression in a heterologous host, *Nature 309*, 462-464.
17. Fernandez-Moreno, M. A., Martinez, E., Boto, L., Hopwood, D. A., and Malpartida, F. (1992) Nucleotide sequence and deduced functions of a set of cotranscribed genes of Streptomyces coelicolor A3(2) including the polyketide synthase for the antibiotic actinorhodin, *J Biol Chem 267*, 19278-19290.
18. Gross, F. L., N. Perlova, O. Gaitatzis, N. Jenke-Kodama, H. (2006) *Archives of Microbiology 185*, 28-38.
19. Magarvey, N. A., Beck, Z. Q., Golakoti, T., Ding, Y., Huber, U., Hemscheidt, T. K., Abelson, D., Moore, R. E., and Sherman, D. H. (2006) Biosynthetic characterization and

chemoenzymatic assembly of the cryptophycins. Potent anticancer agents from cyanobionts, *ACS Chem Biol 1*, 766-779.
20. Jacobsen, J. R., Hutchinson, C. R., Cane, D. E., and Khosla, C. (1997) Precursor-directed biosynthesis of erythromycin analogs by an engineered polyketide synthase, *Science 277*, 367-369.
21. Olano, C., Mendez, C., and Salas, J. A. (2010) Post-PKS tailoring steps in natural product-producing actinomycetes from the perspective of combinatorial biosynthesis, *Natural Product Reports 27*, 571-616.
22. Rix, U., Fischer, C., Remsing, L. L., and Rohr, J. (2002) Modification of post-PKS tailoring steps through combinatorial biosynthesis, *Natural Product Reports 19*, 542-580.
23. Lamb, D. C., Waterman, M. R., Kelly, S. L., and Guengerich, F. P. (2007) Cytochromes P450 and drug discovery, *Curr Opin Biotechnol 18*, 504-512.
24. Machida, K., Aritoku, Y., and Tsuchida, T. (2009) One-pot fermentation of pladienolide D by Streptomyces platensis expressing a heterologous cytochrome P450 gene, *J Biosci Bioeng 107*, 596-598.
25. Lee, S. K., Park, J. W., Kim, J. W., Jung, W. S., Park, S. R., Choi, C. Y., Kim, E. S., Kim, B. S., Ahn, J. S., Sherman, D. H., and Yoon, Y. J. (2006) Neopikromycin and novapikromycin from the pikromycin biosynthetic pathway of Streptomyces venezuelae, *J Nat Prod 69*, 847-849.
26. Yoon, Y. J., Beck, B. J., Kim, B. S., Kang, H. Y., Reynolds, K. A., and Sherman, D. H. (2002) Generation of multiple bioactive macrolides by hybrid modular polyketide synthases in Streptomyces venezuelae, *Chem Biol 9*, 203-214.
27. Desai, R. P., Rodriguez, E., Galazzo, J. L., and Licari, P. (2004) Improved bioconversion of 15-fluoro-6-deoxyerythronolide B to 15-fluoro-erythromycin A by overexpression of the eryK Gene in Saccharopolyspora erythraea, *Biotechnol Prog 20*, 1660-1665.
28. Gibson, M., Nur-e-alam, M., Lipata, F., Oliveira, M. A., and Rohr, J. (2005) Characterization of kinetics and products of the Baeyer-Villiger oxygenase MtmOIV, the key enzyme of the biosynthetic pathway toward the natural product anticancer drug mithramycin from Streptomyces argillaceus, *J Am Chem Soc 127*, 17594-17595.
29. Menendez, N., Nur-e-Alam, M., Brana, A. F., Rohr, J., Salas, J. A., and Mendez, C. (2004) Biosynthesis of the antitumor chromomycin A3 in Streptomyces griseus: analysis of the gene cluster and rational design of novel chromomycin analogs, *Chem Biol 11*, 21-32.
30. Beam, M. P., Bosserman, M. A., Noinaj, N., Wehenkel, M., and Rohr, J. (2009) Crystal structure of Baeyer-Villiger monooxygenase MtmOIV, the key enzyme of the mithramycin biosynthetic pathway, *Biochemistry 48*, 4476-4487.
31. Shen, B., and Hutchinson, C. R. (1993) Tetracenomycin F1 monooxygenase: oxidation of a naphthacenone to a naphthacenequinone in the biosynthesis of tetracenomycin C in Streptomyces glaucescens, *Biochemistry 32*, 6656-6663.
32. Caballero, J. L., Martinez, E., Malpartida, F., and Hopwood, D. A. (1991) Organisation and functions of the actVA region of the actinorhodin biosynthetic gene cluster of Streptomyces coelicolor, *Mol Gen Genet 230*, 401-412.
33. Rafanan, E. R., Le, L., Zhao, L. L., Decker, H., and Shen, B. (2001) Cloning, sequencing, and heterologous expression of the elmGHIJ genes involved in the biosynthesis of the polyketide antibiotic elloramycin from Streptomyces olivaceus Tu2353, *J Nat Prod 64*, 444-449.
34. Shen, B., and Hutchinson, C. R. (1993) Tetracenomycin F2 cyclase: intramolecular aldol condensation in the biosynthesis of tetracenomycin C in Streptomyces glaucescens, *Biochemistry 32*, 11149-11154.

35. Mendez, C., and Salas, J. A. (2001) Altering the glycosylation pattern of bioactive compounds, *Trends Biotechnol 19*, 449-456.
36. Lairson, L. L., Henrissat, B., Davies, G. J., and Withers, S. G. (2008) Glycosyltransferases: structures, functions, and mechanisms, *Annu Rev Biochem 77*, 521-555.
37. Durr, C., Hoffmeister, D., Wohlert, S. E., Ichinose, K., Weber, M., von Mulert, U., Thorson, J. S., and Bechthold, A. (2004) The glycosyltransferase UrdGT2 catalyzes both C- and O-glycosidic sugar transfers, *Angew. Chem. Int. Ed. 43*, 2962-2965.
38. Liu, T., Kharel, M. K., Fischer, C., McCormick, A., and Rohr, J. (2006) Inactivation of gilGT, encoding a C-glycosyltransferase, and gilOIII, encoding a P450 enzyme, allows the details of the late biosynthetic pathway to gilvocarcin V to be delineated, *Chembiochem 7*, 1070-1077.
39. Lozano, M. J., Remsing, L. L., Quiros, L. M., Brana, A. F., Fernandez, E., Sanchez, C., Mendez, C., Rohr, J., and Salas, J. A. (2000) Characterization of two polyketide methyltransferases involved in the biosynthesis of the antitumor drug mithramycin by Streptomyces argillaceus, *J Biol Chem 275*, 3065-3074.
40. Summers, R. G., Wendt-Pienkowski, E., Motamedi, H., and Hutchinson, C. R. (1992) Nucleotide sequence of the tcmII-tcmIV region of the tetracenomycin C biosynthetic gene cluster of Streptomyces glaucescens and evidence that the tcmN gene encodes a multifunctional cyclase-dehydratase-O-methyl transferase, *J Bacteriol 174*, 1810-1820.
41. Decker, H., Motamedi, H., and Hutchinson, C. R. (1993) Nucleotide sequences and heterologous expression of tcmG and tcmP, biosynthetic genes for tetracenomycin C in Streptomyces glaucescens, *J Bacteriol 175*, 3876-3886.
42. Gandecha, A. R., Large, S. L., and Cundliffe, E. (1997) Analysis of four tylosin biosynthetic genes from the tylLM region of the Streptomyces fradiae genome, *Gene 184*, 197-203.
43. Chen, H., Zhao, Z., Hallis, T. M., Guo, Z., and Liu, H.-w. (2001) Insights into the Branched-Chain Formation of Mycarose: Methylation Catalyzed by an (S)-Adenosylmethionine-Dependent Methyltransferase, *Angewandte Chemie International Edition 40*, 607-610.
44. Kreuzman, A. J., Turner, J. R., and Yeh, W. K. (1988) Two distinctive O-methyltransferases catalyzing penultimate and terminal reactions of macrolide antibiotic (tylosin) biosynthesis. Substrate specificity, enzyme inhibition, and kinetic mechanism, *J Biol Chem 263*, 15626-15633.
45. Connors, N. C., Bartel, P. L., and Strohl, W. R. (1990) Biosynthesis of Anthracyclines - Carminomycin 4-O-Methyltransferase, the Terminal Enzymatic Step in the Formation of Daunomycin, *J Gen Microbiol 136*, 1895-1898.
46. Connors, N. C., and Strohl, W. R. (1993) Partial-Purification and Properties of Carminomycin 4-O-Methyltransferase from Streptomyces Sp Strain C5, *J Gen Microbiol 139*, 1353-1362.
47. Weist, S., and Süssmuth, R. D. (2005) Mutational biosynthesis—a tool for the generation of structural diversity in the biosynthesis of antibiotics, *Appl Microbiol Biotechnol 68*, 141-150.
48. Krohn, K., and Rohr, J. (1997) Angucyclines: Total syntheses, new structures, and biosynthetic studies of an emerging new class of antibiotics, *Bioorganic Chemistry Deoxysugars, Polyketides and Related Classes: Synthesis, Biosynthesis, Enzymes 188*, 127-195.
49. Fischer, C., Lipata, F., and Rohr, J. (2003) The complete gene cluster of the antitumor agent gilvocarcin V and its implication for the biosynthesis of the gilvocarcins, *J. Am. Chem. Soc. 125*, 7818-7819.

50. Nakano, H., Matsuda, Y., Ito, K., Ohkubo, S., Morimoto, M., and Tomita, F. (1981) Gilvocarcins, new antitumor antibiotics. 1.Taxonomy, fermentation, isolation and biological activities., *J. Antibiot. 34*, 266-270.
51. Takahashi, K. Y., M.; Tomita, F.; Shirahata, K. (1981) Gilvocarcins, new antitumor antibiotics. 2. Structural elucidation, *J. Antibiot. 43*, 271-275.
52. Morimoto, M. O., S.; Tomita, F.; Marumo, H.;. (1981) Gilvocarcins, new antitumor antibiotics. 3. Antitumor activity, *J. Antibiot. 34*, 701-707.
53. Lytle, C. D., Routson, L. B., and Prodouz, K. N. (1994) Herpes virus infection and repair in cells pretreated with gilvocarcin V or merocyanine 540 and radiation, *J. Photochem. Photobiol. B-Biology 23*, 57-62.
54. Lytle, C. D., Wagner, S. J., and Prodouz, K. N. (1993) Antiviral activity of gilvocarcin V plus UVA radiation, *Photochem. Photobiol. 58*, 818-821.
55. Elespuru, R. K., and Gonda, S. K. (1984) Activation of antitumor agent gilvocarcins by visible light, *Science 223*, 69-71.
56. Tse-Dinh, Y. C., and McGee, L. R. (1987) Light-induced modifications of DNA by gilvocarcin V and its aglycone, *Biochem Biophys Res Commun 143*, 808-812.
57. Oyola, R., Arce, R., Alegria, A. E., and Garcia, C. (1997) Photophysical properties of gilvocarcins V and M and their binding constant to calf thymus DNA, *Photochem. Photobiol. 65*, 802-810.
58. Knobler, R. M., Radlwimmer, F. B., and Lane, M. J. (1993) Gilvocarcin V exhibits both equilibrium DNA binding and UV light induced DNA adduct formation which is sequence context dependent (Vol. 20, pp. 4553, 1992), *Nucleic Acids Res. 21*, 3920-3920.
59. Knobler, R. M., Radlwimmer, F. B., and Lane, M. J. (1992) Gilvocarcin V exhibits both equilibrium DNA binding and UV light induced DNA adduct formation which is sequence context dependent, *Nucleic Acids Res. 20*, 4553-4557.
60. Matsumoto, A., and Hanawalt, P. C. (2000) Histone H3 and heat shock protein GRP78 are selectively cross-linked to DNA by photoactivated gilvocarcin V in human fibroblasts, *Cancer Res. 60*, 3921-3926.
61. Gasparro, F. P., Chan, G., and Edelson, R. L. (1985) Phototherapy and photopharmacology, *Yale J Biol Med 58*, 519-534.
62. Hopper, C. (2000) Photodynamic therapy: a clinical reality in the treatment of cancer, *Lancet Oncol 1*, 212-219.
63. Ochsner, M. (1997) Photophysical and photobiological processes in the photodynamic therapy of tumours, *J Photochem Photobiol B 39*, 1-18.
64. Carter, G. T., Fantini, A. A., James, J. C., Borders, D. B., and White, R. J. (1984) Biosynthesis of ravidomycin- use of ^{13}C-^{13}C double quantum NMR to follow precursor incorporation, *Tetrahedron Lett. 25*, 255-258.
65. Takahashi, K., and Tomita, F. (1983) Gilvocarcins, new antitumor antibiotics. 5. Biosynthesis of gilvocarcins: Incorporation of ^{13}C-labeled compounds into gilvocarcin aglycones, *J. Antibiot. 36*, 1531-1535.
66. Carter, G. T., Fantini, A. A., James, J. C., Borders, D. B., and White, R. J. (1985) Biosynthesis of chrysomycin-A and chrysomycin-B origin of the chromophore, *J. Antibiot. 38*, 242-248.
67. Fischer, C., Lipata, F., and Rohr, J. (2003) The complete gene cluster of the antitumor agent gilvocarcin V and its implication for the biosynthesis of the gilvocarcins, *J Am Chem Soc 125*, 7818-7819.
68. Liu, T., Fischer, C., Beninga, C., and Rohr, J. (2004) Oxidative rearrangement processes in the biosynthesis of gilvocarcin V, *J. Am. Chem. Soc. 126*, 12262-12263.
69. Kharel, M. K., Zhu, L. L., Liu, T., and Rohr, J. (2007) Multi-oxygenase complexes of the gilvocarcin and jadomycin biosyntheses, *J. Am. Chem. Soc. 129*, 3780-3781.

70. Rix, U., Wang, C. C., Chen, Y. H., Lipata, F. M., Rix, L. L. R., Greenwell, L. M., Vining, L. C., Yang, K. Q., and Rohr, J. (2005) The oxidative ring cleavage in jadomycin biosynthesis: a multistep oxygenation cascade in a biosynthetic black box, *Chembiochem 6*, 838-835.
71. Chen, Y. H., Wang, C. C., Greenwell, L., Rix, U., Hoffmeister, D., Vining, L. C., Rohr, J. R., and Yang, K. Q. (2005) Functional analyses of oxygenases in jadomycin biosynthesis and identification of JadH as a bifunctional oxygenase/dehydrase, *J. Biol. Chem. 280*, 22508-22514.
72. Kharel, M. K., Pahari, P., Lian, H., and Rohr, J. (2009) GilR, an unusual lactone-forming enzyme involved in gilvocarcin biosynthesis, *Chembiochem 10*, 1305-1308.
73. Carter, G. T., Fantini, A. A., James, J. C., Borders, D. B., and White, R. J. (1984) Biosynthesis of Ravidomycin. Use of 13C-13C Double Quantum NMR to Follow Precursor Incorporation, *Tetrahedron Lett. 25*, 255-258.
74. Carter, G. T., Fantini, A. A., James, J. C., Borders, D. B., and White, R. J. (1985) Biosynthesis of Chrysomycins A and B. Origin of the Chromophore, *J. Antibiot. 38*, 242-248.
75. Takahashi, K., and Tomita, F. (1983) Gilvocarcins, New Antitumor Antibiotics. 5. Biosynthesis of Gilvocarcins: Incorporation of 13C-Labeled Compounds into Gilvocarcin Aglycones, *J. Antibiot. 36*, 1531-1535.
76. Liu, T., Kharel, M. K., Fischer, C., McCormick, A., and Rohr, J. (2006) Inactivation of *gilGT*, encoding a C-glycosyltransferase, and *gilOlll*, encoding a P450 enzyme, allows the details of the late biosynthetic pathway to gilvocarcin V to be delineated, *Chembiochem 7*, 1070-1077.
77. Liu, T., Kharel, M. K., Zhu, L., Bright, S., and Rohr, J. (2009) Inactivation of the ketoreductase *gilU* gene of the gilvocarcin biosynthetic gene cluster yields new analogues with partly improved biological activity., *Chembiochem 10*, 278-286.
78. Pahari, P., Kharel, M. K., Shepherd, M. D., van Lanen, S. G., and Rohr, J. (2012) Enzymatic Total Synthesis of Defucogilvocarcin M and Its Implications for Gilvocarcin Biosynthesis, *Angew Chem Int Edit 51*, 1216-1220.
79. Shepherd, M. D., Kharel, M. K., Zhu, L. L., van Lanen, S. G., and Rohr, J. (2010) Delineating the earliest steps of gilvocarcin biosynthesis: role of GilP and GilQ in starter unit specificity, *Org Biomol Chem 8*, 3851-3856.
80. Fawaz, F., and Jones, G. H. (1988) Actinomycin synthesis in Streptomyces antibioticus. Purification and properties of a 3-hydroxyanthranilate 4-methyltransferase, *J Biol Chem 263*, 4602-4606.
81. Kharel, M. K., Nybo, S. E., Shepherd, M. D., and Rohr, J. (2010) Cloning and Characterization of the Ravidomycin and Chrysomycin Biosynthetic Gene Clusters, *Chembiochem 11*, 523-532.
82. Srikrishna, A., and Ravikumar, P. C. (2007) The first total synthesis of (+/-)-gamma-herbertenol, a herbertene isolated from a non-herbertus source, *Synthesis-Stuttgart*, 65-74.
83. Shan, M. D., Sharif, E. U., and O'Doherty, G. A. (2010) Total Synthesis of Jadomycin A and a Carbasugar Analogue of Jadomycin B, *Angew Chem Int Edit 49*, 9492-9495.
84. Kitani, Y., Morita, A., Kumamoto, T., and Ishikawa, T. (2002) Synthetic studies on kinamycin antibiotics: Synthesis of a trioxygenated benz[f]indenone and its Diels-Alder reaction to a kinamycin skeleton, *Helv Chim Acta 85*, 1186-1195.
85. Altschul, S. F., Madden, T. L., Schaffer, A. A., Zhang, J. H., Zhang, Z., Miller, W., and Lipman, D. J. (1997) Gapped BLAST and PSI-BLAST: a new generation of protein database search programs, *Nucleic Acids Res 25*, 3389-3402.

86. Altschul, S. F., and Lipman, D. J. (1990) Protein Database Searches for Multiple Alignments, *P Natl Acad Sci USA 87*, 5509-5513.
87. Noinaj, N., Bosserman, M. A., Schickli, M. A., Piszczek, G., Kharel, M. K., Pahari, P., Buchanan, S. K., and Rohr, J. (2011) The Crystal Structure and Mechanism of an Unusual Oxidoreductase, GilR, Involved in Gilvocarcin V Biosynthesis, *Journal of Biological Chemistry 286*, 23533-23543.
88. de Frutos, O., Atienza, C., and Echavarren, A. M. (2001) Synthesis of benzo[b]phenanthridines and related naturally occurring 2-aryl-1,4-naphthoquinones by palladium- and copper-catalyzed coupling of organostannanes with bromoquinones, *Eur J Org Chem*, 163-171.
89. Taft, F., Harmrolfs, K., Nickeleit, I., Heutling, A., Kiene, M., Malek, N., Sasse, F., and Kirschning, A. (2012) Combined Muta- and Semisynthesis: A Powerful Synthetic Hybrid Approach to Access Target Specific Antitumor Agents Based on Ansamitocin P3, *Chem-Eur J 18*, 880-886.
90. Kirschning, A., and Hahn, F. (2012) Merging Chemical Synthesis and Biosynthesis: A New Chapter in the Total Synthesis of Natural Products and Natural Product Libraries, *Angew Chem Int Edit 51*, 4012-4022.
91. Brown, P. M., and Thomson, R. H. (1976) Naturally Occurring Quinones .26. Synthesis of Tetrangulol (1,8-Dihydroxy-3-Methylbenz[a]Anthracene-7,12-Quinone), *J Chem Soc Perk T 1*, 997-1000.
92. Tibrewal, N., Downey, T. E., Van Lanen, S. G., Ul Sharif, E., O'Doherty, G. A., and Rohr, J. (2012) Roles of the Synergistic Reductive O-Methyltransferase GilM and of O-Methyltransferase GilMT in the Gilvocarcin Biosynthetic Pathway, *J Am Chem Soc 134*, 12402-12405.
93. Widboom, P. F., Fielding, E. N., Liu, Y., and Bruner, S. D. (2007) Structural basis for cofactor-independent dioxygenation in vancomycin biosynthesis, *Nature 447*, 342-345.
94. Kharel, M. K., and Rohr, J. (2012) Delineation of gilvocarcin, jadomycin, and landomycin pathways through combinatorial biosynthetic enzymology, *Curr Opin Chem Biol 16*, 150-161.
95. Chen, Y. H., Fan, K. Q., He, Y. Z., Xu, X. P., Peng, Y. F., Yu, T. T., Jia, C. J., and Yang, K. Q. (2010) Characterization of JadH as an FAD- and NAD(P)H-Dependent Bifunctional Hydroxylase/Dehydrase in Jadomycin Biosynthesis, *Chembiochem 11*, 1055-1060.
96. Chung, J. Y., Fujii, I., Harada, S., Sankawa, U., and Ebizuka, Y. (2002) Expression, purification, and characterization of AknX anthrone oxygenase, which is involved in aklavinone biosynthesis in Streptomyces galilaeus, *J Bacteriol 184*, 6115-6122.
97. Leisch, H., Morley, K., and Lau, P. C. (2011) Baeyer-Villiger monooxygenases: more than just green chemistry, *Chem Rev 111*, 4165-4222.
98. Jiang, J., Tetzlaff, C. N., Takamatsu, S., Iwatsuki, M., Komatsu, M., Ikeda, H., and Cane, D. E. (2009) Genome mining in Streptomyces avermitilis: A biochemical Baeyer-Villiger reaction and discovery of a new branch of the pentalenolactone family tree, *Biochemistry 48*, 6431-6440.
99. Sasaki, E., Ogasawara, Y., and Liu, H. W. (2010) A biosynthetic pathway for BE-7585A, a 2-thiosugar-containing angucycline-type natural product, *J Am Chem Soc 132*, 7405-7417.
100. Minto, R. E., and Townsend, C. A. (1997) Enzymology and Molecular Biology of Aflatoxin Biosynthesis, *Chem Rev 97*, 2537-2556.
101. Philmus, B., Abdelwahed, S., Williams, H. J., Fenwick, M. K., Ealick, S. E., and Begley, T. P. (2012) Identification of the product of toxoflavin lyase: degradation via a Baeyer-Villiger oxidation, *J Am Chem Soc 134*, 5326-5330.

102. Bradford, M. M. (1976) Rapid and Sensitive Method for Quantitation of Microgram Quantities of Protein Utilizing Principle of Protein-Dye Binding, *Anal Biochem 72*, 248-254.
103. Borman, S. (1992) Gilvocarcin M Synthesis Wins Praise for Elegance, *Chem Eng News 70*, 56-&.
104. James, C. A., and Snieckus, V. (1997) Combined directed metallation - Cross coupling strategies. Total synthesis of the aglycones of gilvocarcin V, M and E, *Tetrahedron Lett 38*, 8149-8152.
105. Jung, M. E., and Jung, Y. H. (1988) Total Synthesis of the Aglycone of the 8-Methyl Benzonaphthopyrone Antibiotics, Gilvocarcin-M, Virenomycin-M, and Albacarcin-M, *Tetrahedron Lett 29*, 2517-2520.
106. Matsumoto, T., Hosoya, T., and Suzuki, K. (1992) Total Synthesis and Absolute Stereochemical Assignment of Gilvocarcin-M, *J Am Chem Soc 114*, 3568-3570.
107. Beck, Z. Q., Aldrich, C. C., Magarvey, N. A., Georg, G. I., and Sherman, D. H. (2005) Chemoenzymatic synthesis of cryptophycin/arenastatin natural products, *Biochemistry 44*, 13457-13466.
108. Aldrich, C. C., Venkatraman, L., Sherman, D. H., and Fecik, R. A. (2005) Chemoenzymatic synthesis of the polyketide macrolactone 10-deoxymethynolide, *J Am Chem Soc 127*, 8910-8911.
109. Ding, Y., Rath, C. M., Bolduc, K. L., Hakansson, K., and Sherman, D. H. (2011) Chemoenzymatic synthesis of cryptophycin anticancer agents by an ester bond-forming non-ribosomal peptide synthetase module, *J Am Chem Soc 133*, 14492-14495.
110. Kohli, R. M., Burke, M. D., Tao, J., and Walsh, C. T. (2003) Chemoenzymatic route to macrocyclic hybrid peptide/polyketide-like molecules, *J Am Chem Soc 125*, 7160-7161.
111. Fu, X., Albermann, C., Zhang, C., and Thorson, J. S. (2005) Diversifying vancomycin via chemoenzymatic strategies, *Org Lett 7*, 1513-1515.
112. Cameron, D. W., Feutrill, G. I., and Griffiths, P. G. (1981) Regioselective Bromination of 1,4-Naphthoquinones, *Aust J Chem 34*, 1513-1522.
113. Tietze, L. F., Singidi, R. R., and Gericke, K. M. (2007) Total synthesis of the proposed structure of the anthrapyran metabolite delta-indomycinone, *Chemistry 13*, 9939-9947.
114. Barker, D., Brimble, M. A., Do, P., and Turner, P. (2003) Addition of silyloxydienes to 2,6-dibromo-1,4-benzoquinone: an approach to highly oxygenated bromonaphthoquinones for the synthesis of thysanone, *Tetrahedron 59*, 2441-2449.
115. Lopez-Alvarado, P., Avendano, C., and Menendez, J. C. (2002) Efficient, multigram-scale synthesis of three 2,5-dihalobenzoquinones, *Synthetic Commun 32*, 3233-3239.
116. Kimura, M., Ezoe, A., Mori, M., Iwata, K., and Tamaru, Y. (2006) Regio- and stereoselective nickel-catalyzed homoallylation of aldehydes with 1,3-dienes, *J Am Chem Soc 128*, 8559-8568.
117. Savard, J., and Brassard, P. (1984) Reactions of Ketene Acetals .14. The Use of Simple Mixed Vinylketene Acetals in the Annulation of Quinones, *Tetrahedron 40*, 3455-3464.
118. Gattinoni, S., Merlini, L., and Dallavalle, S. (2007) First total synthesis of topopyrone C, *Tetrahedron Lett 48*, 1049-1051.

Vita

Nidhi Tibrewal

EDUCATION

- 83% MS (Pharmaceutical Chemistry) Banasthali Vidyapith, India
- 79% BS (Chemistry) Delhi University, India

AWARDS & FELLOWSHIPS

- Graduate School Academic Year Fellowship, University of Kentucky, 2011-2012
- Certificate for Academic Proficiency, Banasthali Vidyapith, 2006
- Neeta Bhattacharya Memorial Prize, Delhi University, 2003

RESEARCH EXPERIENCE

University of Kentucky, College of Pharmacy Aug 2008 - Current
Graduate Student, Research Advisor: Dr. Jürgen Rohr

- Supervisor for NMR Facility at College of Pharmacy, UK

Projects:

- **Investigating Gilvocarcin biosynthetic pathway for development of novel anti-cancer agents.**
- Synthesized the proposed intermediates of the biosynthetic pathway of Gilvocarcin.
- Cloned the genes into pET28a and expressed in *E. coli* to yield soluble proteins.
- Developed *in vitro* biochemical assay to screen for the substrate.
- Exogenously fed these synthetic substrates to the downstream enzymes involved and studied the different products formed.
- Characterized the products and assigned enzymes their role in the biosynthetic pathway.
- Characterized 3 post PKS enzymes: GilMT, a methyltransferase, GilM, a reductive methyltransferase, and GilOII, a dioxygenase.
- Kinetic analysis of the enzyme-catalyzed reactions.
- Synthesized analogues of the intermediates and tested downstream enzymes for their substrate specificity.
- Exploiting promiscuous nature of GilM and GilMT and generating new aglycons through chemoenzymatic synthesis.
- Engineering GilR, an oxidoreductase, to broaden the substrate specificity of this bottleneck enzyme of the gilvocarcin biosynthetic pathway for the development of novel anti-cancer therapeutics substrate specificity.

- **Synthesis and Evaluation of Adenylosuccinate Synthetase inhibitors.**
- Worked under supervision of Dr. Gregory I. Elliott.
- Synthesized a series of small molecule inhibitors of AdSS.
- Evaluated the synthesized analogues against AdSS.

Intern, Amgen, Thousand Oaks, CA Jun 2011– Aug 2011

- Conducted NMR experiments to characterize the chemical structure of drug metabolites and developed NMR methods for quantification of metabolites in biological matrices.
- Validated NMR based quantification method by using Mass Spectroscopy.

Research Associate, Jubilant Chemsys Ltd., Noida, India Jun 2006 – Apr 2007

- Engaged in the synthesis, purification and characterization of various novel heterocyclic moieties using various name reactions.

Intern, Central Drug Research Institute (CDRI), India Jan 2006 – Jun 2006

- Synthesized a series of 2,4,6-Trisubstituted I,3,5-Triazines as anti-malarial agents.
- Characterized by means of NMR, IR, UV, and Mass Spectroscopy.
- Evaluated in vitro biological activities against Plasmodium falciparum.

PUBLICATIONS

- Tibrewal, N.; Pahari, P.; Wang, G.; Kharel, M. K.; Morris, C.; Downey, T.; Hou, Y.; Bugni, T.S.; Rohr, J. Baeyer-Villiger C-C bond cleavage reaction in gilvocarcin and jadomycin biosynthesis. *J. Am. Chem. Soc.*, **2012**, *134,* 18181. Link
- Tibrewal, N.; Downey, T. E.; Van Lanen, S. G.; Ul Sharif, E.; O'Doherty, G. A.; Rohr, J. Roles of the Synergistic Reductive O-Methyltransferase GilM and of O-Methyltransferase GilMT in the Gilvocarcin Biosynthetic Pathway. *J. Am. Chem. Soc.* **2012**, *134*, 12402. Link
- Britson, S. B.; Chi, X.; Nonaka, K.; Spork, A. P.; Tibrewal, N.; Goswami, A.; Pahari, P.; Ducho, C.; Rohr, J.; Van Lanen, S. G. Amalgamation of Nucleosides and Amino Acids in Antibiotic Biosynthesis: Discovery of an L-Threonine:Uridine-5'-Aldehyde Transaldolase. *J. Am. Chem. Soc.*, **2012**, *134*, 18514. Link
- Tibrewal, N.; Rohr, J.; Elliott, G.I. Design, Synthesis and Evaluation of AdSS bisubstrate inhibitors. *Bioorg. Med. Chem. Lett*. 2012 (Accepted).
- Kharel, M. K.; Pahari, P.; Shepherd, M. D.; Tibrewal, N.; Nybo, S. E.; Shaaban, K. A.; Rohr, J. Angucyclines: Biosynthesis, mode-of-action, new natural products, and synthesis. *Nat. Prod. Rep.* **2012**, *29*, 264.

- Chi, X.; Nonaka, K.; Tibrewal, N.; Baba, S.; Funabashi, M.; Van Lanen, S. G. The muraminomicin biosynthetic gene cluster and enzymatic formation of the 2-deoxyaminoribosyl appendage. **2012**, *MedChemComm.* (Doi: 10.1039/C2MD20245J).
- Tibrewal, N. and Elliott, G. I. Evaluation of hadacidin analogues. *Bioorg. Med. Chem. Lett*. **2011**, *21*, 517.

PRESENTATIONS

- Poster, ICNPR 2012, NYC
- Poster, Amgen 2011, CA
- Talk, American Chemical Society Fall 2010, MA
- Poster, Markey Cancer Center Research Day 2010, KY
- Indian Pharmaceutical Congress 2004, Kolkata, India